University of Alberta

The Effect of Hydrogen on the Performance of Methane-Fuelled S.I. Engines.

by

Curtis Bauer

A thesis submitted to the Faculty of Graduate Studies and Research in partial fulfillment of the requirements for the degree of Master of Science

Department of Mechanical Engineering

Edmonton, Alberta

Fall, 1999

National Library of Canada
Acquisitions and Bibliographic Services
395 Wellington Street
Ottawa ON K1A 0N4
Canada

Bibliothèque nationale du Canada
Acquisitions et services bibliographiques
395, rue Wellington
Ottawa ON K1A 0N4
Canada

Your file Votre référence

Our file Notre référence

The author has granted a non-exclusive licence allowing the National Library of Canada to reproduce, loan, distribute or sell copies of this thesis in microform, paper or electronic formats.

L'auteur a accordé une licence non exclusive permettant à la Bibliothèque nationale du Canada de reproduire, prêter, distribuer ou vendre des copies de cette thèse sous la forme de microfiche/film, de reproduction sur papier ou sur format électronique.

The author retains ownership of the copyright in this thesis. Neither the thesis nor substantial extracts from it may be printed or otherwise reproduced without the author's permission.

L'auteur conserve la propriété du droit d'auteur qui protège cette thèse. Ni la thèse ni des extraits substantiels de celle-ci ne doivent être imprimés ou autrement reproduits sans son autorisation.

0-612-47007-5

Canada

University of Alberta

Library Release Form

Name of Author: Curtis Bauer

Title of Thesis: The Effect of Hydrogen on the Performance of Methane-Fuelled S.I. Engines.

Degree: Master of Science

Year this Degree Granted: 1999

Permission is hereby granted to the University of Alberta Library to reproduce single copies of this thesis and to lend or sell such copies for private, scholarly, or scientific research purposes only.

The author reserves all other publication and other rights in association with the copyright in the thesis, and except as hereinbefore provided, neither the thesis nor any substantial portion thereof may be printed or otherwise reproduced in any material form whatever without the author's prior written permission.

Curtis Bauer

Curtis Bauer
24 Gillian Crescent,
St. Albert, Alberta,
Canada, T8N 0W1

July 16, 1999

University of Alberta

Faculty of Graduate Studies and Research

The undersigned certify that they have read, and recommended to the Faculty of Graduate Studies and Research for acceptance, a thesis entitled *The Effect of Hydrogen on the Performance of Methane-Fuelled S.I. Engines* submitted by Curtis Bauer in partial fulfillment of the requirements for the degree of Master of Science.

A. Bhattacharyya

Dr. A. Bhattacharyya

Dr. M.D. Checkel

Dr. T.W. Forest

Dr. A.E. Mather

June 21, 1999

Abstract

Mixtures of hydrogen and natural gas (hythane) are considered viable alternative fuels to gasoline due to lower overall pollutant emissions. However, as with all compressed gas vehicles, hythane vehicles have less comparable range due to low energy density.

To date, vehicle engines have run on hythane using a fixed hydrogen fraction and air-to-fuel ratio but it is possible to leverage greater advantage from H_2 addition. Hydrogen posses unique lean-burn characteristics which make it possible to control power by the air-to-fuel ratio. In this manner, it is possible to decrease fuel consumption by varying the mixture strength of hydrogen in methane, and varying the air-to-fuel ratio during a driving cycle, without decreasing engine power. Cumulative production of CO_2, CO, and NO can be reduced, but production of unburned hydrocarbons increases due to operation near the partial burn limit. Hydrogen can also be produced on-board by the electrolysis of water, from engine power, and from regenerative braking power. This has the potential to increase engine efficiency, reduce storage requirements and recycle energy. This study presents the results of a one-cylinder engine test with mixtures of hydrogen in methane of 0%, 20%, 40% and 60% by volume. Each fuel was tested at speeds of 700RPM and 900RPM, full & part loads, and equivalence ratios from stoichiometric to the partial burn limit. These engine results are applied to three different driving cycles where engine speed and power requirements are changing. Optimum operating systems are identified given a specified quantity of hydrogen on-board. Furthermore, a simulated electrolyser operating from engine power and regenerative power is determined to offer no advantage.

Table of Contents

1. Introduction..... 1
2. CFR engine test..... 10
    2.1. Equipment used..... 10
    2.2. Test procedure..... 12
    2.3. Data reduction..... 13
    2.4. Full load results..... 16
    2.5. Part load results..... 27
    2.6. Conclusion of CFR engine test..... 32
3. Driving cycle simulation..... 33
    3.1. Driving cycles..... 34
    3.2. Vehicle model..... 35
    3.3. Engine model..... 39
    3.4. Scheme 1, 2, & 3 engine cases..... 41
    3.5. Scheme 1, 2, & 3 cumulative driving cycle results..... 57
        3.5.1. SAE-J-227D cumulative results..... 59
        3.5.2. Highway schedule cumulative results..... 63
        3.5.3. Urban schedule cumulative results..... 67
    3.6. Electrolyser..... 71
        3.6.1. Electrochemical principles..... 72
        3.6.2. Electrolyser design principles..... 73
        3.6.3. Electrolyser response under variable power input..... 75
        3.6.4. Model electrolyser design..... 76
    3.7. Scheme 4 engine cases..... 80
    3.8. Scheme 4 cumulative driving cycle results..... 89
        3.8.1. SAE J-227D cumulative results..... 89
        3.8.2. Highway schedule cumulative results..... 95
        3.8.3. Urban schedule cumulative results..... 101
    3.9. Conclusions and recommendations..... 108

References..... 111
Appendix A. CFR engine raw data..... 115
Appendix B. Uncertainty in CFR data..... 120
Appendix C. CFR best-fit equations..... 130
Appendix D. Model engine case equations..... 133
Appendix E. Second by second model results..... 146
Appendix F. Model sensitivity analysis..... 186
Appendix G. Model computer code..... 188

List of Tables

Table 1.1.Properties of hydrogen, methane & gasoline..... 2

Table 3.1. Summary of engine schemes 1, 2, 3, and 4..... 42

Table 3.2. SAE-J-227D schedule idle and peak fuel consumption and pollutant production (g/s).... 61

Table 3.3. SAE-J-227D schedule percent reduction in consumption of fuel / production of pollutant when using scheme 2 or 3 in place of scheme 1 for equal amounts of hydrogen addition (g/km)..... 63

Table 3.4. SAE-J-227D schedule change in consumption of fuel, production of pollutant (g/km) per g/km of hydrogen addition..... 63

Table 3.5. Highway schedule idle and peak fuel consumption and pollutant production (g/s)..... 65

Table 3.6. Highway schedule percent reduction in consumption of fuel / production of pollutant when using scheme 2 or 3 in place of scheme 1 for equal amounts of hydrogen addition (g/km)..... 66

Table 3.7. Highway schedule change in consumption of fuel, production of pollutant (g/km) per g/km of hydrogen addition..... 67

Table 3.8. Urban schedule idle and peak fuel consumption and pollutant production (g/s)..... 68

Table 3.9. Urban schedule percent reduction in consumption of fuel / production of pollutant when using scheme 2 or 3 in place of scheme 1 for equal amounts of hydrogen addition (g/km)..... 70

Table 3.10. Urban Schedule change in consumption of fuel, production of pollutant (g/km) per g/km of hydrogen addition..... 70

Table A.1. Part load data for CFR engine testing at 700RPM..... 115

Table A.2. Part load data for CFR engine testing at 900RPM..... 116

Table A.3. Full load data for CFR engine testing at 700RPM..... 117

Table A.4. Full load data for CFR engine testing at 900RPM..... 118

Table C.1. Full load data best-fit polynomial coefficients and correlation coefficients with respect to equivalence ratio..... 130

Table C.2. Part load best-fit coefficients and correlation coefficients with respect to engine load.... 132

Table D.1. Best-fit polynomial coefficients and correlation coefficients for case A-G..... 133

Table D.2. Best-fit polynomial coefficients and correlation coefficients for case B-H..... 134

Table D.3. Best-fit polynomial coefficients and correlation coefficients for case C-I..... 135

Table D.4. Best-fit polynomial coefficients and correlation coefficients for case D-J..... 136

Table D.5. Best-fit polynomial coefficients and correlation coefficients for case E-K..... 137

Table D.6. Best-fit polynomial coefficients and correlation coefficients for case D-I..... 138

Table D.7. Best-fit polynomial coefficients and correlation coefficients for case F-I..... 139

Table D.8. Best-fit polynomial coefficients and correlation coefficients for case F-K..... 140

Table D.9. Best-fit polynomial coefficients and correlation coefficients for case C-K..... 141

Table D.10. Best-fit polynomial coefficients and correlation coefficients for case W-K..... 142

Table D.11. Best-fit polynomial coefficients and correlation coefficients for case X-K..... 143
Table D.12. Best-fit polynomial coefficients and correlation coefficients for case Y-K..... 144
Table D.13. Best-fit polynomial coefficients and correlation coefficients for case Z-K..... 145

List of Figures

Figure 1.1. The percentage of CH_4 and H_2 mass, and carbon in the fuel versus volumetric fraction of hydrogen in methane 3
Figure 1.2. The mass and volumetric lower heating value and density of the fuel versus volumetric fraction of hydrogen in methane 4
Figure 1.3. Stoichiometric air-fuel mixtures versus volumetric fraction of hydrogen in methane 5
Figure 2.1. CFR engine test schematic 11
Figure 2.2. Dilution of NO_x sample with atmospheric air 12
Figure 2.3. Test matrix 13
Figure 2.4. Full load experimental results for the CFR partial burn limits 16
Figure 2.5. Full load MBT spark advance BTDC increases with hydrogen addition 17
Figure 2.6. Full load brake power decreases with hydrogen addition 18
Figure 2.7. Full load indicated thermal efficiency decreases with hydrogen addition 19
Figure 2.8. Full load brake thermal efficiency decreases with hydrogen addition 20
Figure 2.9. Full load brake specific fuel consumption at 700RPM decreases with hydrogen addition 21
Figure 2.10. Full load brake specific fuel consumption at 900RPM decreases with hydrogen addition 21
Figure 2.11. Full load brake specific CO_2 production at 700RPM decreases with hydrogen addition 22
Figure 2.12. Full load brake specific CO_2 production at 900RPM decreases with hydrogen addition 23
Figure 2.13. Full load brake specific production of CO at 700RPM and 900RPM is highly dependent on combustion equivalence ratio 24
Figure 2.14. Full load brake specific production of unburned hydrocarbons at 700RPM decreases with hydrogen addition 25
Figure 2.15. Full load brake specific production of unburned hydrocarbons at 900RPM decreases with hydrogen addition 25
Figure 2.16. Full load brake specific production of NO_x (as NO) at 700RPM increases with hydrogen addition 26
Figure 2.17. Full load brake specific production of NO_x (as NO) at 900RPM increases with hydrogen addition 27
Figure 2.18. Brake specific fuel consumption increases with decreasing load for all fuels, equivalence ratios and engine speeds 28
Figure 2.19. Brake specific production of CO_2 increases with decreasing load for all fuels, equivalence ratios and engine speeds 28

Figure 2.20. Brake specific production of CO increases with decreasing loads for all fuels, equivalence ratios and engine speeds 29
Figure 2.21. Brake specific production of HCs increase with decreasing load for all fuels, equivalence ratios and engine speeds 30
Figure 2.22. Brake specific NO production dependence on equivalence ratio at part load 31
Figure 2.23. Brake specific production of NO decreases with decreasing load for equivalence ratios below 0.9, and increases for equivalence ratios above 0.9, for all fuels and engine speeds 31
Figure 3.1. Driving cycle, vehicle and engine model architecture 33
Figure 3.2. SAE-J-227D schedule 34
Figure 3.3. Highway Fuel Economy Test schedule 35
Figure 3.4. 1972 Federal Test Procedure schedule 35
Figure 3.5. Vehicle model 36
Figure 3.6. SAE-J-227D schedule required engine speed and power 37
Figure 3.7. Highway Fuel Economy Test schedule required engine speed and power 38
Figure 3.8. 1972 Federal Test Procedure schedule required engine speed and power 39
Figure 3.9. Control of f, ϕ, and throttle position with the pedal 41
Figure 3.10. Power map of the model engine at 1000RPM and 5kW 43
Figure 3.11. Brake specific fuel consumption of the model engine at 1000RPM and 5kW 44
Figure 3.12. Power map of the model engine at 1800RPM and 35kW 44
Figure 3.13. Brake specific fuel consumption of the model engine at 1800RPM and 35kW 45
Figure 3.14. Engine case A-G 46
Figure 3.15. Engine case B-H 47
Figure 3.16. Engine case C-I 49
Figure 3.17. Engine case D-J 50
Figure 3.18. Engine case E-K 51
Figure 3.19. Engine case D-I 53
Figure 3.20. Engine case F-I 54
Figure 3.21. Engine case F-K 55
Figure 3.22. Engine case C-K 56
Figure 3.23. SAE-J-227D schedule brake power, and engine speed combinations with respect to pedal position 59
Figure 3.24. SAE J-227D cumulative results versus H_2 consumption for schemes 1, 2, and 3 62
Figure 3.25. Highway schedule brake power, and engine speed combinations with respect to pedal position 64
Figure 3.26. Highway cumulative results versus H_2 consumption for schemes 1, 2 and 3 66
Figure 3.27. Urban schedule brake power, and engine speed combinations versus pedal position 67
Figure 3.28. Urban cumulative results versus H_2 consumption for schemes 1, 2 and 3 69

Figure 3.29. Comparing a scheme 1,2, or 3 engine to a scheme 4 engine with electrolyser 71
Figure 3.30. Typical alkaline electrolysis cell 74
Figure 3.31. Brossard electrolyser hydrogen production rate with respect to input power 76
Figure 3.32. Model electrolyser hydrogen production rate with respect to input power 77
Figure 3.33. Regenerative braking provides additional power to the electrolyser 78
Figure 3.34. Negative tractive energy captured in the HOT-505 schedule 79
Figure 3.35. HOT-505 schedule cumulative negative tractive energy captured by regenerative braking 79
Figure 3.36. Model engine power map at 1000RPM and full load 82
Figure 3.37. Model engine brake specific fuel consumption map at 1000RPM and full load 83
Figure 3.38. Engine case W-K operation with respect to pedal position 85
Figure 3.39. Engine case X-K operation with respect to pedal position 86
Figure 3.40. Engine case Y-K operation with respect to pedal position 87
Figure 3.41. Engine case Z-K operation with respect to pedal position 88
Figure 3.42. Case W-K SAE-J-227D schedule second-by-second engine / electrolyser power, and hydrogen consumption / production 90
Figure 3.43. Case X-K SAE-J-227D schedule second-by-second engine / electrolyser power, and hydrogen consumption / production 91
Figure 3.44. Case Y-K SAE-J-227D schedule second-by-second engine / electrolyser power, and hydrogen consumption / production 91
Figure 3.45. Case Z-K SAE-J-227D schedule second-by-second engine / electrolyser power, and hydrogen consumption / production 92
Figure 3.46. SAE-J-227D cumulative hydrogen consumption and production with respect to engine energy for cases E-K, W-K, X-K, Y-K and Z-K 93
Figure 3.47. SAE-J-227D cumulative fuel consumption and pollutant production with respect to total hydrogen consumption for scheme 4 95
Figure 3.48. Case W-K Highway schedule second-by-second engine / electrolyser power, and hydrogen consumption / production 96
Figure 3.49. Case X-K Highway schedule second-by-second engine / electrolyser power, and hydrogen consumption / production 97
Figure 3.50. Case Y-K Highway schedule second-by-second engine / electrolyser power, and hydrogen consumption / production 98
Figure 3.51. Case Z-K Highway schedule second-by-second engine / electrolyser power, and hydrogen consumption / production 98
Figure 3.52. Highway cumulative hydrogen consumption and production with respect to engine energy for cases E-K, W-K, X-K, Y-K and Z-K 100
Figure 3.53. Highway cumulative fuel consumption and pollutant production with respect to total

hydrogen consumption for scheme 4 101
Figure 3.54. Case W-K Urban schedule second-by-second engine / electrolyser power, and hydrogen consumption / production 102
Figure 3.55. Case X-K Urban schedule second-by-second engine / electrolyser power, and hydrogen consumption / production 103
Figure 3.56. Case Y-K Urban schedule second-by-second engine / electrolyser power, and hydrogen consumption / production 104
Figure 3.57. Case Z-K Urban schedule second-by-second engine / electrolyser power, and hydrogen consumption / production 104
Figure 3.58. Urban cumulative hydrogen consumption and production with respect to engine energy for cases E-K, W-K, X-K, Y-K and Z-K 106
Figure 3.59. Urban cumulative fuel consumption and pollutant production with respect to total hydrogen consumption for scheme 4 107
Figure B.1. Absolute error in equivalence ratio for 700RPM and 900RPM 122
Figure B.2. Absolute error in indicated thermal efficiency for 700RPM and 900RPM 123
Figure B.3. Absolute error in brake thermal efficiency for 700RPM and 900RPM 123
Figure B.4. Relative error in brake specific fuel consumption for 700RPM and 900RPM 124
Figure B.5. Relative error in brake specific CO_2 production for 700RPM and 900RPM 124
Figure B.6. Relative error in brake specific CO production for 700RPM and 900RPM 125
Figure B.7. Relative error in brake specific HC production for 700RPM and 900RPM 125
Figure B.8. Relative error in brake specific NO production for 700RPM and 900RPM 126
Figure B.9. Relative error in part load percentage of full load BSFC 127
Figure B.10. Relative error in part load percentage of full load $BSCO_2$ 127
Figure B.11. Relative error in part load percentage of full load BSCO 128
Figure B.12. Relative error in part load percentage of full load BSHC 128
Figure B.13. Relative error in part load percentage of full load BSNO 129
Figure E.1. Case A-G SAE-J-227D schedule second-by-second results 147
Figure E.2. Case B-H SAE-J-227D schedule second-by-second results 148
Figure E.3. Case C-I SAE-J-227D schedule second-by-second results 149
Figure E.4. Case D-J SAE-J-227D schedule second-by-second results 150
Figure E.5. Case E-K SAE-J-227D schedule second-by-second results 151
Figure E.6. Case D-I SAE-J-227D schedule second-by-second results 152
Figure E.7. Case F-I SAE-J-227D schedule second-by-second results 153
Figure E.8. Case F-K SAE-J-227D schedule second-by-second results 154
Figure E.9. Case C-K SAE-J-227D schedule second-by-second results 155
Figure E.10. Case W-K SAE-J-227D schedule second-by-second results 156
Figure E.11. Case X-K SAE-J-227D schedule second-by-second results 157

Figure E.12. Case Y-K SAE-J-227D schedule second-by-second results 158
Figure E.13. Case Z-K SAE-J-227D schedule second-by-second results 159
Figure E.14. Case A-H Highway schedule second-by-second results 160
Figure E.15. Case B-H Highway schedule second-by-second results 161
Figure E.16. Case C-I Highway schedule second-by-second results 162
Figure E.17. Case D-J Highway schedule second-by-second results 163
Figure E.18. Case E-K Highway schedule second-by-second results 164
Figure E.19. Case D-I Highway schedule second-by-second results 165
Figure E.20. Case F-I Highway schedule second-by-second results 166
Figure E.21. Case F-K Highway schedule second-by-second results 167
Figure E.22. Case C-K Highway schedule second-by-second results 168
Figure E.23. Case W-K Highway schedule second-by-second results 169
Figure E.24. Case X-K Highway schedule second-by-second results 170
Figure E.25. Case Y-K Highway schedule second-by-second results 171
Figure E.26. Case Z-K Highway schedule second-by-second results 172
Figure E.27. Case A-H Urban schedule second-by-second results 173
Figure E.28. Case B-H Urban schedule second-by-second results 174
Figure E.29. Case C-I Urban schedule second-by-second results 175
Figure E.30. Case D-J Urban schedule second-by-second results 176
Figure E.31. Case E-K Urban schedule second-by-second results 177
Figure E.32. Case D-I Urban schedule second-by-second results 178
Figure E.33. Case F-I Urban schedule second-by-second results 179
Figure E.34. Case F-K Urban schedule second-by-second results 180
Figure E.35. Case C-K Urban schedule second-by-second results 181
Figure E.36. Case W-K Urban schedule second-by-second results 182
Figure E.37. Case X-K Urban schedule second-by-second results 183
Figure E.38. Case Y-K Urban schedule second-by-second results 184
Figure E.39. Case Z-K Urban schedule second-by-second results 185
Figure F.1. Effect of increasing the mass of the vehicle model from 1250 kg to 1550 kg on energy, fuel consumption and pollutant production 187
Figure F.2. The effect of increasing the thermal efficiency of the engine by 1% (absolute) compared to the effect of increasing mass on the fuel consumption 187

List of Symbols, Nomenclature, and Abbreviations

ϕ	equivalence ratio
η_{cycle}	cycle efficiency
η_E	electrolysis efficiency
$\eta_{electrolyser}$	electrolyser efficiency over the driving cycle
η_G	generator efficiency
$\eta_{th,brake}$	brake thermal efficiency
$\eta_{th,indicated}$	indicated thermal efficiency
ρ	density
A	effective frontal area
AFR	air-to-fuel ratio, stoichiometric
AFA	air-to-fuel ratio, actual
BMEP	brake mean effective pressure
bp	brake power
$BSFC$	brake specific fuel consumption
$BSCO_2$	brake specific production of carbon dioxide
$BSCO$	brake specific production of carbon monoxide
$BSHC$	brake specific production of unburned hydrocarbons
$BSNO$	brake specific production of nitric oxide
C_D	coefficient of drag
CFR	coordinating fuels research
C_R	rolling coefficient
d_{cycle}	driving cycle distance
deg BTDC	degrees before top dead center
$E_{drivetrain}$	cycle cumulative drivetrain energy
$E_{fulltime}$	cycle cumulative fulltime energy used by the electrolyser
E_{input}	cycle cumulative fuel energy input
$E_{regeneration}$	cycle cumulative regenerative energy provided by braking
f	volumetric fraction of hydrogen
F_D	drag force

F_R	rolling resistance
F_I	inertial force
fp	friction power
LHV	lower heating value
LHV_f	lower heating value of hydrogen/methane mixture
load	engine load
m	mass
M	molar mass
MBT	minimum spark advance for best torque
m_{fuel}	cumulative consumption of fuel over a driving cycle
$\dot{m}_{fuel}$	instantaneous mass flow rate of fuel
$\dot{m}_{H2,E}$	instantaneous mass flow rate of H_2 produced by the electrolyser
NGV	natural gas vehicle
P_G	engine power supplied to the full-time generator
ppm	parts per million
P_R	regenerative power
RPM	revolutions per minute
SEC_t	thermoneutral specific energy consumption
v	vehicle speed
V_p	electrolyser voltage required at pressure
WOT	wide open throttle
x	molar fraction
y	hydrogen-to-carbon ratio

1. Introduction

Hydrogen is a potential alternative to gasoline in the future. It is considered a near perfect energy storage medium, as it can be created from fossil [1] or non-fossil sources [2]. Its use in conventional combustion engines has generally shown decreased pollutant emissions [3,4,5] primarily due to lean burn and a reduction of carbon in the fuel. When hydrogen and oxygen are reacted in a fuel cell, the only products are electricity and water. However, hydrogen is currently a rare commodity when compared to hydrocarbon fuels. Due to a lack of infrastructure, its introduction is a long-term prospect. Current use of hydrogen must be limited to small-scale advantage.

Natural gas vehicles (NGVs) are a potential alternative to gasoline vehicles in the short term. They are less polluting, and the fuel is widely available. However, in an effort to reduce their pollutants further, NGVs have been run on "hythane" (mixtures of H_2 and CH_4) with a fixed hydrogen fraction and air-to-fuel ratio. These vehicles have lower comparable range due to lower on-board energy density. To make up for this, it is desirable to decrease fuel consumption (and increase range), by leveraging more advantage from the hydrogen. This is possible by varying its mixture strength with methane, and varying the air-to-fuel ratio, during a driving cycle. This can also be achieved without negatively affecting engine power and emissions.

Hydrogen is an excellent additive to methane or gasoline due to its unique characteristics. Based on an examination of the properties in Table 1.1, it is seen that hydrogen is able to burn ultra-lean at an equivalence ratio[1] of 0.1. Methane and gasoline are capable of burning at equivalence ratios no lower than of 0.53 and 0.70 respectively. Hydrogen's mass specific lower heating value (LHV)[2] of 119 930kJ/kg is nearly three times that of methane or gasoline. However, hydrogen's density of 0.083764kg/m^3 at STP[3], results in a volumetric LHV of 10 046kJ/m^3, which is lower than methane (32 573kJ/m^3) or gasoline (195 800kJ/m^3). Although its stoichiometric air-to-fuel ratio is higher, hydrogen occupies a greater proportion of volume with respect to the air (0.290), than does methane (0.095) or gasoline (0.018). This in effect counters hydrogen's low

---

[1] Equivalence Ratio (ϕ) is the ratio of the stoichiometric air-to-fuel ratio to the actual air to fuel ratio.
[2] LHV is the chemical energy released during complete combustion with the water product as vapor.
[3] STP denotes standard temperature (293.15K) and pressure (1atm).

volumetric LHV, so that with stoichiometric mixtures, hydrogen/air contains slightly less energy (2913kJ/m^3) than stoichiometric methane/air (3088kJ/m^3) and stoichiometric gasoline/air (3446kJ/m^3). An approximate seven-fold increase in the burning speed of a hydrogen flame (265cm/s-325cm/s) over methane or gasoline results in shorter burn times. This shorter burn time is reflected in less heat transfer from a hydrogen flame (17%-25%) to the environment when compared to methane (22%-33%) and gasoline (30%-42%). Hydrogen's quenching distance (usually defined as the minimum gap between parallel plates in which a flame will propagate [6]), of 0.064cm is approximately 1/3 that of methane or gasoline. Hydrogen generally burns hotter (2318K) than methane (2148K), but cooler than gasoline (2470K), based on flame temperatures in air.

Table 1.1.Properties of hydrogen, methane & gasoline.

	Hydrogen (H_2)	Methane (CH_4)	Gasoline (C_8H_{18})
Equivalence ratio ignition lower limit in STP air* [7]	0.10	0.53	0.70
Mass Lower Heating Value (kJ/kg) [8]	119 930	50 020	44 500
Density of Gas @ STP (kg/m^3)* [8]	0.083764	0.65119	4.4
Volumetric Lower Heating Value @ STP (kJ/m^3)*†	10 046	32 573	195 800
Stoichiometric Air to Fuel Ratio (kg/kg)†	34.20	17.19	15.08
Volumetric Fraction of Fuel in Air, ϕ=1 @ STP*†	0.290	0.095	0.018
Volumetric Lower Heating Value in air, ϕ=1 @ STP (kJ/m^3)*†	2913	3088	3446
Burning Speed in STP air (cm/s)* [8]	265 – 325	37 - 45	37 – 43
% thermal energy radiated from flame to surroundings [8]	17 – 25	23 – 33	30 – 42
Molar Carbon to Hydrogen Ratio†	0	0.25	0.44
Quenching Distance in STP air (cm)* [8]	0.064	0.203	0.2
Flame Temperature in air (K) [8]	2318	2148	2470

*STP denotes standard temperature (293.15K) and pressure (1atm)

†Author's calculations (using density of air = 1.17kg/m^3 where applicable)

With H_2-gasoline mixtures, the gasoline must be evaporated first before it can be mixed with hydrogen. With H_2-CH_4 mixtures, both fuels are in the gaseous state at STP, and readily diffuse into each other to form homogeneous mixtures. Fuel delivery can be pre-mixed in the storage tanks, or mixed on-board the vehicle. The mixture properties

are proportional to the amount of hydrogen and methane contained within. For sake of convenience, mixtures are defined in terms of volumetric fractions. The volumetric fraction of hydrogen in methane is the ratio of the volume of hydrogen to the total volume of hydrogen and methane. Due to hydrogen's lower density compared to methane, significant amounts of hydrogen mass only appear at high volumetric fractions as seen in Figure 1.1. The addition of H_2 effectively decreases the amount of carbon in the fuel faster than the decrease in the mass of CH_4, because carbon is being displaced volumetrically according to $C_{(1-f)}H_{(4-2f)}$. This assumes that hydrogen and methane mixtures are approximated as ideal gasses.

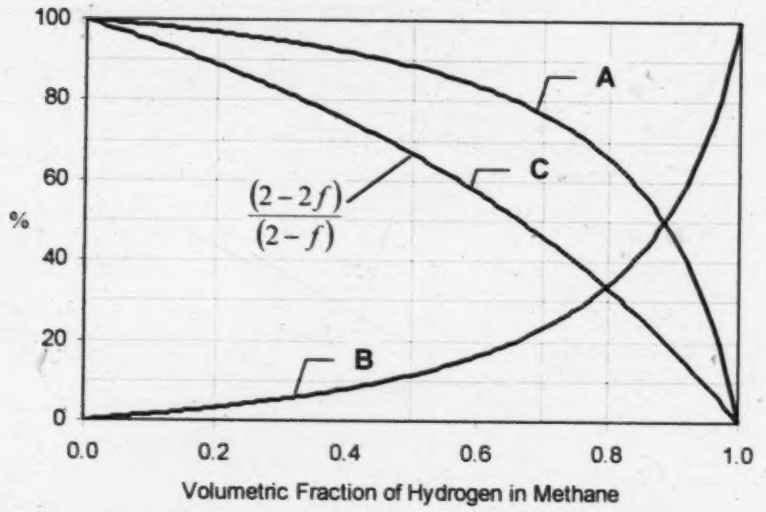

Figure 1.1. The percentage of CH_4 and H_2 mass, and carbon in the fuel versus volumetric fraction of hydrogen in methane. **(A)** The percentage mass of CH_4 in the fuel decreases while **(B)** the percentage mass of H_2 increases with hydrogen addition. **(C)** The percentage of carbon in the fuel (where CH_4 = 100%) decreases with hydrogen addition.

Addition of hydrogen increases the LHV of the mixture per unit mass, but decreases its density. This results in a lower LHV per unit volume as hydrogen is added as seen in Figure 1.2. When air /fuel mixtures are considered as seen in Figure 1.3, the volume of fuel in air increases as hydrogen is added despite an increasing air-to-fuel

ratio. This increase in volume of fuel in air counters the dropping volumetric energy content of the fuel so that there is only a slight decrease in fuel/air energy content with H_2 addition.

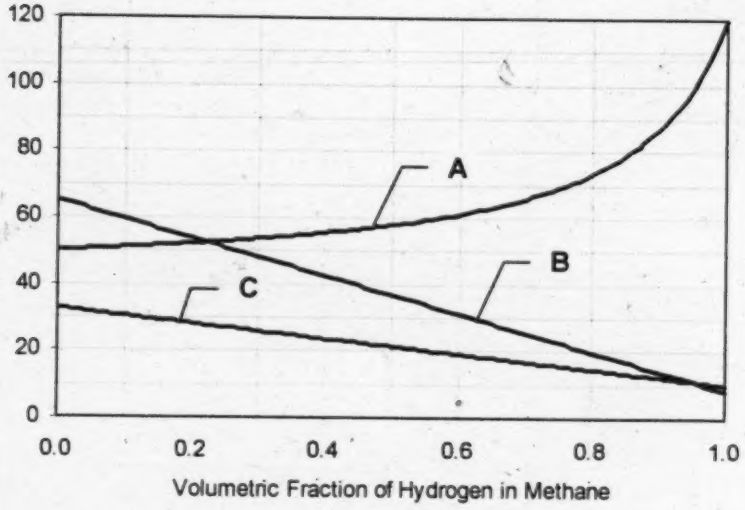

Figure 1.2. The mass and volumetric lower heating value and density of the fuel versus volumetric fraction of hydrogen in methane. The mass specific LHV (**A**) in MJ/kg, increases with H_2 addition, but the density (**B**) in $g/m^3 \times 10^1$, decreases so that the volumetric LHV (**C**) in MJ/m^3 decreases.

Depending on engine design, it may not be possible to reach the lower ignition limit, but rather a partial burn limit [9]. The partial burn limit is effectively the greatest air-to-fuel ratio for vehicle use, as any lower would result in unacceptable misfiring. Conversely, the upper equivalence ratio is bounded by the engine's knock limit. Knock occurs when unburned fuel opposite the flame front reaches its auto-ignition temperature and pressure [10]. Higher compression ratios, fuel enriched mixtures, and hydrogen addition all increase peak cylinder temperature and pressure independently, thus leading to a greater inclination to knock. The addition of hydrogen to methane raises the fuel /air effective polytropic index of compression. Therefore, for a fixed compression ratio, the addition of hydrogen contributes to an increase in peak cylinder pressure (and temperature) at identical equivalence ratios.

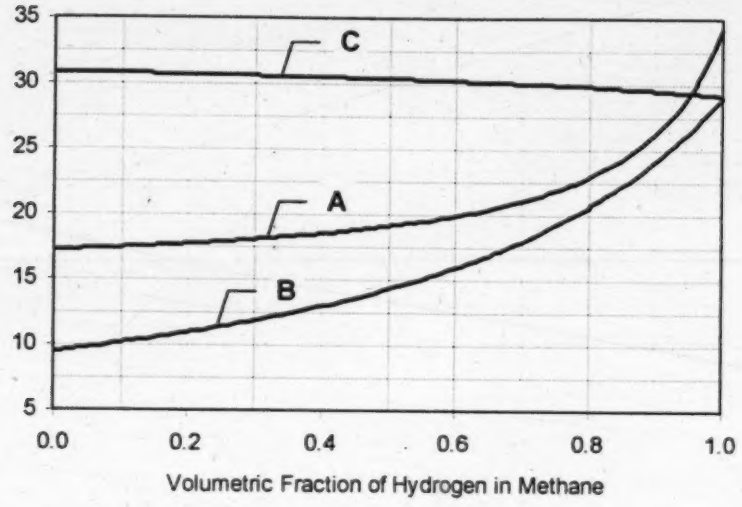

Figure 1.3. Stoichiometric air-fuel mixtures versus volumetric fraction of hydrogen in methane. The stoichiometric air-to-fuel ratio (**A**) increases with hydrogen addition, but the volumetric percentage of fuel in air (**B**) also increases, so that there is a decrease in the stoichiometric mixture volumetric energy content (**C**) in $kJ/m^3 \times 10^2$.

In an effort to capitalize on the properties of hydrogen, without a fully dedicated operating system, mixtures of hydrogen and conventional fuels have previously been examined. The feasibility of hydrogen addition to gasoline was first demonstrated in a series of experiments looking at emissions reduction through lean combustion. Experiments on one-cylinder research engines [11, 12, 13] showed hydrogen's ability to extend the lean limit of combustion, and generally reduce carbon monoxide (CO) and unburned hydrocarbons (HCs), but increase oxides of nitrogen (NO_x) at identical equivalence ratios. Thermal efficiency was found highly dependent on equivalence ratio, but less dependent on the fuel type. Experiments performed on production engines confirmed that hydrogen addition could decrease emissions, and increase thermal efficiency in conjunction with operating the engine at a specified lean equivalence ratio [14, 15].

With strict legislation came the development of less polluting natural gas vehicles. In an effort to reduce pollutants ever further, hydrogen addition to natural gas was

examined. As with gasoline engines, hydrogen addition in natural gas engines was also found to decrease carbon-based emissions. To date, Hythane (premixed to 20% hydrogen in methane by volume) vehicles have undergone road testing in California, Colorado and Pennsylvania, claiming emissions reductions over baseline natural gas [16]. In addition, several studies were done on production and research engines. One of the first studies was carried out on a one-cylinder research engine in Germany by Nagalingam et al. [17] in 1983. Mixtures of hydrogen in methane of 0%, 20%, 50%, and 100% by volume were studied at one engine speed. Hydrogen addition was found to extend the lean limit of combustion due to its inherent nature, but it decreased the power due to an overall lower volumetric heating value. Indicated thermal efficiency decreased with H_2 addition, possibly due to a decreasing ratio of brake power to friction power and increasing heating value of the fuel. Optimum spark time decreased by up to 20deg BTDC for mixtures of pure hydrogen indicating increased flame speed. Emissions of NO_x increased for pure hydrogen due to higher combustion temperature, with the peak occurring at a leaner equivalence ratio. Unburned hydrocarbons and carbon monoxide emissions decreased due to direct displacement of a carbon-based fuel with hydrogen. All trends behaved as expected, with power peaking around stoichiometric equivalence ratio, efficiency and NO_x emissions peaking around $\phi = 0.8$ to 0.9, and hydrocarbons reaching a minimum around $\phi = 0.8$ to 0.9. Carbon monoxide was only produced by mixtures above $\phi = 0.95$. This experiment did not analyze engine speed and engine load (throttle position).

In 1992, a study was done at the University of Melbourne on a one-cylinder research engine at 1200RPM [18]. The thrust of the study was to reduce cycle-to-cycle variability, by supplementing natural gas at the ignition site with hydrogen. This was expected to increase flame propagation speed and widen the flammability limits. The process is referred to as hydrogen assisted jet ignition (HAJI), and uses a prechamber to control the hydrogen jet. The amount of hydrogen used varied from 2% to 10% by mass of methane. Three different inlet manifold pressures were studied. Equivalence ratios examined were simply defined as "lower limit" or "maximum efficiency" referring to the base condition with pure methane. Adding hydrogen separately effectively enriches the fuel mixture and therefore alters the operation of the engine. In general, hydrogen addition was found to increase thermal efficiency, power, and NO_x, while decreasing

MBT spark advance, and unburned hydrocarbons. However, it is difficult to say if this is entirely the result of the unique properties of hydrogen, or of a shift in combustion stoichiometry. This experiment did not examine the effect of varying engine speed on the results.

In 1993, a test was carried out on a 1.6 liter Toyota four-cylinder engine by Swain [19], to determine the effect of hythane (premixed to 20% hydrogen in methane by volume) on a production engine. The test was performed at 1000RPM, Best Efficiency Spark Advance (BESA) and at "light loading condition". Compared to methane, hythane (at identical equivalence ratios) was found to increase brake thermal efficiency and NO_x, while decreasing BESA, unburned HCs, and CO. In addition, the use of hythane decreased the lower limit equivalence ratio from 0.61 to 0.54 (defined as 38% of cycles not firing). The experiment did not analyze various fractions of hydrogen in methane, the effect of varying engine speed, or load.

A more theoretically based experiment was carried out by Karim [20] on a CFR engine in 1995. Fuel mixtures up to 80% hydrogen in methane by volume were tested while varying equivalence ratio and spark advance at 900RPM and full load. Again, hydrogen addition was shown to decrease optimum spark timing. Results for indicated power output, and average indicated output efficiency were reported at spark timings of 10deg BTDC, 20deg BTDC, and 30deg BTDC at equivalence ratios from 0.65 to 1.30. Spark timing was shown to have an adverse effect on thermal efficiency. The knocking region was defined for different compression ratios and different mixtures of methane/hydrogen. The experiment did not analyze the effect of engine speed, or load (throttle position). Equivalence ratios near the partial burn limit were not examined.

In 1995 a study was done on a 3.1-liter 6-cylinder production engine with 15% hydrogen in methane by volume mixture to examine its impact on engine operation [21]. Speed, load, and spark timing were varied, at equivalence ratios from 1 to 1.03. Results showed that 15% hydrogen fuel generally had better efficiency, lower HC, CO, and CO_2 emissions over baseline methane, but higher NO_x emissions. The experiment did not analyze various mixtures of hydrogen in methane, or equivalence ratios near the partial burn limit.

In 1996, a comprehensive study was done on a 4.6-liter 8-cylinder production engine [22]. Mixtures of 0%, 10%, 20%, 30%, 40%, and 50% hydrogen in methane by volume were studied. Hydrogen addition was found to increase production of NO_x, and decrease production of HC in the lean region at 1700RPM. For the particular case of a 30% hydrogen mixture, at an equivalence ratio of 0.65, the engine was tested at various speeds (1700RPM, 2350RPM, 3000RPM), and various loads (100BMEP to 500 BMEP). Production of NO_x was found to increase with increasing load, somewhat independent of speed. Hydrocarbon production was found to decrease with increasing load independent of speed. Brake thermal efficiency was found to improve with increasing load at 2350RPM. This particular case did not analyze various mixtures of hydrogen at different equivalence ratios. In a follow-up paper [23], the test was expanded so that 0%, 30%, and 100% hydrogen in methane mixtures were tested in a one-cylinder research engine. The testing was carried out at full load and 1800RPM. The objective was to find operating conditions that would result in production of NO_x below the Equivalent Zero Emission Vehicle (EZEV) limits without the use of a catalytic converter. NO_x, power and indicated thermal efficiency were reported while varying the spark timing and equivalence ratio. The 0% H_2 mixture was tested with equivalence ratios from 0.62 to 0.72, the 30% H_2 mixture from $\phi = 0.53$ to 0.67, and the 100% H_2 mixture from $\phi = 0.35$ to 0.45. It was found that operating the engine with a 30% H_2 mixture, an equivalence ratio of 0.53 and at best efficiency spark timing, the engine would be capable of reaching the EZEV limit for NO_x of 8.9ppm. The experiment did not study the effect of engine speed or load. Although lean equivalence ratios were studied, the partial burn limits were not reached.

Universal among the results shown was the ability to achieve leaner combustion as the amount of hydrogen was increased. Traditional gasoline engines have been designed to run at near stoichiometric air-to-fuel ratios, with power controlled by the throttle plate. Current natural gas engines are, for the most part, adaptations of existing gasoline engines. Vehicle engines need a wide power band, due to varying driver requirements. Conventionally due to narrow ignition limits, it is necessary to employ a throttle plate to control engine power. However, by utilizing the unique lean-burn property of hydrogen, power control can be achieved by altering the air/fuel ratio. This

leads us to ask if we can obtain a decrease in fuel consumption, and a decrease in pollutant emissions, by utilizing the unique lean-burn property of hydrogen to control power by air-to-fuel ratio. However, in order to make a realistic assessment of hydrogen addition in a vehicle, a driving cycle simulation must be developed, to analyze the cumulative effects of several different operating systems.

2. CFR Engine Test

Although many tests have been previously conducted on engines with hydrogen / methane mixtures, there is a lack of data to examine and compare one set of operating conditions to another in a driving cycle. During such a cycle, the two parameters of engine speed, and required power are changing. Depending on the operating system, the fraction of hydrogen in methane, and equivalence ratio can also be changing throughout a cycle, for a total of four parameters. Many tests examined two or three of these parameters, but a complete test with all four parameters was found to be lacking (from one engine). Due to this shortfall, a one-cylinder research engine was tested with various mixtures of hydrogen/methane, at different engine speeds, loads and equivalence ratios in the lean region to obtain input data for the entire operational range.

2.1. Equipment used

To obtain the required data set, a one-cylinder research engine was tested under laboratory conditions. The CFR (Coordinating Fuel Research) engine is a 0.61L one-cylinder engine built in 1960 originally designed to determine knock properties of fuels. Although adjustable for compression ratio, the engine was maintained at a compression ratio of 8.5 for the duration of testing. The engine has controls to alter fuel flow, spark timing, and load (by throttle position). The engine was connected to an electric dynamometer that was capable of maintaining constant engine speed through feedback control. A schematic of the test setup can be seen in Figure 2.1.

Mass flow rate of air into the engine was measured with a long radius flow nozzle, calibrated to atmospheric pressure and temperature. The air was routed through a large volume drum, which provided for damping of small flow fluctuations. Fuels of 0%, 20%, 40% and 60% hydrogen in methane by volume were supplied via compressed gas cylinders at 18MPa (2600 psi) regulated to a gauge pressure of approximately 10KPa (1.5psi). The fuel line was run through a volumetric gas flow meter, but since it was only calibrated for natural gas, the air flow measurement was used in subsequent stoichiometric calculations.

Exhaust gas was led from a sample line through a cold water bath at 7°C (to eliminate water), and then to emissions sampling equipment. A Snap-On emissions

analyzer was used to sample CO_2, CO, O_2, and unburned hydrocarbons. The analyzer was calibrated with known concentrations of calibration gasses before testing. The analyzer's infrared unburned hydrocarbon detector was calibrated with hexane (C_6H_{14}), and then corrected for methane by multiplying the instrument reading by a factor of 6. However, a post-test calibration revealed that the infrared detector underestimated the amount of CH_4 in the exhaust stream by a factor of 3.95. This is not critical, as it was more important to obtain relative readings with hydrogen addition, as opposed to absolute values.

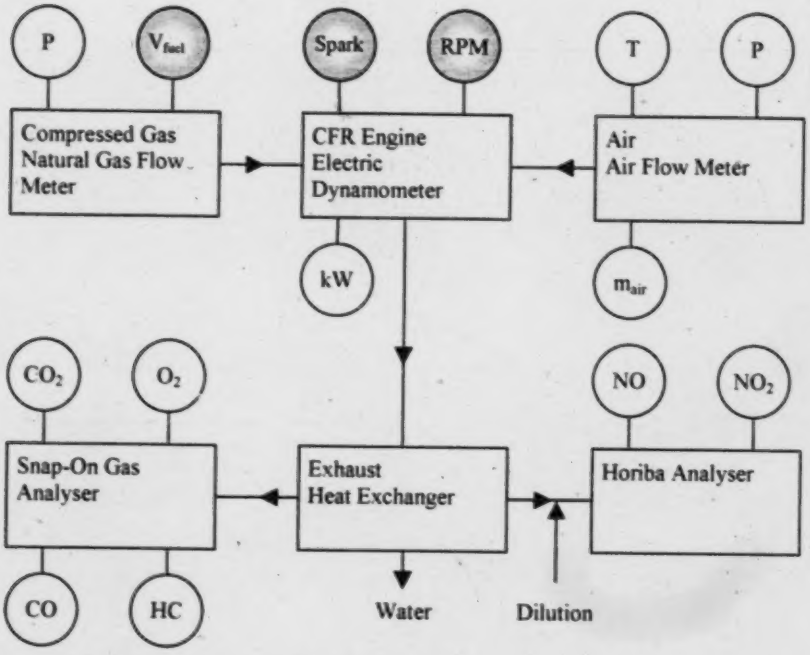

Figure 2.1. CFR engine test schematic. ◉ = adjustable control, ○ = measurement only
P = atmospheric pressure, T = atmospheric temperature, V_{fuel} = volumetric flow rate of fuel, Spark = spark timing, RPM = engine speed, kW = engine power, m_{air} = mass flow rate of air, CO_2 = % CO_2 (dry), O_2 = % O_2 (dry), CO = % CO (dry), HC = ppm C6 (dry), NO = ppm NO (dry), NO_2 = ppm NO_2 (dry).

A Horiba chemical reaction cell NO_x analyzer was used to sample for NO and NO_2. Since the unit was range limited at 2500ppm, which is exceeded under certain conditions, all NO_x samples were diluted with atmospheric air. As seen in Figure 2.2,

dilution air was drawn into the exhaust stream at a constant flow rate by maintaining a constant water column height. The dilution factor used was determined to be 2.69 (i.e. 1000ppm reading = 2690ppm actual concentration) by calibrating with known NO_x concentrations before testing. Only NO_x samples were diluted.

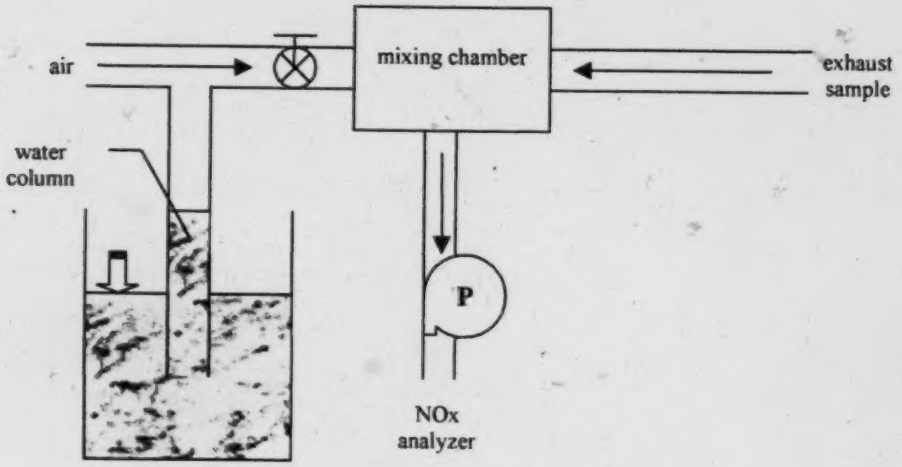

Figure 2.2. Dilution of NO_x sample with atmospheric air. The dilution factor is consistent by maintaining a constant water column height, during calibration and testing.

2.2. Test procedure

During testing, ambient temperatures ranged from 20°C to 22°C, and pressures ranged from 92KPa (690mmHg) to 94KPa (708mmHg). Wet bulb temperatures ranged from 10°C to 12°C. No environmental correction factors were used for power or emissions.

Testing was carried out at constant speed, and at MBT spark (minimum spark advance for best torque). MBT spark was bracketed by trial and error during testing. Fuels of 0%, 20%, 40%, and 60% hydrogen in methane by volume were tested (in order). Fuels above 60% hydrogen were not examined because of the danger of knock and/or intake manifold explosions. The fuel and air were drawn into a gas mixer and fed into the engine past a throttle plate. For each fuel, speed was set to 700RPM and 900RPM in

turn according to Figure 2.3. Before taking data, the engine oil temperature was allowed to stabilize at 62^{0}C. At this oil temperature, the friction power needed by the engine was 0.90kW at 700RPM and 1.43 kW at 900RPM. The oil was not changed for the duration of the test. Initially, the throttle plate was held wide open (load=1) and a "sweep" of air-to-fuel ratios was then performed. The air-to-fuel ratios were varied from near stoichiometric to the partial burn limit by reducing the flow rate of fuel supplied to the engine at constant speed. The partial burn limit was determined by reducing the fuel flow rate until the engine started to misfire. Once the full load values were established, the throttle plate was closed so that load[4] was approximately 2/3 then 1/3 in turn. At each throttle plate setting, an air-to-fuel ratio sweep was again performed. No external exhaust gas recirculation (EGR) was used in this experiment, and no catalytic conversion was used.

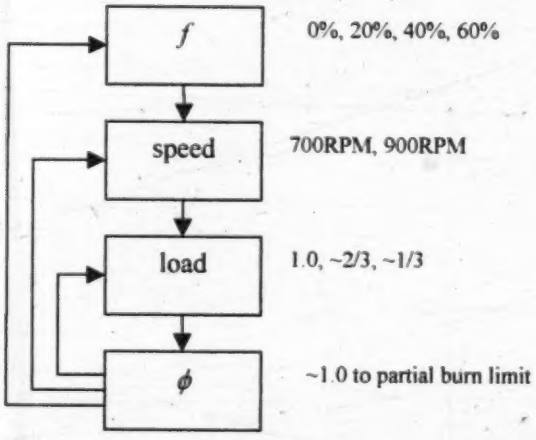

Figure 2.3. Test matrix. For each hydrogen fraction, the engine was tested at various speed, each which was tested at various load, each which was tested at various equivalence ratio.

2.3. Data reduction

In order to provide meaningful data for the input model, the raw engine test results were reduced through stoichiometric analysis. Knowing the fraction of hydrogen

[4] Load is defined as the fraction of power produced at part load to that produced at full load.

(f) a stoichiometric balance can be done assuming complete combustion as seen in equation 1.

$$(1-f)CH_4 + fH_2 + (2-1.5f)(O_2 + 3.76N_2) \rightarrow \quad (1)$$
$$(1-f)CO_2 + (2-f)H_2O + (2-1.5f)3.76N_2$$

The stoichiometric air-to-fuel ratio (AFS) can be determined from equation 2.

$$AFS = \frac{(2-1.5f)4.76M_{air}}{(1-f)M_{CH4} + fM_{H2}} \quad (2)$$

From exhaust gas analysis, the actual air-to-fuel ratio was found by stoichiometric balance with the method detailed by Heywood [24]. The equivalence ratio is determined using equation 3.

$$\phi = \frac{AFS}{AFA} \quad (3)$$

The stoichiometric balance was then completed in equation 4 by assuming all unburned hydrocarbons to be CH_4, and all NO_x to be NO (since NO_2 is only a small fraction of NO_x in S.I. engines [25]). The stoichiometric balance is:

$$CH_y + \frac{n_{O2}}{\phi}(O_2 + 3.76N_2) \rightarrow \quad (4)$$
$$n_p\left(x_{CHy}CH_y + x_{co}CO + x_{CO2}CO_2 + x_{O2}O_2 + x_{N2}N_2 + x_{NO}NO + x_{H2O}H_2O + x_{H2}H_2\right)$$

where n_{O2} are the number of moles or air, and n_p are the number of moles of combustion product. The hydrogen to carbon ratio is known from the fuel composition in equation 5.

$$y = \frac{4(1-f)+2f}{1-f} \quad (5)$$

Knowing the mass flow rate of air, the subsequent consumption of fuel and production of products can be solved for on a brake power specific basis (equation 6):

$$bs_q = \frac{m_{air} x_q M_q 3600}{(0.5x_{CO} + x_{CO2} + 0.5x_{NO} + x_{O2} + 0.5x_{H2O}) 4.76 M_{air} bp} \quad (g/kWhr) \quad (6)$$

where q represents the fuel (CH_y) consumed or pollutant CO_2, CO, CH_4, NO produced. The lower heating value of the hythane mixture is dependent on the proportions of hydrogen (LHV = 119 930 kJ/kg) and methane (LHV = 50 020 kJ/kg), as seen in equation 7.

$$LHV_f = \frac{LHV_{H2}\rho_{H2} f + LHV_{CH4}\rho_{CH4}(1-f)}{\rho_{H2} f + \rho_{CH4}(1-f)} \quad (7)$$

The indicated thermal efficiency is a measure of how much total power the engine produces with respect to the chemical energy input rate (equation 8).

$$\eta_{th,indicated} = \frac{bp + fp}{m_{fuel} LHV_f} \quad (8)$$

Brake thermal efficiency gives a more realistic assessment of engine performance, as friction power is not available to do useful work. As seen in equation 9, brake thermal efficiency is a measure of how much available power is produced with respect to the chemical energy input rate.

$$\eta_{th,brake} = \frac{bp}{m_{fuel} LHV_f} \quad (9)$$

2.4. Full load results

The engine was first tested at full load (WOT). Stable combustion is only possible in a region between the knock and ignition limits as seen in Figure 2.4. The partial burn limit of the engine was defined by the onset of misfire. A dramatic drop in power is indicative of a misfire. The results show that the partial burn limits for the CFR engine occur slightly above the ignition limits for the speeds of 700RPM, and 900RPM. For pure methane the partial burn limit was found to occur at approximately $\phi = 0.58$. Hydrogen addition to 60% lowered the partial burn limit to approximately $\phi = 0.34$.

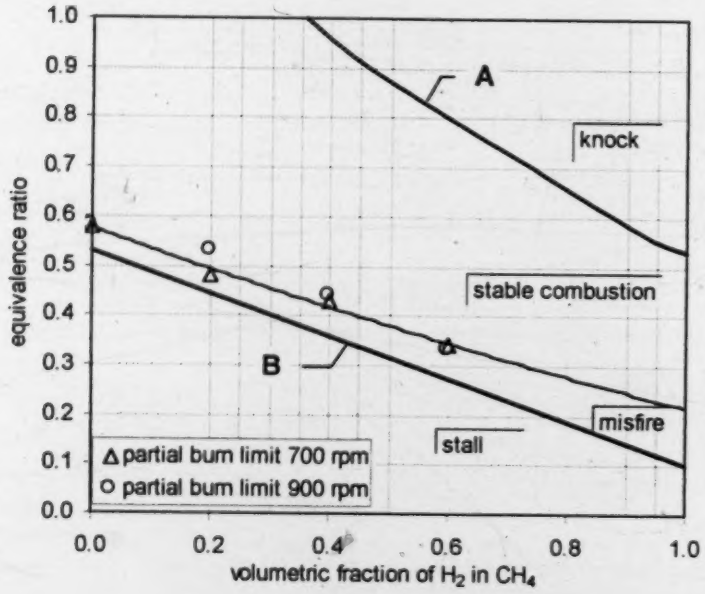

Figure 2.4. Full load experimental results for the CFR partial burn limits. Shown are the knock limit (**A**) as estimated for a 9:1 compression ratio based on data from [20], and the ignition limit (**B**) as estimated based on data from [8]. The data points as determined by experiment for 700RPM and 900RPM are shown for the CFR test. Hydrogen addition lowers the partial burn limit for the CFR engine. The uncertainty in equivalence ratio ranges from +/- 0.02 to +/- 0.04 (see Appendix A for detailed uncertainty analysis).

Spark timing is dependent on the flame speed. Faster flame speed results in a decrease in the crank angle before top dead center at which the spark is applied. Flame speed reaches a maximum near stoichiometric air/fuel, and decreases either lean or rich

[26]. The results of testing, as seen in Figure 2.5, confirmed that minimum spark timings were found at around stoichiometric ϕ due to faster overall flame speed. Adding hydrogen decreased the spark timing further by increasing the average flame speed. Hydrogen addition up to 60% by volume decreased spark timing by 6deg BTDC to 14deg BTDC at identical equivalence ratios. Increasing the engine speed to 900RPM increased the spark timing by approximately 2.5deg BTDC, due to a shorter time in which the flame can burn.

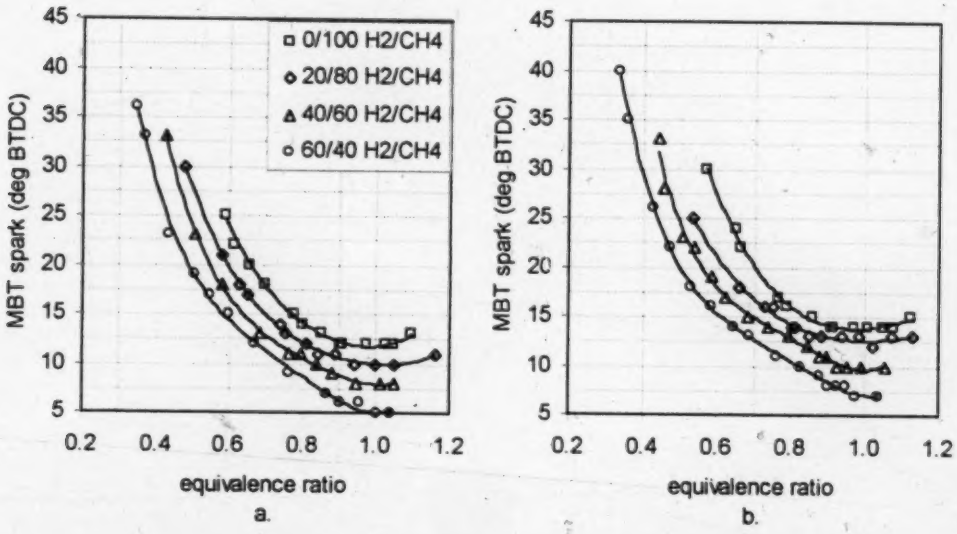

Figure 2.5. Full load MBT spark advance BTDC increases with hydrogen addition. (**a**.) Spark is more advanced at 700RPM than at (**b**.) 900RPM due to slower piston speed. The uncertainty in MBT spark is +/- 1deg BTDC.

Power produced at MBT spark is a maximum near stoichiometric ϕ, where there is an optimum amount of air and fuel. Air to fuel ratios rich of stoichiometric decrease engine power due to decreasing combustion efficiency [27]. Air to fuel ratios lean of stoichiometric decrease engine power due to a reduction in the volumetric LHV of the intake mixture, despite increasing combustion efficiency. Hydrogen addition also decreases power due to a reduction in volumetric LHV. As seen in Figure 2.6, hydrogen addition to 60% by volume decreased the engine power by approximately 0.2kW at ϕ=

1.0. However, the addition of 60% hydrogen allowed power production at lower equivalence ratios, although power produced at the partial burn limit is approximately 1/5 of the peak value at $\phi = 1.0$.

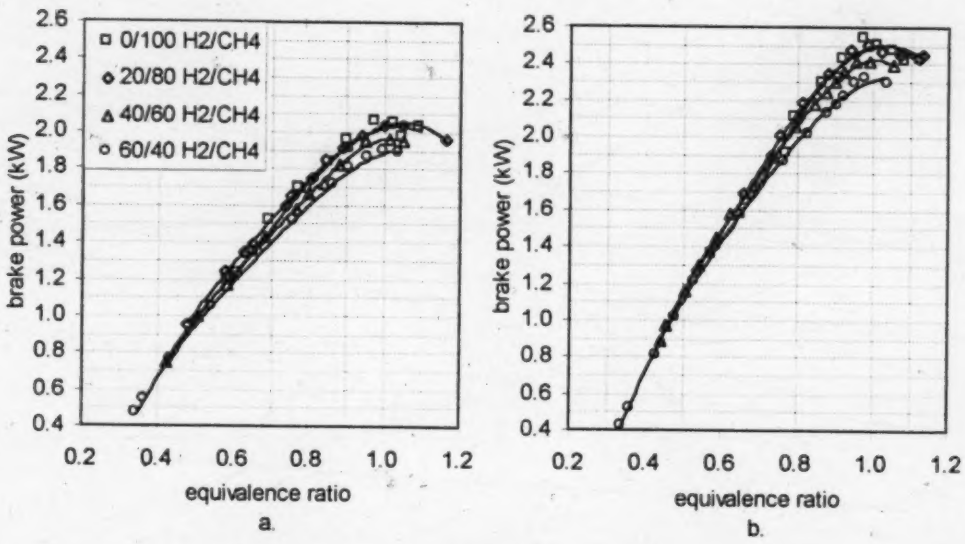

Figure 2.6. Full load brake power decreases with hydrogen addition. (**a**.) Brake power is lower at 700RPM than at (**b**.) 900RPM. The uncertainty in brake power is estimated at +/- 0.03 kW.

Indicated thermal efficiency is partially dependent on combustion efficiency. Combustion efficiency is high when using lean equivalence ratios, as shown by the small amount of products of incomplete combustion. Combustion efficiency decreases for rich equivalence ratios by approximately $1/\phi$ as there is insufficient oxygen to complete combustion [28]. Indicated thermal efficiency, as seen in Figure 2.7, shows an increase in the proportion of energy captured from the fuel as the equivalence ratio decreases. Indicated thermal efficiency drops by approximately 2% (absolute) with the addition of 60% hydrogen due to an increase in the energy input of the fuel without an increase in power. The decrease in thermal efficiency with hydrogen addition was an unexpected result, as the fast burn speed of hydrogen and its greater ratio of specific heats should result in less heat transfer out of the cylinder. However, this may be offset by the high flame temperature of hydrogen, and the research engine's cooling system (designed to

run at constant temperature). This effect may be common with research engines, as Nagalingam et al. [17] noticed a similar decrease in efficiency when hydrogen was added.

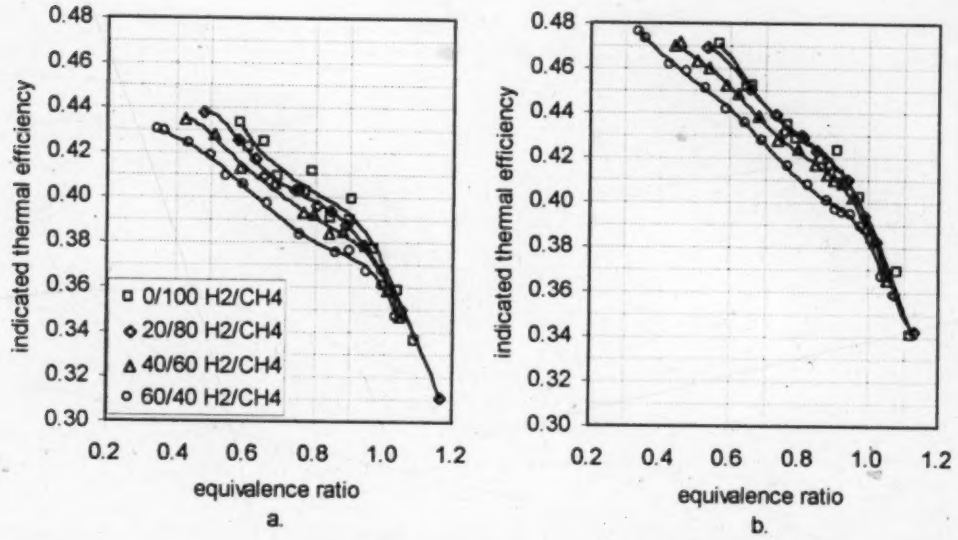

Figure 2.7. Full load Indicated thermal efficiency decreases with hydrogen addition. (**a**.) Indicated thermal efficiency is lower at 700RPM than at (**b**.) 900RPM due to a higher proportion of friction power to brake power at 700RPM. The uncertainty in indicated thermal efficiency ranges from +/- 0.01 to +/- 0.06.

Brake thermal efficiency does not include the speed dependent friction power needed by the engine. As seen in Figure 2.8, brake thermal efficiency peaks where the brake power and the combustion efficiency are high, around equivalence ratios of 0.9. As the brake power decreases so does the brake thermal efficiency, as a greater proportion of the fuel energy is being used to overcome friction. Hydrogen addition to 60% by volume decreased brake efficiency by approximately 2% (absolute).

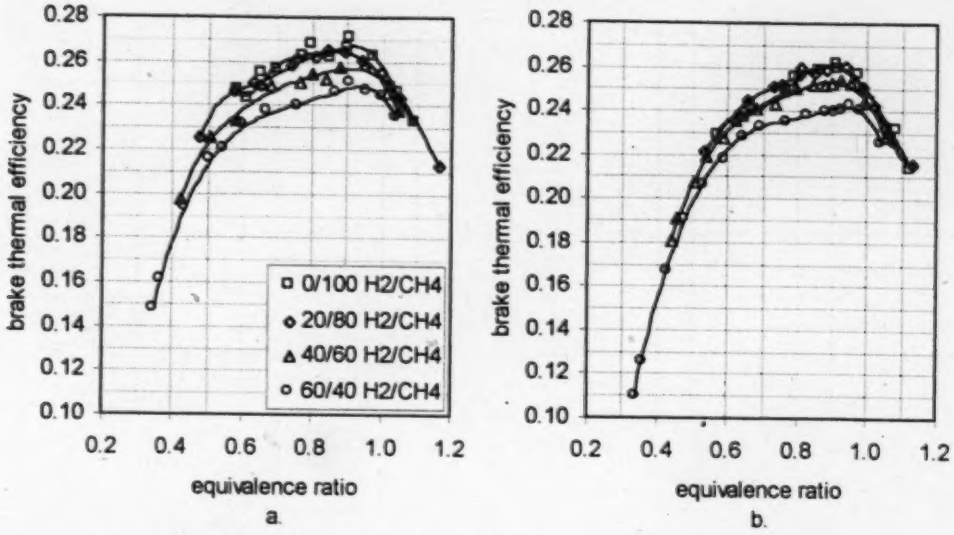

Figure 2.8. Full load brake thermal efficiency decreases with hydrogen addition. (a.) Brake thermal efficiency is higher at 700RPM than (b.) 900RPM due to a greater proportion of chemical energy delivered being used to produce brake power. The uncertainty in brake thermal efficiency ranges from +/- 0.01 to +/- 0.02.

Brake specific fuel consumption (*BSFC*) is the mass flow rate of fuel with respect to brake power and is therefore inversely proportional to brake thermal efficiency. As seen in Figure 2.9, the lowest *BSFC* can be found around $\phi = 0.9$ where the thermal efficiency is highest and the brake power produced is proportionally high. The addition of hydrogen decreases *BSFC* on a mass basis, because of the higher energy content of the fuel. Higher engine speeds increase the *BSFC* due to increased friction power. Hydrogen addition up to 60% decreases *BSFC* by up to 50g/kWhr (14%). Figure 2.10 shows an increase in *BSFC* of approximately 5g/kWhr (1%) for fuels at identical ϕ when the speed is increased to 900RPM. This slight increase is possibly due to the increase in friction power at higher speeds. Subsequently, since the fuel consumption per unit of brake power is higher at 900RPM, it is expected that the brake specific pollutants produced are also higher at 900RPM.

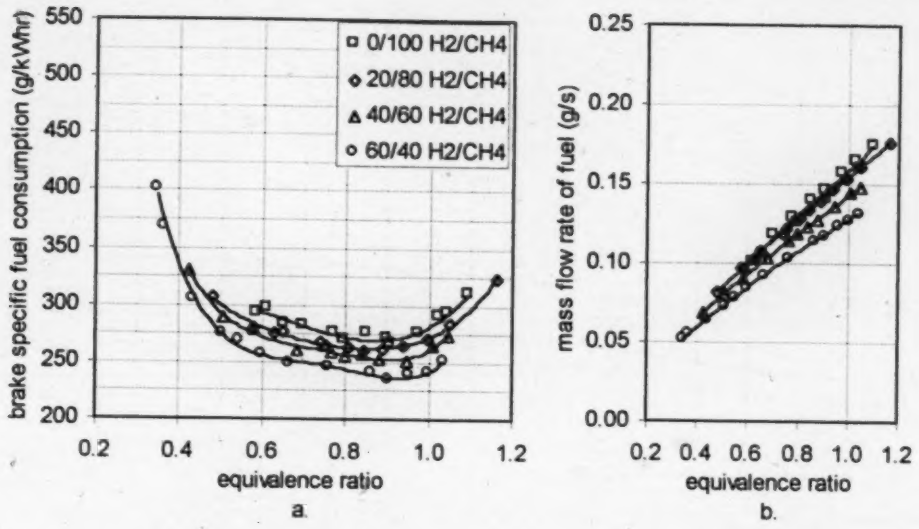

Figure 2.9. Full load brake specific fuel consumption at 700RPM decreases with hydrogen addition. (**a**.) *BSFC* (**b**.) Mass flow rate of fuel. The uncertainty in *BSFC* ranges from +/-4% to +/-14%.

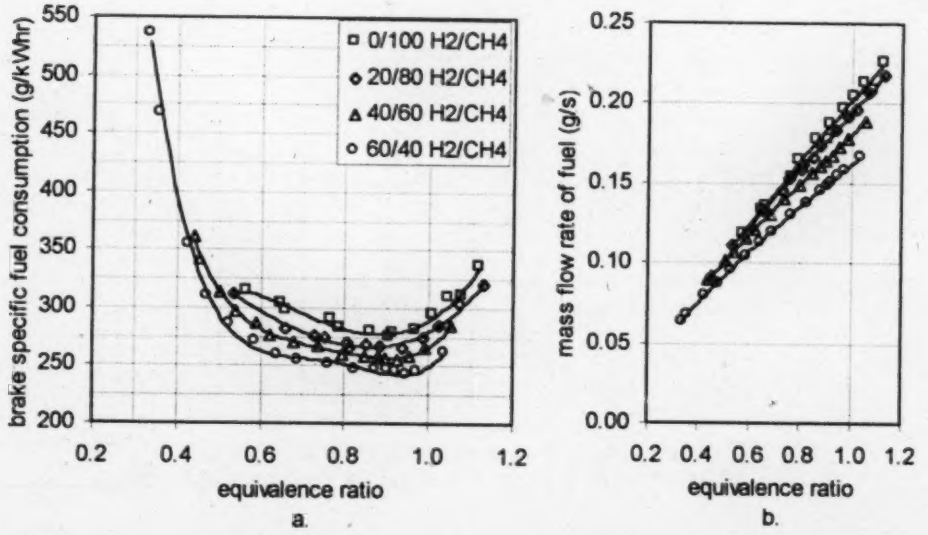

Figure 2.10. Full load brake specific fuel consumption at 900RPM decreases with hydrogen addition. (**a**.) *BSFC* (**b**.) Mass flow rate of fuel. Brake specific fuel consumption is slightly higher at 900RPM (than 700RPM) due to decreased thermal efficiency. The uncertainty in *BSFC* ranges from +/-4% to +/-14%.

Carbon dioxide is considered a product of complete combustion of a hydrocarbon fuel. As seen in Figures 2.11 and 2.12, the molar fraction of CO_2 in the products peaks at an equivalence ratio of 0.9, where combustion efficiency is highest, irrespective of speed. From $\phi = 0.9$, the molar fraction of CO_2 decreases for both lean equivalence ratios due to a reduction in fuel carbon, and for rich equivalence ratios where there is insufficient air to fully form CO_2. However, brake specific production of carbon dioxide ($BSCO_2$) increases at lean equivalence ratios, as the power reduction is proportionally greater than the reduction in CO_2 concentration in the exhaust. Hydrogen addition up to 60% decreases $BSCO_2$ by approximately 250g/kWhr (26%) at identical equivalence ratios. The increase in speed to 900RPM increases $BSCO_2$ by approximately 25g/kWhr (3%).

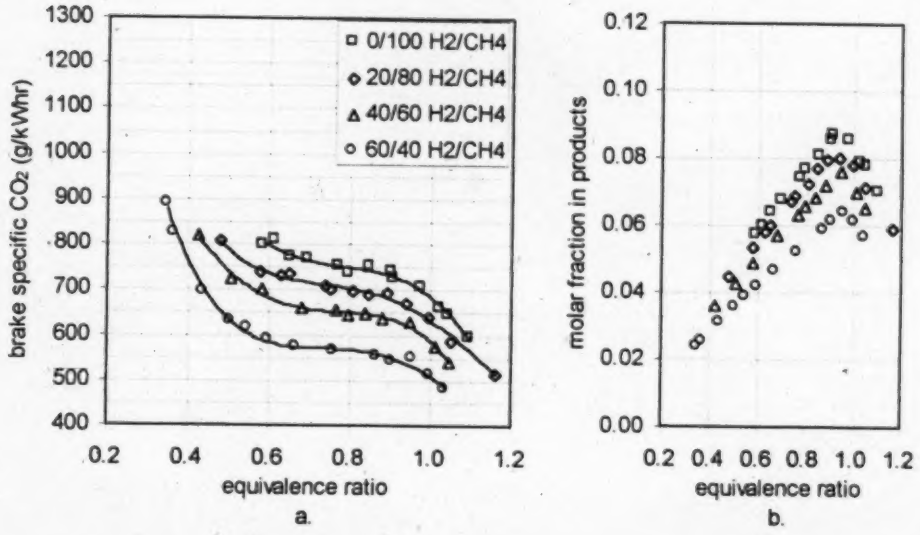

Figure 2.11. Full load brake specific CO_2 production at 700RPM decreases with hydrogen addition. (**a.**) $BSCO_2$ (**b.**) Molar fraction of CO_2 in the exhaust products. The uncertainty in $BSCO_2$ ranges from +/-5% to +/-18%.

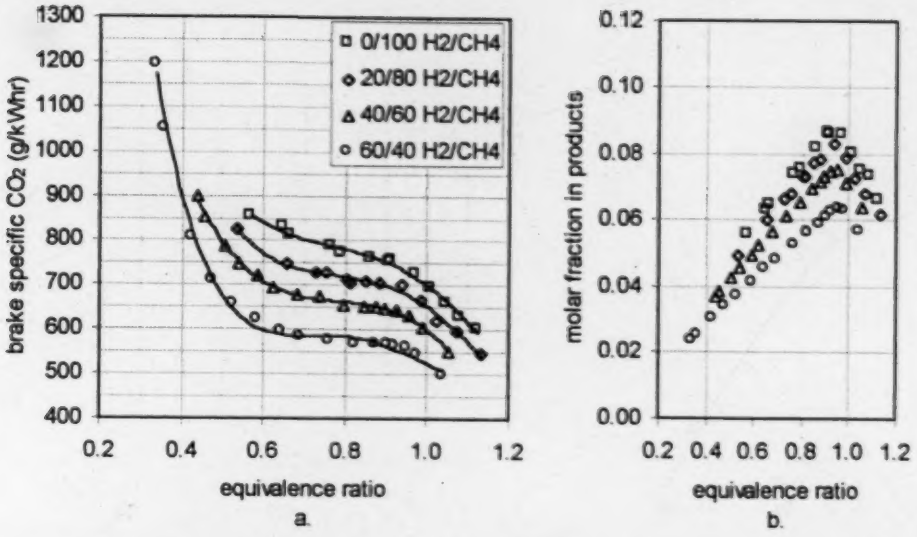

Figure 2.12. Full load brake specific CO_2 production at 900RPM decreases with hydrogen addition. (**a**.) $BSCO_2$ (**b**.) Molar fraction of CO_2 in the exhaust products. Brake specific production of CO_2 at 900RPM is slightly higher due to lower brake thermal efficiency at 900RPM. The uncertainty in $BSCO_2$ ranges from +/-5% to +/-18%.

Production of carbon monoxide primarily occurs in rich combustion when there is a lack of O_2 to fully form CO_2 [29]. As seen in Figure 2.13, its production is highly dependent on combustion stoichiometry and less so on engine speed. In the rich region ($\phi > 0.95$), there is a general reduction in *BSCO* with the addition of hydrogen, due to the reduction of carbon in the fuel. Hydrogen addition up to 60% by volume decreased *BSCO* by up to 20g/kWhr (40%) at $\phi = 1$. In the ultra-lean region ($\phi < 0.40$), an increase in *BSCO* can be noted; due to incomplete combustion combined with sharply dropping power [30].

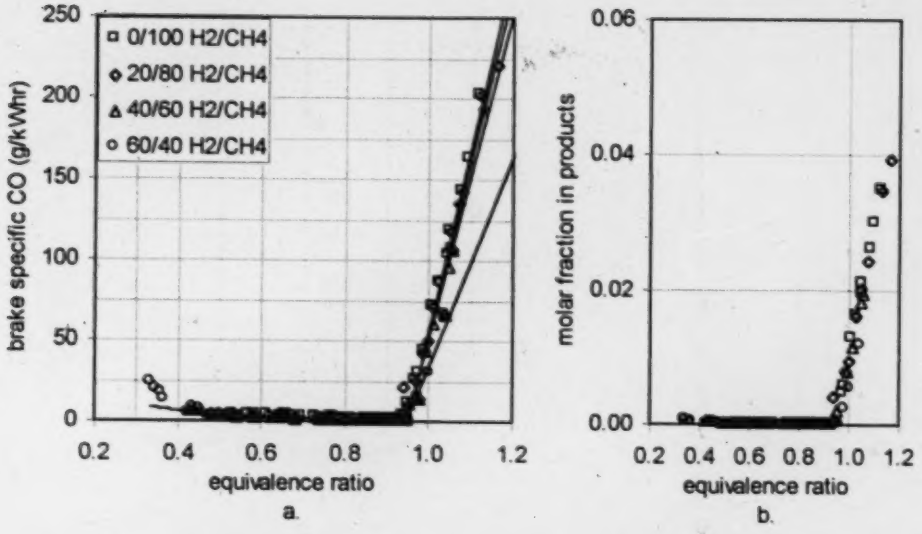

Figure 2.13. Full load brake specific production of CO at 700RPM and 900RPM is highly dependent on combustion equivalence ratio. (a.) *BSCO* (b.) The molar fraction of CO in the exhaust products. The uncertainty in *BSCO* ranges from +/-10% to +/-13%.

Unburned hydrocarbons are found in the exhaust stream whenever there is incomplete combustion in the cylinder. HCs include fuel, partially oxidized fuel, and lubricating oil. They are thought to form in the "quench zone" at the cool cylinder walls and the crevice volumes where the flame is extinguished [31]. Lean combustion slows the burn speed, and at cooler cylinder temperatures the quench zone is larger. The presence of unburned HCs also increases in the rich region due to insufficient O_2 available to ensure a complete reaction with the fuel. As seen in Figures 2.14 and 2.15, brake specific hydrocarbon production (*BSHC*) is lowest around $\phi = 0.9$, where the combustion efficiency is highest, burning speed is fastest, and cylinder temperatures are high. Hydrogen addition decreases *BSHC* due to the reduction of carbon present in the fuel, a smaller quenching distance, and higher combustion temperatures. Hydrogen addition up to 60% reduced *BSHC* from 0.5g/kWhr (50%) to 2.0g/kWhr (60%) at identical ϕ. However, at ultra-lean conditions (ϕ<0.40), there is a large increase in *BSHC* possibly due to a larger quench zone, partial burning, and a drop in power.

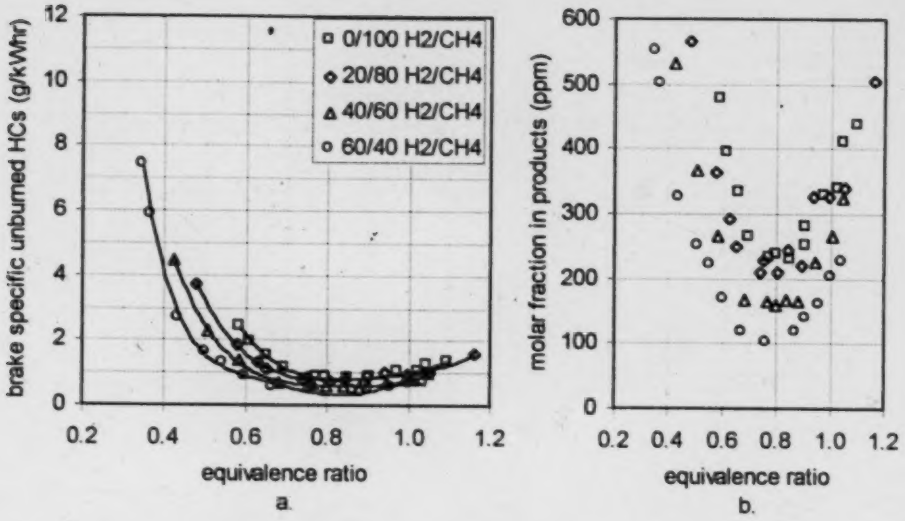

Figure 2.14. Full load brake specific production of unburned hydrocarbons at 700RPM decreases with hydrogen addition. (**a.**) *BSHC* (**b.**) Molar fraction of HCs (as C1) in the exhaust products. The uncertainty in *BSHC* varies from +/-10% to +/-53%.

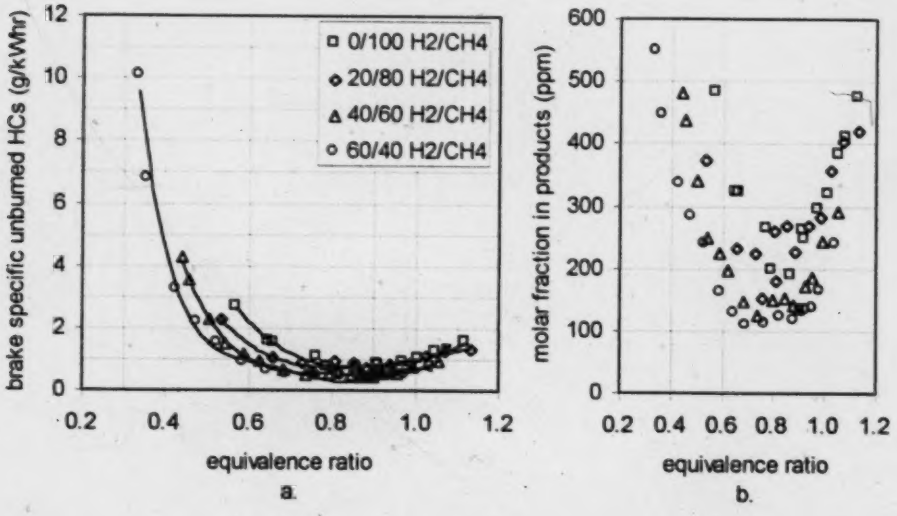

Figure 2.15. Full load brake specific production of unburned hydrocarbons at 900RPM decreases with hydrogen addition. (**a.**) *BSHC* (**b.**) Molar concentration of HCs (as C1) in the exhaust products. The uncertainty in *BSHC* varies from +/-10% to +/-53%.

Oxides of nitrogen (NO & NO_2) form in atmospheric oxygen and nitrogen at high temperatures in a reaction separate from combustion. In an S.I. engine, due to limited residence time in the cylinder, the concentration of NO_x is "frozen" above its equilibrium level [32]. Engine NO_x usually peaks around $\phi = 0.8$ to 0.9, where combustion temperatures are high, and there is an abundance of oxygen. From peak production, the concentration decreases for richer equivalence ratios (although combustion temperatures are still high), due to a decreasing amount of oxygen. For leaner equivalence ratios, the decrease in NO_x is primarily a reflection of decreasing combustion temperature. Figures 2.16 and 2.17 show that brake specific production of oxides of nitrogen ($BSNO_x$) peaks around $\phi = 0.85$. The addition of hydrogen increases $BSNO_x$ due to its higher flame temperatures. Hydrogen addition to 40% increased peak $BSNO_x$ approximately 5g/kWhr (30%). However the ability of hydrogen allows the engine to run ultra-lean while producing very low amounts of NO_x.

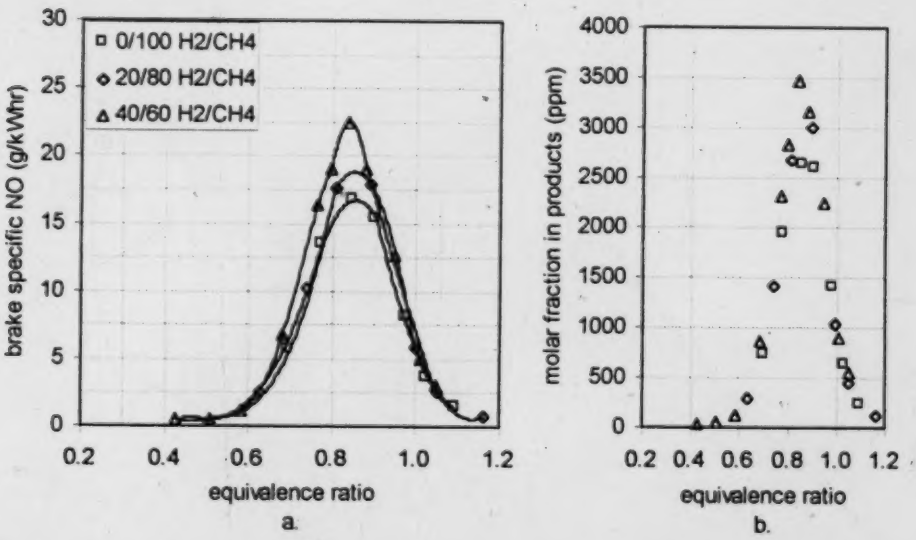

Figure 2.16. Full load brake specific production of NO_x (as NO) at 700RPM increases with hydrogen addition. (**a**.) *BSNO* (**b**.) Molar concentration of NO_x in the exhaust products (as NO + NO_2). The uncertainty in *BSNO* ranges from +/-9% +/-10%.

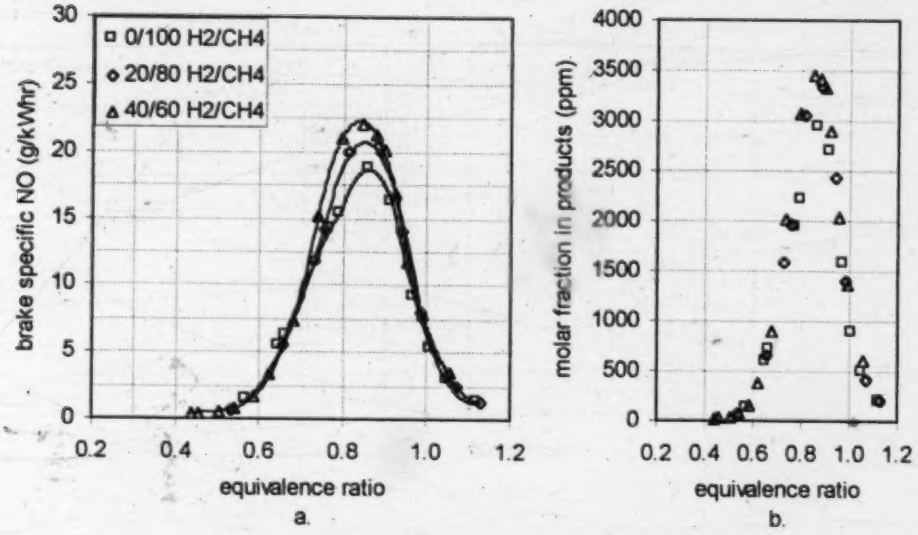

Figure 2.17. Full load brake specific production of NO_x (as NO) at 900RPM increases with hydrogen addition. (a.) *BSNO* (b.) Molar concentration of NO_x in the exhaust products (as NO + NO_2). The uncertainty in *BSNO* ranges from +/-9% +/-10%.

2.5. Part load results

The engine was then tested at part load. Conventionally, spark ignition engines have used a throttle plate to control engine power. When the throttle plate is closed, intake pressure, and fuel flow is reduced, resulting in less power. However, closing the throttle plate increases pumping loss [33] which results in lower thermal efficiencies and increased brake specific fuel consumption. This effect is clearly seen in Figure 2.18 where decreasing the load by the throttle plate results in an increase in *BSFC*. Decreasing the load to 0.2 increased *BSFC* to approximately 260% of its full load value. The results also show that the trend is the same for all tested hydrogen fractions, equivalence ratios, and engine speeds.

Brake specific production of CO_2 at part load also followed a pattern similar to *BSFC* as seen in Figure 2.19. As the efficiency drops, the amount of fuel used per unit of energy produced increases. Therefore, products of combustion follow accordingly. Reducing load to 0.2 increased $BSCO_2$ to approximately 260% of the full load value.

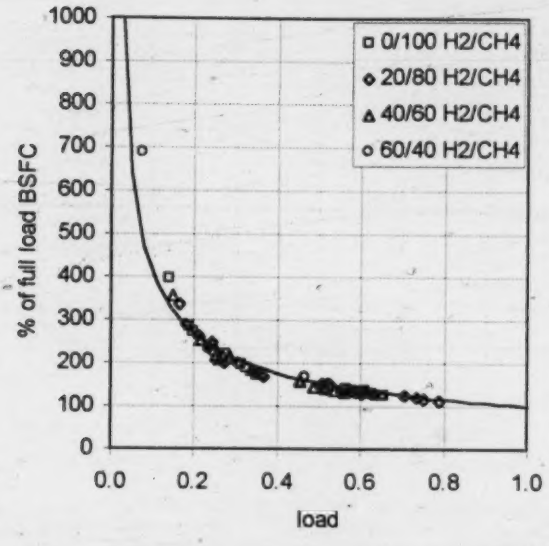

Figure 2.18. Brake specific fuel consumption increases with decreasing load for all fuels, equivalence ratios and engine speeds. The relative uncertainty ranges from +/-6% to +/-11%.

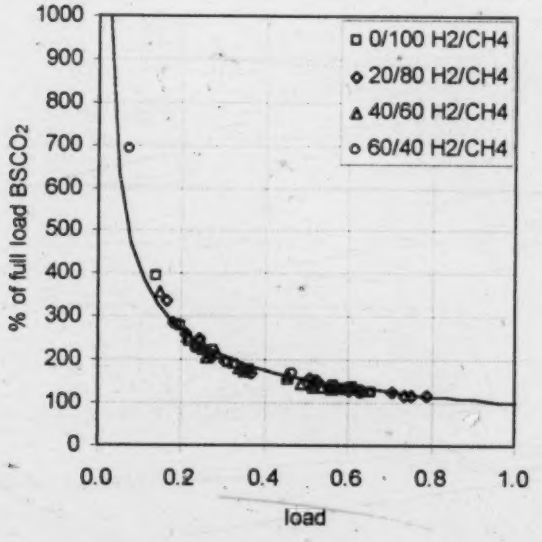

Figure 2.19. Brake specific production of CO_2 increases with decreasing load for all fuels, equivalence ratios and engine speeds. The relative uncertainty ranges from +/-6% to +/-15%.

Significant production of brake specific carbon monoxide only occurs above equivalence ratios of 0.95. Below this, the production of CO is small, but still increases with decreasing load. The increase in *BSCO* at part load as seen in Figure 2.20, follows the same trend as $BSCO_2$. Decreasing the load to 0.2 increased *BSCO* to approximately 350% of its full load value. As seen in Figure 2.21, similar amounts of unburned hydrocarbons are produced at part load. Decreasing the load to 0.2 increased *BSHC* by approximately 375% of its full load value. This can be attributed to decreased cylinder temperatures and pressures due to the closing throttle plate, which may increase the quench zone, and provide less oxidization of unburned fuel in the cooler exhaust stream.

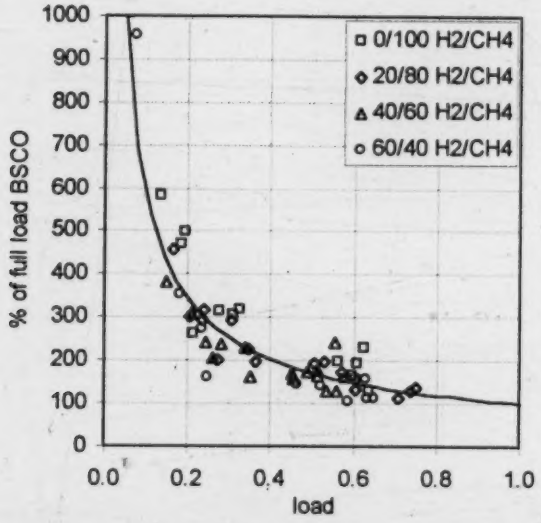

Figure 2.20. Brake specific production of CO increases with decreasing loads for all fuels, equivalence ratios and engine speeds. The relative uncertainty ranges from +/-13% to +/-42%.

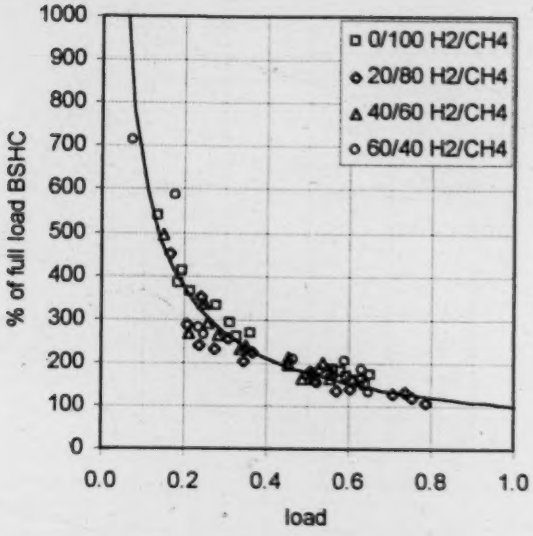

Figure 2.21. Brake specific production of HCs increase with decreasing load for all fuels, equivalence ratios and engine speeds. The relative uncertainty ranges from +/-17% to +/-65%.

Production of NO_x is unique in that its formation is not directly part of the combustion, but a separate reaction. Brake specific production of NO_x at part load behaves differently than other pollutants because closing the throttle plate reduces peak combustion temperature and increases the residual gas fraction. NO_x formation is reduced at lower temperatures and the unburned gas fraction acts as a diluent, bringing NOx concentrations down further [34]. Part load *BSNO* is also dependent on equivalence ratio. Figure 2.22 shows that part load *BSNO* decreases for equivalence ratios below 0.9, and increases for equivalence ratios above 0.9. This trend suggests that although NO_x production is reduced at part load, its peak may be progressively displaced to richer equivalence ratios by the increasing residual fraction. As seen in Figure 2.23, the test range is bracketed by best-fit equations for data points where $\phi = 1.00$, and 0.66. At an equivalence ratio of 1.0, decreasing the load to 0.2 increases *BSNO* to approximately 150% of its full load value. At an equivalence ratio of 0.66, decreasing the load to 0.2 decreases *BSNO* to approximately 50% of its full load.

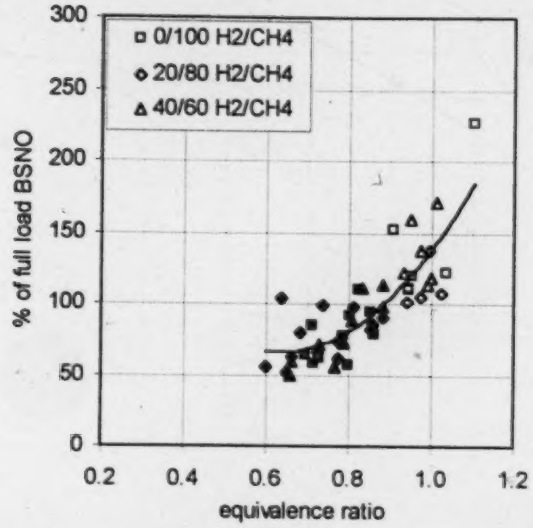

Figure 2.22. Brake specific NO production dependence on equivalence ratio at part load. Percentage of full load *BSNO* decreases for equivalence ratios below 0.9 at part engine loads. o = equivalence ratios greater than 0.9, • = equivalence ratios less than 0.9.

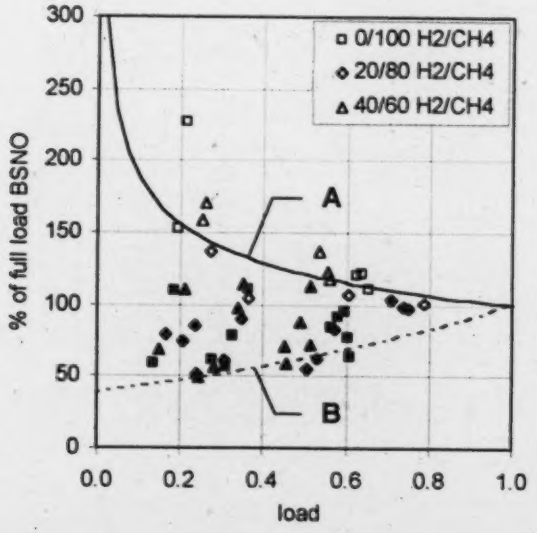

Figure 2.23. Brake specific production of NO decreases with decreasing load for equivalence ratios below 0.9, and increases for equivalence ratios above 0.9, for all fuels and engine speeds. The area of interest is bracketed by the best-fit equations for $\phi = 1.00$ **(A)**, and $\phi = 0.66$ **(B)**. o = equivalence ratios greater than 0.9, • = equivalence ratios less than 0.9. The relative uncertainty ranges from +/-13% to +/-24%.

2.6. Conclusion of CFR engine test

Data now exist for a driving cycle analysis using different mixtures of hydrogen and methane, equivalence ratios, speeds, and loads. The best-fit curves can be used to analyze fuel consumption and pollutant production at any operating condition. When compared to pure methane, hydrogen addition to 60% by volume, was shown to:

- lower the partial burn limit from an equivalence ratio of 0.58 to 0.34.
- decrease brake power up to 8% (at $\phi = 1$).
- decrease *BSFC* up to 14% (from $\phi = 0.58$ to 1.00).
- decrease $BSCO_2$ up to 26% (from $\phi = 0.58$ to 1.00).
- decrease *BSCO* up to 40% (for $\phi > 0.95$).
- decrease *BSHC* up to 60% (from $\phi = 0.58$ to $\phi = 1.00$).
- increase peak *BSNO* at $\phi = 0.83$ approximately 30% (for f=40%).

Changing engine speed from 700RPM to 900RPM had a small effect on fuel consumption and pollutant production, when compared to the effect of equivalence ratio and hydrogen addition. For all tested hydrogen fractions, equivalence ratios and engine speeds, using the throttle to achieve a part load of 0.2 was shown to:

- increase *BSFC* to approximately 260% of its full load value.
- increase $BSCO_2$ to approximately 260% of its full load value.
- increase *BSCO* production to approximately 350% of its full load value.
- increase *BSHC* production to approximately 375% of its full load value.
- increase *BSNO* production to approximately 150% of its full load value when ϕ=1.
- decrease *BSNO* production to approximately 50% of its full load value when ϕ=0.66.

The results agree with the less extensive engine tests cited using hythane fuels. Relationships for fuel consumption and pollutant production with respect to equivalence ratio, and engine load now exist for one engine. In the next section, these relationships are used to develop different engine operating "cases" which are evaluated according to varying engine power, speed and load in a driving cycle simulation.

3. Driving cycle simulation

In order for a realistic assessment of hydrogen addition in a vehicle, its effect must be examined under conditions of varying power and engine speed. In this way, the cumulative effects of fuel consumption and pollutant production can be compared. Similar vehicle models have been used in driving cycles to estimate fuel consumption and pollutant production with gasoline-hydrogen mixtures. A study by Hacohen et al. [35] used a theoretically based engine model to estimate the impact of H_2 addition on a gasoline engine. In general, it predicted a decrease in fuel consumption, and pollutant production with H_2 addition depending on the operational equivalence ratio. However, it is not clear if these improvements are due to changing the equivalence ratio, or due to the addition of hydrogen. The thrust of this study is to determine if there is an operating strategy that results in the minimum amount of fuel consumed, given a certain quantity of hydrogen stored on-board. In order to determine this, data from the CFR engine were used to develop an engine model for use in a vehicle model in a driving cycle simulation as seen in Figure 3.1.

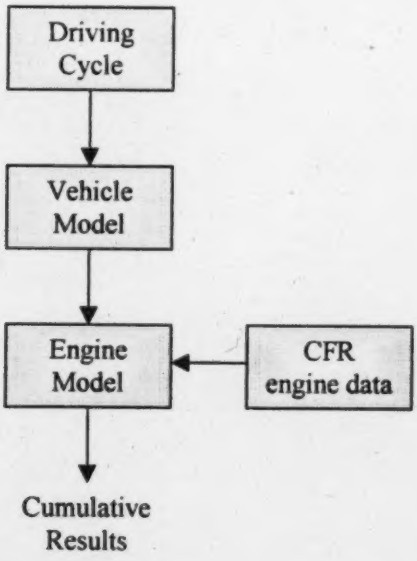

Figure 3.1. Driving cycle, vehicle and engine model architecture. A realistic assessment of hydrogen addition can be obtained from the cumulative amount of fuel consumed and pollutant produced in a driving cycle simulation.

3.1. Driving cycles

Driving cycles, given as a speed versus time trace, are based on typical driving conditions encountered. Different conditions are encountered during city, highway or combined driving. Three different cycles are considered in this study, so it can be seen if cumulative fuel consumption and pollutant production results are cycle dependent. The standardized driving schedules examined in this study are the SAE-J-227D, the Highway Fuel Economy Test and the 1972 Federal Test Procedure [36]. As seen in Figure 3.2, SAE-J-227D is a basic cycle of accelerating, cruising, braking, and idling. This schedule lasts for 122 seconds and covers a distance of 1.54km at an average speed of 45.3km/hr. Speeds reach a maximum of 72km/hr.

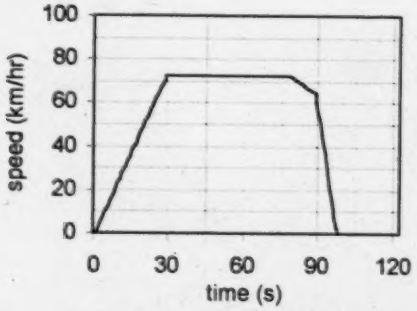

Figure 3.2. SAE-J-227D schedule.

The Highway Fuel Economy Test schedule, as seen in Figure 3.3, contains many periods of accelerating, cruising, braking, and idling. The pattern is typical of the sustained high speeds and minimal braking encountered during highway driving. It lasts for 765 seconds during which the vehicle travels 16.4km at an average speed of 77.7km/hr. Maximum speed reached is 96.4km/hr.

The 1972 Federal Test Procedure schedule, as seen in Figure 3.4, is representative of stop and go driving typical in an urban center, with many periods of idling. The schedule runs for 1372s, covering a distance of 12.1km at an average speed of 31.4km/hr. A maximum speed of 91.2km/hr is reached during the cycle.

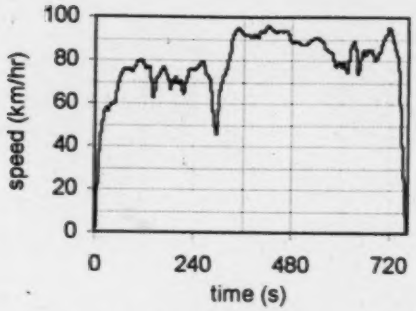

Figure 3.3. Highway Fuel Economy Test schedule.

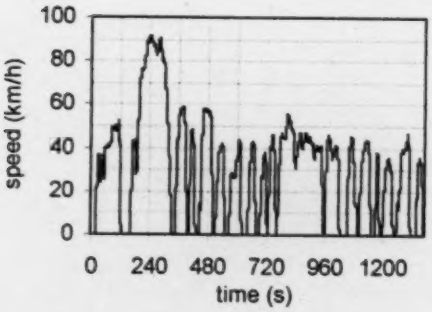

Figure 3.4. 1972 Federal Test Procedure schedule.

3.2. Vehicle model

The purpose of the vehicle model is to obtain from the speed versus time, the corresponding engine power and RPM with time. This engine power and RPM is then applied to the engine model (which is based on CFR data), from which the cumulative fuel consumption and pollutant production can be determined for the cycle.

A kinematic vehicle model has been developed [37] that is capable of obtaining vehicle power from a cycle speed versus time trace. As seen in Figure 3.5, a dynamic force balance is performed on aerodynamic drag, rolling resistance, and inertial force. The resultant force times the speed of the vehicle determines the power required (which can be either positive or negative). Presumably, the model engine will provide the positive power required, and the brakes will deliver the negative power required. Drivetrain efficiency is neglected in this comparative analysis. The drag coefficient,

rolling resistance coefficient, and frontal area are estimated from a 1992 Ford Escort Hatchback.

F_D (Aerodynamic Drag) = $C_D A \rho_{air} v^2 / 2$
F_R (Rolling Resistance) = $C_R m g$
F_I (Inertial Force) = $m a$

Required Power = $v (F_D + F_R + F_I)$

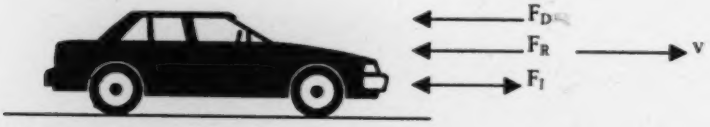

C_D (Coefficient of Drag) = 0.38
C_R (Rolling Coefficient) = 0.013
A (Effective Frontal Area) = 1.85m^2
m (mass) = 1250kg
ρ_{air} (density of air) = 1.17kg/m^3

Gear Ratios
1 = 3.46
2 = 1.94
3 = 1.29
4 = 0.97
5 = 0.81

Final Drive Ratio = 3.67
Upshift = 2000RPM
Downshift = 1300RPM
Idle = 1000RPM

Figure 3.5. Vehicle model. The power required by a vehicle is dependent upon its speed with time, and its parameters of C_D, C_R, A, and m. Engine speed is determined by transmission gearing.

To relate engine RPM to the vehicle speed, the model makes use of gearing ratios. Except when idling or braking, the vehicle model is in gear at all times during the driving cycle. When in gear, the vehicle's speed determines what the engine speed should be through the appropriate gear ratio. The driver upshifts when an engine speed of 2000RPM or higher is reached, and downshifts when it falls below 1300RPM. When not in gear, the engine speed is set to its idle at 1000RPM. To make the model as realistic as possible, the gear ratios represent typical values for a small passenger vehicle (1988 Volkswagen Cabriolet).

The required power and engine speed is determined for each cycle on a second-by-second basis. As seen in Figure 3.6, the SAE-J-227D schedule runs through gears 1 to 5, at an average engine speed of 1487RPM. Power required by the vehicle ranges from -34.9kW to +23.2kW at an average of 3.8kW.

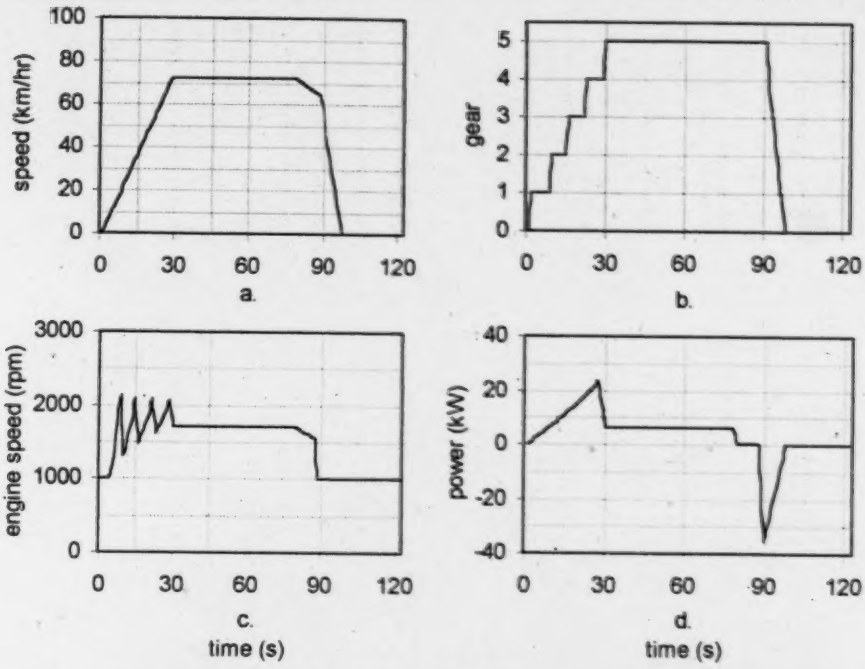

Figure 3.6. SAE-J-227D schedule required engine speed and power. (**a**.) Given speed with time, it is possible to (**b**.) determine gear (**c**.) engine speed and (**d**.) required power of the vehicle model.

In a similar manner, the highway schedule (Figure 3.7) uses all five gears, with most of its time spent in fifth gear. Consequently, the average engine speed is higher at 1874RPM. Required power varies between –27.2kW and +22.4kW, with an average of 8.03kW.

As seen in Figure 3.8, the urban schedule changes gear quite often, which results in engine speed ranging from 1000RPM to 2700RPM at an average of 1404RPM. Braking is generally lighter and acceleration harder than the other two schedules, as the required power ranges from –20.0kW to +27.8kW. However, due to periods of idling, the average required power is lower than the other schedules at 2.18kW.

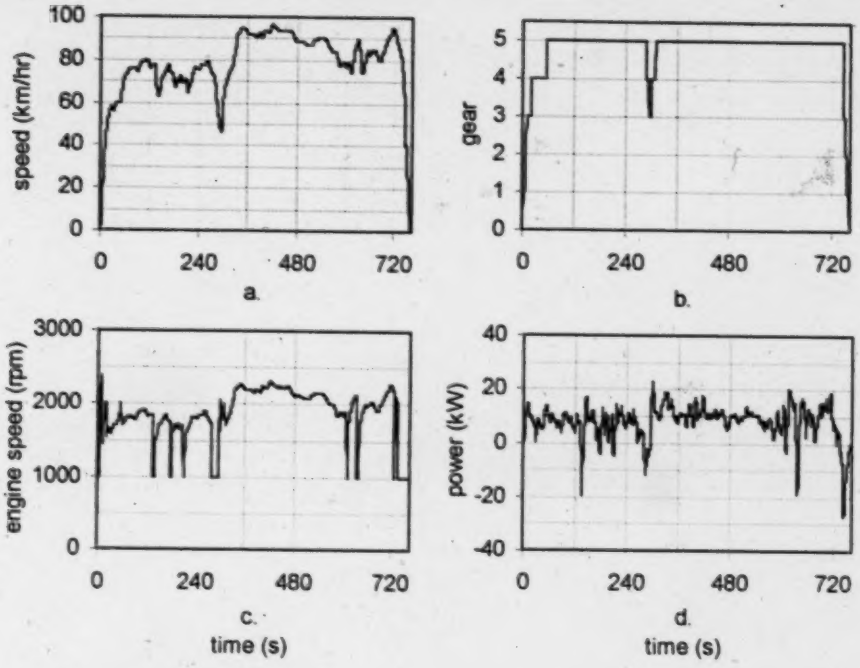

Figure 3.7. Highway Fuel Economy Test schedule required engine speed and power. (**a**.) Given speed with time, it is possible to (**b**.) determine gear (**c**.) engine speed and (**d**.) required power of the vehicle model.

In order for valid comparisons to be made, model parameters must be held constant throughout the analysis. For example, when using hydrogen as a fuel, the container storage weight and volume can be considerable. It is estimated that for compressed gas stored at 20.7MPa, a storage weight of 63.3kg and a volume of 408.8L is required to store 4.7kg of hydrogen [38]. However, vehicle mass will be considered constant for comparison purposes in the model. Also, the gearing of the vehicle plays an important role with respect to engine loading, and therefore is kept constant.

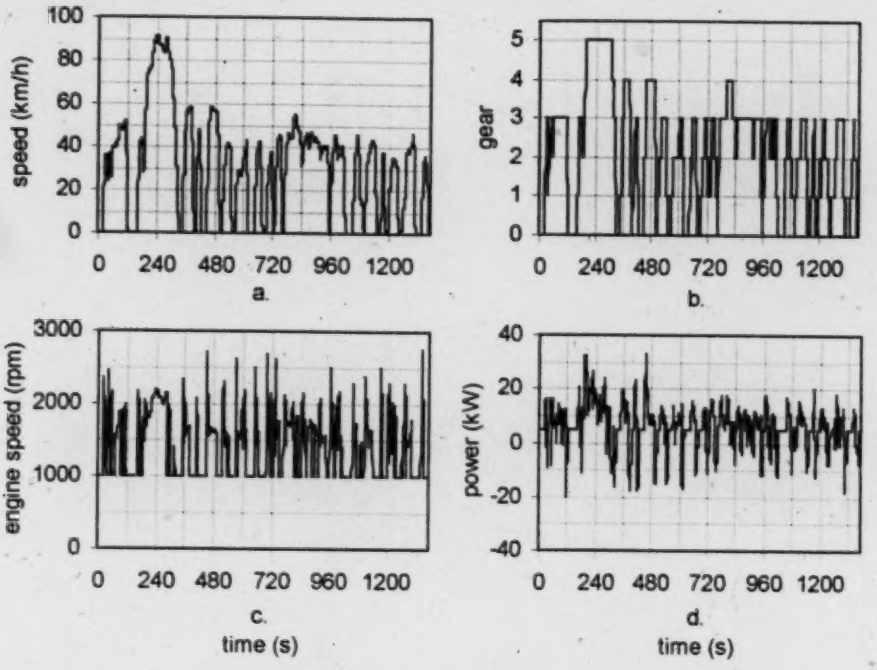

Figure 3.8. 1972 Federal Test Procedure schedule required engine speed and power. (**a**.) Given speed with time, it is possible to (**b**.) determine gear (**c**.) engine speed and (**d**.) required power of the vehicle model.

3.3. Engine model

An engine model is needed to provide positive tractive power to the vehicle model. Data on brake power, *BSFC*, $BSCO_2$, *BSCO*, *BSHC*, and *BSNO* were obtained from the CFR engine while varying its operational parameters f, ϕ, RPM, and load. This data is used to build various engine model "cases". Practically speaking, engine cases must fit in with one of four realistic operational schemes:

- Scheme 1: The vehicle has premixed fuel (a fixed hydrogen fraction), and is operating at stoichiometric equivalence ratios with power control by means of a throttle plate (conventional operation). This will be taken as the base case for comparison purposes.
- Scheme 2: The vehicle has premixed fuel but is operating at lean equivalence ratios where the best *BSFC* occurs. The equivalence ratio and throttle plate combine to control power.

- Scheme 3: The vehicle has fuel mixed on-board (the hydrogen fraction varies while driving), and is operating at lean equivalence ratios where the best *BSFC* occurs. The hydrogen fraction, equivalence ratio, and throttle plate combine to control power.
- Scheme 4: The vehicle has fuel mixed on-board, and is operating at lean equivalence ratios, but is completely unthrottled. Power control is accomplished by splitting the engine power between an electrolyser and the drivetrain.

Unthrottled operation with the use of hydrogen has been suggested previously [39] for mixtures of methanol and hydrogen but no driving cycle analysis was performed. For each scheme, there are nearly an infinite number of cases based on all the different combinations of hydrogen fraction, equivalence ratio, and load. A systematic approach is carried out in the next section, which identifies the key "cases" where the fuel consumption is lowest.

In order for it to fit in with the vehicle model, it was necessary to scale-up the brake power produced and the speed of the CFR engine. The scaling of the engine power and speed does not effect comparable results, as long as their factors are held constant for all cases. The brake power of the CFR engine was scaled up by a factor of 15 in order to approximate a real production engine. This is not indicative of displacement, as the CFR engine is a simplistic design, and has a relatively low power to displacement ratio. In order to fit in with the gearing, the speed of the CFR engine was scaled up by a factor of 2, to be more representative of a modern production engine. Engine power and speed can be scaled differently, as they can both be altered through engine design. Brake specific fuel consumption and pollutant production are assumed to be unchanged by scaling with power, as they are normalized with respect to power (i.e. $BSFC_{CFR} = BSFC_{MODEL}$). By scaling the speed, the CFR brake specific fuel consumption and pollutant production is assumed to equal the engine model at speeds of 2 times faster (i.e. $BSFC_{CFR,\ 700RPM} = BSFC_{MODEL,\ 1400RPM}$).

The engine operating characteristics of any fuel composition between 0% and 60% hydrogen are found by linear interpolation between existing data points (at 0%, 20%, 40% and 60%). Likewise, the engine operating characteristics at any engine speed are solved for by linear interpolation between existing data points (at 1400RPM and 1800RPM in the model). Linear interpolation can be used since no unusual behavior is

indicated in the test data. Certain engine parameters must be held constant in the model so that valid comparisons can be made. Although it is possible to improve engine operation (for fuel type, and equivalence ratio) by varying the compression ratio, spark type & duration and/or the combustion chamber design [40], these variables are not examined in the model.

3.4. Scheme 1, 2, & 3 engine cases

Varying the fraction of hydrogen, equivalence ratio, and load (throttle plate position) can control power either individually or in combination. As seen in Figure 3.9, for driver control, these parameters can each independently be a function of the "pedal" position. The pedal is similar to a conventional accelerator pedal. The amount of hydrogen fraction and the equivalence ratio can be changed with respect to the pedal position by means of electronically or hydraulically activated valves. The throttle can be controlled by means of a mechanical linkage with the pedal.

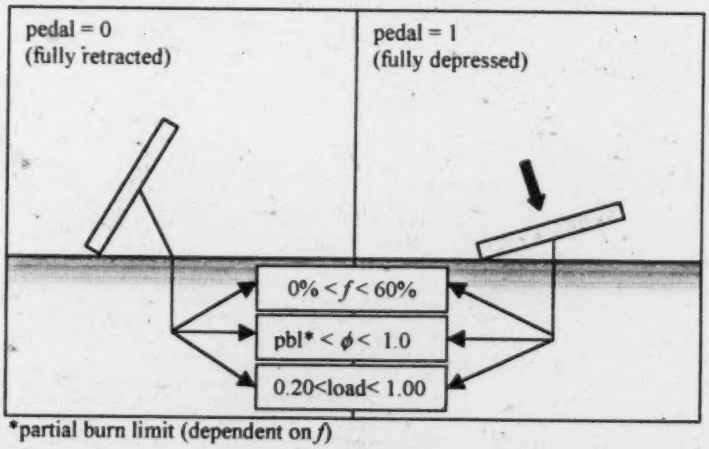

Figure 3.9. Control of f, ϕ, and load (throttle) with the pedal. The driver controls fraction of hydrogen used, equivalence ratio, and throttle plate position through pre-programmed linkage with the pedal.

As previously mentioned, there are virtually an infinite number of operating systems when all the combinations of hydrogen fraction, equivalence ratio, and throttle position are considered with respect to the pedal position. The rationale behind finding

an optimum operating system is to minimize the consumption of methane with a given amount of hydrogen in a driving cycle. Hence, several key cases of engine operating system will be considered for each scheme as seen in Table 3.1.

Table 3.1. Summary of engine schemes 1, 2, 3 and 4.

Scheme 1	**f = constant**	**ϕ = 1.0**	**0.2<load<1.0**
Scheme 2	**f = constant**	**pbl<ϕ < 1.0**	**0.2<load<1.0**
Scheme 3	**0%<f < 60%**	**pbl<ϕ < 1.0**	**0.2<load<1.0**
Scheme 4	**0%<f < 60%**	**pbl<ϕ < 1.0**	**load=1.0**

Throughout the analysis, each engine case is designed so that the engine idles at 5kW at 1000RPM (pedal=0), and produces 35kW at 1800RPM (pedal=1). The model engine is allowed to reach speeds (and powers) beyond 1800RPM (and 35kW) depending on the cycle requirements. However, by requiring each engine case to conform to the power targets (5kW minimum at 1000 RPM, and 35kW maximum at 1800RPM), ensures that the cumulative engine energy used will be nearly constant from case to case. In addition, the engine will have the same "performance" from case to case. For the sake of driver perception, the power must increase linearly or near-linearly as the pedal is depressed.

Figure 3.10 shows a map of all the conditions at which the scaled-up CFR engine is capable of producing 5kW at 1000RPM. At this power and speed, all combinations of hydrogen fraction & equivalence ratio can be used, within the partial burn limit and the knock limit. At equivalence ratios below the partial burn limit, the engine misfires and eventually stalls. At equivalence ratios above the knock limit, engine damage is possible [20]. Hydrogen addition increases the tendency to knock, but enables the use of lower equivalence ratios, which decreases the tendency to knock. Points A-F on the operational boundaries are used to define the idle conditions for each engine case. The contour lines, representing equal engine load, show that as the equivalence ratio decreases, and the hydrogen fraction increases, less throttling is required to bring the engine down to 5kW.

For example, at $f = 0$, and $\phi = 1$ (point A), throttling is required to bring the engine load to 0.2 to produce 5kW. At $f = 0.6$, and $\phi = 0.34$ (point F), throttling down to a load of only 0.65 is necessary (to produce 5kW).

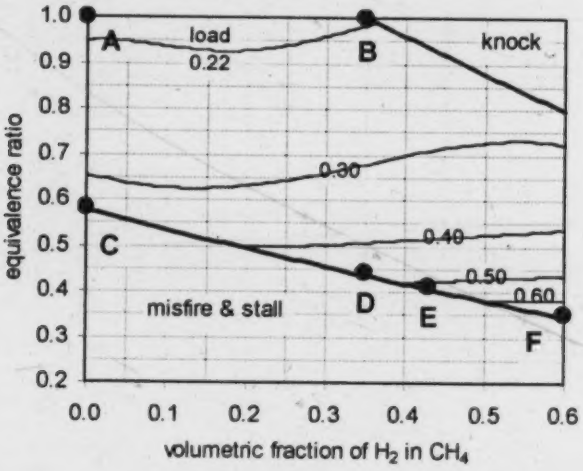

Figure 3.10. Power map of the model engine at 1000RPM and 5kW. Decreasing the equivalence ratio, and increasing the hydrogen fraction reduces the dependence on throttling to bring power down to 5kW. Contour lines represent equal engine load.

In order to optimize cases for fuel consumption, it is necessary to identify at which points the *BSFC* is lowest. Figure 3.11 shows the brake specific fuel consumption of hydrogen and methane for the model engine operating at 5kW and 1000RPM. Points A to F are the same as on the power map (Figure 3.10). *BSFC* generally decreases with increasing hydrogen due to a reduction in the mass of fuel consumed. *BSFC* also decreases with increasing engine load due to a reduction in pumping losses incurred as the throttle plate is opened. Indeed, this effect is significant, as the *BSFC* is lowest at the partial burn limit (points C, D, E, F) where the engine load is highest.

Next consider the model engine operation at 1800RPM. It is not possible to achieve 35kW at all combinations of hydrogen fractions, equivalence ratios, and engine loads at this speed. As seen in Figure 3.12, this limits the operational conditions to hydrogen fractions from 0 to 0.43, equivalence ratios from 0.88 to 1.00, and loads from 0.93 to 1.00. Points I, J, K are on a line at wide open throttle (WOT). Below this line,

the engine is not capable of producing 35kW at 1800RPM. Points G-K on the operational boundaries are used to define the 1800RPM and pedal = 1 condition for each case.

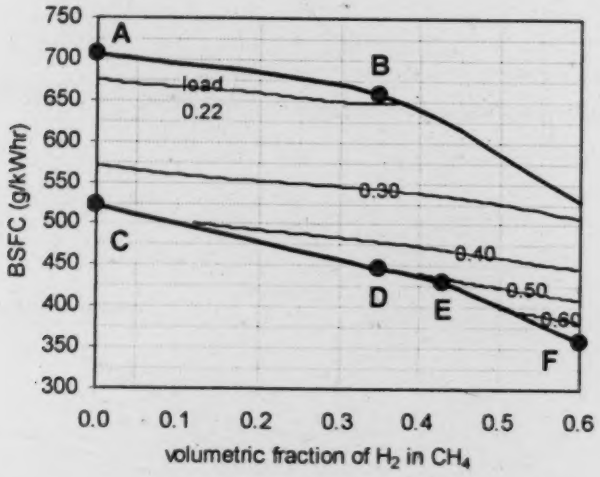

Figure 3.11. Brake specific fuel consumption of the model engine at 1000RPM and 5kW. Increasing hydrogen fraction and engine load (contour lines are represent equal load) decrease the *BSFC*.

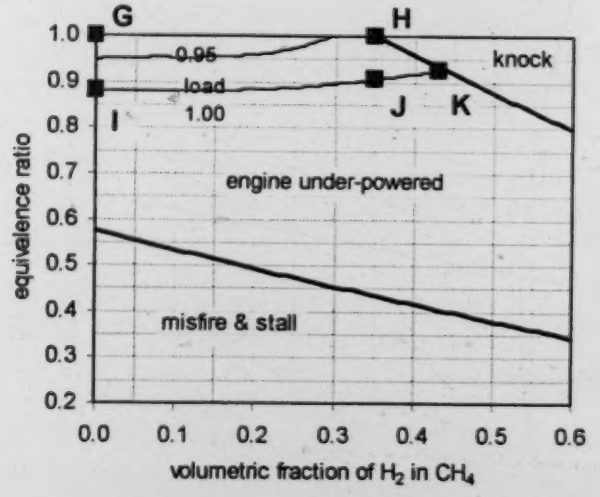

Figure 3.12. Power map of the model engine at 1800RPM and 35kW. The engine is capable of producing 35kW at near full load and above equivalence ratios from 0.88 to 0.93. Below the load=1.00 contour, the engine is under-powered. Using fractions of hydrogen above 0.43 will result in engine knock.

Figure 3.13 shows the brake specific fuel consumption map for 1800kW and 35kW. Again, it is shown that increasing the hydrogen fraction and increasing the engine load decreases the *BSFC*. The lowest *BSFC* is found when the engine is at wide open throttle (Points I-J-K). Note that the *BSFC* is lower at 1800RPM than at 1000RPM because the engine is operating at higher loads.

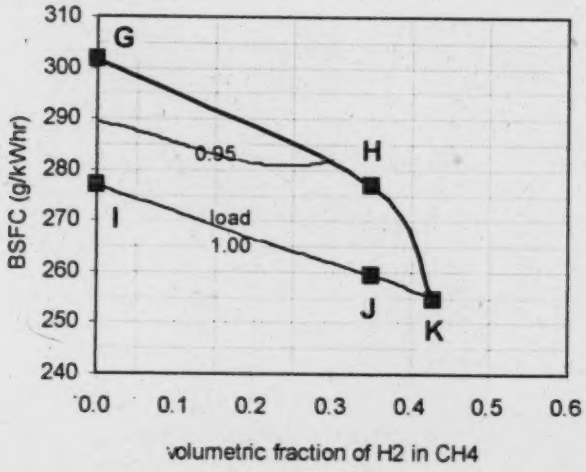

Figure 3.13. Brake specific fuel consumption of the model engine at 1800RPM and 35kW. Brake specific fuel consumption is lowest when the engine is essentially unthrottled (load = 1).

With the 1000RPM, 5kW and 1800RPM, 35kW points defined, several key cases from each scheme can now be examined. The cases are labeled after the operational points from Figures 3.10 to 3.13, with the first letter representing the 5kW and 1000RPM point, and the second letter representing the 35kW and 1800RPM operating point.

For scheme 1, case A-G (as seen in Figure 3.14) represents a conventional throttled engine operating on pure methane at a stoichiometric equivalence ratio. The throttle is used to control power so that the engine operates from point A (pedal = 0) to point G (pedal = 1). As the pedal position increases, the engine brake specific fuel consumption and pollutant production decrease due to higher engine loads. At 1800RPM, and increasing pedal from 0 to 1, *BSFC* ranges from 746g/kWhr to 302g/kWhr, $BSCO_2$ from 1810g/kWhr to 732g/kWhr, *BSCO* from 188g/kWhr to 6g/kWhr 1, *BSHC* from

3.46g/kWhr to 1.04g/kWhr and *BSNO* from 9.58g/kWhr to 6.37g/kWhr. Only curves for 1800RPM are shown, as the difference between engine speeds (to 1000RPM) are small compared to difference due to pedal position. The production of CO is significant due to equivalence ratios above 0.95.

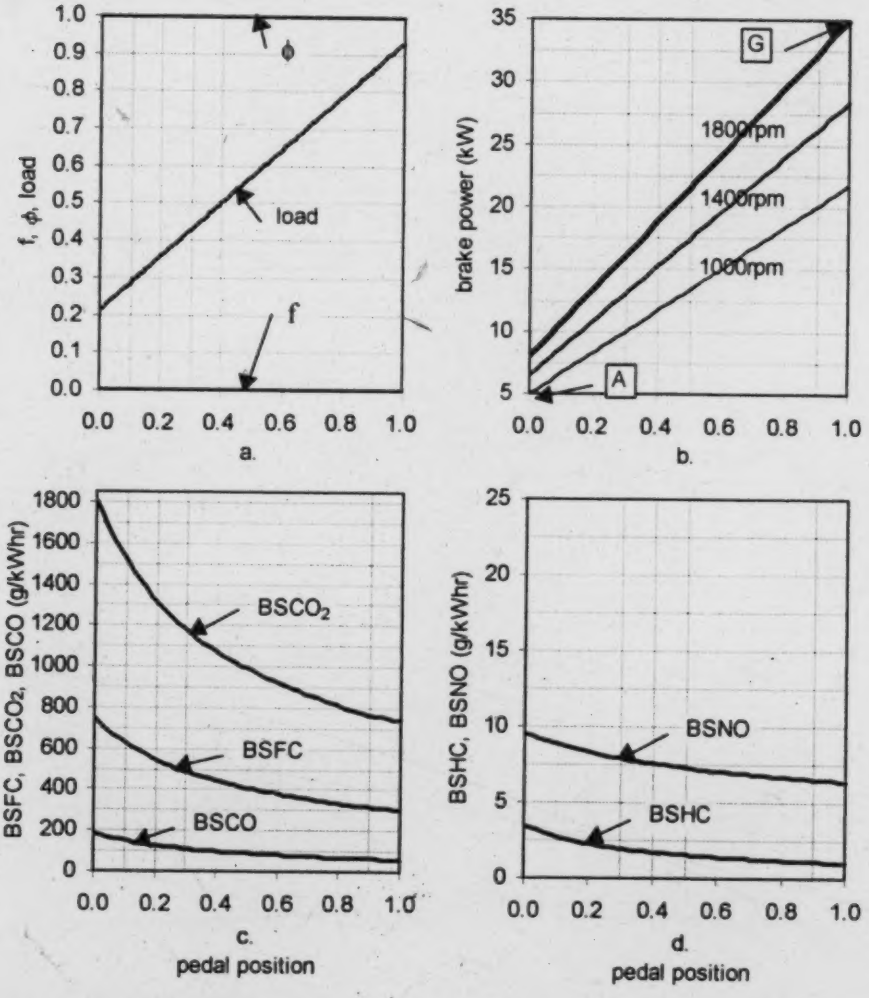

Figure 3.14. Engine case A-G. (**a**.) Engine *f*, ϕ, and load (**b**.) brake power (**c**.) brake specific fuel consumption and production of CO_2 and CO and (**d**.) brake specific production of HCs and NO with respect to pedal position. The *f*, ϕ, and load with pedal position are designed so that the resultant brake power is 5kW, 1000RPM (Figure 3.9) at zero pedal, and 35kW, 1800RPM (Figure 3.11) at full pedal.

Case B-H (as seen in Figure 3.15) represents scheme 1 operation with the maximum amount of hydrogen possible. Operating at a stoichiometric equivalence ratio limits the volumetric hydrogen fraction to 35%, as any greater than this would result in engine knock. Compared to case A-G, brake specific fuel consumption is slightly lower, as is production of CO_2, CO, and HC, due to hydrogen addition and increased engine load. However, NO production is slightly higher due to hydrogen addition.

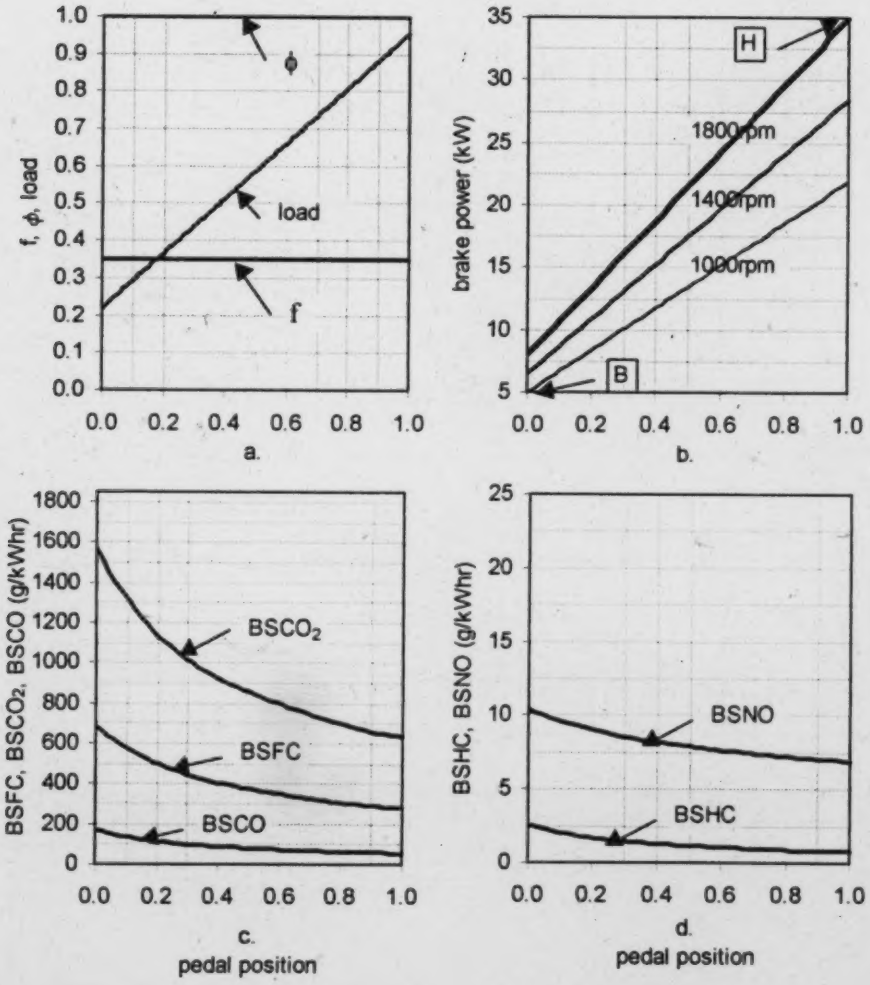

Figure 3.15. Engine case B-H. (**a.**) Engine *f*, ϕ, and load (**b.**) brake power (**c.**) brake specific fuel consumption and production of CO_2 and CO and (**d.**) brake specific production of HCs and NO with respect to pedal position.

When increasing the pedal from 0 to 1 in case B-H, *BSFC* changes from 687g/kWhr to 277g/kWhr, $BSCO_2$ from 1566g/kWhr to 631g/kWhr, *BSCO* from 167g/kWhr to 54g/kWhr, *BSHC* from 2.59g/kWhr to 0.77g/kWhr and *BSNO* from 10.39g/kWhr to 6.90g/kWhr (at 1800RPM).

For scheme 2, the fuel is still premixed, but now the equivalence ratio and throttle plate combine to control power. Case C-I (Figure 3.16) represents scheme 2 operation with pure methane fuel. Compared to conventional operation (case A-G), there is a reduction in brake specific fuel consumption and brake specific CO_2 production at higher engine load. *BSCO* drops to negligible amounts as equivalence ratios below 0.95 are used. However, *BSHC* is generally higher due to the use of equivalence ratios near the partial burn limit. *BSNO* is lower at idle, but peaks higher at equivalence ratios of 0.8 to 0.9 where the combustion temperature is high, and oxygen is abundant. At 1800RPM, and increasing the pedal from 0 to 1, *BSFC* ranges from 585g/kWhr to 277g/kWhr, $BSCO_2$ from 1595g/kWhr to 759g/kWhr, *BSCO* from 6g/kWhr to 1g/kWhr, and *BSHC* from 5.76g/kWhr to 0.75g/kWhr. *BSNO* increases from a minimum of 0.61g/kWhr to a maximum of 18.57g/kWhr.

Case D-J, (as seen in Figure 3.17) is used for comparison with case B-H, as both use a 35% hydrogen mixture. However, due to scheme 2 operation at higher engine load, case D-J has lower brake specific fuel consumption and production of CO_2. *BSCO* is negligible, but *BSHC* increases due to the use of equivalence ratios near the partial burn limit. Again, production of NO is lower at ultra-lean equivalence ratios, but peaks higher when the equivalence ratio passes through 0.8 to 0.9. At 1800RPM, and increasing the pedal from 0 to 1, *BSFC* ranges from 548g/kWhr to 259g/kWhr, $BSCO_2$ from 1421g/kWhr to 658g/kWhr, *BSCO* from 9g/kWhr to 1g/kWhr, and *BSHC* from 7.47g/kWhr to 0.59g/kWhr. *BSNO* increases from a minimum of 0.08g/kWhr to a peak of 21.58g/kWhr.

Another benefit to scheme 2 operation is that a higher fraction of premixed hydrogen can be used, as the lean equivalence ratios used reduce the tendency to knock. The maximum premixed fuel possible due to knock limitation increases to 43% hydrogen. This is represented by case E-K, as seen in Figure 3.18. Compared to D-J, the brake specific fuel consumption and pollutant productions are relatively unchanged.

However, a greater proportion of hydrogen can be used, consequently requiring less methane. At 1800RPM, and increasing the pedal from 0 to 1, *BSFC* ranges from 578g/kWhr to 255g/kWhr, $BSCO_2$ from 1400g/kWhr to 626g/kWhr, *BSCO* from 10g/kWhr to 1g/kWhr, and *BSHC* from 8.81g/kWhr to 0.51g/kWhr. *BSNO* increases from a minimum of 0.06g/kWhr to a peak of 22.15g/kWhr.

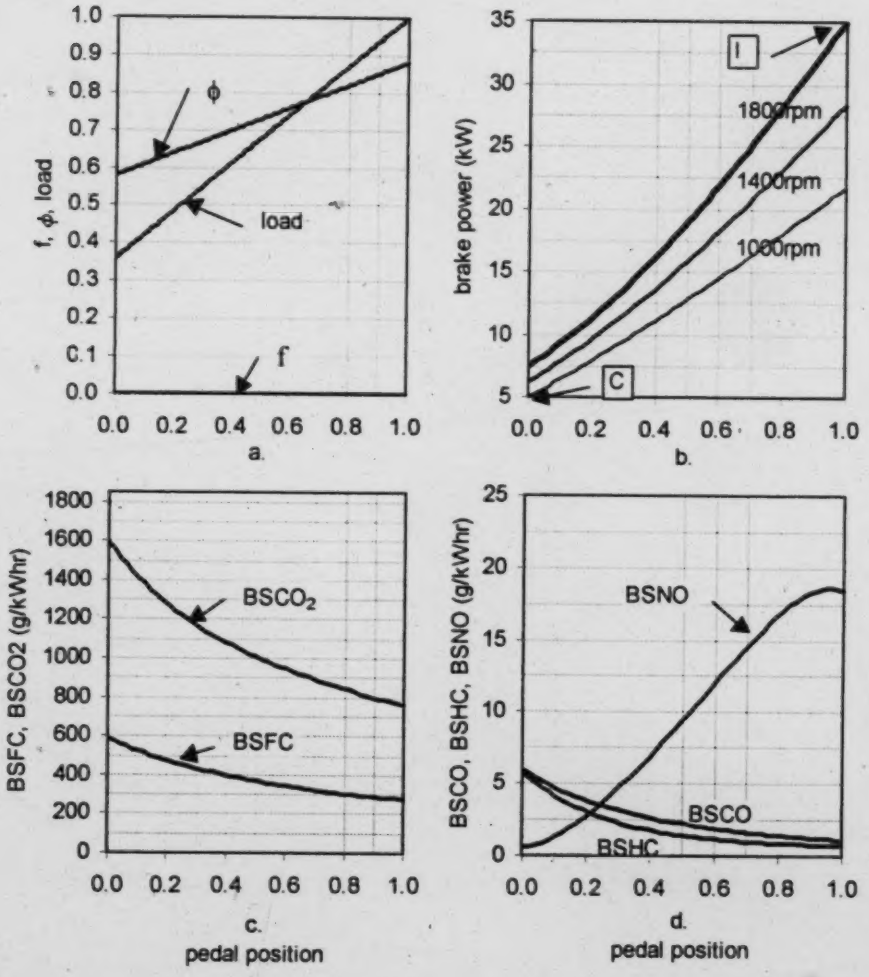

Figure 3.16. Engine case C-I. (a.) Engine *f*, ϕ, and load (b.) brake power (c.) brake specific fuel consumption and production of CO_2 and (d.) brake specific production of CO, HCs and NO with respect to pedal position.

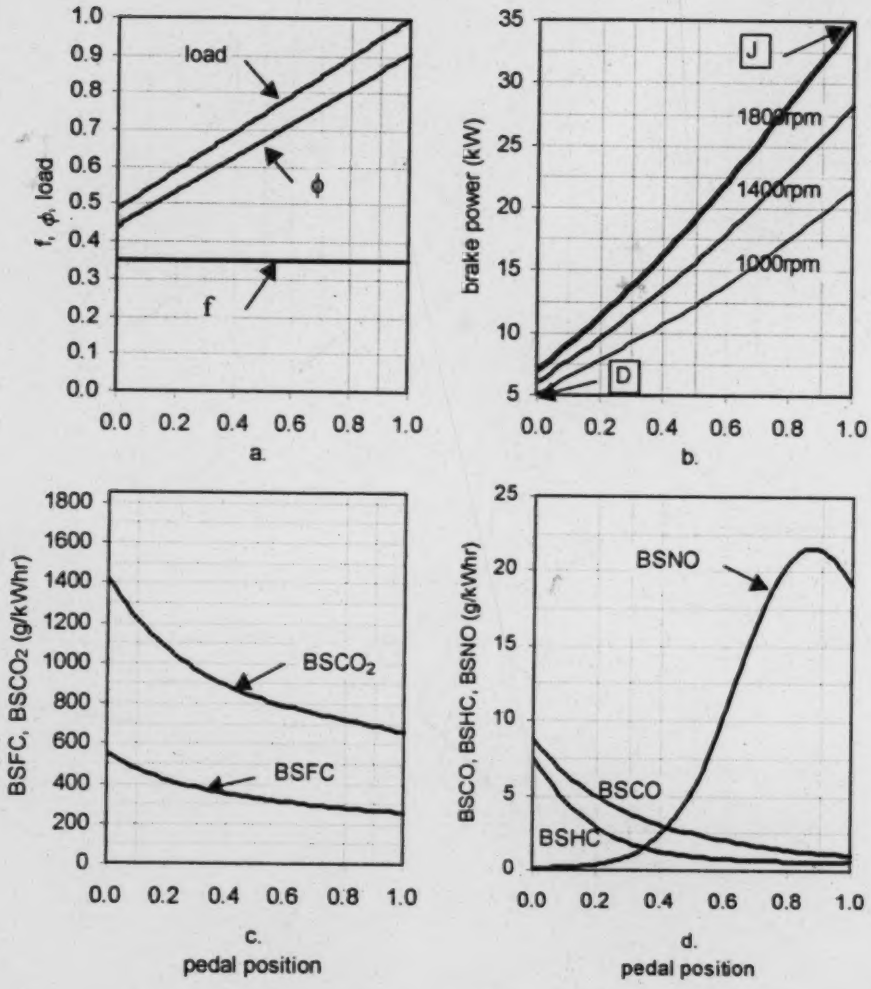

Figure 3.17. Engine case D-J. (**a**.) Engine f, ϕ, and load (**b**.) brake power (**c**.) brake specific fuel consumption and production of CO_2 and (**d**.) brake specific production of CO, HCs and NO with respect to pedal position.

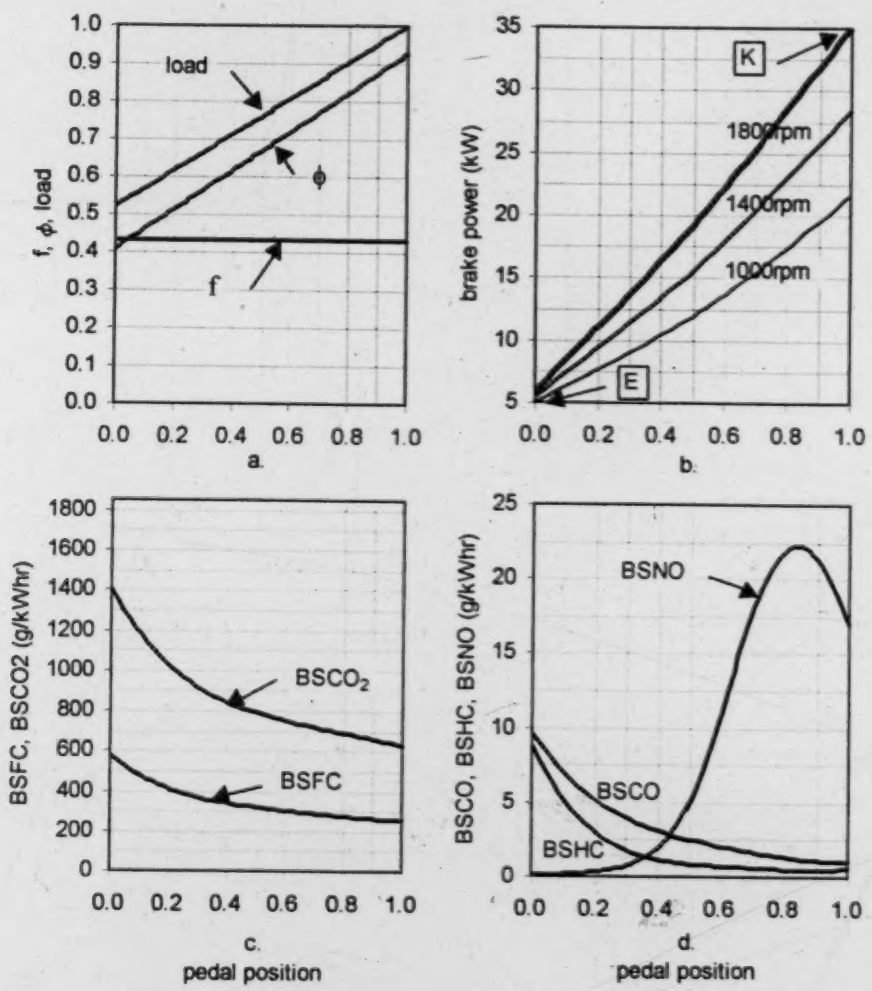

Figure 3.18. Engine case E-K. (**a**.) Engine *f*, ϕ, and load (**b**.) brake power (**c**.) brake specific fuel consumption and production of CO_2 and (**d**.) brake specific production of CO, HCs and NO with respect to pedal position.

It was revealed previously, that by operating the engine at higher loads, it is possible to decrease *BSFC*. However, the requirement that the fuel be premixed limits the maximum hydrogen fraction usable to 43%. Scheme 3 operation proposes using the equivalence ratio, hydrogen fraction, and throttle plate in combination to control power. At low pedal positions (and low power requirements), the fraction of hydrogen used can

be high and at high pedal positions (and high power requirements), the fraction of hydrogen used can be low. At all times the engine load will be high due to the use of lean equivalence ratios. This involves mixing the fuel on-board. One scheme 3 operating system is case D-I, as seen in Figure 3.19. The fraction of hydrogen used changes from 35% at 0 pedal to 0%, at 1 pedal. Compared to case E-K (scheme 2), brake specific fuel consumption and production of pollutants are relatively unchanged. However, D-I has the potential to consume less hydrogen because of the declining hydrogen fraction with the application of the pedal. At 1800RPM, and increasing the pedal from 0 to 1, *BSFC* ranges from 548g/kWhr to 277g/kWhr, $BSCO_2$ from 1421g/kWhr to 759g/kWhr, *BSCO* from 9g/kWhr to 1g/kWhr, and *BSHC* from 7.47g/kWhr to 0.75g/kWhr. *BSNO* increases from a minimum of 0.08g/kWhr to a peak of 18.79g/kWhr.

Another scheme 3 operating system is case F-I, as seen in Figure 3.20. The hydrogen fraction decreases from 60% to 0% with the application of the pedal. Engine load is higher than any previous case, due to the ultra-lean equivalence ratios at 0 pedal. However, as shown in the CFR engine test, at ultra-lean equivalence ratios there is an increase in *BSFC* due to a rapid loss of power. Consequently, compared to case E-K (scheme 2), brake specific fuel consumption actually increases, while CO_2 and CO production is relatively unchanged. A further drawback is that case F-I has a higher *BSHC* due to the use of ultra-lean equivalence ratios near the partial burn limit. However, *BSNO* is decreased due to the use of lower hydrogen fractions as it peaks at equivalence ratios of 0.8 to 0.9. At 1800RPM, and increasing the pedal from 0 to 1, *BSFC* ranges from 612g/kWhr to 277g/kWhr, $BSCO_2$ from 1369g/kWhr to 759g/kWhr, *BSCO* from 11g/kWhr to 1g/kWhr, and *BSHC* from 10.87g/kWhr to 0.75g/kWhr. *BSNO* increases from a minimum of 0.07g/kWhr to a peak of 18.95g/kWhr. Although there is no appreciable decrease in *BSFC* by using this case, the amount of methane used can be reduced by increasing the amount of hydrogen consumed.

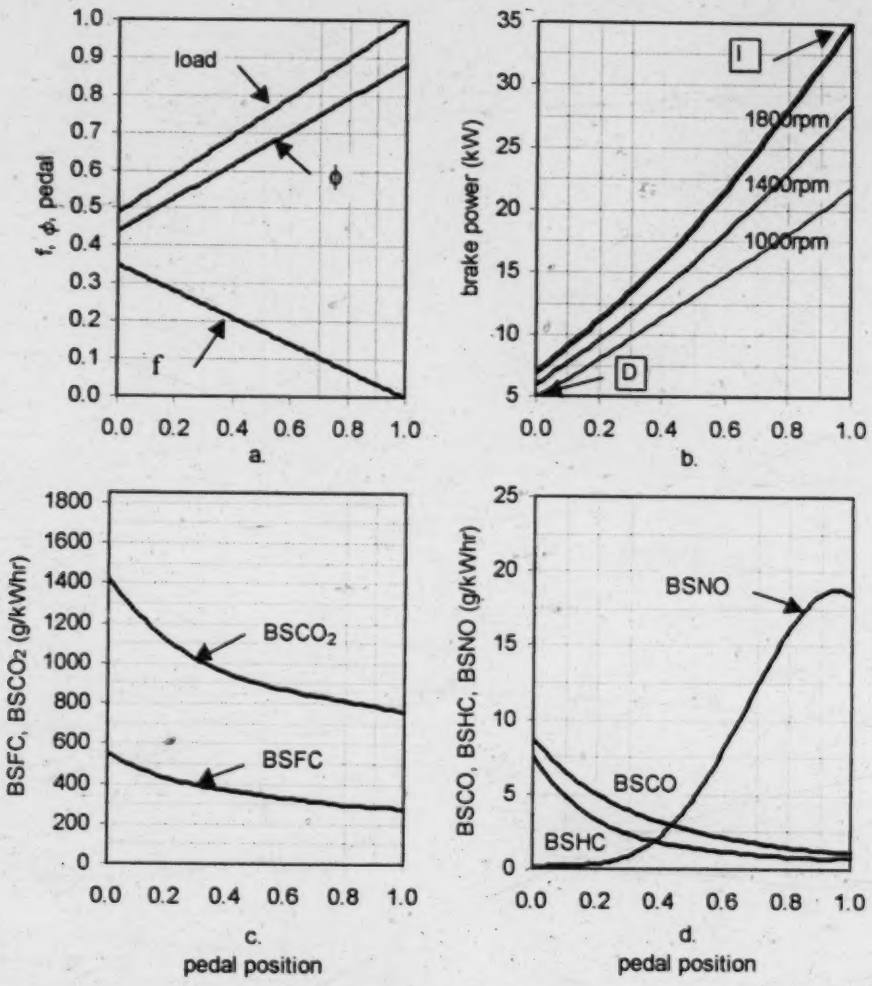

Figure 3.19. Engine case D-I. (a.) Engine *f*, ϕ, and load (b.) brake power (c.) brake specific fuel consumption and production of CO_2 and (d.) brake specific production of CO, HCs and NO with respect to pedal position.

In a similar manner, case F-K is proposed. As seen in Figure 3.21, this case uses the greatest possible amount of H_2. The concentration of hydrogen varies from 60% to 43% as the pedal is increased from 0 to 1. Consequently the load is very high, but that is not enough to account for the increase in *BSFC* is due to the use of ultra-lean equivalence ratios. Compared to F-I, brake specific fuel consumption and production of pollutants is relatively unchanged, except peak *BSNO* is increased due to the increased amount of

hydrogen used as the equivalence ratio passes through 0.8 to 0.9. Again, it is presumable that the amount of methane consumed will be reduced due to more hydrogen being used. At 1800RPM, and increasing the pedal from 0 to 1, *BSFC* ranges from 612g/kWhr to 255g/kWhr, $BSCO_2$ from 1369g/kWhr to 626g/kWhr, *BSCO* from 11g/kWhr to 1g/kWhr, and *BSHC* from 10.87g/kWhr to 0.51g/kWhr. *BSNO* increases from a minimum of 0.07g/kWhr to a peak of 22.56g/kWhr.

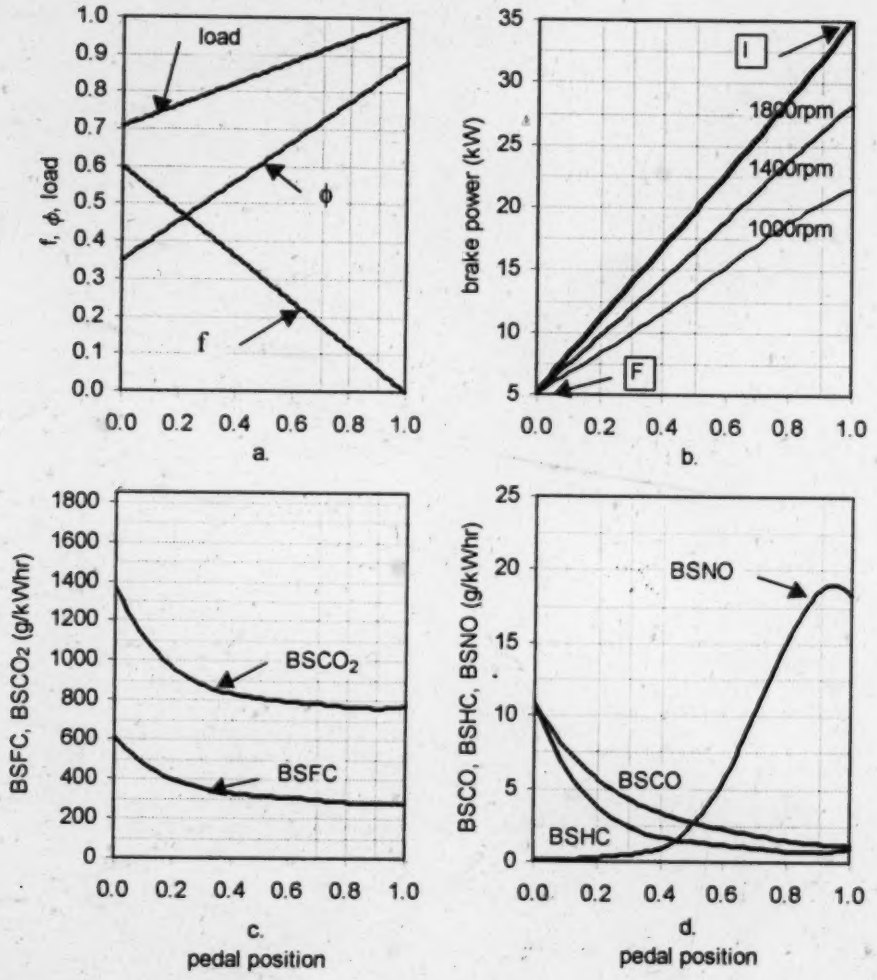

Figure 3.20. Engine case F-I. (**a**.) Engine f, ϕ, and load (**b**.) brake power (**c**.) brake specific fuel consumption and production of CO_2 and (**d**.) brake specific production of CO, HCs and NO with respect to pedal position.

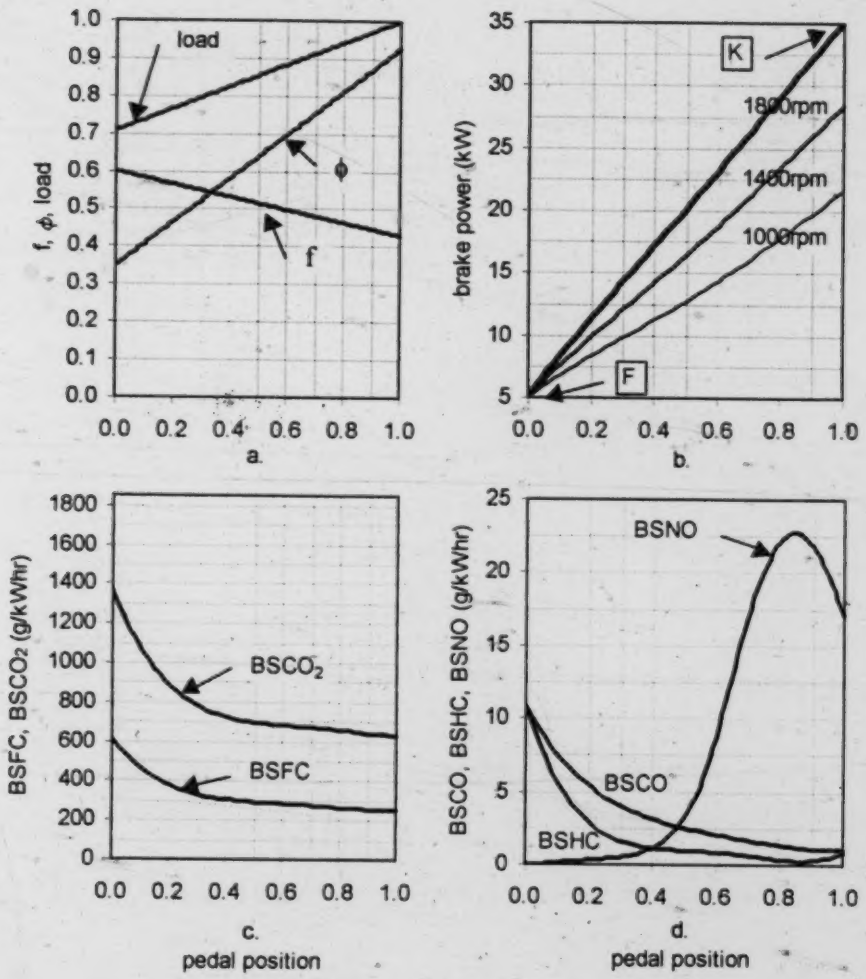

Figure 3.21. Engine case F-K. (**a**.) Engine f, ϕ, and load (**b**.) brake power (**c**.) brake specific fuel consumption and production of CO_2 and (**d**.) brake specific production of CO, HCs and NO with respect to pedal position.

As seen in the previous results, there is no clear advantage in using ultra-lean equivalence ratios to increase engine load. In addition, the previous cases may consume a prohibitive amount of hydrogen in a driving cycle due to the large fractions used. In order to potentially reduce the cumulative amount of hydrogen consumed, case C-K (as seen in Figure 3.22) is proposed where the hydrogen fraction increases from 0% to 43% as the pedal position increases from 0 to 1. Compared to case F-K, case C-K generally

has a lower *BSFC*, *BSHC*, and *BSNO*. However, $BSCO_2$ is increased due to a greater amount of carbon in the fuel at a pedal position of zero. At 1800RPM, and increasing the pedal from 0 to 1, *BSFC* ranges from 585g/kWhr to 255g/kWhr, $BSCO_2$ from 1595g/kWhr to 626g/kWhr, BSCO from 6g/kWhr to 1g/kWhr, and *BSHC* from 5.76g/kWhr to 0.51g/kWhr. *BSNO* increases from a minimum of 0.61g/kWhr to a peak of 21.19g/kWhr. This case will highlight the impact that the fraction of hydrogen variation with pedal position has on the cumulative hydrogen consumption.

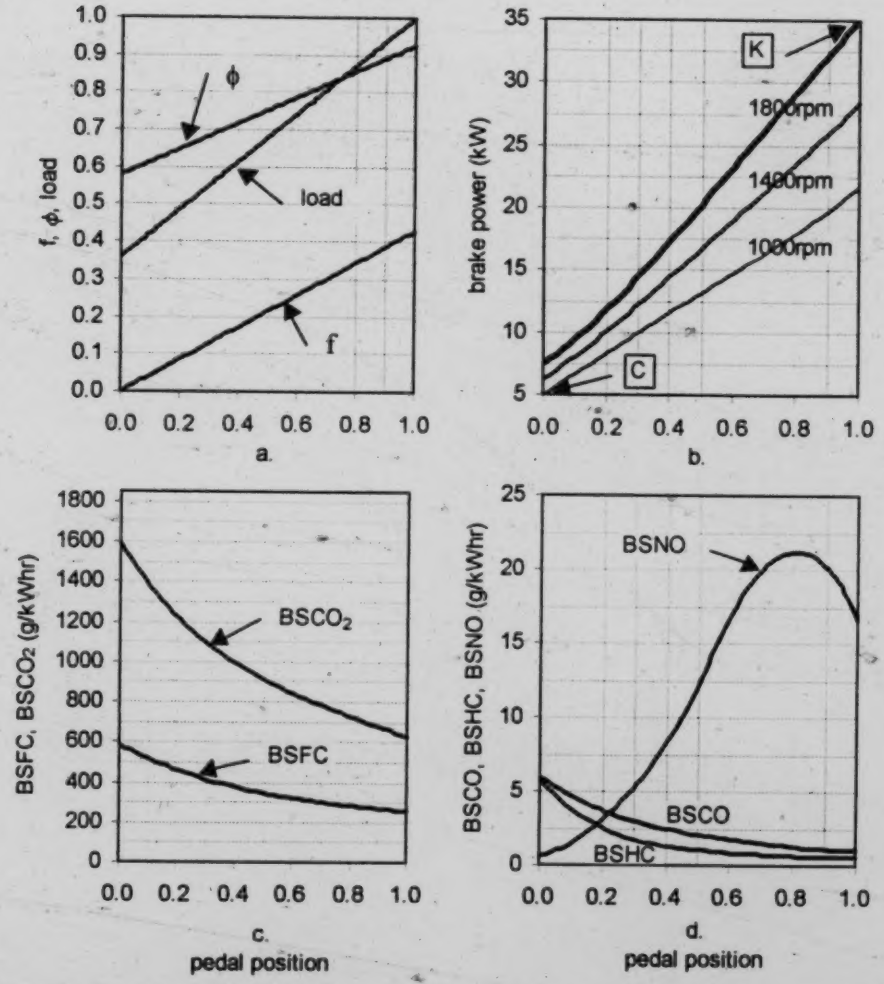

Figure 3.22. Engine case C-K. (a.) Engine *f*, ϕ, and load (b.) brake power (c.) brake specific fuel consumption and production of CO_2 and (d.) brake specific production of CO, HCs and NO with respect to pedal position.

3.5. Scheme 1, 2, & 3 cumulative driving cycle results

To move the vehicle model through the driving cycle at its required speed-time trace, its engine provides positive required power, while the brakes provide negative required power. When the vehicle is braking, or is at rest, the engine is considered to be idling. The model engine requires 5kW to account for accessory power, so the engine must supply 5kW (at all times) in addition to the power required to move the vehicle through the cycle. Equation 10 shows that the consumption of fuel is dependent on the engine power and the brake specific fuel consumption:

$$\dot{m}_{fuel} = \frac{BSFC\ P_{engine}}{3600} \qquad \left[\frac{g}{s}\right] \qquad (10)$$

where *BSFC* is a function of f, ϕ, engine load and speed.

The cumulative amount of fuel consumed is normalized with respect to the cycle distance according to equation 11, so that comparisons may be made between driving cycles.

$$m_{fuel} = \frac{\sum_{1}^{n} \dot{m}_{fuel}\,\Delta t}{d_{cycle}} \qquad \left[\frac{g}{km}\right] \qquad (11)$$

The cumulative production of each pollutant (CO_2, CO, HCs, and NO) is determined similarly. In this manner, the pollution produced during a driving cycle can be compared to the government limits for CO (2.5g/km), HC (0.25g/km), and NO (0.62g/km) production [41]. However, it should be noted that the model does not account for any reduction by catalytic conversion of the exhaust products.

The cycle efficiency is defined as the ratio of cumulative engine energy to the cumulative heating value of the fuel consumed according to equation 12. This measure will allow us to gauge the efficiency of fuel use depending on the engine operating system.

$$\eta_{cycle} = \frac{\sum_{1}^{n} P_{engine} \Delta t}{\sum_{1}^{n} (\dot{m}_{CH4} LHV_{CH4} + \dot{m}_{H2} LHV_{H2}) \Delta t} \qquad (12)$$

At each second in the cycle, fuel consumption, and production of carbon dioxide, carbon monoxide, unburned hydrocarbons and NO are calculated. Multi-cylinder and transient effects, such as too-lean or too-rich operation, or time needed to change gears are neglected.

Scheme 1, 2, and 3 engine cases (A-G to C-K) were put in the vehicle model and run through each driving cycle. The cumulative energy produced by the engine is greater than the cumulative positive energy required by the vehicle due engine production of 5kW for accessories. However, the cumulative energy produced by each engine case is nearly constant (due to the uniformity of engine power from case to case). Similarly, the pedal position with respect to time is nearly identical for all cases. But as seen in the previous section, each combination of pedal position and engine speed yields different engine characteristics of *BSFC*, $BSCO_2$, *BSCO*, *BSHC*, and *BSNO*.

3.5.1. SAE-J-227D cumulative results

The brake power, pedal position, and engine speed required from the SAE-J-227D schedule can be seen in Figure 3.23. Engine power ranged from 5kW to approximately 28.2kW, averaging 10.5kW. An average pedal position of 0.14 was used. The highest pedal position used of 0.67 indicates that the engine has reserve power that is not needed in this particular driving cycle. Over the entire cycle, the engine consumes 827kJ/km.

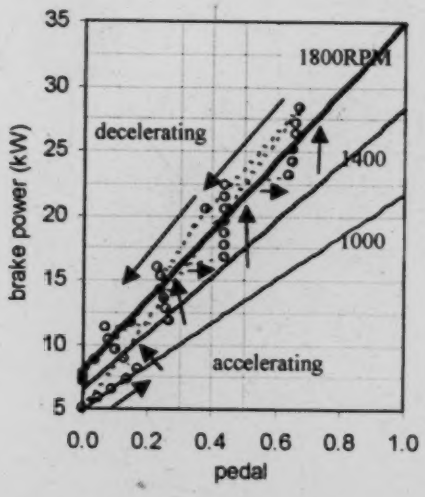

Figure 3.23. SAE-J-227D schedule brake power, and engine speed combinations with respect to pedal position. These combinations are used for each engine case (each point represents one second of operation).

Usually peak fuel consumption and pollutant production rates occur at the maximum required power during a driving cycle, because that is where the flow rate of fuel is highest. However depending on the engine case, this is not always so, as some engine characteristics decrease with increasing power demand (i.e. f). Although the power produced at idle (5kW) is the same for all cases, the idle conditions (f, ϕ, engine load) may be different depending on the idle set point. Over the course of the schedule, fuel consumption and pollutant production vary from idle to peak conditions (g/s). Generally compared to scheme 1, scheme 2 and 3 had lower idle and peak consumption of CH_4 at the expense of increasing H_2 consumption. Also, idle CO_2 production is

reduced due to higher engine load, but the peak is largely unchanged due to the increase in $BSCO_2$ with decreasing equivalence ratio. Idle and peak CO levels are reduced to near negligible levels due to the use of equivalence ratios below 0.95. Hydrocarbon production is increased at idle due to operation near the partial burn limit. Idle NO production is negligible due to the use of lean equivalence ratios equal to or below 0.58, but peak NO production is increased due to the higher combustion temperatures found at equivalence ratios from 0.8 to 0.9. It is interesting to note that case C-K has the highest peak production of NO, due to simultaneous increasing of hydrogen fraction and equivalence ratio during peak power demand. A summary of the idle and peak values for each case is found in Table 3.2.

The second-by-second results (which can be found for pedal position, f, ϕ, engine load, CH_4 and H_2 consumption, and CO_2, CO, HC, and NO production in Appendix E), can not tell us how much hydrogen storage is required on board a vehicle. Since the storage and/or cost of hydrogen are critical issues, the cases must be compared on a cumulative basis. In this manner, an optimal operating system can be selected based on the amount of on-board hydrogen storage available. As seen in Figure 3.24, the effect of hydrogen addition (g/km) is noted on CH_4 consumption, and CO_2, CO, HC, and NO production for each different operating scheme.

The addition of hydrogen for scheme 1 cases (A-G, B-H), decreases the consumption of CH_4 by displacing it, and the production of CO_2, CO, and HCs, is reduced by the reduction of carbon in the fuel. However, hydrogen addition increases the production of NO by increasing combustion temperatures. For every g/km of hydrogen addition, there is an approximate 2.34g/km decrease in CH_4 consumption. Likewise, cumulative CO_2 production is reduced by 5.67g/km, CO by 0.45g/km, and HC by 0.02g/km for every g/km of hydrogen addition. However NO increased by 0.03g/km for every g/km of hydrogen.

Table 3.2. SAE-J-227D schedule idle and peak fuel consumption and pollutant production (g/s).

	CH_4		H_2		CO_2		CO		HC		NO	
	idle	*peak*	*idle*	*peak*	*idle*	*peak*	*idle*	*peak*	*idle*	*peak*	*idle*	*peak*
Scheme 1; f = fixed, $\phi = 1$												
A-G	0.977	2.896	0.000	0.000	2.398	7.004	0.260	0.602	0.005	0.010	0.011	0.057
B-H	0.852	2.475	0.059	0.171	2.069	6.033	0.232	0.534	0.004	0.007	0.014	0.060
Scheme 2; f = fixed, partial burn limit < ϕ < 1												
C-I	0.724	2.567	0.000	0.000	2.000	7.135	0.008	0.014	0.008	0.012	0.000	0.119
D-J	0.579	2.152	0.040	0.149	1.542	5.900	0.012	0.018	0.011	0.014	0.000	0.144
E-K	0.543	2.068	0.053	0.201	1.468	5.666	0.013	0.018	0.010	0.014	0.000	0.155
Scheme 3; 0% < f < 60%, partial burn limit < ϕ < 1												
D-I	0.579	2.406	0.040	0.076	1.542	6.644	0.012	0.018	0.011	0.014	0.000	0.120
F-I	0.417	2.276	0.081	0.156	1.094	6.179	0.015	0.019	0.011	0.015	0.000	0.099
F-K	0.417	1.973	0.081	0.235	1.094	5.378	0.015	0.019	0.011	0.015	0.000	0.139
C-K	0.724	2.267	0.000	0.126	2.000	6.265	0.008	0.013	0.008	0.012	0.000	0.162

For operating scheme 2, the use of lean equivalence ratios decreases the fuel consumption and pollutant production (except unburned hydrocarbons) beyond that from scheme 1 operation. Scheme 2 cases (C-I, D-J, E-K) show the effects of using hydrogen to increase the engine load by operating at lean equivalence ratios. When compared to scheme 1, scheme 2 reduces the cumulative consumption of CH_4 (g/km) by 21% to 31% for equal amounts of hydrogen addition. Similarly, CO_2 production is reduced by 12% to 23%, and CO production is reduced 96% to 97%. However, cumulative HC production increases from 18% to 71%. Production of NO is reduced by 39% to 70%. These results are summarized in Table 3.3. In addition, scheme 2 operation increases the cycle efficiency to approximately 16-17% from 12-13%.

Similar to scheme 1, for every g/km of hydrogen addition in scheme 2, there is a decrease in CH_4 consumption of approximately 3.12g/km and an 8.59g/km reduction in CO_2. Due to the use of equivalence ratios below 0.95, CO production is negligible. However, HC production is increased by 0.01g/km for every g/km of hydrogen, due to the use of equivalence ratios near the partial burn limit. Although peak production of NO is higher for scheme 2 cases, this is offset by lower idle production, so that the

cumulative NO production is decreased by 0.06g/km for every g/km of hydrogen addition.

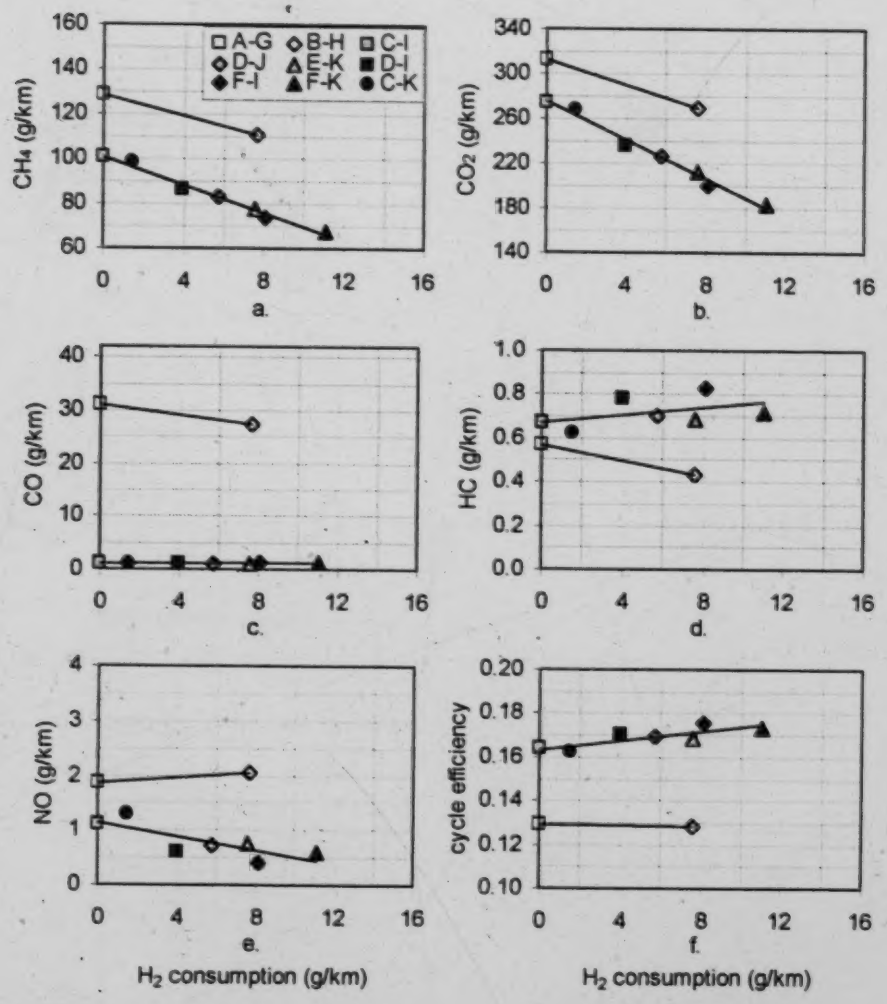

Figure 3.24. SAE J-227D cumulative results versus H_2 consumption for scheme 1 (□), scheme 2 (▣), and scheme 3 (■). (**a**.) Consumption of methane (**b**.) Production of CO_2 (**c**.) Production of CO (**d**.) Production of HC (**e**.) Production of NO. (**f**.) Cycle efficiency.

Table 3.3. SAE-J-227D schedule percent reduction in consumption of fuel / production of pollutant when using scheme 2 or 3 in place of scheme 1 for equal amounts of hydrogen addition (g/km).

CH_4	CO_2	CO	HC	NO
21 to 31	12 to 23	96 to 97	-18 to -71*	39 to 70

*negative value indicates an increase

Scheme 3 cases (D-I, F-I, F-K, C-K) show that allowing the hydrogen fraction to vary with the pedal position at lean equivalence ratios provides no appreciable difference over scheme 2. However, using a scheme 3 operating system would allow for a greater amount of total hydrogen usage (g/km). Scheme 3 case F-K (where hydrogen fraction varies from 0.43 to 0.60) is capable of using 46% more hydrogen than scheme 2 case E-K (where the hydrogen fraction is knock-limited to a maximum of 0.43). It is interesting to note that case C-K, where the fraction of hydrogen increases with pedal position, is shown to follow closely the same trend as other scheme 2 and 3 cases on a cumulative basis. The change in fuel consumption or pollutant production with hydrogen addition is summarized in Table 3.4 for each scheme.

Table 3.4. SAE-J-227D schedule change in consumption of fuel, production of pollutant (g/km) per g/km of hydrogen addition (each based on the slope of a best-fit linear trendline).

	CH_4	CO_2	CO	HC	NO
scheme1	-2.34	-5.67	-0.45	-0.02	0.03
scheme 2&3	-3.12	-8.59	0.04	0.01	-0.06

3.5.2. Highway schedule cumulative results

For the Highway schedule, there are a greater number of different combinations of brake power and pedal position than SAE-J-227D. As seen in Figure 3.25, the engine power ranges from 5kW to approximately 27.4kW at an average of 13.78kW. The higher average power requires a higher average pedal position of 0.19. The highest pedal position of 0.81 again indicates that the engine has reserve power not needed in this driving cycle. The engine consumes 639kJ/km of energy over the entire schedule.

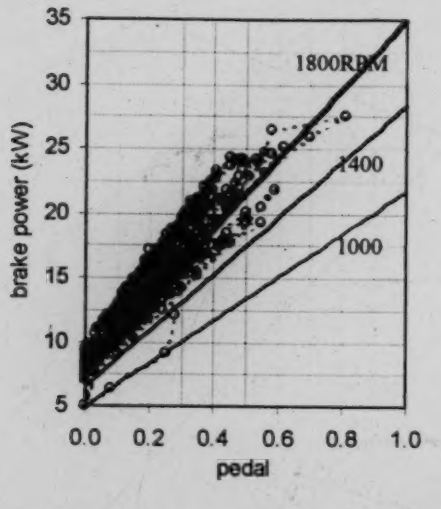

Figure 3.25. Highway schedule brake power, and engine speed combinations with respect to pedal position. These combinations are used for each engine case (each point represents one second of operation).

Idle and peak fuel consumption and pollutant production (g/s) results for each case are summarized in Table 3.5. Compared to SAE-J-227D, idle values are unchanged, but the peak values are generally higher due to higher engine speeds and powers.

Figure 3.26 shows the cumulative results for each operating scheme. Compared to the SAE-J-227D schedule, the highway schedule has a lower consumption of fuel and production of pollutants per kilometer due to the vehicle spending more time at higher speeds, and covering more distance for a given amount of acceleration. However, the addition of hydrogen has the same relative effect on CH_4, CO_2, CO, HC, NO, and cycle efficiency for schemes 1, 2 and 3 as previously seen in Figure 3.24.

For scheme 1, there is an approximate 2.43g/km decrease in CH_4 consumption for every g/km addition of hydrogen, and a 5.64g/km reduction in CO_2. CO production is reduced by 0.44g/km and HC production by 0.02g/km, but NO is increased by 0.02g/km for every g/km of hydrogen addition.

Again, scheme 2 displays a further change in consumption and production when compared to scheme 1. Scheme 2, when compared to scheme 1 reduces the cumulative consumption of CH_4 (g/km) by 20% to 27% for equal amounts of hydrogen addition. Similarly, CO_2 production is reduced by 11% to 19%, and CO production is reduced 96%

to 97%. However, cumulative HC production increases from 5% to 42%. Production of NO is reduced by 31% to 81%. These results are summarized in Table 3.6. In addition, scheme 2 operation increases the cycle efficiency to approximately 17% from 13%.

Table 3.5. Highway schedule idle and peak fuel consumption and pollutant production (g/s).

	CH_4		H_2		CO_2		CO		HC		NO	
	idle	*peak*	*idle*	*peak*	*idle*	*peak*	*idle*	*peak*	*idle*	*peak*	*idle*	*peak*
Scheme 1; f = fixed, $\phi = 1$												
A-G	0.977	2.949	0.000	0.000	2.398	7.108	0.260	0.626	0.005	0.011	0.011	0.055
B-H	0.852	2.509	0.059	0.174	2.069	6.121	0.232	0.554	0.004	0.007	0.014	0.057
Scheme 2; f = fixed, partial burn limit < ϕ < 1												
C-I	0.724	2.553	0.000	0.000	2.000	7.029	0.008	0.015	0.008	0.014	0.000	0.134
D-J	0.579	2.100	0.040	0.145	1.542	5.725	0.012	0.019	0.011	0.016	0.000	0.161
E-K	0.543	2.016	0.053	0.196	1.468	5.494	0.013	0.019	0.010	0.016	0.000	0.169
Scheme 3; 0% < f < 60%, partial burn limit < ϕ < 1												
D-I	0.579	2.330	0.040	0.083	1.542	6.345	0.012	0.019	0.011	0.016	0.000	0.129
F-I	0.417	2.162	0.081	0.172	1.094	5.871	0.015	0.020	0.011	0.017	0.000	0.120
F-K	0.417	1.879	0.081	0.243	1.094	5.093	0.015	0.020	0.011	0.017	0.000	0.171
C-K	0.724	2.288	0.000	0.139	2.000	6.249	0.008	0.015	0.008	0.014	0.000	0.158

Schemes 2 & 3 appear to have no appreciable difference in cumulative result. For schemes 2 & 3, there is an approximate 2.97g/km decrease in CH_4 consumption for every g/km addition of hydrogen, and a 7.94g/km reduction in CO_2. CO production is negligible while HC production is nearly uniform for every g/km of hydrogen addition. Cumulative NO production is decreased by 0.12g/km for every g/km of hydrogen addition. Case C-K, where the fraction of hydrogen increases with pedal position, is shown to follow the same trend as other scheme 2 and 3 cases on a cumulative basis. These results are summarized in Table 3.7.

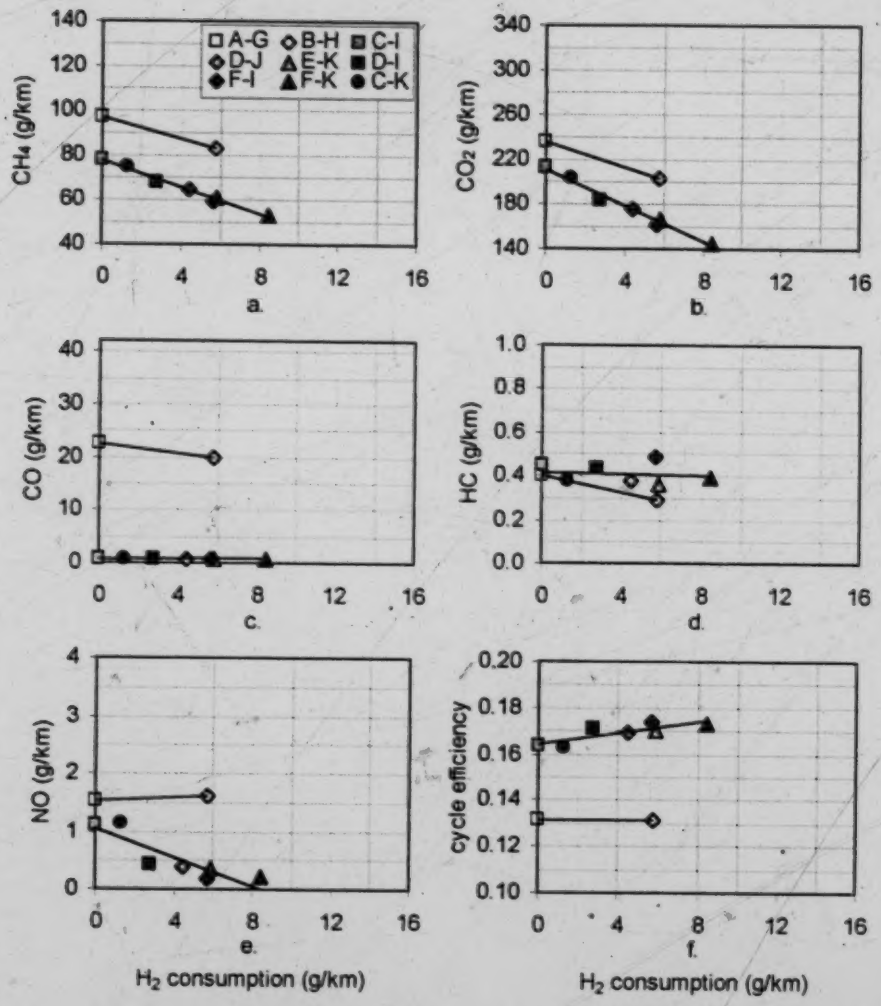

Figure 3.26. Highway cumulative results versus H_2 consumption for scheme 1 (□), scheme 2 (▣), and scheme 3 (■). (**a**.) Consumption of methane (**b**.) Production of CO_2 (**c**.) Production of CO (**d**.) Production of HC (**e**.) Production of NO. (**f**.) Cycle efficiency.

Table 3.6. Highway schedule percent reduction in consumption of fuel / production of pollutant when using scheme 2 or 3 in place of scheme 1 for equal amounts of hydrogen addition (g/km).

CH_4	CO_2	CO	HC	NO
20 to 27	11 to 19	96 to 97	-5 to -42*	31 to 81

* negative value indicates an increase

Table 3.7. Highway schedule change in consumption of fuel, production of pollutant (g/km) per g/km of hydrogen addition (each based on the slope of a best-fit linear trendline).

	CH_4	CO_2	CO	HC	NO
scheme1	-2.43	-5.64	-0.44	-0.02	0.02
scheme 2&3	-2.97	-7.94	0.03	0.00	-0.12

Although there is no appreciable difference between schemes 2 and 3 with respect to cumulative fuel consumption or pollution production, using a scheme 3 operating system would allow for a greater amount of hydrogen usage (g/km). Scheme 3 case F-K is capable of using 44% more hydrogen than scheme 2 case E-K.

3.5.3. Urban schedule cumulative results

The combinations of engine brake power, pedal position, and speed can be seen in Figure 3.27 for each second of operation. It can be seen that engine power ranged from 5kW to approximately 32.3kW at an average of 8.58kW. The average pedal position is low at 0.08 due to the periods of idle. The highest pedal position used is 0.85, which indicates that the engine has additional power reserve that is not needed by the driving cycle. The engine consumes 982kJ/km of energy over the entire schedule.

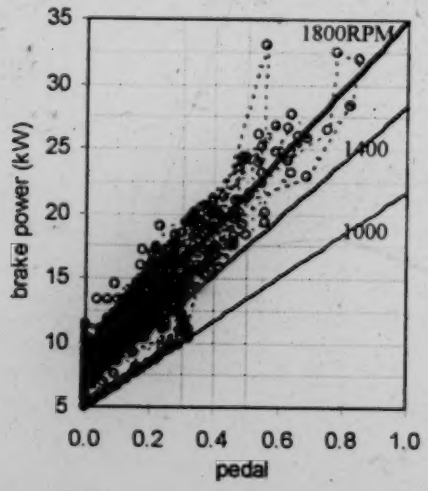

Figure 3.27. Urban schedule brake power, and engine speed combinations with respect to pedal position. These combinations are used for each engine case (each point represents one second of operation).

Idle and peak fuel consumption and pollutant production (g/s) results for each case are summarized in Table 3.8. Again idle production and consumption values are the same as for the other schedules. However, peak fuel consumption and pollutant production are higher due to the increase in peak power required.

Table 3.8. Urban schedule idle and peak fuel consumption and pollutant production (g/s).

	CH_4		H_2		CO_2		CO		HC		NO	
	idle	*peak*	*idle*	*peak*	*idle*	*peak*	*idle*	*peak*	*idle*	*peak*	*idle*	*peak*
Scheme 1; f = fixed, $\phi = 1$												
A-G	0.977	3.805	0.000	0.000	2.398	9.115	0.260	0.769	0.005	0.012	0.011	0.078
B-H	0.852	3.215	0.059	0.223	2.069	7.855	0.232	0.680	0.004	0.008	0.014	0.075
Scheme 2; f = fixed, partial burn limit < ϕ < 1												
C-I	0.724	3.486	0.000	0.000	2.000	9.707	0.008	0.018	0.008	0.016	0.000	0.160
D-J	0.579	2.729	0.040	0.189	1.542	7.425	0.012	0.022	0.011	0.017	0.000	0.198
E-K	0.543	2.605	0.053	0.253	1.468	7.105	0.013	0.022	0.010	0.018	0.000	0.203
Scheme 3; 0% < f < 60%, partial burn limit < ϕ < 1												
D-I	0.579	3.073	0.040	0.105	1.542	8.313	0.012	0.022	0.011	0.017	0.000	0.166
F-I	0.417	2.849	0.081	0.220	1.094	7.544	0.015	0.023	0.011	0.020	0.000	0.161
F-K	0.417	2.445	0.081	0.312	1.094	6.632	0.015	0.022	0.011	0.019	0.000	0.202
C-K	0.724	2.911	0.000	0.171	2.000	8.013	0.008	0.017	0.008	0.015	0.000	0.203

Figure 3.28 shows that the cumulative fuel consumption and pollutant production (g/km) are higher in the urban schedule than the other schedules. This is because not as much distance is covered due to the periods of low speed and idle. However, the same trends in fuel consumption and pollutant production can be seen with respect to the other two schedules.

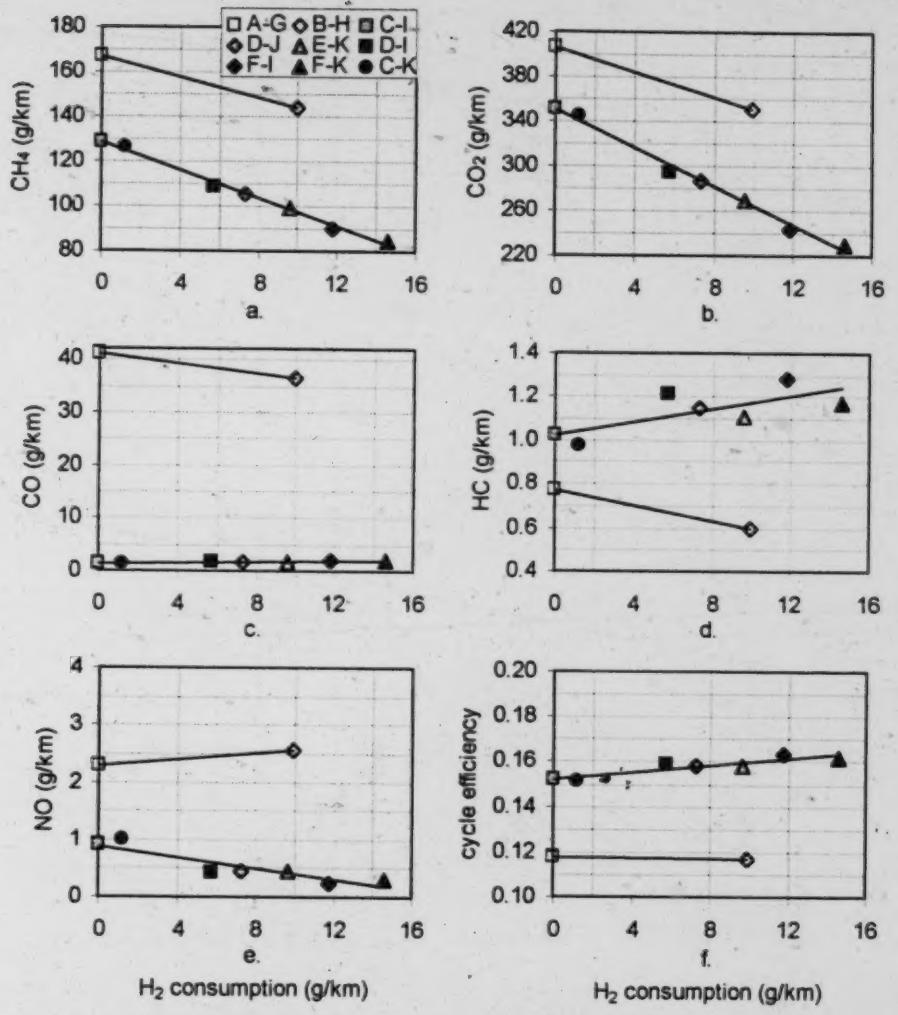

Figure 3.28. Urban cumulative results versus H_2 consumption for scheme 1 (□), scheme 2 (▣), and scheme 3 (■). (a.) Consumption of methane (b.) Production of CO_2 (c.) Production of CO (d.) Production of HC (e.) Production of NO. (f.) Cycle efficiency.

For scheme 1, there is an approximate 2.30g/km decrease in CH_4 consumption for every g/km addition of hydrogen, and a 5.63g/km reduction in CO_2. Production of CO is reduced by 0.46g/km and HC production is reduced by 0.02g/km, but NO production is increased by 0.03g/km.

Schemes 2 and 3, when compared to scheme 1, again reduce the cumulative consumption of CH_4 (g/km) by 23% to 32% for equal amounts of hydrogen addition.

Similarly, CO_2 production is reduced by 14% to 25%, and CO production is reduced 97% to 98%. However, cumulative HC production increases from 33% to 97%. Production of NO is reduced by 61% to 84%. These results are summarized in Table 3.9. In addition, scheme 2 increases the cycle efficiency from 12% to 16%.

Table 3.9. Urban schedule percent reduction in consumption of fuel / production of pollutant when using scheme 2 or 3 in place of scheme 1 for equal amounts of hydrogen addition (g/km).

CH_4	CO_2	CO	HC	NO
23 to 32	14 to 25	97 to 98	-33 to -97*	61 to 84

*negative value indicates an increase

Schemes 2 and 3 appear to have no appreciable difference in cumulative result. For schemes 2 and 3, there is an approximate 3.10g/km decrease in CH_4 consumption for every g/km addition of hydrogen, and an 8.69g/km reduction in CO_2. Production of CO is at negligible levels while HC production increases by 0.02g/km for every g/km of hydrogen addition. However, cumulative NO production is decreased by 0.05g/km for every g/km of hydrogen addition.

Although there is no appreciable difference between schemes 2 and 3 with respect to cumulative fuel consumption or pollution production, using a scheme 3 operating system would allow for a greater amount of hydrogen usage (g/km). Scheme 3 is capable of using 51% more hydrogen. Case C-K, where the fraction of hydrogen increases with pedal position, is shown to follow the same trend as other scheme 2 and 3 cases on a cumulative basis. These results are summarized in Table 3.10.

Table 3.10. Urban Schedule change in consumption of fuel, production of pollutant (g/km) per g/km of hydrogen addition (each based on the slope of a best-fit linear trendline).

	CH_4	CO_2	CO	HC	NO
scheme1	-2.30	-5.63	-0.46	-0.02	0.03
scheme 2&3	-3.10	-8.69	-0.05	0.02	-0.05

3.6. Electrolyser

As seen from the previous results, increasing the engine load by reducing dependence on the throttle plate yields significant gains in fuel economy. For best fuel economy, the engine would ideally be operated continually at full load (unthrottled). For schemes 1, 2 and 3 the power band available by adjusting the air-to-fuel ratio was not wide enough, so that some part load throttling was still needed. However, a 4th scheme is possible where the engine is run constantly at full load. This is possible by dividing the engine power between the drivetrain and an electrically powered electrolyser. As seen in Figure 3.29, the increase in engine efficiency must be large enough to offset the increased fuel consumption used to power the electrolyser.

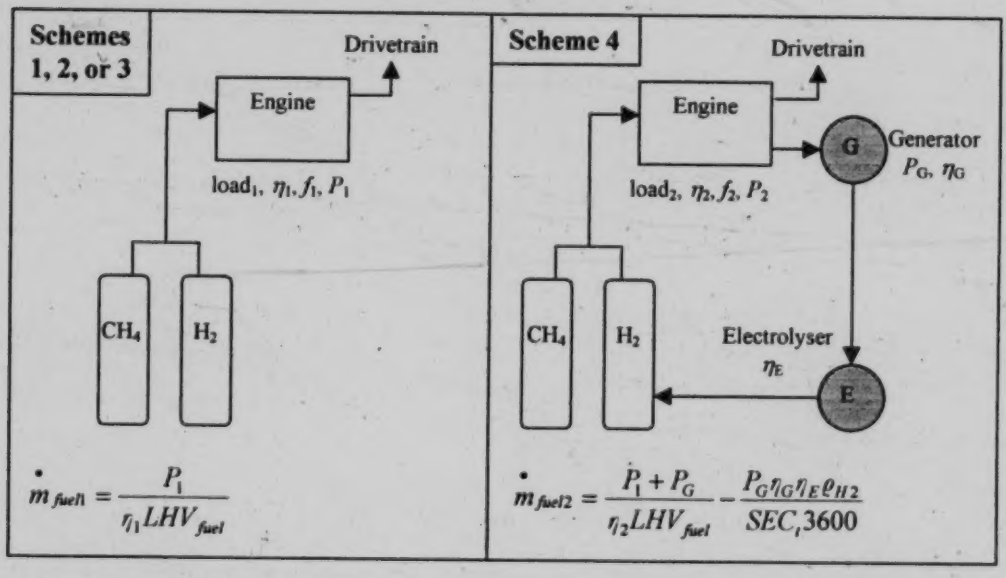

Figure 3.29. Comparing a scheme 1,2 or 3 engine to a scheme 4 engine with electrolyser. Scheme 4 engine is unthrottled ($load_2 = 1.0 > load_1$), which results in higher thermal efficiency ($\eta_2 > \eta_1$), but uses more power ($P_2 = P_1 + P_G$). Both engines use the same hydrogen fraction ($f_2 = f_1$). In order for scheme 4 to be of benefit the engine must produce enough hydrogen fuel to make up for its increased consumption (ie. $m_{fuel2} < m_{fuel1}$). SEC_t = thermoneutral specific energy consumption (3.30kWhr/m^{3}H$_2$).

Powering an electrolyser from a combustion engine represents a net loss of energy due to the conversion efficiency from chemical energy to mechanical to electrical back to chemical. Therefore, the use of an electrolyser will only be beneficial if there is a substantial increase in engine efficiency due to addition of hydrogen and operation at full load. When considering storage requirements, the cumulative effect must be considered through a driving cycle according to equation 13.

$$\sum_{1}^{n} \dot{m}_{fuel2}\,\Delta t < \sum_{1}^{n} \dot{m}_{fuel1}\,\Delta t \tag{13}$$

In addition, the use of an electrolyser has the potential to decrease the on-board storage requirement of hydrogen. However, this is only possible when the electrolyser production exceeds the increased consumption in hydrogen fuel.

3.6.1. Electrochemical principles

Water can be decomposed into its elemental components through a process called electrolysis. The resulting products are hydrogen and oxygen.

$$H_2O \xrightarrow{2F} H_2 + \frac{1}{2}O_2 \tag{14}$$

To make the reaction in equation 14 proceed, a voltage and current is passed through an electrolytic solution of water via two electrodes. Through thermodynamic property relations, the energy change for this reaction at 25°C and 1atm can be described in equation 15 as:

$$\Delta H^{\circ}_{f} = \Delta G^{\circ}_{f} + T\Delta S^{\circ} \tag{15}$$

where ΔH°_{f} is the change in enthalpy, ΔG°_{f} is the minimum electrical energy required, and $T\Delta S^{\circ}$ is the thermal energy required for the reaction to proceed. At 25°C and 1atm, ΔG°_{f} = 237kJ/mol for liquid water, and using Faraday's constant, the minimum electrical voltage required is found to be $1.23V$ [42]. However, at this voltage, thermal energy

must be drawn from the surroundings (ΔH^{o}_{f} = 286kJ/mol). For thermoneutral operation (where the reaction body does not absorb heat or give it off), a voltage of 1.48V is required. For electrolysers, thermoneutral voltage is considered to be 100% efficient, and the production rate at this efficiency is 3.30kWhr/m^{3}H$_2$[5]. Electrolysis efficiency is defined by equation 16.

$$\eta_E = \left(\frac{1.48}{V}\right)_{CELL} \qquad (16)$$

If an external source of heat energy is available (such as waste heat from an engine), it is possible to operate the electrolyser at a higher temperature. In this manner, electrical energy can be displaced by heat energy resulting in higher electrical efficiency. There is a potential to increase electrolysis efficiency by using waste heat from a combustion engine, but this is not considered any further in this study. Electrolysis cells can also be operated at elevated pressures, thus reducing or eliminating the need for compressing the hydrogen produced. As found by Bohacik et al. [43], increasing the electrolysis pressure (P in atmospheres) according to equation 17, demands an increase in input voltage.

$$V_P = V_{1atm} + 0.0435 \log P \qquad (17)$$

The increase in input energy is required for the compression of the electrolysis products.

3.6.2. Electrolyser design principles

Cell voltage varies directly with current, and therefore increases proportionally with current applied. This means that the electrolysis efficiency decreases with increasing current. Despite high efficiency, it is not practical to operate at low current, as the hydrogen production rate is small. Typical electrolysers operate at 1.8 to 2.2V (82% to 67% efficiency) per cell to strike a compromise between efficiency and production rate. Maximum current is limited by the current density the electrodes are able to maintain. At high current, the electrodes are limited by material properties, and become

[5] Volume of hydrogen at standard temperature and pressure (293.15K, 1atm)

saturated with charge. The electrolyte may be composed of any water-based solution that conducts electricity. However, the most common electrolyte is alkaline potassium hydroxide (*KOH*), at 20% to 30% by weight. As seen in Figure 3.30, the reaction proceeds at the cathode with water and potassium to produce hydrogen atoms. The hydrogen atoms bond to the cathode surface, where they combine to form diatomic hydrogen gas. Likewise, hydroxyl molecules migrate towards the anode, where they combine to form water and atomic oxygen. The oxygen collects on the anode surface and then combines to form diatomic oxygen gas. Usually, the electrodes are coated with a catalyst (i.e. nickel-platinum), that assists in the combining of atomic hydrogen and oxygen. The catalyst also helps to increase current density. An ion-permeable membrane separates the flow of hydrogen and oxygen gasses.

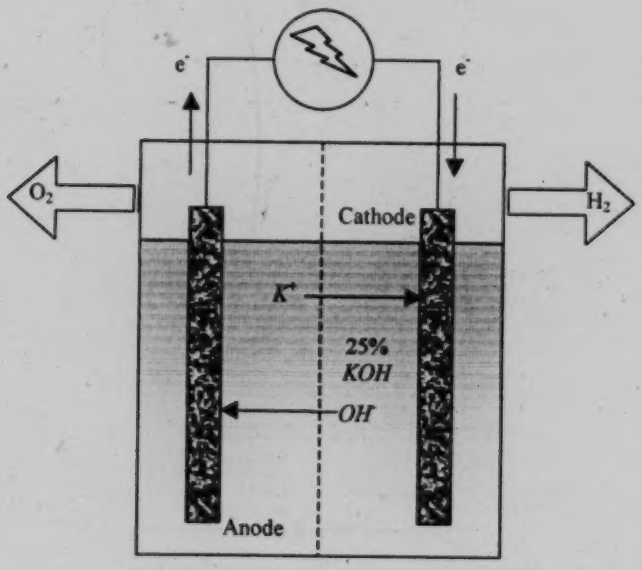

Figure 3.30. Typical alkaline electrolysis cell. When voltage & current is applied to a 25% solution of KOH, hydrogen forms at the cathode and oxygen at the anode.

To achieve a certain hydrogen production rate, multiple electrolysis cells are combined in an electrolyser. Electrolysers are classified as unipolar or bipolar. In a unipolar type, electrolysis cells are connected in parallel. This design occupies a large volume, but if one cell fails, the unit will continue to function. The bipolar design is

more compact, but since the cells are connected in series, the unit will not function if one cell fails. Hydrogen can be produced on-board a vehicle by an electrolyser connected to a generator. The generator(s) can be run directly off engine power (full time), and/or off braking power (regeneration). The electrolyser and its subsidiary components like the generator(s) and electrolyte tank, adds weight to the vehicle, which may result in increased overall fuel consumption. Stationary commercial electrolyser units weigh anywhere from 278kg to 454kg with displacement volume of $0.97m^3$ to $1.70m^3$ for 8kW and 82.5kW units respectively.[6] Presumably, practical electrolysers for automotive applications would have to be reduced with respect to both mass and volume if they are shown to be viable.

3.6.3. Electrolyser response under variable power input

An electrolyser running in an automotive application would have variable power input, whether full-time or during regeneration. Several studies examined electrolysers under variable input from solar sources [44, 45]. However, the power changes due to solar energy occur at a slower rate (minutes, hours), than it would in an engine (seconds). A study by Brossard et al. [46] found that a small electrolyser operating under variable power input (from a windmill) suffers no additional loss in efficiency due to transient effects. The electrochemical reactions proceed at a rate much faster than the change in power applied (Faradaic efficiency is close to 100% regardless of constant or variable power). Hence, no additional loss of energy is incurred due to transient power input. However, as seen in the previous section, the efficiency of the cell varies depending on the power input. The Brossard 5-cell bipolar unit was designed to operate at a maximum voltage of $2.4V$ / cell and current of $250A$. This is equivalent to 3kW of input power ($P = VI$). The authors noted that below $50A$ of current, the content of hydrogen in the oxygen produced increases (creating a safety hazard). It is assumed that the maximum current is $250A$ due to the material limitations of the electrodes. The characteristic of the electrolyser was estimated (as seen in Figure 3.31) by fitting a logarithmic curve to the existing data. Figure 3.30 shows the characteristic voltage-current and the specific

[6] Teledyne Brown Engineering, electrolyser models ALTUS-20 & HM-200

energy consumption (*SEC*) relationship. Although *SEC* increases with voltage, so does the production rate of hydrogen up to a maximum of 0.0026g/s.

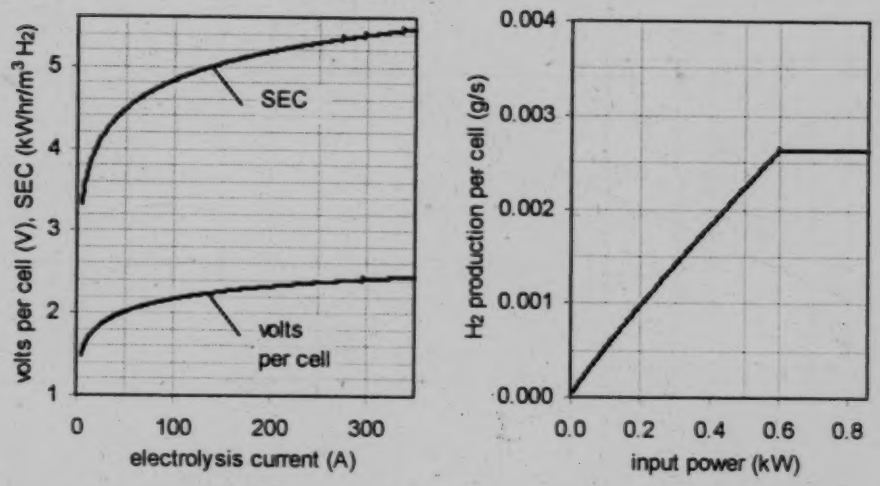

a. b.

Figure 3.31. Brossard electrolyser hydrogen production rate with respect to input power (derived from [46]). The voltage per cell (a.) increases with current according to $V = 0.2267\,Ln(I) + 1.1218$. The Specific Energy Consumption increases with voltage, but the hydrogen production rate (b.) is higher at higher power ($P = IV$). Above 250*A*, the cell production is limited by the electrode maximum current density.

3.6.4. Model electrolyser design

The hypothetical model electrolyser is based on the Brossard electrolyser, except that 50 cells are used instead of 5, bringing the maximum effective input power up to 30kW. Such a large electrolyser might have in reality a low power cutoff around 2.5kW (50*A*) when the current is low, due to increased amounts of hydrogen being created at the anode. However, this effect is neglected for the sake of the model, as overall production below 2.5kW is small. The production rate of hydrogen with respect to input power of the model electrolyser can be seen in Figure 3.32. Increasing the input power to 30kW results in a maximum hydrogen production rate of approximately 0.13g/s. Above 30kW of input power, there is no additional increase in production rate due to maximum electrode current density.

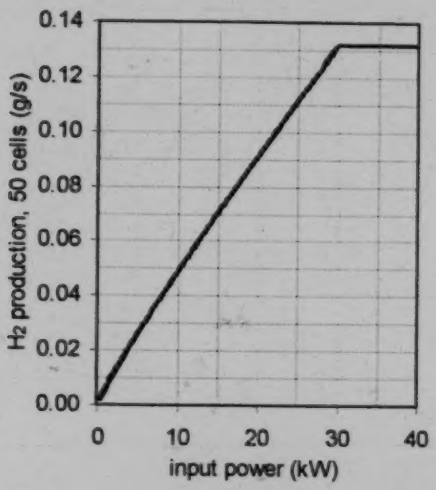

Figure 3.32. Model electrolyser hydrogen production rate with respect to input power (50 electrolysis cells in series). Production is limited at 250*A*, due to electrode maximum current density.

To power the electrolyser on a full-time basis, an electrical generator is required to supply the current and voltage. The generator would be directly coupled to the engine running at full load by means of a clutch. Depending on the driver input (which is determined by the cycle power requirements), the power produced by the engine is divided between the generator and the drivetrain. The generator (at a conversion efficiency of 90%) then supplies electrical power to the electrolyser, to create hydrogen.

Additional electrical generation can be achieved by recapturing energy used to provide vehicle braking (regeneration). As seen in Figure 3.33, power can be supplied to the electrolyser both full-time from the engine and on an intermittent basis during braking. Regenerative capture of braking energy has been previously demonstrated. The regeneration model is built around the University of Alberta's successfully operated hybrid-electric vehicles (HEV)[47, 48, 49]. An HEV uses a combination of electric motors and a combustion engine to power a vehicle, in an effort to reduce fuel consumption and pollutants. The U of A HEV used its electric motors in reverse to generate electricity when braking. During braking, a portion of the energy is absorbed by the electric motors (used as generators) and a portion by the hydraulic brakes. The amount of energy absorbed by the motors was dependent on both the vehicle speed, and

the brake pedal position determined by driver input. Yung [50] found that regeneration captured on average 62.7% of the braking energy in a HOT-505 cycle.

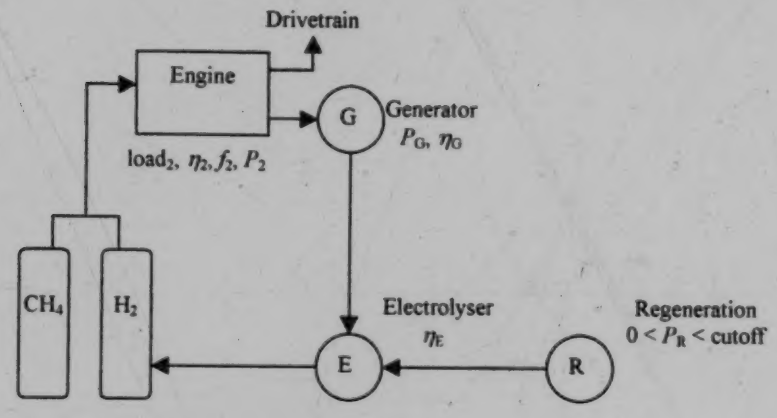

$$\dot{m}_{fuel2} = \frac{P_1 + P_G}{\eta_2 LHV_{fuel}} - \frac{(P_G \eta_G + P_R)\eta_E \varrho_{H2}}{SEC_t 3600}$$

Figure 3.33. Regenerative braking provides additional power to the electrolyser.

For the purposes of the model, it is necessary to define a regenerative "cutoff power". As seen in Figure 3.34, in the cutoff power was set at 6.88kW in the HOT-505 cycle. In this manner, regeneration can absorb all braking power up to the cutoff, beyond which the hydraulic brakes are activated. Note that this is not actually how the actual HEV regeneration system works, but only a simplification that results in an equivalent amount of cumulative regenerative energy. Figure 3.35 shows that using a cutoff power of 6.88kW results in a recovery of approximately 62.7% of the braking energy in a HOT-505 cycle.

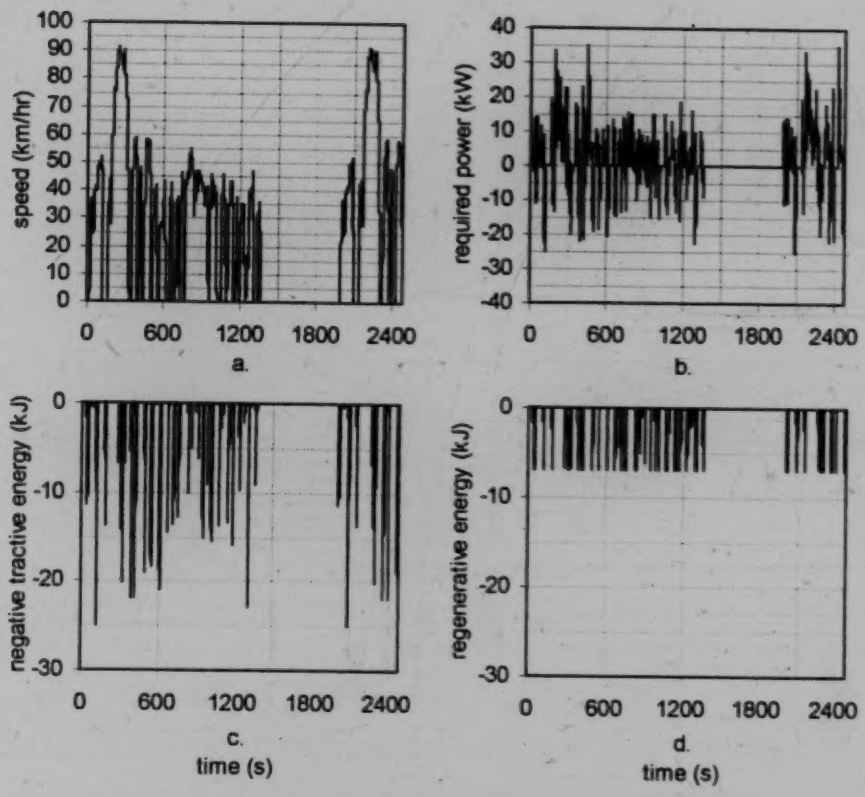

Figure 3.34. Negative tractive energy captured in the HOT-505 schedule (vehicle mass = 1545kg). (**a**.) Speed versus time, (**b**.) Required power. (**c**.) Negative tractive energy (braking). (**d**.) Regenerative energy limited to 6.88kW.

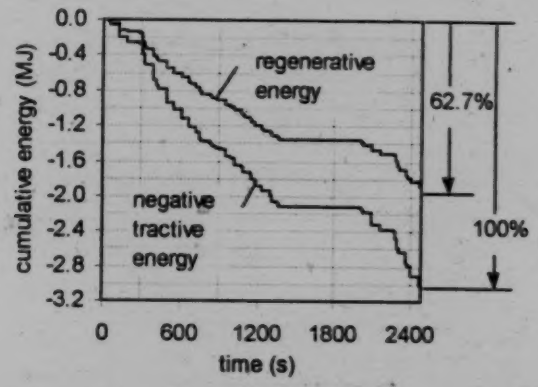

Figure 3.35. HOT-505 schedule cumulative negative energy captured by regenerative braking. Using a regenerative power cutoff of 6.88kW, the cumulative regenerative energy accounts for 62.7% of the cumulative negative tractive energy.

In the model, the full-time and regenerative power are combined and supplied to the electrolyser so that the amount of hydrogen produced by the electrolyser is determined by equation 18. The electrolysis efficiency is a function of this input power.

$$\dot{m}_{H2,E} = \frac{(P_G \eta_G + P_R)\eta_E \varrho_{H2}}{SEC_t 3600} \tag{18}$$

In order to gauge the effectiveness of the electrolyser, its cumulative efficiency over a driving cycle must be determined. The cycle electrolyser efficiency, in equation 19, is a measure of how much chemical energy is produced, compared to the energy used to create it.

$$\eta_{electrolyser} = \frac{\sum_1^n \dot{m}_{H2,E}\, LHV_{H2} \Delta t}{\sum_1^n (P_G + P_R)\Delta t} \tag{19}$$

A simple energy balance on the required energy input to the engine results in equation 20. It is seen that additional energy input is required to power the electrolyser. The only way for an electrolyser to be of benefit is to allow an increase the cycle efficiency through unthrottled engine operation, and by recapturing regenerative energy.

$$E_{input} = \frac{E_{drivetrain}}{\eta_{cycle}} + E_{fulltime}\left(\frac{1}{\eta_{cycle}} - \eta_{electrolyser}\right) - E_{regeneration}\eta_{electrolyser} \tag{20}$$

3.7. Scheme 4 engine cases

The advantage to operating an engine unthrottled is that its efficiency can be improved, due to the reduction in pumping losses. However driving cycle requirements mean that a realistic vehicle engine must have a wide power band. Power control with an unthrottled engine can be accomplished by two methods:

- using lean equivalence ratios. (method 1)

and/or

- dividing engine power between the drivetrain and an electrolyser (method 2).

With an engine operating at full load, and a fixed hydrogen fraction, it is possible to select an operating condition with the lowest *BSFC* based on equivalence ratio alone. Typically, the lowest *BSFC* (at each engine speed) occurs at slightly lean equivalence ratios from 0.8 to 0.9 regardless of fuel type. However, to achieve low power by method 1, it is necessary to use equivalence ratios near the partial burn limit where the *BSFC* may be as much as 3 times higher.

Method 2 suggests that instead of lowering the engine power, it can be uniformly high, with a portion being sent to the wheels, or the electrolyser based on driver input. In this manner, the engine can be run consistently at the equivalence ratio where the best *BSFC* is found. The drawback is that the greater the amount of power produced by the engine (and the greater amount of power sent to the electrolyser), the greater its fuel consumption will be. It is necessary to determine if the increase in engine efficiency, and the production of hydrogen by the electrolyser, is enough to compensate for the increase in fuel consumption.

With scheme 4, the engine is to operate at full load (wide open throttle) at all speeds. The power sent to the drivetrain is controlled by a combination of equivalence ratio and full-time electrolyser power. A hydrogen fraction of 43% is chosen for demonstration purposes, as this is the largest fraction that can be used premixed and therefore is applicable to both engine schemes 2 and 3. Figure 3.36 shows a power map of the unthrottled model engine at 1000RPM. It can be seen that for $f = 0.43$, at arbitrarily selected points W, X, Y, & Z the engine is producing powers of 9.6kW, 13.9kW, 17.3kW and 21.1kW respectively. Point W represents operation at the partial burn limit, while point Z represents operation at the lowest *BSFC*.

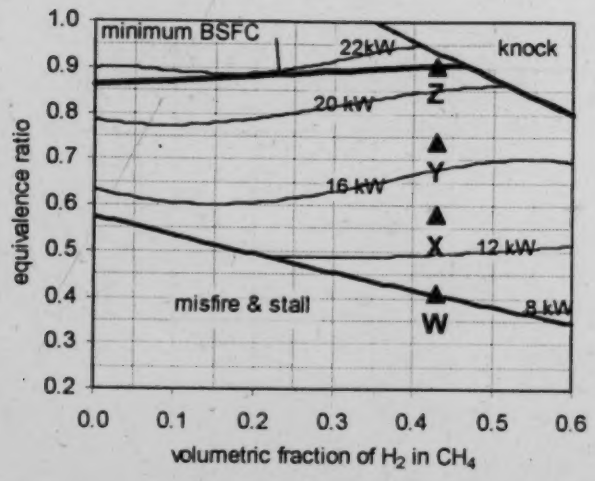

Figure 3.36. Model engine power map at 1000RPM and full load. The contour lines represent equal power. The power increases with equivalence ratio with the minimum *BSFC* occurring between the 20kW and 22kW.

Figure 3.37 shows the corresponding *BSFC* map for the model engine operating unthrottled at 1000RPM. It can be seen that point W has the highest *BSFC* while point Z has the lowest. This is a reflection of the improved combustion efficiency as the equivalence ratio approaches 0.8 to 0.9.

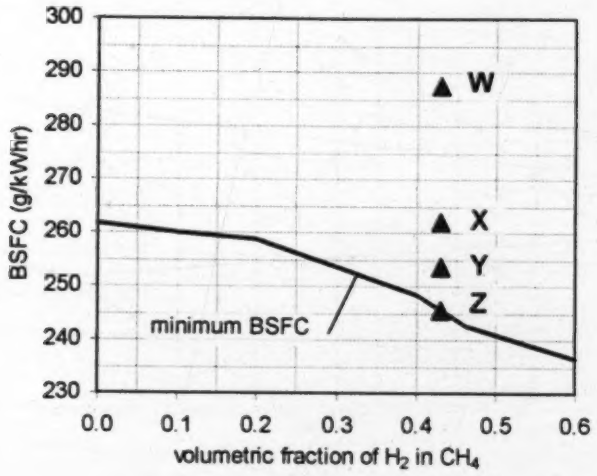

Figure 3.37. Model engine brake specific fuel consumption map at 1000RPM and full load. Point W has the highest *BSFC* and Point Z has the lowest (at a hydrogen fraction of 0.43).

At all points W to Z, the engine power exceeds the 5kW criterion established previously at 1000RPM, necessitating a split between power sent to the drivetrain and to the electrolyser. As the line of minimum *BSFC* from point W to Z is approached, the power produced by the engine increases. Therefore, when operating at point Z, a greater amount of engine power is sent to the electrolyser than at point W, so that drivetrain power is maintained at 5kW at 1000RPM.

At 1800RPM and full pedal, the engine must still meet the requirement of 35kW, making point K (as seen in Figure 3.12) the only one possible to meet this criteria at full load and $f = 0.43$. Therefore, all scheme 4 cases go through point K at 1800RPM. All scheme 4 cases employ full-time and regenerative power supplied to the electrolyser[7].

In scheme 4 cases, the operational equivalence ratio alone determines the brake specific fuel consumption and production of pollutants. As the equivalence ratio approaches the line of best fuel consumption, $BSCO_2$ and *BSHC* decrease due to improving combustion efficiency. *BSCO* is insignificant as long as equivalence ratios are kept below 0.95. However, *BSNO* increases as the line of best *BSFC* is approached, as its peak is reached around equivalence ratios from 0.8 to 0.9.

[7] Increased vehicle mass due to the electrolyser and its components is not considered here.

As seen in Figure 3.38, case W-K uses a constant hydrogen fraction of 0.43 at full load, with the equivalence ratio increasing from 0.42 to 0.93 as the pedal is increased from 0 to 1. Since the engine produces 9.6kW at 1000RPM and zero pedal, its power is split between the electrolyser (4.6kW) and the drivetrain (5kW). The electrolyser power decreases linearly to 0kW as the pedal is depressed. Due to the use of equivalence ratios near the partial burn limit, a noticeable increase in *BSFC*, $BSCO_2$, *BSCO*, and *BSHC* can be seen at low pedal positions. *BSNO* peaks as the equivalence ratio passes through 0.8 to 0.9.

Compared to case W-K, several trends can be noted for cases X-K (Figure 3.39), Y-K (Figure 3.40), and Z-K (Figure 3.41). Although the fraction of hydrogen remains constant, the equivalence ratios used (at low pedal positions) increase from case W-K to Z-K. For case Z-K, the equivalence ratio is nearly constant with pedal position. Consequently, the power supplied to the electrolyser progressively increases[8], but the *BSFC* decreases from case W-K to Z-K. For case Z-K, *BSFC* essentially reaches the lowest possible with scheme 4. Other trends as the cases go from W-K to Z-K, are decreasing $BSCO_2$, *BSCO*, and *BSHC*, but increasing *BSNO* due to the use of equivalence ratios between 0.8 and 0.9. At full pedal and 1800RPM, all the cases are operating at the same point.

[8] Electrolyser power also increases with engine speed for cases X-K, Y-K and Z-K to account for the increasing power as equivalence ratios approach 0.93.

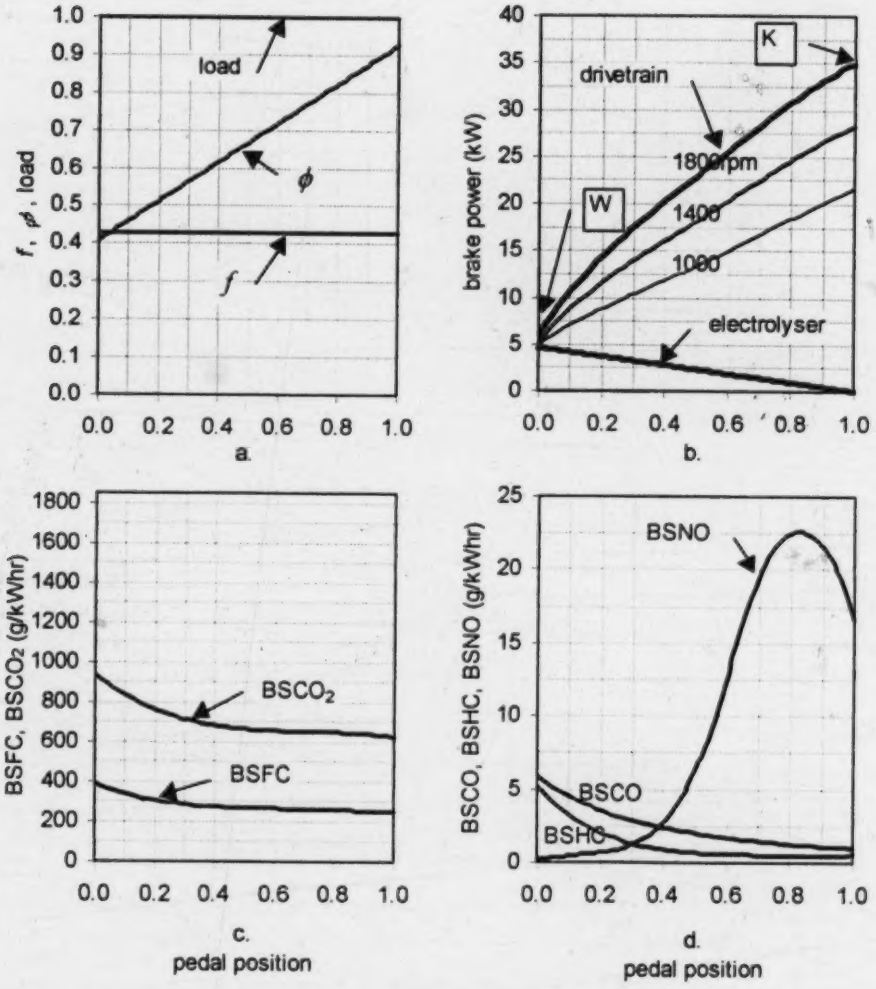

Figure 3.38. Engine case W-K operation with respect to pedal position. (a.) Operation at full load with f=0.43 and $0.41 < \phi < 0.93$. (b.) Engine power is divided between the drivetrain and the electrolyser. (c.) Resultant *BSFC* and $BSCO_2$ at 1800RPM. (d.) Resultant *BSCO*, *BSHC* and *BSNO* at 1800RPM.

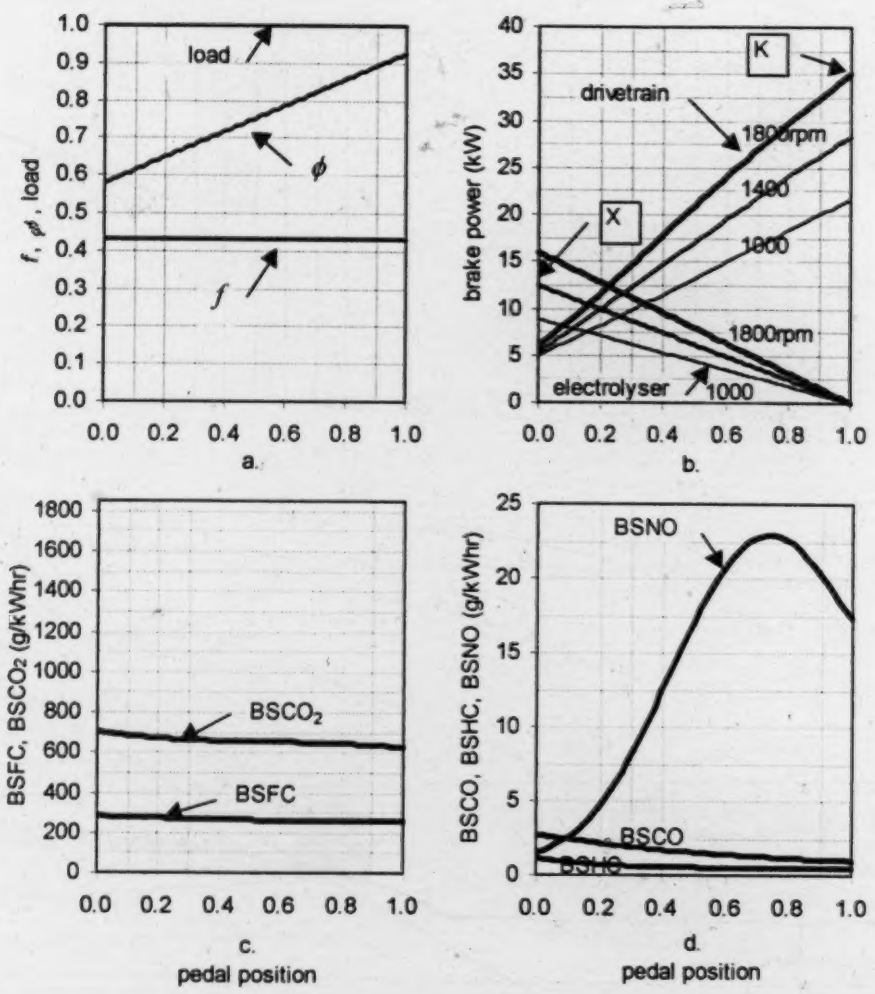

Figure 3.39. Engine case X-K operation with respect to pedal position. (a.) Operation at full load with f=0.43 and $0.58 < \phi < 0.93$. (b.) Engine power is divided between the drivetrain and the electrolyser. (c.) Resultant *BSFC* and $BSCO_2$ at 1800RPM. (d.) Resultant *BSCO*, *BSHC* and *BSNO* at 1800RPM.

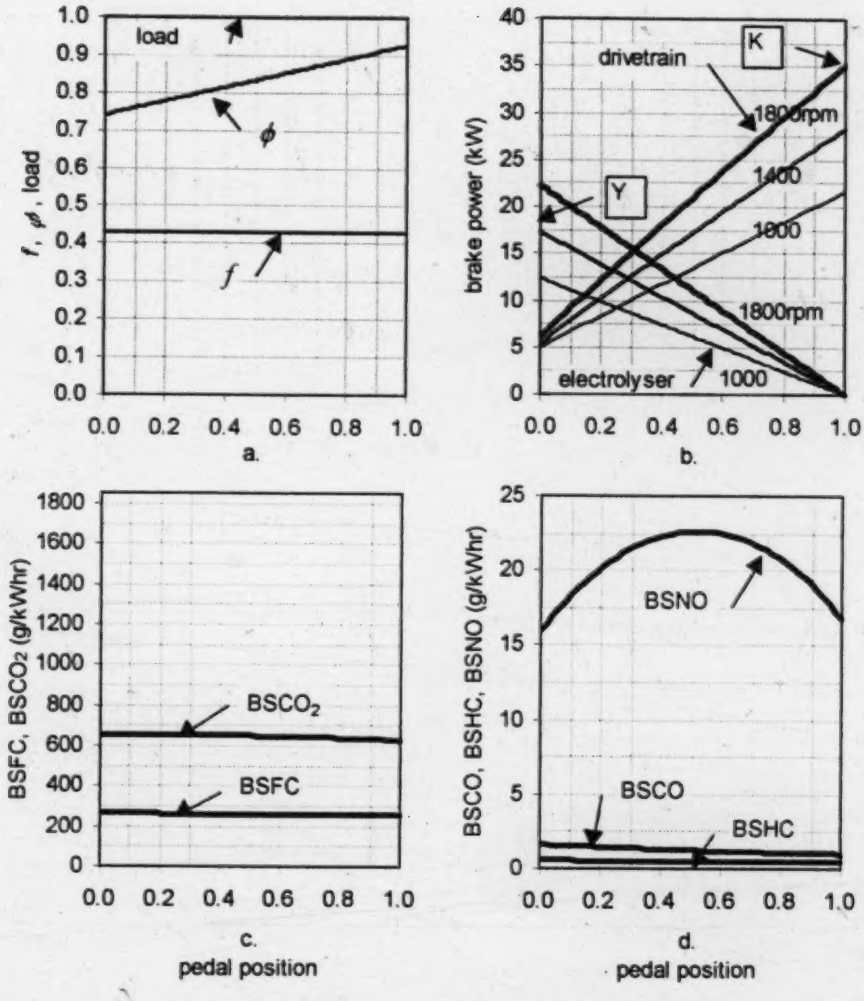

Figure 3.40. Engine case Y-K operation with respect to pedal position. (a.) Operation at full load with f=0.43 and $0.74 < \phi < 0.93$. (b.) Engine power is divided between the drivetrain and the electrolyser. (c.) Resultant *BSFC* and $BSCO_2$ at 1800RPM. (d.) Resultant *BSCO*, *BSHC* and *BSNO* at 1800RPM.

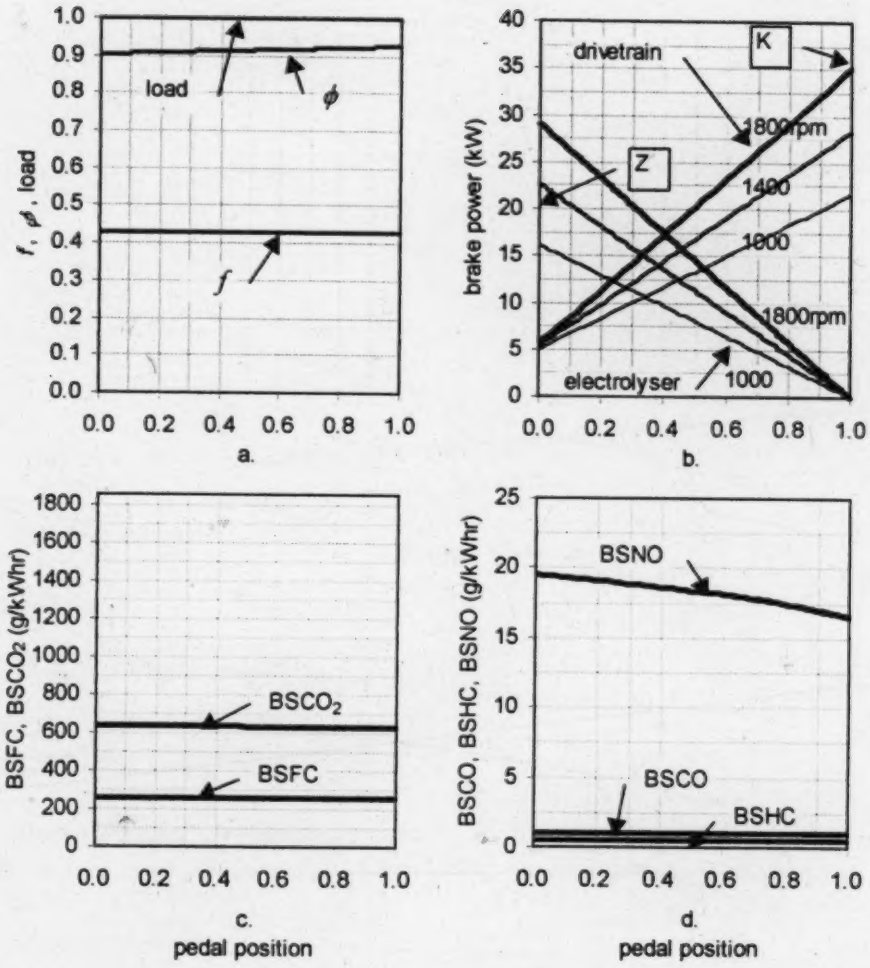

Figure 3.41. Engine case Z-K operation with respect to pedal position. (a.) Operation at full load with f=0.43 and $0.90 < \phi < 0.93$. (b.) Engine power is divided between the drivetrain and the electrolyser. (c.) Resultant *BSFC* and $BSCO_2$ at 1800RPM. (d.) Resultant *BSCO*, *BSHC* and *BSNO* at 1800RPM.

Note that for each case the power provided to the electrolyser decreases with increasing pedal position. Therefore, when peak power is required, the portion of engine power sent to the drivetrain is larger.

3.8. Scheme 4 cumulative driving cycle results

Scheme 4 cases (W-K, X-K, Y-K, and Z-K) are different from scheme 1, 2 and 3 cases in that they both consume and produce hydrogen. These cases use a constant hydrogen fraction of 43% but consumption and production of hydrogen is not the same for each, due to changing power sent to the electrolyser. Since the drivetrain power with respect to pedal is nearly equal for all cases, the pedal position with respect to time is consistent for each driving cycle. However, cumulative engine energy output is different depending on the amount of power provided to the electrolyser for each case. At no time during any of the driving cycles does the electrolyser production of hydrogen equal that consumed by the engine. Hence, on-board hydrogen storage is still necessary. The regenerative power delivered to the electrolyser is different for each driving cycle, but maximum regenerative power is the same for all limited to 6.88kW. The regenerative power supplied during a driving cycle is not dependent on which engine case is used, as it depends only on vehicle braking. Maximum electrolyser input power is limited to 30kW, at which point hydrogen production is 0.13g/s due to the maximum current density of the electrodes. Production of CO is negligible for all cases, due to use of equivalence ratios below 0.95.

3.8.1. SAE J-227D cumulative results

It can be seen in Figure 3.42 that for case W-K, a maximum engine output of 30kW is required to satisfy the driving cycle. At this point the peak hydrogen consumption is 0.20g/s. The case uses the least amount of engine power for the electrolyser. Full time electrolyser power varies from 2kW to 4kW, which results in a hydrogen production rate from 0.01g/s to 0.02g/s. Regenerative power appears when the vehicle is braking, and is limited to its maximum cutoff power of 6.88kW. During this time, the production of hydrogen from regenerative power reaches a maximum of 0.03g/s.

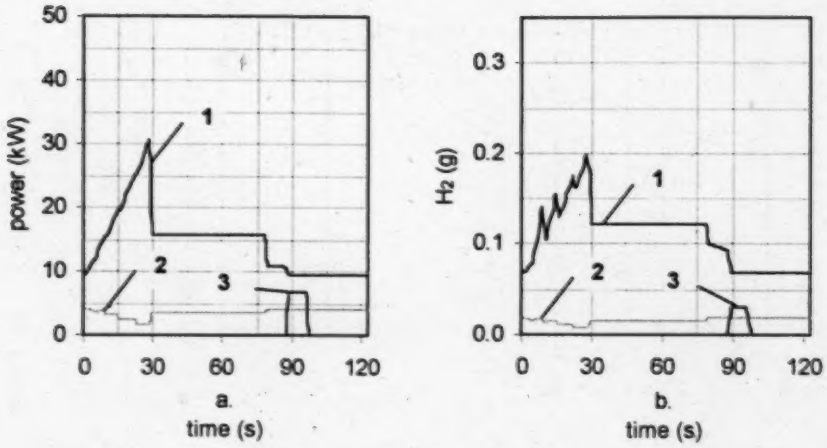

Figure 3.42. Case W-K SAE-J-227D schedule second-by-second engine / electrolyser power, and hydrogen consumption / production. (a.) (1.) Total engine power. (2.) Full-time engine power supplied to the electrolyser. (3.) Regenerative braking power supplied to the electrolyser. (b.) (1.) Engine consumption of hydrogen. (2.) Electrolyser full-time hydrogen production. (3.) Regenerative hydrogen production.

Case X-K (compared to case W-K), sends more engine power to the electrolyser. It can be seen in Figure 3.43 that, compared to case W-K, the peak engine power rises to 35kW (for the same driving cycle), due to increased electrolyser power. Peak hydrogen consumed by the engine increases to 0.22g/s, while full time hydrogen production ranges from 0.03g/s to 0.06g/s. Regenerative hydrogen produced is unchanged at a maximum of 0.03g/s during braking.

The electrolyser power progressively increasing in case Y-K (Figure 3.44) and then case Z-K (Figure 3.45) increases both hydrogen production, and hydrogen consumption. Case Y-K full time hydrogen production varies from 0.03g/s to 0.09g/s, while peak consumption is 0.23g/s. Case Z-K full time hydrogen production varies from 0.04g/s to 0.12g/s but peak consumption increases to 0.25g/s. For case Z-K, the electrolyser consumes anywhere from 17% to 42% of the total engine power.

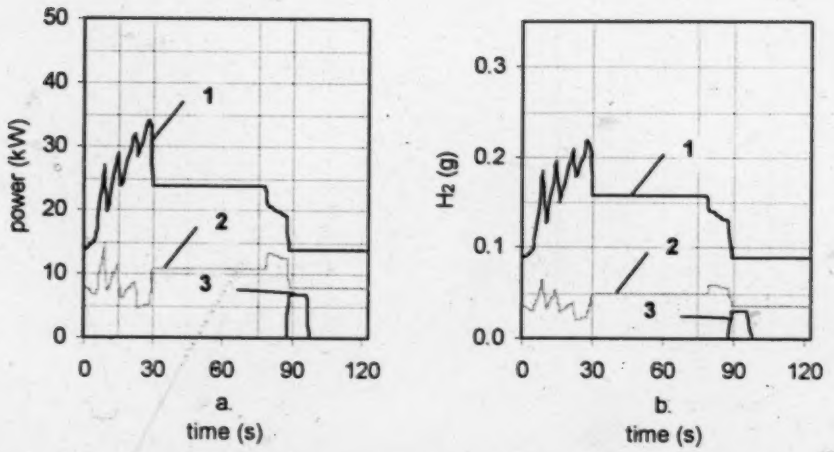

Figure 3.43. Case X-K SAE-J-227D schedule second-by-second engine / electrolyser power, and hydrogen consumption / production. (**a**.) (1.) Total engine power. (2.) Full-time engine power supplied to the electrolyser. (3.) Regenerative braking power supplied to the electrolyser. (**b**.) (1.) Engine consumption of hydrogen. (2.) Electrolyser full-time hydrogen production. (3.) Regenerative hydrogen production.

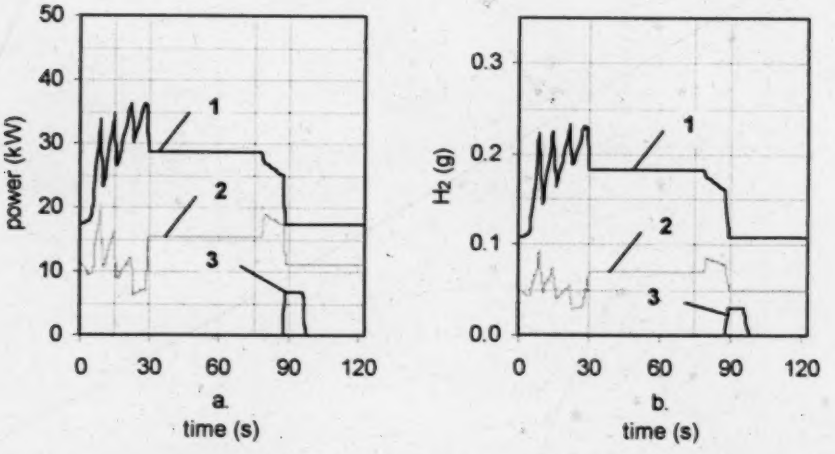

Figure 3.44. Case Y-K SAE-J-227D schedule second-by-second engine / electrolyser power, and hydrogen consumption / production. (**a**.) (1.) Total engine power. (2.) Full-time engine power supplied to the electrolyser. (3.) Regenerative braking power supplied to the electrolyser. (**b**.) (1.) Engine consumption of hydrogen. (2.) Electrolyser full-time hydrogen production. (3.) Regenerative hydrogen production.

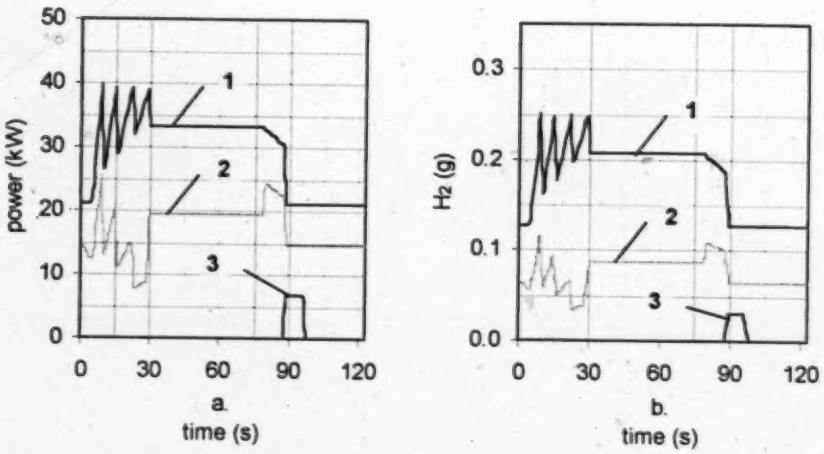

Figure 3.45. Case Z-K SAE-J-227D schedule second-by-second engine / electrolyser power, and hydrogen consumption / production. (**a**.) (1.) Total engine power. (2.) Full-time engine power supplied to the electrolyser. (3.) Regenerative braking power supplied to the electrolyser. (**b**.) (1.) Engine consumption of hydrogen. (2.) Electrolyser full-time hydrogen production. (3.) Regenerative hydrogen production.

Along with hydrogen, the consumption of methane, and production of pollutants changes depending on the engine case. Generally, peak consumption of fuel and pollutant production occurs at the peak required power. Peak methane consumption is smallest for case W-K (2.1g/s) and largest for case Z-K (2.6g/s) despite improving *BSFC*. Likewise, production of CO_2 is largest for case Z-K (7.0g/s). HC production is highest for case W-K (0.016g/s) when equivalence ratios near the partial burn limit are used. Peak NO production is highest for case Z-K (0.23g/s) due to operating at equivalence ratios from 0.90 to 0.93 where combustion temperatures are high. (The second-by second results for each case fuel consumption and pollutant production can be seen in Appendix E.)

Figure 3.46 shows the cumulative hydrogen production and consumption results for SAE J-227D. Scheme 2 case E-K is included for comparison purposes, as it also uses a constant hydrogen fraction of 0.43 but has no electrolyser. The overall impact of adding an electrolyser is to increase the cumulative engine energy from approximately 800kJ/km (case E-K) to 2300kJ/km (case Z-K). For case Z-K, the electrolyser is producing approximately 6g/km over the entire cycle. However, increasing the

cumulative engine energy increases the amount of hydrogen consumed, from approximately 8g/km (case E-K) to 14g/km (case Z-K). The cumulative amount of regenerative hydrogen produced is relatively small at approximately 0.17g/km, and is the same regardless of engine operating case. When the total hydrogen is considered (engine consumption minus electrolyser production), the cumulative effect is neutral (i.e. total hydrogen consumed is a relatively consistent 8g/km for each engine case).

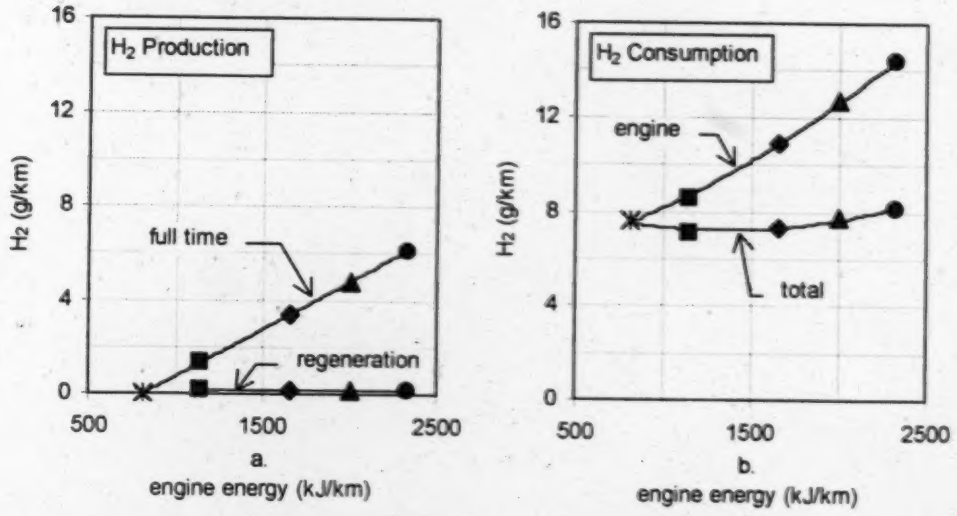

Figure 3.46. SAE-J-227D cumulative hydrogen production and consumption with respect to engine energy for cases E-K (✱), W-K (■), X-K (◆), Y-K (▲), and Z-K (●). (a.) Cumulative hydrogen production from full time and regenerative power. (b.) Cumulative hydrogen consumption by the engine and total hydrogen consumption (consumption – production).

If only hydrogen consumption was considered, the overall effect of the electrolyser could be described as neutral (i.e. does not provide a benefit or a disadvantage with respect to hydrogen consumption). However, since the engine is operating at 43% hydrogen, the remainder of the fuel is methane. Therefore, the methane consumption also increases with electrolyser power.

Figure 3.47 shows the cumulative effect of cases W-K, X-K, Y-K, and Z-K on fuel consumption and pollutant production with respect to total hydrogen consumption for the SAE-J-227D schedule. The previous scheme 1, 2, and 3 cases are represented by

best-fit linear equations as described in section 3.5.1. For equal amounts of total hydrogen consumed, case E-K (no electrolyser) shows the lowest methane consumption and CO_2 production, while case Z-K (with the greatest electrolyser power) shows the highest. CO production is low for all scheme 4 cases regardless of electrolyser power, as equivalence ratios used are below 0.95. Generally, unburned hydrocarbons are large for case W-K, as the equivalence ratios include those near the partial burn limit of 0.41. However, cases X-K, Y-K, and W-K generally show low HC emissions due to the use of equivalence ratios from 0.7 to 0.9. Unfortunately, the use of these equivalence ratios results in an increase in cumulative NO produced as case Z-K is approached. It is important to note that as predicted the cycle efficiency (defined by equation 12) increases from 17% (for scheme 2 and 3 cases) to approximately 21% to 26% for scheme 4 cases. This represents a cumulative increase in fuel usage efficiency by the engine. However, this increase in efficiency is not enough to make up for the increased fuel consumption due to power supplied to the electrolyser. The cumulative electrolyser efficiency (as defined by equation 19) for the entire driving cycle is approximately 54% for each case.

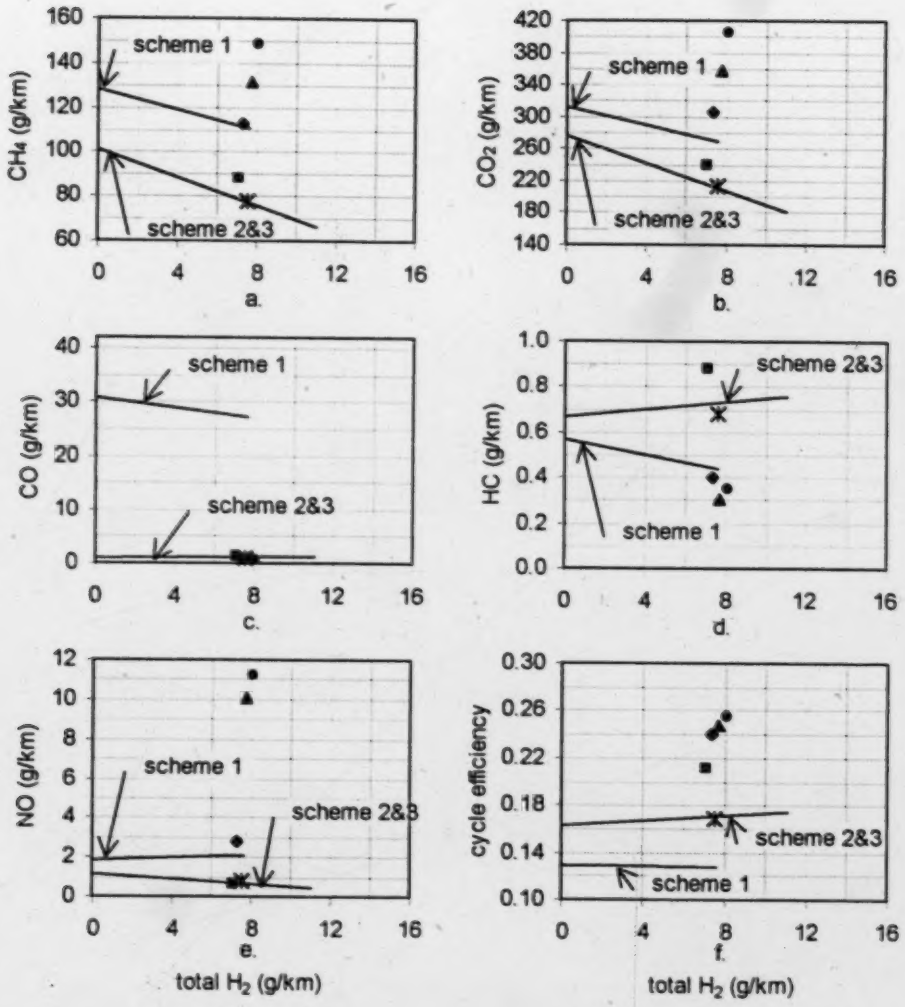

Figure 3.47. SAE-J-227D cumulative fuel consumption and pollutant production with respect to total hydrogen consumption for cases E-K (✱), W-K (■), X-K (◆), Y-K (▲), and Z-K (●). (a.) CH_4 consumption. (b.) CO_2 production. (c.) CO production. (d.) HC production. (e.) NO production (f.) cycle efficiency.

3.8.2. Highway schedule cumulative results

The highway schedule is similar to SAE-J-227D in that the peak power required is close to the same value. However, it is different in that there are more engine power

and speed combinations over a longer time. Generally high engine speeds, required powers and pedal positions are found in the highway schedule.

It can be seen in Figure 3.48 that for case W-K, a maximum engine output of 29kW is required to satisfy the driving cycle. At this point the peak hydrogen consumption is 0.19g/s. Full time power consumed by the electrolyser again varies from 2kW to 4kW, which results in a production rate from 0.01g/s to 0.02g/s. Regenerative power is developed when the vehicle is braking, again limited to a maximum cutoff power of 6.88kW, during which the production of hydrogen from regenerative power reaches a maximum of 0.03g/s.

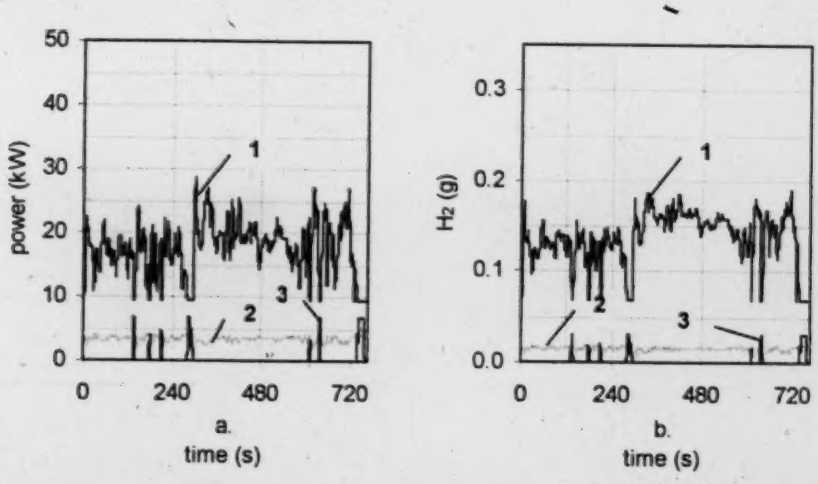

Figure 3.48. Case W-K Highway schedule second-by-second engine / electrolyser power, and hydrogen consumption / production. (**a**.) (1.) Total engine power. (2.) Full-time engine power supplied to the electrolyser. (3.) Regenerative braking power supplied to the electrolyser. (**b**.) (1.) Engine consumption of hydrogen. (2.) Electrolyser full-time hydrogen production. (3.) Regenerative hydrogen production.

For case X-K, the peak engine power rises to 35kW due to increased power delivered to the electrolyser as seen in Figure 3.49. Peak hydrogen consumed by the engine increases to 0.23g/s, while full time hydrogen production ranges from 0.03g/s to 0.07g/s.

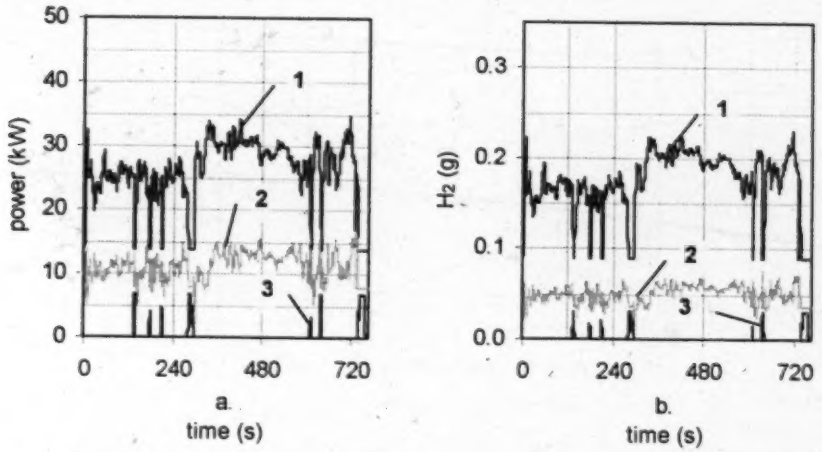

Figure 3.49. Case X-K Highway schedule second-by-second engine / electrolyser power, and hydrogen consumption / production. (**a**.) (1.) Total engine power. (2.) Full-time engine power supplied to the electrolyser. (3.) Regenerative braking power supplied to the electrolyser. (**b**.) (1.) Engine consumption of hydrogen. (2.) Electrolyser full-time hydrogen production. (3.) Regenerative hydrogen production.

With the electrolyser power progressively increasing in case Y-K (Figure 3.50), and Z-K (Figure 3.51) increasing hydrogen production and consumption is again seen. Case Y-K peak full time hydrogen production increases to 0.10g/s, while peak consumption increases to 0.25g/s. Case Z-K peak full time hydrogen production increases to 0.13g/s, at which point (based on electrolyser design), it is limited by electrode current density. Peak hydrogen consumption increases to 0.28g/s for case Z-K. From peak to idle, the case Z-K electrolyser consumes anywhere from 15% to 42% of the total engine power.

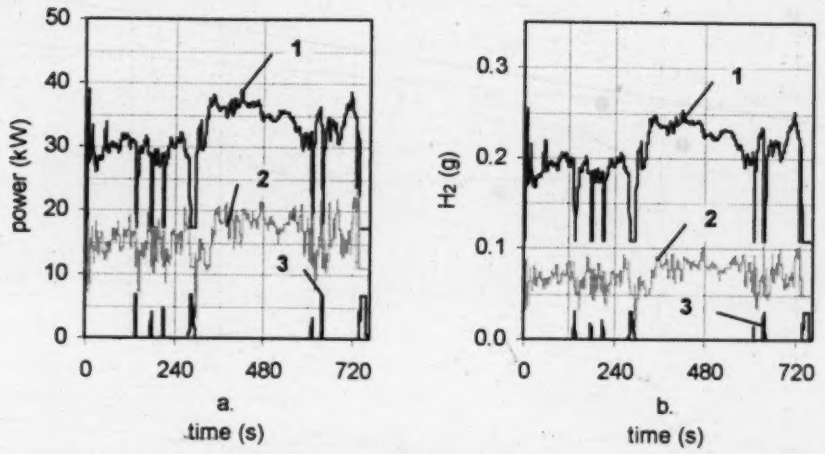

Figure 3.50. Case Y-K Highway schedule second-by-second engine / electrolyser power, and hydrogen consumption / production. (a.) (1.) Total engine power. (2.) Full-time engine power supplied to the electrolyser. (3.) Regenerative braking power supplied to the electrolyser. (b.) (1.) Engine consumption of hydrogen. (2.) Electrolyser full-time hydrogen production. (3.) Regenerative hydrogen production.

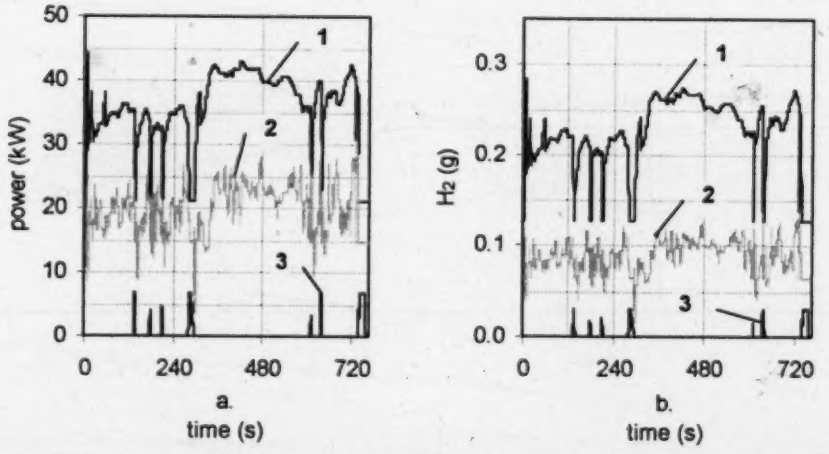

Figure 3.51. Case Z-K Highway schedule second-by-second engine / electrolyser power, and hydrogen consumption / production. (a.) (1.) Total engine power. (2.) Full-time engine power supplied to the electrolyser. (3.) Regenerative braking power supplied to the electrolyser. (b.) (1.) Engine consumption of hydrogen. (2.) Electrolyser full-time hydrogen production. (3.) Regenerative hydrogen production.

Along with hydrogen, the consumption of methane, and production of pollutants is again different for each case. Peak methane consumption is smallest for case W-K

(2.0g/s) and largest for case Z-K (3.0g/s) despite improving BSFC. Likewise, production of CO_2 is largest for Z-K (8.0g/s). HC production is highest for W-K (0.018g/s) when equivalence ratios near the partial burn limit are used. Peak NO production is highest for Z-K (0.29g/s) due to operating at equivalence ratios from 0.90 to 0.93 where combustion temperatures are high. (The second-by second results for each case fuel consumption and pollutant production can be seen in Appendix E.)

Figure 3.52 shows the cumulative hydrogen production and consumption results for the Highway schedule. The overall impact of adding an electrolyser is again shown to increase the cumulative engine energy from approximately 600kJ/km (case E-K) to 1600kJ/km (case Z-K). For case Z-K, the cumulative electrolyser production is highest at approximately 4g/km. Increasing the engine energy causes an increase in the hydrogen consumed, from approximately 6g/km (case E-K) to 10.5g/km (case Z-K). Cumulative regenerative hydrogen produced is relatively small at approximately 0.08g/km, and is the same for all cases as it is not dependent on the engine operating case. Hydrogen production by regenerative braking is smallest for the Highway schedule, as there is less braking over the distance traveled. When the total hydrogen is considered (engine consumption minus electrolyser production), the cumulative effect is again neutral (i.e. total hydrogen consumed is relatively stable around 6g/km).

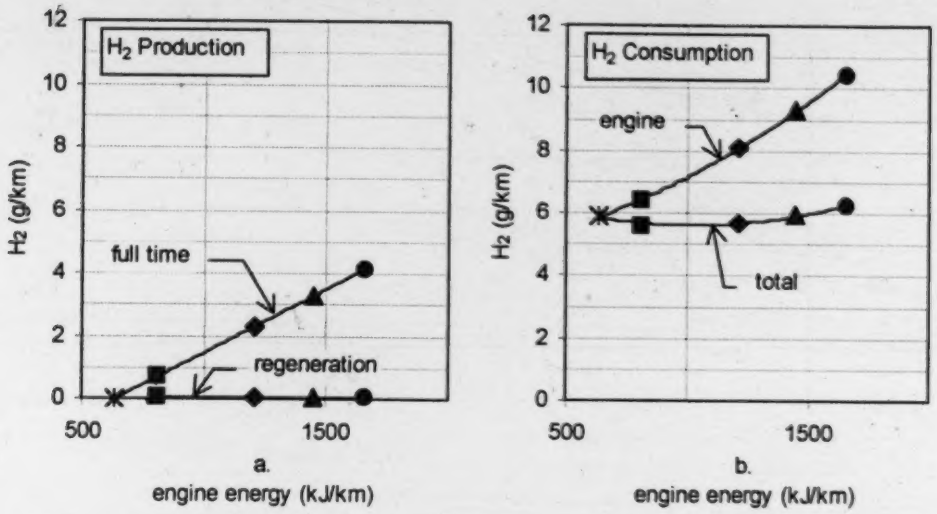

Figure 3.52. Highway cumulative hydrogen production and consumption with respect to engine energy for cases E-K (✱), W-K (■), X-K (◆), Y-K (▲), and Z-K (●). (**a**.) Cumulative hydrogen production from full time and regenerative power. (**b**.) Cumulative hydrogen consumption by the engine and total hydrogen consumption (consumption – production).

Figure 3.53 shows the Highway schedule cumulative effect of cases W-K, X-K, Y-K, and Z-K on fuel consumption and pollutant production with respect to total hydrogen consumption. The previous scheme 1, 2, and 3 cases are represented by best-fit linear equations as described in section 3.5.2. Again, for equal amounts of total hydrogen consumed, case E-K (no electrolyser) shows the lowest methane consumption and CO_2 production, while case Z-K (greatest electrolyser power) shows the highest. Again, unburned hydrocarbons are lowest for case W-K, as the equivalence ratios used are near the partial burn limit, and highest for case Z-K, where the equivalence ratios used are from 0.90 to 0.93. However, for case Z-K, the equivalence ratios used results in a substantial increase in cumulative NO produced. Again, cycle efficiency (as defined by equation 12) increases from 17% (for scheme 2 and 3 cases) to approximately 25% as case Z-K is approached. This increase in efficiency is not enough to make up for the increased fuel consumption due to power supplied to the electrolyser. The cumulative electrolyser efficiency (defined by equation 19) is approximately 54% for each case.

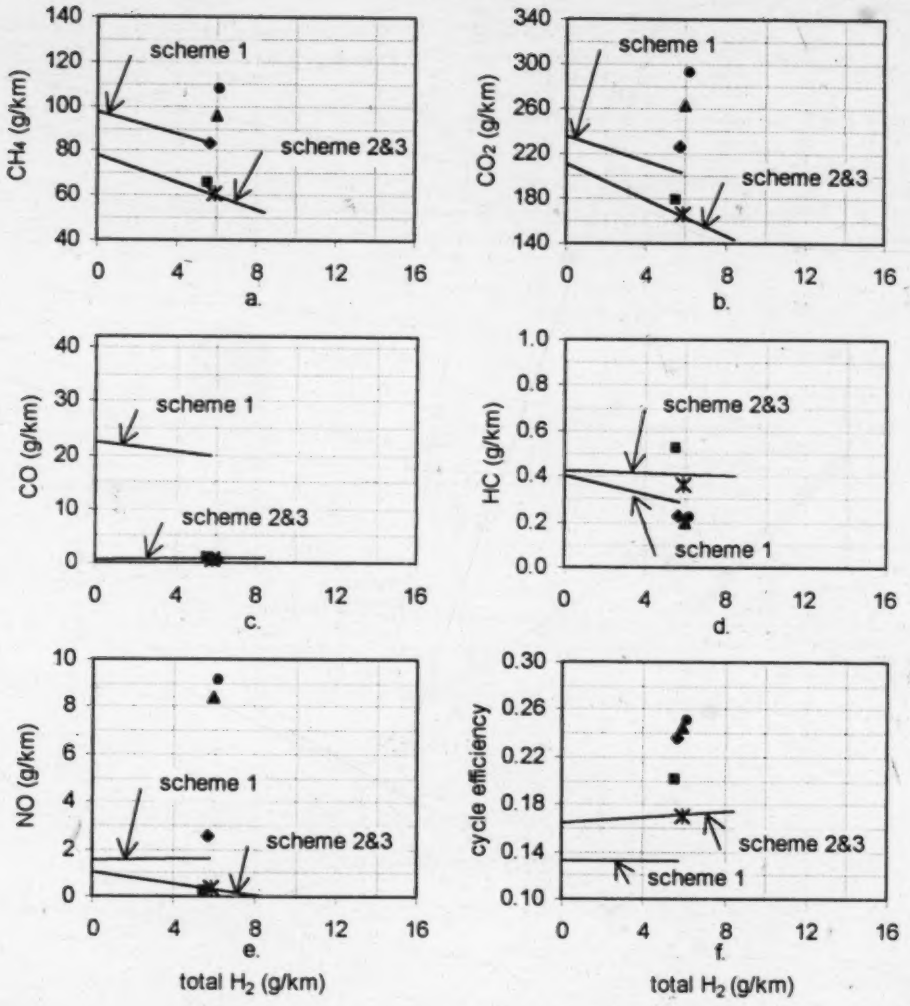

Figure 3.53. Highway cumulative fuel consumption and pollutant production with respect to total hydrogen consumption for cases E-K (✱), W-K (■), X-K (◆), Y-K (▲), and Z-K (●). (a.) CH_4 consumption. (b.) CO_2 production. (c.) CO production. (d.) HC production. (e.) NO production (f.) cycle efficiency.

3.8.3. Urban schedule cumulative results

The Urban schedule is different from the Highway schedule in that there is higher power required of the engine, and there are many more periods of idle. Generally, the Urban schedule has lower average engine speeds, required powers, and consequently pedal positions.

It can be seen for case W-K (Figure 3.54) that a maximum engine output of 36kW is required to satisfy the driving cycle. At this point the peak hydrogen consumption is 0.25g/s. Full time power consumed by the electrolyser varies from 2kW to 4kW, which results in a production rate from 0.01g/s to 0.02g/s. Compared to the Highway schedule, regenerative power is developed more frequently, but again limited to a maximum cutoff power of 6.88kW. During this time, the production of hydrogen from regenerative power reaches a maximum of 0.03g/s. Regenerative hydrogen produced is the same regardless of engine case.

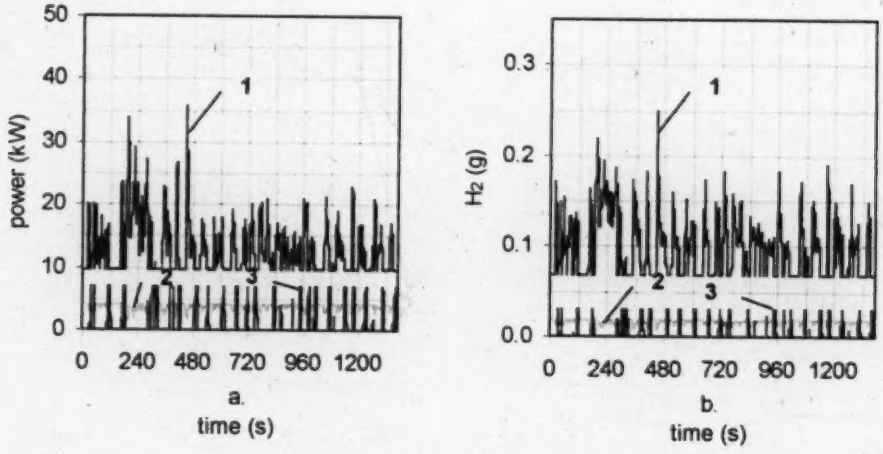

Figure 3.54. Case W-K Urban schedule second-by-second engine / electrolyser power, and hydrogen consumption / production. (a.) (1.) Total engine power. (2.) Full-time engine power supplied to the electrolyser. (3.) Regenerative braking power supplied to the electrolyser. (b.) (1.) Engine consumption of hydrogen. (2.) Electrolyser full-time hydrogen production. (3.) Regenerative hydrogen production.

For case X-K (Figure 3.55), the peak engine power rises to 43kW due to increased electrolyser power. Consequently full time hydrogen production ranges from 0.03g/s to 0.07g/s, but peak hydrogen consumption increases to 0.29g/s.

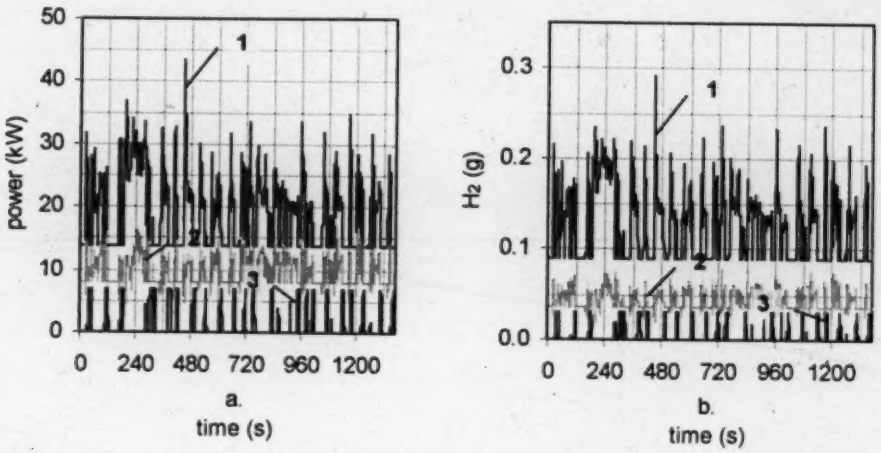

Figure 3.55. Case X-K Urban schedule second-by-second engine / electrolyser power, and hydrogen consumption / production. (**a**.) (1.) Total engine power. (2.) Full-time engine power supplied to the electrolyser. (3.) Regenerative braking power supplied to the electrolyser. (**b**.) (1.) Engine consumption of hydrogen. (2.) Electrolyser full-time hydrogen production. (3.) Regenerative hydrogen production.

With the electrolyser power progressively increasing in case Y-K (Figure 3.56), and Z-K (Figure 3.57) it is again seen that there is a corresponding increase in hydrogen production and consumption. Case Y-K peak full time hydrogen production increases to 0.10g/s, while peak consumption increases to 0.31g/s. For case Z-K, peak consumption increases to 0.33g/s, and the electrolyser consumes anywhere from 14% to 42% of the total engine power. Consequently, case Z-K full time production ranges from 0.03g/s to a maximum of 0.13g/s, at which point it is limited by electrode current density.

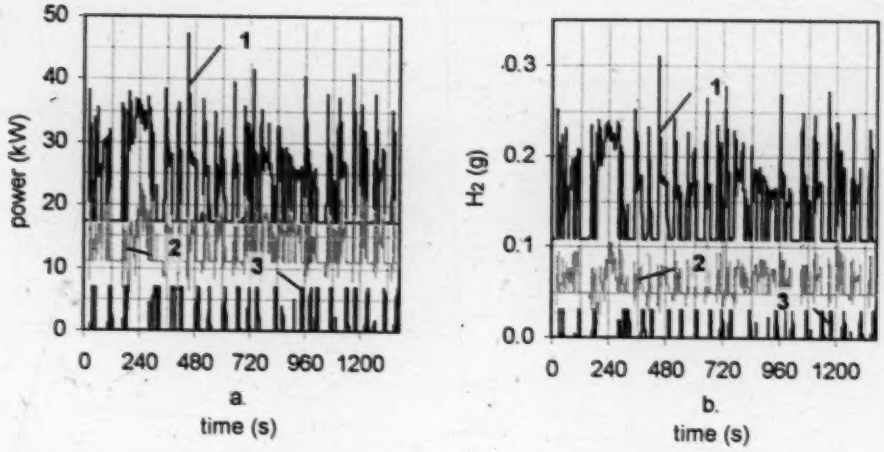

Figure 3.56. Case Y-K Urban schedule second-by-second engine / electrolyser power, and hydrogen consumption / production. (**a**.) (1.) Total engine power. (2.) Full-time engine power supplied to the electrolyser. (3.) Regenerative braking power supplied to the electrolyser. (**b**.) (1.) Engine consumption of hydrogen. (2.) Electrolyser full-time hydrogen production. (3.) Regenerative hydrogen production.

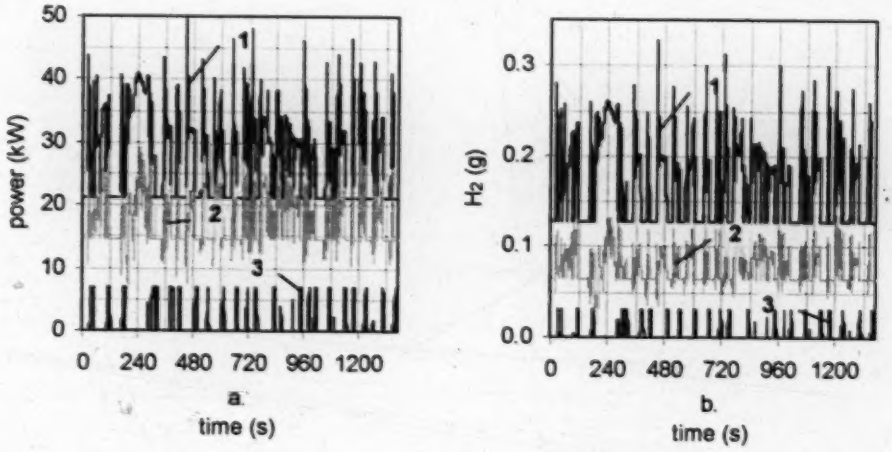

Figure 3.57. Case Z-K Urban schedule second-by-second engine / electrolyser power, and hydrogen consumption / production. (**a**.) (1.) Total engine power. (2.) Full-time engine power supplied to the electrolyser. (3.) Regenerative braking power supplied to the electrolyser. (**b**.) (1.) Engine consumption of hydrogen. (2.) Electrolyser full-time hydrogen production. (3.) Regenerative hydrogen production.

Again, the consumption of methane, and production of pollutants is different for each case. Peak methane consumption is again smallest for case W-K (2.6g/s) and largest for case Z-K (3.4g/s) despite improving BSFC. Likewise, production of CO_2 is largest for Z-K (9.0g/s). HC production is highest for W-K (0.019g/s) when equivalence ratios near the partial burn limit are used, peak NO production is highest for Z-K (0.35g/s) due to operating at equivalence ratios from 0.90 to 0.93. (The second-by second results for each case fuel consumption and pollutant production can be seen in Appendix E.)

Figure 3.58 shows the cumulative hydrogen production and consumption results for the Urban schedule. The overall impact of adding an electrolyser is to increase the cumulative engine energy from approximately 1000kJ/km (case E-K) to 3100kJ/km (case Z-K). For case Z-K, the cumulative electrolyser production is highest at approximately 9g/km. However, increasing the engine energy causes an increase in the amount of hydrogen consumed, from approximately 10g/km (case E-K) to 20g/km (case Z-K). Cumulative regenerative hydrogen produced is still relatively small at approximately 0.46g/km, despite the increased frequency of braking. When the total hydrogen is considered (engine consumption minus electrolyser production), the cumulative effect is once again relatively neutral (i.e. total hydrogen consumed is relatively stable around 10g/km.

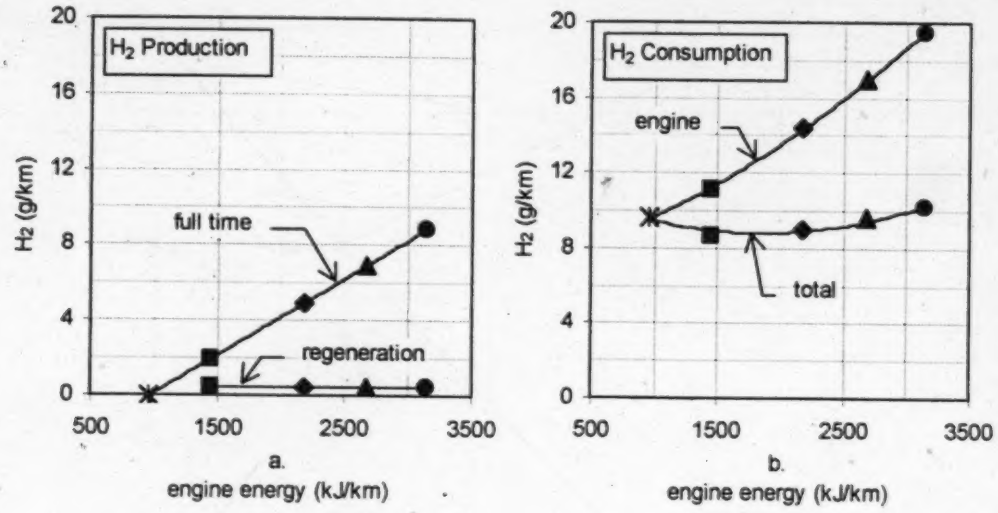

Figure 3.58. Urban cumulative hydrogen production and consumption with respect to engine energy for cases E-K (✱), W-K (■), X-K (●), Y-K (▲), and Z-K (●). (a.) Cumulative hydrogen production from full time and regenerative power. (b.) Cumulative hydrogen consumption by the engine and total hydrogen consumption (consumption – production).

Figure 3.59 shows the cumulative effect of cases W-K, X-K, Y-K, and Z-K on fuel consumption and pollutant production with respect to total hydrogen consumption for the Urban schedule. The previous scheme 1, 2, and 3 cases are represented by best-fit linear equations as described in section 3.5.3. Similar to the results for the other schedules, for equivalent total hydrogen consumed, case E-K (no electrolyser) shows the lowest methane consumption and CO_2 production, while case Z-K (greatest electrolyser power) shows the highest. Again, case W-K shows the greatest production of unburned hydrocarbons while case Z-K shows the greatest production of NO. The cycle efficiency (as defined by equation 12) increases from 16% (for scheme 2 and 3 cases) to approximately 26% for case Z-K. Again, this increase in efficiency is not enough to make up for the increased fuel consumption due to power supplied to the electrolyser. The cumulative electrolyser efficiency (defined by equation 19) for the entire driving cycle is approximately 54% for each case.

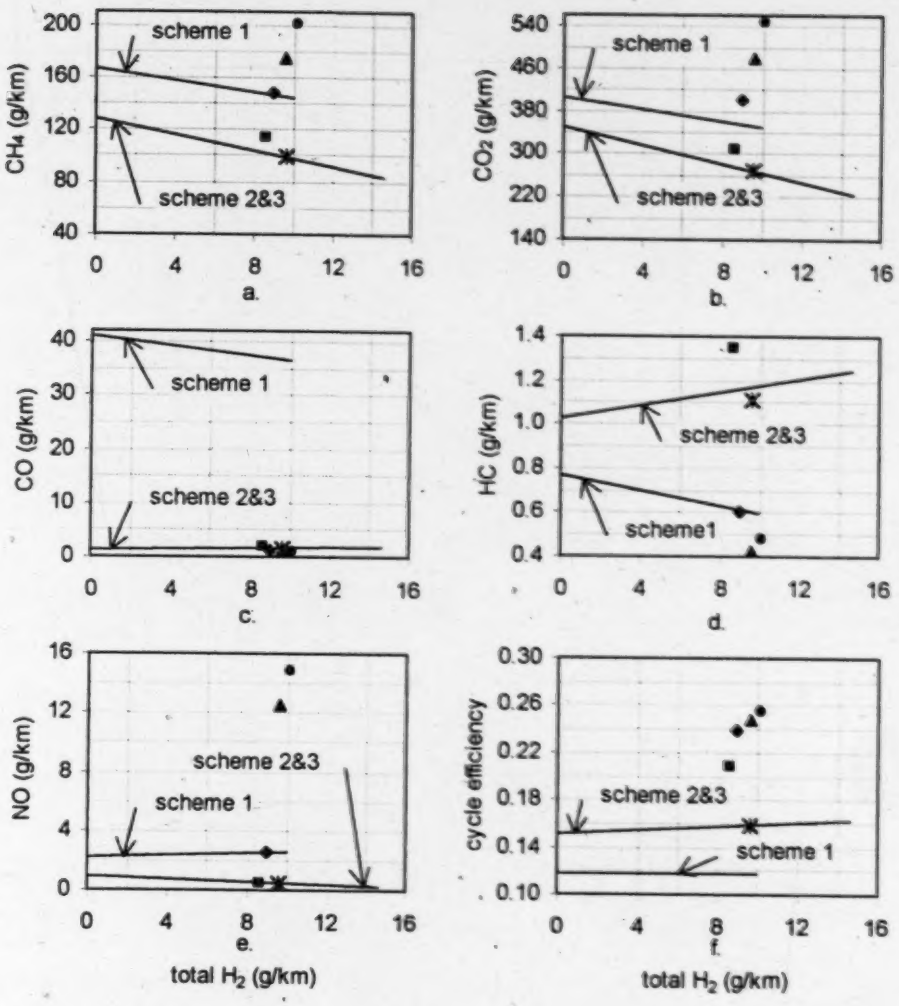

Figure 3.59. Urban cumulative fuel consumption and pollutant production with respect to total hydrogen consumption for cases E-K (✱), W-K (■), X-K (◆), Y-K (▲), and Z-K (●). (a.) CH_4 consumption. (b.) CO_2 production. (c.) CO production. (d.) HC production. (e.) NO production (f.) cycle efficiency.

3.9. Conclusions and recommendations

Although only a simulation, the driving cycle model vehicle and selected engine cases have provided several noticeable trends and conclusions. In general, hydrogen addition was found to be beneficial, both in terms of its potential to reduce methane consumption and pollutant production. The driving cycle simulation revealed the following important trends:

1. The relative effect of hydrogen addition is consistent regardless of driving cycle used. For example, for every g/km of hydrogen addition to scheme 1, the methane consumption decreased by 2.43g/km for the Highway schedule and 2.30g/km for the Urban schedule. A similar constancy also appears for pollutant production for each of the driving cycles examined. In this respect, it can be concluded that although the driving cycle may change the absolute value of fuel consumed and pollutant produced the relative effect of hydrogen addition remains consistent.
2. Using a pre-mixed fraction of hydrogen in the fuel and operating at stoichiometric equivalence ratios (scheme 1) reduces methane consumption 2.30g/km to 2.43g/km for every g/km of hydrogen addition. This is primarily a result of displacing methane with hydrogen. Due to a reduction of carbon present in the fuel, CO_2 is reduced 5.63g/km to 5.67g/km, CO is reduced 0.44g/km to 0.46g/km, and HCs are reduced approximately 0.02g/km with every g/km of hydrogen addition. However, NO is increased approximately 0.02g/km to 0.03g/km with every g/km of hydrogen addition due to increasing flame temperatures. The cycle efficiency is approximately 12% to 13%.
3. Modifying the engine to use lean equivalence ratios (partial burn limit $< \phi < 1.0$), enables higher engine loads and less throttling (scheme 2). This increases cycle efficiency to 15% to 17%. Compared to scheme 1 operation, scheme 2 operation consumes 20% to 32% less methane, and produces 11% to 25% less CO_2 for equal amounts of hydrogen addition (in g/km). CO production is reduced by 96% to 98% due to the use of equivalence ratios below 0.95. However, unburned hydrocarbon production is higher by 5% to 97%, due to the use of ultra-lean equivalence ratios near the partial burn limit. Peak production rates of NO are higher, but on a

cumulative basis, NO decreases by 31% to 84% due to lower overall combustion temperatures at lean equivalence ratios. Also, a lean strategy allows the use of higher pre-mixed hydrogen fractions before the knock limit is reached.

In scheme 2 engines, every g/km of hydrogen addition reduces CH_4 consumption 2.97g/km to 3.12g/km, and reduces CO_2 production 7.94g/km to 8.69g/km due to direct displacement of the CH_4 fuel, and increasing cycle efficiency. HC production increases approximately 0.02g/km due to the progressively leaner equivalence ratios used with every g/km of hydrogen addition. However, this leaning of equivalence ratio decreases NO production from 0.05g/km to 0.12g/km for every g/km of hydrogen addition. CO produced is negligible

4. Mixing hydrogen and methane fuel on-board allows greater hydrogen fractions and leaner equivalence ratios to be used before knock limitations are reached (scheme 3). Scheme 3 appears to have no appreciable difference with respect to the cumulative fuel consumption or pollutant production over scheme 2 operation. However, the use of greater hydrogen fractions (up to 60% by volume), allows 44% to 51% more hydrogen to be used during a driving cycle. If the hydrogen storage capability permits, this allows a further reduction in methane consumption.
5. Dividing the engine power between an electrolyser and the drivetrain allows the engine to be operated at full load (scheme 4). This increases the cycle efficiency to 20% to 25%. However, the additional power used by the electrolyser consumes more fuel than is produced, despite increased cycle efficiency. At no time does the hydrogen produced by the electrolyser equal or exceed that consumed by the engine when $f = 0.43$. The model electrolyser efficiency is approximately 54%.
6. The cumulative hydrogen produced by regenerative braking power is a small fraction (1% to 4%) of that consumed by the engine when $f = 0.43$. On a cumulative basis, the model electrolyser running off regenerative braking produces 0.17g/km in the SAE-J-227D schedule, 0.08g/km in the Highway schedule and 0.46g/km in the Urban schedule.

Implementing a lean strategy (scheme 2) has an equal or greater effect on NGV operation than the addition of hydrogen alone. The lean strategy also provides the most

benefit with the least increase in complexity and is therefore the superior operating system. However, the results in this study were obtained using data from a one-cylinder CFR engine. In order to refine the model, additional testing should be done on a production engine to determine the impact of:

1. friction power, as the CFR engine's high friction power would tend to overestimate the difference between scheme 1 and scheme 2 operation.
2. multi-cylinder effects, where the equivalence ratio may change from cylinder to cylinder.
3. transient effects, when changing the pedal position rapidly can result in the equivalence ratio varying too rich or too lean of the target.
4. operation at ultra-lean equivalence ratios, where the cycle to cycle variability may be unacceptably high for vehicle use.
5. thermal efficiency differences based on engine design, when small changes in thermal efficiency can have a major impact on fuel consumption (see Appendix F).
6. operating system design, including control of fuel flow, equivalence ratio, and throttle position by electronically or hydraulically actuated valves linked to the pedal position and "programmed" with respect to engine speed.
7. reduced catalytic converter efficiency, due to lower exhaust temperatures during lean operation.

References

1. Jamai, Y., M.L. Wyszynski, "On-Board Generation of Hydrogen-Rich Gaseous Fuels – A Review", *Int. J. Hydrogen Energy*, Vol.19, No.7, pp. 557-572, 1994
2. Winter, C., J. Nitsch, Hydrogen as an Energy Carrier, Springer-Verlag, 1988, pp. 209-231
3. DeLuchi, M.A., "Hydrogen Vehicles: An Evaluation of Fuel Storage Performance, Safety, Environmental Impacts, and Cost", *Int. J. Hydrogen Energy*, Vol.14, No.2, pp. 81-130, 1989
4. Norbeck, J.M, Hydrogen Fuel for Surface Transportation, Society of Automotive Engineers, 1996, pp. 75-93
5. Kukkonen, C.A., M. Shelef, "Hydrogen as an Alternative Automotive Fuel: 1993 Update", SAE 940766, 1994
6. Lewis, von Elbe, Combustion, Flames and Explosions of Gases, 3rd Ed., Academic Press, 1987, pp. 246-248
7. Das, L.M., "Hydrogen Engines: A View of the Past and a Look into the Future", *Int. J. Hydrogen Energy*, Vol.15, No.6, pp. 425-443, 1990
8. Peschka, W., Liquid Hydrogen – Fuel of the Future, Springer-Verlag, 1992, pp. 283-286
9. Heywood, J.B., Internal Combustion Engine Fundamentals, McGraw-Hill, 1988, pp. 424-427
10. Ibid., pp. 457-458
11. Stebar, R.F., F.B. Parks, "Emission Control with Lean Operation Using Hydrogen-Supplemented Fuel", SAE 740187, 1974
12. Parks, F.B., "A Single-Cylinder Engine Study of Hydrogen-Rich Fuels", SAE 760099, 1976
13. Varde, K.S., "Combustion Characteristics of Small Spark Ignition Engines Using Hydrogen Supplemented Fuel Mixtures", SAE 810921, 1981
14. Houseman, J., F.W. Hoehn, "A Two-Charge Engine Concept: Hydrogen Enrichment", SAE 741169, 1974

15. Finegold, J.G., "Hydrogen: Primary or Supplementary Fuel for Automotive Engines", SAE 760609, 1976

16. Raman, V., J. Hansel, J. Fulton, F. Lynch, and D. Bruderly, "Hythane – An Ultraclean Transportation Fuel", Hydrogen Fuel For Surface Transportation, SAE Publication, 1996, pp. 47-56

17. Nagalingam, B., F. Duebel, K. Schmillen, "Performance Study using Natural Gas, Hydrogen Supplemented Natural Gas and Hydrogen in AVL Research Engine", *Int. J. Hydrogen Energy*, Vol.8, No.9, pp. 715-720, 1983

18. Kyaw, Z.H., "Chemical Control of S.I. Engine Combustion", Ph.D. Thesis, Department of Mechanical and Manufacturing Engineering, The University of Melbourne, 1992, pp. 38-45

19. Swain, M.R., M.J. Yusuf, Z. Dulger, M.N. Swain, "The Effects of Hydrogen Addition on Natural Gas Engine Operation", SAE 932775, 1993

20. Karim, G.A., I. Wierzba and Y. Al-Alousi, "Methane-Hydrogen Mixtures as Fuels", *Int. J. Hydrogen Energy*, Vol.21, No.7, pp. 625-631, 1996

21. Cattelan, A., J. Wallace, "Exhaust Emission and Energy Consumption Effects from Hydrogen Supplementation of Natural Gas", SAE 952497, 1995

22. Collier, K., R.L. Hoekstra, N. Mulligan, C. Jones, D. Hahn, "Untreated Exhaust Emissions of a Hydrogen-Enriched CNG Production Engine Conversion", SAE 960858, 1996

23. Hoekstra, R.L., P. Van Blarigan, N. Mulligan, "NO_x Emissions and Efficiency of Hydrogen, Natural Gas, and Hydrogen / Natural Gas Blended Fuels", SAE 961103, 1996

24. Heywood, pp. 149-151

25. Ibid., pp. 577-578

26. Lewis, pp. 395-403

27. Heywood, pp. 830-831

28. Ibid., pp. 81-82

29. Ibid., pp. 592-595

30. Ibid., pp. 596

31. Ibid., pp. 611-613

32. Ibid., pp. 578-585

33. Ibid., pp. 102, 304-307

34. Ibid., pp. 582-585

35. Hacohen, J., G. Pinhasi, Y. Putterman and E. Sher, "Driving Cycle Simulation of a Vehicle Motored by a S.I. Engine Fuelled with H_2-Enriched Gasoline", *Int. J. Hydrogen Energy*, Vol.16, No.10, pp. 695-702, 1991

36. "Emission Test Driving Schedules – SAEJ1506 Apr93: SAE Information Report", 1996 SAE Handbook, Vol.1, pp. 13.135-142, 1996

37. Sovran, G., M.S. Bohn, "Formulae for the Tractive Energy Requirements of Vehicles Driving the EPA Schedules", SAE 810184, 1981

38. Norbeck, pp. 16-22

39. Schafer, F., "An Investigation of the Addition of Hydrogen to Methanol on the Operation of an Unthrottled Otto Engine", SAE 810776, 1981

40. Beck, N.J., W.P. Johnson, P.W. Peterson, "Optimized E.F.I. for Natural Gas Fueled Engines," SAE 911650, 1991

41. Canada, Industrial Programs Branch, "International New Vehicle Emissions Standards (Internal Report)", Unpublished report by N. Ostrouchov, (Ottawa: Environment Canada)

42. Winter, pp. 178

43. Bohacik, T., S. DeMaria, C. Trowbridge, W. Saman, "Combustion Characteristics of Electrolytically Produced Hydrogen-Oxygen Mixtures", SAE 971703, 1997

44. Brinner, A., H. Bussmann, W. Hug, W. Seeger, "Test Results of the Hysolar 10 kW PV-Electrolysis Facility", *Int. J. Hydrogen Energy*, Vol.17, No.3, pp. 187-197, 1992

45. Hug, W., H. Bussmann, A. Brinner, "Intermittent Operation and Operation Modeling of an Alkaline Electrolyser", *Int. J. Hydrogen Energy*, Vol.18, No.12, pp. 973-977, 1993

46. Brossard, L., G. Belanger, G. Trudel, "Behavior of a 3 kW Electrolyser Under Constant and Variable Input", *Int. J. Hydrogen Energy*, Vol.9, No.1/2, pp. 67-72, 1984

47. Duckworth, V., K. Workun, D. Checkel, "The University of Alberta Hybrid Electric Vehicle Project Final Technical Report", SAE Publication SP-980, pp. 1-11, 1994

48. Checkel, M.D., V. E. Duckworth, J. B. Lybbert, V. Yung, "Development of the University of Alberta Entry for the 1994 HEV Challenge", SAE Publication SP-1103, pp. 1-13, 1995

49. Yung, V., et al., "Development of the University of Alberta Entry in the 1995 Hybrid Electric Vehicle Challenge", The 1995 HEV Challenge, SAE Publication SP-1170, pp.111-124

50. Yung, V., "Energy and Emissions of a Range-Extending HEV", M.Sc. Thesis, Department of Mechanical Engineering, The University of Alberta, 1997, pp. 62-64

Appendix A. CFR engine raw data

Unreduced data are given here for the CFR engine test. All pollutant results are obtained as dry percent volumetric fraction of the exhaust. NO_x values were not obtained for the 60% hydrogen mixture, as the NO_x analyzer was unavailable at this time. Data for part load tests can be seen in Table A.1 for 700RPM and in Table A.2 for 900RPM. Part load tests were taken at approximately 2/3 and 1/3 throttle opening. Data for the full load tests can be seen in Table A.3 for 700RPM and in Table A.4 for 900RPM. Full load tests were performed at wide open throttle.

Table A.1. Part load data for CFR engine testing at 700RPM.

speed (rpm)	f (% vol)	spark (°BTDC)	CO_2 (%)	CO (%)	O_2 (%)	HC (ppmC6)	NO_x (ppm)	bp (kW)	m_{air} (g/s)
700	0.0	12	10.65	0.28	1.17	77	1950	1.25	2.17
		12	9.70	0.03	3.23	61	2299	1.10	2.20
		14	9.05	0.03	4.40	60	1846	1.01	2.21
		20	7.91	0.04	6.46	66	605	0.85	2.22
		22	10.65	0.15	1.32	94	1474	0.72	1.69
		25	9.81	0.04	3.08	67	1362	0.61	1.71
		13	9.06	0.04	4.56	67	773	0.54	1.72
		12	8.13	0.04	6.16	72	348	0.43	1.73
	19.8	10	10.16	0.07	1.32	55	2714	1.56	2.42
		11	8.76	0.03	4.25	46	2741	1.33	2.47
		13	7.83	0.03	5.87	46	1340	1.19	2.50
		17	6.72	0.03	8.22	55	354	0.97	2.53
		21	9.84	0.81	1.17	84	1256	0.74	1.68
		30	9.56	0.03	2.64	58	1874	0.66	1.70
		10	8.29	0.04	5.14	54	727	0.52	1.73
		11	6.85	0.04	7.93	71	108	0.34	1.76
	39.9	8	8.97	1.15	1.03	71	1416	1.10	1.97
		8	9.45	0.04	1.48	51	2639	1.06	2.00
		8	7.80	0.03	4.88	39	1634	0.84	2.03
		9	6.45	0.03	7.69	46	263	0.62	2.07
		11	9.09	0.97	1.03	71	1128	0.69	1.62
		10	8.98	0.03	2.66	47	2045	0.62	1.67
		11	7.61	0.03	5.47	39	725	0.45	1.70
		13	6.42	0.03	7.83	49	131	0.33	1.71

Table A.2. Part load data for CFR engine testing at 900RPM.

speed (rpm)	f (% vol)	spark (°BTDC)	CO_2 (%)	CO (%)	O_2 (%)	HC (ppmC6)	NO_x (ppm)	bp (kW)	m_{air} (g/s)
900	0.0	14	10.60	0.26	1.34	77	2236	1.61	2.79
		17	8.92	0.03	4.76	51	1496	1.25	2.84
		22	7.79	0.04	6.85	63	596	1.06	2.90
		24	8.29	3.98	1.19	132	240	0.53	1.86
		30	10.35	0.04	2.09	73	1886	0.47	1.88
		15	9.33	0.04	3.96	57	1231	0.41	1.89
		14	8.01	0.04	6.46	69	226	0.25	1.93
	19.8	12	9.15	1.90	1.03	78	886	1.51	2.66
		13	9.19	0.03	3.25	45	2398	1.30	2.71
		14	6.99	0.04	7.69	56	331	0.89	2.78
		16	6.32	0.04	9.01	64	103	0.75	2.81
		18	9.67	1.10	1.03	76	1081	0.68	1.89
		25	9.33	0.03	3.25	47	1459	0.54	1.94
		13	8.33	0.03	5.17	43	792	0.43	1.96
		13	7.23	0.04	7.25	57	246	0.29	1.98
	39.9	10	9.32	0.54	1.03	59	2137	1.29	2.40
		10	8.95	0.03	2.66	38	3441	1.17	2.44
		10	8.05	0.03	4.44	33	2337	1.02	2.46
		10	7.20	0.03	6.21	34	991	0.85	2.51
		11	8.72	1.47	1.03	68	1026	0.63	1.81
		11	9.58	0.10	1.18	57	2000	0.60	1.83
		12	8.36	0.03	3.84	32	1825	0.46	1.87
		13	7.13	0.03	6.36	38	390	0.28	1.89
	60.0	7	7.32	1.68	0.92	60	n/a	1.47	2.59
		7	8.14	0.50	0.92	52	n/a	1.50	2.56
		8	7.89	0.02	2.13	39	n/a	1.40	2.59
		8	6.79	0.02	4.87	27	n/a	1.16	2.64
		8	5.20	0.03	8.68	35	n/a	0.79	2.74
		9	4.38	0.03	10.65	48	n/a	0.57	2.77
		10	7.60	1.35	0.92	61	n/a	0.55	1.75
		11	8.33	0.31	0.92	55	n/a	0.57	1.76
		13	7.15	0.03	4.11	32	n/a	0.37	1.78
		14	5.92	0.04	7.16	30	n/a	0.13	1.83

Table A.3. Full load data for CFR engine testing at 700RPM.

speed (rpm)	f (% vol)	spark (°BTDC)	CO_2 (%)	CO (%)	O_2 (%)	HC (ppmC6)	NO_x (ppm)	bp (kW)	m_{air} (g/s)
700	0.0	12	9.56	2.40	0.90	84	544	1.97	2.64
		12	10.53	0.03	1.93	57	4069	1.91	2.67
		14	9.13	0.03	4.47	47	3725	1.68	2.71
		20	7.35	0.04	7.75	64	1020	1.35	2.79
		22	6.83	0.04	8.64	75	485	1.22	2.82
		25	6.50	0.04	9.23	90	112	1.19	2.83
		13	8.54	3.68	1.02	89	290	2.03	2.75
		12	9.63	1.99	1.02	69	773	2.05	2.78
		12	10.42	0.70	1.02	67	1731	2.06	2.78
		12	10.34	0.02	2.06	51	3146	1.95	2.79
		13	9.66	0.02	3.23	46	3142	1.83	2.83
		15	8.76	0.03	4.99	46	2282	1.69	2.87
		18	7.84	0.03	6.75	51	849	1.51	2.91
	19.8	10	9.86	0.50	1.64	67	3578	1.98	2.76
		11	9.30	0.02	3.42	49	4621	1.85	2.81
		13	8.14	0.03	5.59	45	3118	1.66	2.87
		17	6.91	0.03	7.91	48	683	1.39	2.93
		21	6.06	0.04	9.50	69	132	1.25	2.97
		30	4.95	0.04	11.59	105	52	0.95	3.01
		10	8.77	2.50	1.02	70	555	2.04	2.72
		11	7.21	4.84	1.02	103	150	1.96	2.69
		10	9.61	1.18	1.02	67	1278	2.04	2.73
		11	9.69	0.02	2.35	45	3659	1.92	2.78
		12	8.67	0.02	4.25	42	3198	1.75	2.82
		14	7.92	0.03	5.87	41	1676	1.60	2.85
		18	6.64	0.03	8.37	56	342	1.35	2.92
	39.9	8	8.18	2.27	1.03	68	689	1.95	2.62
		8	8.76	1.45	1.03	56	1120	1.96	2.64
		8	9.54	0.09	1.18	47	2812	1.95	2.66
		9	8.88	0.02	2.66	34	3893	1.82	2.69
		11	7.96	0.02	4.59	32	3436	1.66	2.74
		10	8.37	0.02	3.55	34	4242	1.72	2.72
		11	7.57	0.02	5.33	33	2777	1.58	2.76
		13	6.68	0.02	7.25	33	1011	1.43	2.82
		18	5.59	0.03	9.46	51	137	1.17	2.89
		23	4.83	0.03	11.09	69	55	1.00	2.94
		33	3.95	0.05	12.71	98	37	0.75	2.99
	60.0	5	7.38	1.55	0.75	49	n/a	1.89	2.53
		5	7.96	0.73	0.75	44	n/a	1.90	2.54
		6	7.82	0.02	2.26	30	n/a	1.80	2.59
		6	8.30	0.03	1.05	35	n/a	1.86	2.57
		7	7.40	0.02	3.17	25	n/a	1.71	2.62
		9	6.43	0.02	5.59	21	n/a	1.51	2.70
		12	5.61	0.02	7.70	24	n/a	1.34	2.76
		15	4.96	0.02	9.21	33	n/a	1.19	2.81
		17	4.49	0.02	10.28	43	n/a	1.05	2.85
		19	4.12	0.02	11.18	48	n/a	0.96	2.87
		23	3.49	0.03	12.54	61	n/a	0.76	2.93
		33	2.83	0.07	13.90	92	n/a	0.54	2.99
		36	2.65	0.09	14.35	101	n/a	0.47	3.00

Table A.4. Full load data for CFR engine testing at 900RPM.

speed (rpm)	f (% vol)	spark (°BTDC)	CO_2 (%)	CO (%)	O_2 (%)	HC (ppmC6)	NO_x (ppm)	bp (kW)	m_{air} (g/s)
900	0.0	14	10.53	0.03	1.93	53	3961	2.33	3.37
		17	8.71	0.03	5.21	52	2298	1.92	3.46
		22	7.47	0.04	7.59	62	841	1.65	3.53
		24	7.27	0.03	7.86	62	698	1.58	3.53
		30	6.35	0.04	9.67	91	160	1.36	3.58
		15	8.08	4.26	1.04	96	243	2.43	3.48
		14	9.18	2.59	1.04	78	615	2.48	3.49
		14	9.84	1.60	1.04	65	1092	2.51	3.50
		14	10.47	0.59	1.04	60	1922	2.54	3.50
		14	10.44	0.03	1.79	50	3279	2.43	3.52
		15	9.79	0.02	2.98	38	3521	2.30	3.55
		16	8.98	0.02	4.62	39	2616	2.11	3.59
	19.8	12	8.98	1.98	1.09	73	1695	2.47	3.39
		13	9.37	0.03	3.27	54	4683	2.22	3.45
		14	8.80	0.03	4.35	52	4090	2.11	3.48
		16	7.85	0.03	6.14	44	1871	1.90	3.54
		18	7.00	0.03	7.74	45	756	1.69	3.58
		25	5.58	0.03	10.42	70	68	1.28	3.67
		13	7.62	4.26	1.03	86	263	2.45	3.41
		13	8.41	2.99	1.03	83	511	2.45	3.43
		13	9.76	0.97	1.03	58	1727	2.51	3.45
		13	10.21	0.07	1.33	55	3002	2.48	3.46
		13	9.55	0.02	2.52	46	4053	2.35	3.50
		14	8.75	0.02	4.14	36	3644	2.19	3.53
		16	8.05	0.02	5.47	30	2312	2.01	3.60
	39.9	10	8.04	2.44	1.05	61	754	2.39	3.32
		10	8.98	1.01	1.05	51	1712	2.41	3.33
		10	9.49	0.25	1.19	39	2561	2.41	3.35
		10	9.38	0.03	1.64	36	3613	2.36	3.36
		11	9.07	0.02	2.23	28	4129	2.30	3.39
		11	8.84	0.02	2.68	29	4219	2.24	3.40
		12	8.51	0.02	3.42	31	4237	2.18	3.42
		13	7.94	0.02	4.62	30	3727	2.06	3.47
		14	7.30	0.02	5.96	25	2413	1.89	3.52
		15	6.68	0.03	7.30	29	1057	1.74	3.55
		17	6.10	0.03	8.64	38	435	1.58	3.60
		19	5.70	0.03	9.39	43	189	1.45	3.63
		22	5.21	0.02	10.35	47	84	1.30	3.67
		23	4.80	0.03	11.09	64	46	1.16	3.71
		28	4.26	0.05	12.13	81	31	0.97	3.75
		33	4.10	0.05	12.42	89	28	0.89	3.76

Table A.4. **(Continued)** Full load data for CFR engine testing at 900RPM.

speed (rpm)	f (% vol)	spark (°BTDC)	CO_2 (%)	CO (%)	O_2 (%)	HC (ppmC6)	NO_x (ppm)	bp (kW)	m_{air} (g/s)
		7	7.40	1.55	0.76	52	n/a	2.30	3.20
		7	8.18	0.33	0.92	36	n/a	2.33	3.23
		8	8.26	0.03	1.23	30	n/a	2.30	3.25
		8	8.03	0.02	1.84	29	n/a	2.23	3.27
		8	7.77	0.02	2.29	29	n/a	2.18	3.28
		9	7.51	0.01	2.91	25	n/a	2.13	3.30
		10	7.06	0.02	4.14	26	n/a	2.02	3.34
900	60.0	11	6.47	0.02	5.52	23	n/a	1.87	3.39
		13	5.80	0.02	7.21	22	n/a	1.71	3.47
		14	5.42	0.02	8.28	26	n/a	1.58	3.50
		16	4.89	0.02	9.50	32	n/a	1.40	3.56
		18	4.33	0.02	10.73	46	n/a	1.21	3.62
		22	3.87	0.02	11.81	54	n/a	1.02	3.66
		26	3.45	0.03	12.88	63	n/a	0.81	3.70
		35	2.78	0.07	14.16	82	n/a	0.52	3.75
		40	2.59	0.08	14.62	100	n/a	0.43	3.78

Appendix B. Uncertainty in CFR data

Uncertainty error was calculated assuming measurement uncertainty was the machine accuracy. When machine accuracy did not exist, they were estimated based on ½ of the smallest measurable increment. The estimated accuracies used were as follows:

1. Horiba™ NOx analyzer error

The manufacturer gave the machine error at 2% full scale. The dilution error was estimated by calibrating the water column at its largest observed deviation and noting the effect on the NO reading. The error due to spark was obtained by changing the spark by it's resolution (+/- 1deg) and noting the effect on the NO reading. It was necessary to use relative error values for NO, as its range varied from near zero to ~4000ppm.

$$\left(\frac{\varepsilon_{NO}}{NO}\right)_{machine} = +/- 0.02 \qquad \left(\frac{\varepsilon_{NO}}{NO}\right)_{dilution} = +/- 0.07$$

$$\left(\frac{\varepsilon_{NO}}{NO}\right)_{spark} = +/- 0.02$$

2. Snap-On™ gas analyzer error

The manufacturer gave the machine error for each concentration value. It was necessary to use relative error for CO, as its range varied from near zero to ~4%.

$$\varepsilon_{CO2} = +/- 0.4\ \% \qquad \frac{\varepsilon_{CO}}{CO} = +/- 0.10$$

$$\varepsilon_{O2} = +/- 0.2\ \% \qquad \varepsilon_{HC} = +/- 66\text{ppm}$$

3. Dynamometer error

The dynamometer error was estimated by observing the normal deviation on the digital readout.

$$\varepsilon_{power} = +/- 0.03\text{kW}$$

4. Air flow error

The air flow error was estimated from the error in room temperature and pressure and the resolution error in the reading scale.

$$\frac{\varepsilon_{mair}}{m_{air}} = +/- 0.02$$

5. Additional error

Additional error may have been caused by the cycle-to-cycle variation in readings. However, this effect was observed to be minimal as the single-cylinder engine combustion was stable above the partial burn limit (large deviations in readings were only observed below the partial burn limit). Error due to cycle-to-cycle variation is neglected in this analysis.

The mean square method was used to determine error with the basic formulation:

$$\varepsilon_q^{\,2} = \sum_{i=1}^{n} \left(\frac{\partial q}{\partial a_i} \right)^2 \varepsilon_i^{\,2}$$

$$q = q(a_1, a_2, a_3, \ldots, a_n)$$

The full load error is based on the estimated errors in the measured concentrations in the exhaust gas, and the mass flow rate of air, so that:

$$q = q(CO_2, CO, HC, NO, O_2, m_{air})$$

The part load value was represented as a percentage of the full load value. Therefore the error in the part load value was dependent on the estimated errors in the measured concentrations in the exhaust gas, the mass flow rate of air, and the estimated error found previously.

$$q = q(CO_2, CO, HC, NO, O_2, m_{air}, full.load.value)$$

The error in thermal efficiency was dependent on the estimated error in power, and the mass flow rate of air.

$$q = q(m_{air}, power)$$

The lower heating value does not contribute error, as the exact composition of the fuel was known.

B.1. Full Load Error

The equivalence ratio error varied from +/- 0.022 to +/- 0.045 as seen in Figure B.1. The error was due to uncertainties in the exhaust product concentrations. Error is highest where the concentration of CO_2 is low.

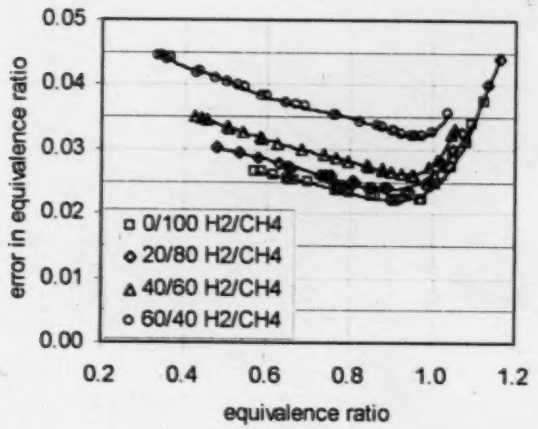

Figure B.1. Absolute error in equivalence ratio for 700RPM and 900RPM (+/-).

The error in indicated thermal efficiency varied from +/- 0.012 to +/-0.059 as seen in Figure B.2. The error is primarily due to uncertainties in brake power, and mass flow rates. In a similar manner, the error in brake thermal efficiency varied from +/- 0.008 to +/- 0.022, as seen in Figure B.3.

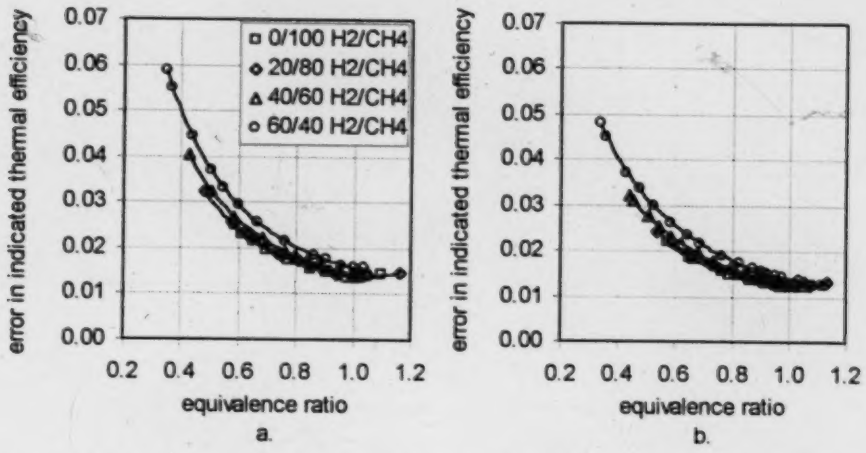

Figure B.2. Absolute error in indicated thermal efficiency for (a.) 700RPM and (b.) 900RPM (+/-).

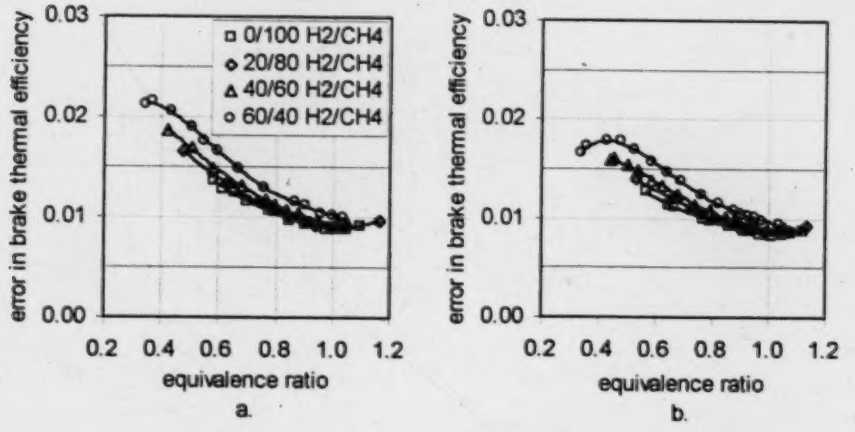

Figure B.3. Absolute error in brake thermal efficiency for (a.) 700RPM and (b.) 900RPM (+/-).

The error in brake specific fuel consumption varied from approximately +/- 4% to +/- 14% as seen in Figure B.4. The largest errors are found at low equivalence ratios, where the relative errors in brake power, mass flow rate of air, CO_2, and ϕ are large.

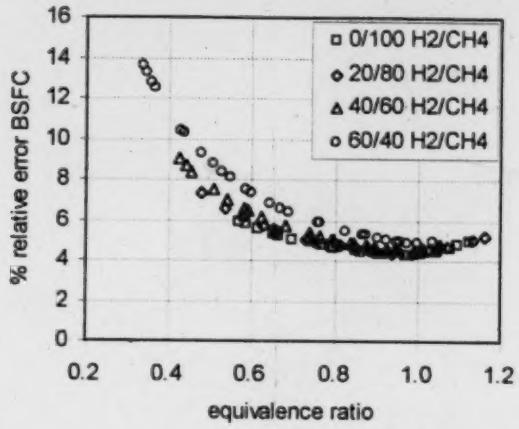

Figure B.4. Relative error in brake specific fuel consumption for 700RPM and 900RPM (+/-).

The error in brake specific production of CO_2 varied from approximately +/- 5% to +/- 18% as seen in Figure B.5. Once again, large errors are found where the relative errors in brake power, mass flow rate of air, CO_2, and ϕ are large.

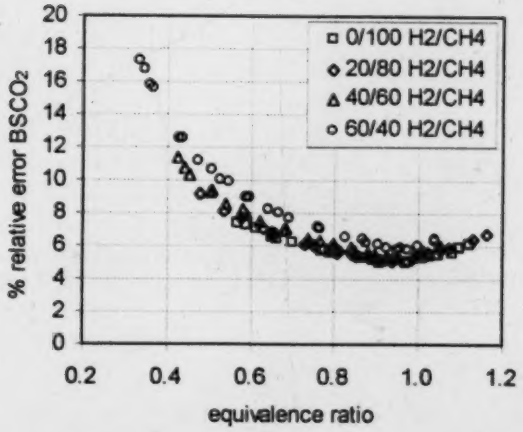

Figure B.5. Relative error in brake specific CO_2 production for 700RPM and 900RPM (+/-).

The relative error in CO was relatively stable at +/- 11% to +/- 13%as seen in Figure B.6. The error was primarily due to the uncertainty in CO concentration in the exhaust products. It was necessary to use a relative error estimate for CO, as an absolute error is unusable when the CO production is small.

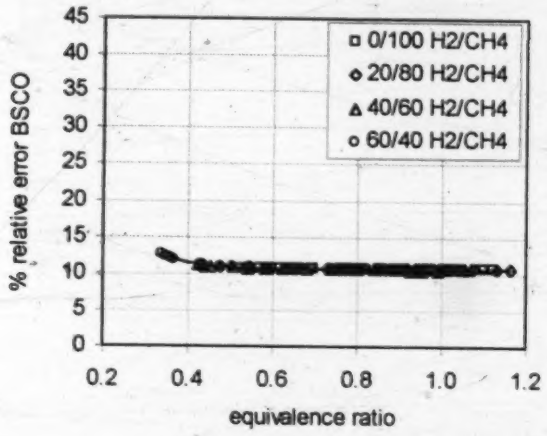

Figure B.6. Relative error in brake specific CO production for 700RPM and 900RPM (+/-).

The error in brake specific HC production varied from +/- 10% to +/- 53% as seen in Figure B.7. The error was primarily due to the uncertainty of unburned HC in the exhaust products. Large relative errors are found where the production of unburned hydrocarbons is small in comparison to the uncertainty.

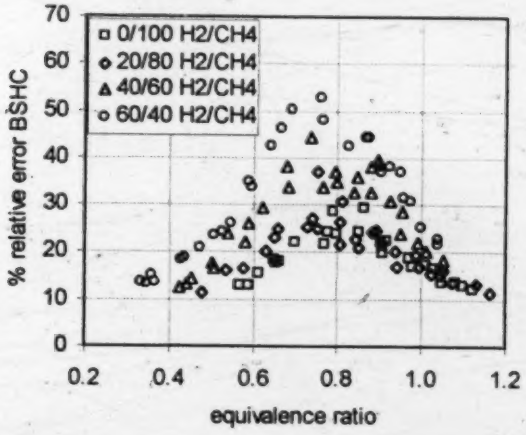

Figure B.7. Relative error in brake specific HC production for 700RPM and 900RPM (+/-).

The relative error in brake specific NO production was relatively stable at +/- 9% to +/- 10% as seen in Figure B.8. It was necessary to use a relative error as an absolute value was unusable when NO production is small. The error in NO was primarily due to the error caused by dilution of the NO sample.

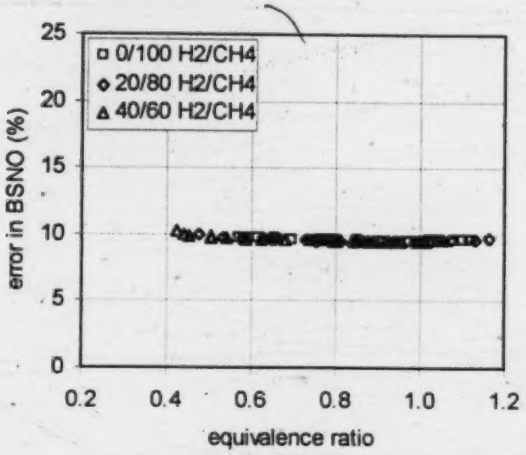

Figure B.8. Relative error in brake specific NO production for 700RPM and 900RPM (+/-).

B.2. Part Load Error

The part load errors are larger than their respective full load errors, because they are based not only on machine uncertainties, but also on the error in the full load value. As seen in Figure B.9, the relative error in the part load % of full load *BSFC* varied from +/- 6% to +/- 11%. The absolute error becomes large as the magnitude of the value becomes large.

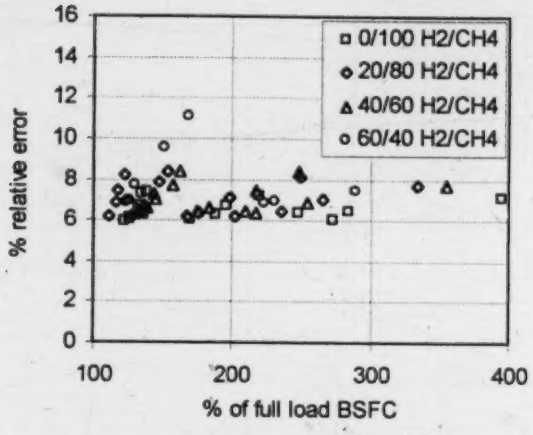

Figure B.9. Relative error in part load percentage of full load *BSFC* (+/-).

The relative error in part load % of full load $BSCO_2$ ranged from +/- 6% to +/- 15% as seen in Figure B.10. The absolute error becomes large with the magnitude of the base value.

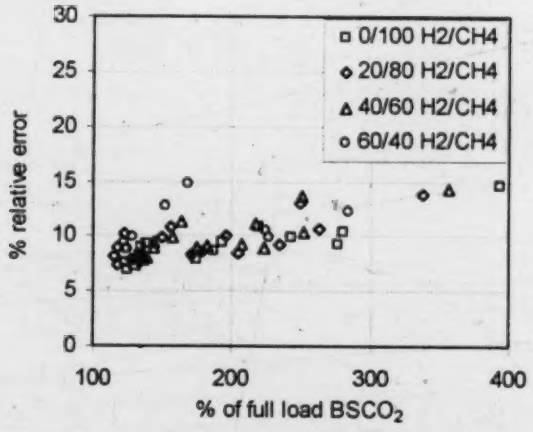

Figure B.10. Relative error in part load percentage of full load $BSCO_2$ (+/-).

The relative error in part load % of full load *BSCO* varied from +/- 13% to +/- 42% as seen in Figure B.11. The relative error is higher at high magnitudes of the part load value because the full load value is based on a relative error.

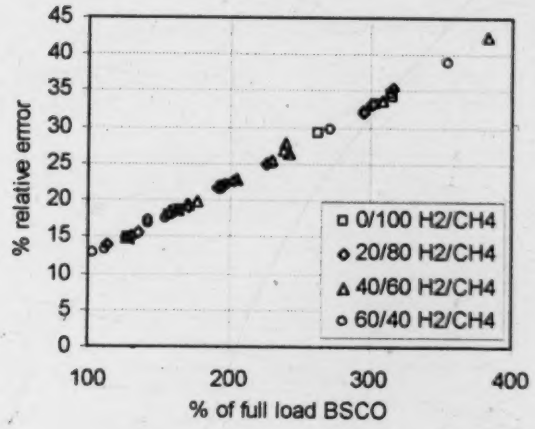

Figure B.11. Relative error in part load percentage of full load *BSCO* (+/-).

The relative error in part load % of full load *BSHC* varies from +/- 17% to +/- 65% as seen in Figure B.12. The error is large where the concentration of unburned hydrocarbons is small compared to the machine uncertainty.

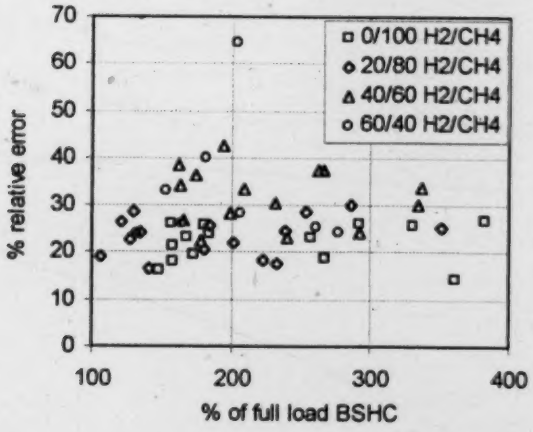

Figure B.12. Relative error in part load percentage of full load *BSHC* (+/-).

The relative error in part load % of full load *BSNO* varied from approximately +/- 13% to +/- 24% as seen in Figure B.13. The error increases with the magnitude of the part load value because the full load error it is based on is relative.

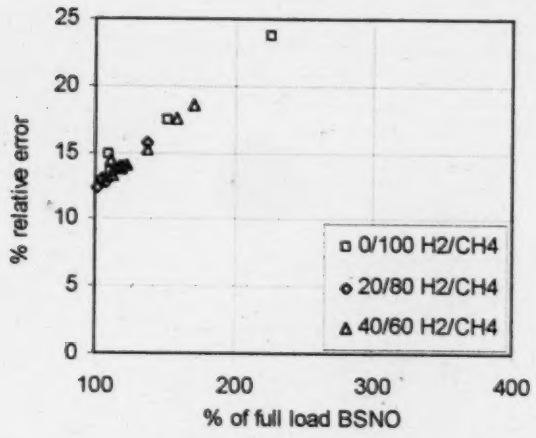

Figure B.13. Relative error in part load percentage of full load *BSNO* (+/-).

Appendix C. CFR best-fit equations

Best fit polynomials were used to form the full load data into a continuous relationship with equivalence ratio according to equation A1.

$$q = C_5\phi^5 + C_4\phi^4 + C_3\phi^3 + C_2\phi^2 + C_1\phi^1 + C_0\phi^0 \quad \text{(A1)}$$

A summary of the polynomial coefficients, along with the correlation coefficients with respect to equivalence ratio is given in table C.1.

Table C.1. Full load data best-fit polynomial coefficients and correlation coefficients with respect to equivalence ratio.

Full Load		ϕ^5	ϕ^4	ϕ^3	ϕ^2	ϕ^1	ϕ^0	R^2
Brake Power								
700 rpm	0%		1.37	-10.54	17.24	-7.86	1.82	0.99
	20%		-4.87	11.70	-11.39	7.77	-1.18	1.00
	40%		-18.93	53.03	-55.50	27.91	-4.54	1.00
	60%		-9.91	26.99	-28.02	15.28	-2.45	1.00
900 rpm	0%		16.73	-69.15	97.74	-54.59	11.77	0.99
	20%		7.87	-33.28	45.57	-22.29	4.61	0.99
	40%		-22.39	63.05	-67.18	34.96	-6.02	1.00
	60%		-9.55	25.79	-27.49	16.42	-2.86	1.00
Fuel Consumption								
700 rpm	0%		83.90	669.33	-1547.24	951.13	124.10	0.94
	20%		1369.34	-4079.34	4798.96	-2683.41	866.42	0.99
	40%		4190.03	-12565.88	14139.59	-7140.78	1637.48	0.99
	60%		5409.99	-16348.88	18369.62	-9155.26	1966.15	1.00
900 rpm	0%		-385.22	2476.15	-3995.82	2326.51	-132.55	0.97
	20%		224.49	-221.48	163.30	-359.42	472.55	0.98
	40%		5537.29	-17018.05	19672.57	-10208.85	2282.90	1.00
	60%		8670.05	-26677.07	30488.76	-15394.49	3161.47	1.00
Carbon Dioxide								
700 rpm	0%		-986.48	-819.98	5625.69	-5529.93	2396.82	0.98
	20%		3784.06	-14507.18	19648.48	-11491.85	3200.06	0.99
	40%		-2373.83	3145.56	1268.04	-3263.90	1811.75	0.99
	60%		3845.89	-15058.87	20692.22	-12146.54	3176.51	0.99
900 rpm	0%		2790.49	-12080.55	17908.52	-11392.92	3475.62	0.99
	20%		4645.60	-18884.97	27110.26	-16765.65	4546.93	0.99
	40%		718.38	-6920.87	13619.66	-10056.19	3239.58	1.00
	60%		11256.75	-38601.91	48375.94	-26421.67	5914.50	1.00

Table C.1. **(Continued)** Full load data best-fit polynomial coefficients and correlation coefficients.

		ϕ^5	ϕ^4	ϕ^3	ϕ^2	ϕ^1	ϕ^0	R^2
Carbon Monoxide								
ϕ>0.95	0%					1130.46	-1073.00	1.00
	20%					1062.55	-1008.50	1.00
	40%					1006.28	-955.00	0.99
	60%					652.57	-619.00	0.97
ϕ<0.95	ALL	= 0.824*equiv ^ -2.1986						
Hydrocarbons								
700	0%		90.54	-340.01	484.69	-309.01	74.81	1.00
rpm	20%		74.06	-272.06	378.18	-234.55	55.33	1.00
	40%		112.86	-375.40	472.61	-266.96	57.66	1.00
	60%	-677.62	2571.40	-3846.66	2844.59	-1045.48	154.45	1.00
900	0%		43.50	-169.82	258.77	-178.89	47.42	0.99
rpm	20%		39.38	-153.78	228.89	-151.72	38.23	0.94
	40%		161.48	-531.21	655.89	-360.47	74.97	1.00
	60%	-904.89	3435.16	-5133.15	3782.04	-1379.41	200.98	0.99
Nitric Oxide								
700rpm								
ϕ<=0.775	0%			512.26	-741.64	357.17	-56.64	1.00
0.775<ϕ<0.905	0%				-549.00	938.46	-384.34	1.00
ϕ>0.905	0%				289.02	-652.08	368.80	1.00
ϕ<=0.806	20%			267.89	-310.17	111.78	-11.46	1.00
0.806<ϕ<0.997	20%				-622.75	1061.81	-433.77	1.00
ϕ>0.997	20%				265.02	-603.13	343.70	1.00
ϕ<=0.798	40%	-24131.00	69539.43	-78671.47	43853.98	-12075.32	1316.52	1.00
0.798<ϕ<0.875	40%				-2010.73	3373.54	-1392.52	1.00
ϕ>0.875	40%				73.59	-240.82	174.19	0.99
ϕ<0.58	ALL	= 0.0545*EXP(5.0229*equiv)						
900rpm								
ϕ<=0.793	0%			-1467.72	3058.75	-2043.53	444.30	1.00
0.793<ϕ<0.917	0%				-749.47	1287.72	-534.48	1.00
ϕ>0.917	0%				376.83	-840.57	470.00	1.00
ϕ<=0.775	20%				232.70	-238.05	61.43	1.00
0.775<ϕ<0.982	20%				-693.59	1178.95	-480.31	0.98
ϕ>0.982	20%				313.87	-711.99	405.05	1.00
ϕ<=0.739	40%			851.63	-1234.56	598.39	-96.45	1.00
0.739<ϕ<0.920	40%				-705.02	1182.73	-473.76	1.00
ϕ>0.920	40%				567.84	-1225.38	664.32	1.00
ϕ<0.58	ALL	= 0.0054*EXP(9.4629*equiv)						

The selection of the order of polynomial was based on the confidence interval, combined with an aesthetic fit. In certain cases, (i.e. when fitting *BSNO* with equivalence ratio), the curve was broken into several segments to ensure a good fit.

Part load data were best-fit using a power equation according to equation A2.

$$q = A(load)^B \tag{A2}$$

The equations are valid for all different fuels (0% to 60% H_2), speeds (700RPM to 900RPM), and equivalence ratios (partial burn limit to 1.0). It is questionable whether the power equation is valid for low engine loads below 0.2. For this reason, the model engine cases do not use loads lower than 0.2. Part load NO is different in that its value varies with equivalence ratio. The best-fit coefficients and correlation coefficients with respect to engine load are summarized in Table C.2.

Table C.2. Part load best-fit coefficients and correlation coefficients with respect to engine load.

Part Load $\%= A*load^B$		A	B	R^2
% full load BSFC	ALL	100.00	-0.62	0.77
% full load $BSCO_2$	ALL	100.00	-0.62	0.78
% full load BSCO	ALL	99.98	-0.77	0.78
% full load BSHC	ALL	100.00	-0.82	0.87
% full load NO				
ϕ = 1.00	ALL	99.95	-0.28	0.64
ϕ = 0.66	ALL	=39.5421*EXP(0.9383*load)		0.98

Appendix D. Model engine case equations

Based on the CFR data, best-fit polynomials were used in the engine model in the computer code with respect to pedal position according to equation D1.

$$q = K_5 pedal^5 + K_4 pedal^4 + K_3 pedal^3 + K_2 pedal^2 + K_1 pedal^1 + K_0 pedal^0 \qquad \text{(D1)}$$

Summaries of the best-fit polynomial coefficients along with the correlation coefficients for all engine cases are given in Tables D.1 – D.13.

Table D.1. Best-fit polynomial coefficients and correlation coefficients for case A-G.

A-G	$pedal^5$	$pedal^4$	$pedal^3$	$pedal^2$	$pedal^1$	$pedal^0$	R^2
f	0.0000	0.0000	0.0000	0.0000	0.0000	0.0000	
ϕ	0.0000	0.0000	0.0000	0.0000	0.0000	1.0000	
throttle	0.0000	0.0000	0.0000	0.0000	0.7190	0.2140	
Brake Power							
1400rpm	0.0000	0.0010	-0.0022	0.0017	21.8499	6.5035	1.0000
1800rpm	0.0000	-0.0009	0.0020	-0.0015	26.9597	8.0240	1.0000
Fuel Consumption							
1400rpm	0.0000	792.1689	-2139.5241	2282.0377	-1364.1614	726.1327	0.9998
1800rpm	0.0000	814.3231	-2199.3594	2345.8594	-1402.3134	746.4409	0.9998
Carbon Dioxide							
1400rpm	0.0000	1932.0727	-5218.2668	5565.9487	-3327.3667	1771.4041	0.9998
1800rpm	0.0000	1974.4369	-5332.6869	5687.9924	-3400.3254	1810.2454	0.9998
Carbon Monoxide							
ALL	0.0000	277.2370	-740.3538	770.9915	-433.8348	187.6951	0.9997
Hydrocarbons							
1400rpm	0.0000	5.7792	-15.3804	15.9025	-8.7905	3.5924	0.9997
1800rpm	0.0000	5.5721	-14.8293	15.3328	-8.4757	3.4638	0.9997
NOx 1.00 >=pedal							
1400rpm	0.0000	3.4217	-9.5109	10.8027	-7.6407	8.7889	0.9999
1800rpm	0.0000	3.7309	-10.3692	11.7756	-8.3272	9.5775	0.9999
1.00 <pedal							
1400rpm	0.0000	0.0000	0.0000	0.0000	0.0000	0.0000	
1800rpm	0.0000	0.0000	0.0000	0.0000	0.0000	0.0000	

The selection of the order of polynomial was based on the confidence interval, combined with an aesthetic fit. In certain cases, (for example when fitting *BSNO* with pedal position), it was necessary to break the curve into several segments to ensure a good fit.

Table D.2. Best-fit polynomial coefficients and correlation coefficients for case B-H.

B-H	pedal^5	pedal^4	pedal^3	pedal^2	pedal^1	pedal^0	R^2
f	0.0000	0.0000	0.0000	0.0000	0.0000	0.3500	
ϕ	0.0000	0.0000	0.0000	0.0000	0.0000	1.0000	
throttle	0.0000	0.0000	0.0000	0.0000	0.7380	0.2180	
Brake Power							
1400rpm	0.0000	-0.0012	0.0026	-0.0020	21.9457	6.4824	1.0000
1800rpm	0.0000	-0.0003	0.0007	-0.0005	26.9971	7.9747	1.0000
Fuel Consumption							
1400rpm	0.0000	743.0429	-2004.7592	2134.1780	-1271.0042	672.2607	0.9998
1800rpm	0.0000	759.7648	-2049.8761	2182.2084	-1299.6092	687.3908	0.9998
Carbon Dioxide							
1400rpm	0.0000	1689.3721	-4559.3782	4853.7940	-2890.7877	1529.2331	0.9998
1800rpm	0.0000	1730.3591	-4668.6141	4970.0829	-2960.0456	1565.8704	0.9998
Carbon Monoxide							
ALL	0.0000	250.3730	-667.9419	694.2951	-389.2764	167.3761	0.9997
Hydrocarbons							
1400rpm	0.0000	4.5900	-12.2032	12.5940	-6.9368	2.8174	0.9997
1800rpm	0.0000	4.2120	-11.1983	11.5571	-6.3658	2.5855	0.9997
NOx 1.00 >=pedal							
1400rpm	0.0000	3.9846	-11.0629	12.5386	-8.8317	10.0910	0.9999
1800rpm	0.0000	4.1028	-11.3902	12.9083	-9.0910	10.3865	0.9999
1.00 <pedal							
1400rpm	0.0000	0.0000	0.0000	0.0000	0.0000	0.0000	1.0000
1800rpm	0.0000	0.0000	0.0000	0.0000	0.0000	0.0000	1.0000

Table D.3. Best-fit polynomial coefficients and correlation coefficients for case C-I.

C-I	pedal^5	pedal^4	pedal^3	pedal^2	pedal^1	pedal^0	R^2
f	0.0000	0.0000	0.0000	0.0000	0.0000	0.0000	
ϕ	0.0000	0.0000	0.0000	0.0000	0.3010	0.5800	
throttle	0.0000	0.0000	0.0000	0.0000	0.6400	0.3600	
Brake Power							
1400rpm	0.0000	-1.6086	0.1496	3.3183	15.2599	6.2367	1.0000
1800rpm	0.0000	-4.0231	2.6056	12.3303	16.5634	7.4842	1.0000
Fuel Consumption							
1400rpm	0.0000	171.6420	-508.8144	699.7643	-646.4770	553.7764	1.0000
1800rpm	0.0000	169.2322	-502.0147	710.0236	-685.1869	585.3052	1.0000
Carbon Dioxide							
1400rpm	0.0000	609.6805	-1903.2241	2454.1515	-1941.5226	1519.1695	1.0000
1800rpm	0.0000	676.3352	-2062.3809	2588.9095	-2037.3019	1595.2129	1.0000
Carbon Monoxide							
ALL	0.0000	5.8279	-17.1004	20.7740	-14.3740	5.9798	1.0000
Hydrocarbons							
1400rpm	0.0000	10.7823	-31.4962	36.4636	-20.7485	5.8463	0.9999
1800rpm	0.0000	8.5672	-25.2863	30.4232	-18.6906	5.7629	0.9999
NOx 1.00	>=pedal						
1400rpm	0.0000	-75.6077	99.8031	-12.9360	4.2059	0.3643	0.9990
1800rpm	-63.1623	135.4695	-126.7849	71.8808	0.3752	0.6136	0.9997
1.00	<pedal						
1400rpm	0.0000	0.0000	0.0000	0.0000	0.0000	0.0000	
1800rpm	0.0000	0.0000	0.0000	0.0000	0.0000	0.0000	

Table D.4. Best-fit polynomial coefficients and correlation coefficients for case D-J.

D-J	pedal^5	pedal^4	pedal^3	pedal^2	pedal^1	pedal^0	R^2
f	0.0000	0.0000	0.0000	0.0000	0.0000	0.3500	
ϕ	0.0000	0.0000	0.0000	0.0000	0.4660	0.4400	
throttle	0.0000	0.0000	0.0000	0.0000	0.5130	0.4870	
Brake Power							
1400rpm	0.0000	-6.6780	12.7452	-1.5525	17.8443	5.9346	1.0000
1800rpm	0.0000	-8.0527	12.3999	2.8214	20.9591	6.8750	1.0000
Fuel Consumption							
1400rpm	0.0000	348.4946	-951.6268	1042.6209	-680.9198	497.1908	1.0000
1800rpm	0.0000	438.7369	-1221.1482	1363.9811	-869.4880	548.0294	1.0000
Carbon Dioxide							
1400rpm	0.0000	347.5126	-1433.5855	2123.6981	-1657.3353	1266.3981	1.0000
1800rpm	0.0000	677.5721	-2439.3603	3304.5399	-2304.2816	1420.9293	1.0000
Carbon Monoxide							
ALL	0.0000	12.7091	-36.4706	42.0901	-25.9668	8.7036	0.9999
Hydrocarbons							
1400rpm	0.0000	17.7019	-52.3681	59.7570	-31.9514	7.5485	0.9999
1800rpm	0.0000	20.6421	-60.0844	66.4423	-33.8301	7.4679	0.9999
NOx 0.50	>=pedal						
1400rpm	0.0000	99.6245	-12.8549	-4.2030	1.8126	0.1189	0.9994
1800rpm	0.0000	54.5839	28.7539	-11.0089	2.1385	0.0831	0.9995
0.50	<pedal						
1400rpm	0.0000	-126.6646	-54.6447	446.9177	-314.8568	65.1129	0.9974
1800rpm	0.0000	656.8324	-2206.0271	2598.5651	-1241.4950	211.2196	0.9999

Table D.5. Best-fit polynomial coefficients and correlation coefficients for case E-K.

E-K	pedal^5	pedal^4	pedal^3	pedal^2	pedal^1	pedal^0	R^2
f	0.0000	0.0000	0.0000	0.0000	0.0000	0.4300	
ϕ	0.0000	0.0000	0.0000	0.0000	0.5160	0.4100	
throttle	0.0000	0.0000	0.0000	0.0000	0.4790	0.5210	
Brake Power							
1400rpm	0.0000	-11.2943	23.2463	-10.0030	20.9835	5.3936	1.0000
1800rpm	0.0000	-12.8660	25.3010	-10.6562	27.4435	5.7905	1.0000
Fuel Consumption							
1400rpm	0.0000	558.1438	-1483.2747	1509.8654	-837.0905	503.4808	1.0000
1800rpm	0.0000	800.4436	-2184.7527	2267.5633	-1204.9609	577.7268	1.0000
Carbon Dioxide							
1400rpm	0.0000	272.7895	-1394.9734	2234.0061	-1724.0472	1228.8028	1.0000
1800rpm	0.0000	817.0030	-2956.2205	3909.4751	-2542.6258	1400.2499	1.0000
Carbon Monoxide							
ALL	0.0000	17.4656	-48.9874	54.3741	-31.4679	9.6521	0.9999
Hydrocarbons							
1400rpm	0.0000	25.8024	-71.7777	76.1796	-37.6776	8.1281	0.9998
1800rpm	0.0000	34.3750	-94.1481	96.4989	-44.9325	8.8146	0.9997
NOx 0.50	>=pedal						
1400rpm	0.0000	247.9047	-137.1268	24.7241	-0.1324	0.1020	0.9997
1800rpm	0.0000	180.6166	-78.8961	13.7183	0.3670	0.0624	0.9998
0.50	<pedal						
1400rpm	0.0000	612.4803	-2311.5357	2925.8282	-1475.2925	261.6297	0.9917
1800rpm	0.0000	864.1655	-2840.2144	3267.5651	-1527.1694	252.6678	0.9992

Table D.6. Best-fit polynomial coefficients and correlation coefficients for case D-I.

D-I	pedal^5	pedal^4	pedal^3	pedal^2	pedal^1	pedal^0	R^2
f	0.0000	0.0000	0.0000	0.0000	-0.3500	0.3500	
ϕ	0.0000	0.0000	0.0000	0.0000	0.4410	0.4400	
throttle	0.0000	0.0000	0.0000	0.0000	0.5130	0.4870	
Brake Power							
1400rpm	0.0000	-0.2880	-0.0790	5.9402	16.9023	5.9346	1.0000
1800rpm	0.0000	-12.3991	23.6633	-4.5827	21.4028	6.8750	1.0000
Fuel Consumption							
1400rpm	0.0000	327.4623	-891.2334	979.6584	-643.0161	497.1908	0.9999
1800rpm	0.0000	593.3074	-1495.1826	1477.4751	-844.3095	548.0294	0.9997
Carbon Dioxide							
1400rpm	0.0000	542.1942	-1773.5592	2226.3587	-1524.8095	1266.3981	1.0000
1800rpm	0.0000	391.4458	-1782.8293	2738.6324	-2010.4025	1420.9293	1.0000
Carbon Monoxide							
ALL	0.0000	11.6435	-33.7223	39.5415	-25.0403	8.7036	0.9999
Hydrocarbons							
1400rpm	0.0000	13.2652	-39.5528	47.1118	-27.5255	7.5485	1.0000
1800rpm	0.0000	23.2772	-62.3283	63.6577	-31.2463	7.4679	0.9996
NOx 0.50	<=pedal						
1400rpm	0.0000	-17.4317	63.5016	-20.0007	2.7170	0.1189	0.9979
1800rpm	0.0000	-3.1930	67.3026	-20.0679	2.6885	0.0831	0.9988
0.50	<pedal						
1400rpm	0.0000	-53.4701	-141.7369	465.0045	-323.9740	70.2288	0.9987
1800rpm	0.0000	-60.5588	7.9643	146.4695	-92.5071	16.9846	0.9999

Table D.7. Best-fit polynomial coefficients and correlation coefficients for case F-I.

F-I	pedal^5	pedal^4	pedal^3	pedal^2	pedal^1	pedal^0	R^2
f	0.0000	0.0000	0.0000	0.0000	-0.6000	0.6000	
ϕ	0.0000	0.0000	0.0000	0.0000	0.5310	0.3500	
throttle	0.0000	0.0000	0.0000	0.0000	0.2920	0.7080	
Brake Power							
1400rpm	0.0000	-7.7961	13.3802	-6.0367	23.6836	5.0644	0.9999
1800rpm	0.0000	-1.5892	5.8259	-4.5883	30.3014	5.1316	0.9999
Fuel Consumption							
1400rpm	-897.1280	2991.1432	-3943.3398	2661.2096	-1028.4107	485.1620	1.0000
1800rpm	-1389.9878	4889.3696	-6771.3820	4720.9846	-1784.3860	611.6620	1.0000
Carbon Dioxide							
1400rpm	-2401.4189	6826.1876	-7746.6478	4679.2472	-1704.4293	1078.4596	0.9990
1800rpm	-5225.2248	15182.798	-17411.491	10353.516	-3516.2513	1368.7644	0.9997
Carbon Monoxide							
ALL	0.0000	22.0620	-60.8060	65.6613	-36.5477	10.7998	0.9998
Hydrocarbons							
1400rpm	-78.0759	230.7136	-264.6085	153.9271	-50.6660	9.4116	0.9993
1800rpm	-86.5396	261.0495	-309.9275	187.9361	-62.7751	10.8724	0.9990
NOx 0.50	<=pedal						
1400rpm	630.2595	-595.4172	194.5575	-23.4324	1.7116	0.1474	0.9965
1800rpm	638.3312	-583.5789	189.8272	-21.7388	1.4126	0.0691	0.9977
0.50	<pedal						
1400rpm	0.0000	-842.8627	2165.9167	-1999.9612	817.7464	-124.9873	0.9986
1800rpm	0.0000	-140.7555	129.2610	152.7454	-160.0655	37.0429	0.9998

Table D.8. Best-fit polynomial coefficients and correlation coefficients for case F-K.

F-K	pedal^5	pedal^4	pedal^3	pedal^2	pedal^1	pedal^0	R^2
f	0.0000	0.0000	0.0000	0.0000	-0.1700	0.6000	
ϕ	0.0000	0.0000	0.0000	0.0000	0.5760	0.3500	
throttle	0.0000	0.0000	0.0000	0.0000	0.2920	0.7080	
Brake Power							
1400rpm	0.0000	-10.2003	23.6351	-16.4402	26.2966	5.0644	1.0000
1800rpm	0.0000	-8.9332	19.2521	-13.3116	32.9460	5.1316	1.0000
Fuel Consumption							
1400rpm	0.0000	875.8960	-2339.2384	2305.5638	-1075.9024	485.1620	0.9999
1800rpm	0.0000	1484.8719	-4012.8864	3986.6174	-1812.9678	611.6620	0.9999
Carbon Dioxide							
1400rpm	0.0000	910.2034	-3001.4097	3590.0265	-1957.9056	1078.4596	0.9999
1800rpm	0.0000	2334.4608	-6900.0353	7481.6456	-3652.0289	1368.7644	0.9998
Carbon Monoxide							
ALL	0.0000	25.4458	-69.1478	72.8635	-38.8889	10.7998	0.9997
Hydrocarbons							
1400rpm	-80.1106	252.0713	-307.9853	187.0369	-59.9030	9.4116	0.9999
1800rpm	-105.4559	331.1729	-402.8985	241.3457	-74.6067	10.8724	0.9998
NOx 0.52 >=pedal							
1400rpm	861.3874	-762.8628	232.1433	-25.6702	1.7544	0.1474	0.9994
1800rpm	0.0000	252.6735	-176.6972	42.1378	-2.0620	0.0691	0.9987
0.52 <pedal							
1400rpm	0.0000	878.9427	-3283.1747	4194.7930	-2176.8047	399.3266	0.9910
1800rpm	0.0000	1512.9199	-4947.2522	5772.1511	-2810.2724	489.5756	0.9985

Table D.9. Best-fit polynomial coefficients and correlation coefficients for case C-K.

C-K	pedal^5	pedal^4	pedal^3	pedal^2	pedal^1	pedal^0	R^2
f	0.0000	0.0000	0.0000	0.0000	0.4300	0.0000	
ϕ	0.0000	0.0000	0.0000	0.0000	0.3460	0.5800	
throttle	0.0000	0.0000	0.0000	0.0000	0.6400	0.3600	
Brake Power							
1400rpm	0.0000	8.4558	-19.4668	16.9403	16.2073	6.2367	1.0000
1800rpm	0.0000	9.3176	-27.7070	29.5728	16.4179	7.4842	1.0000
Fuel Consumption							
1400rpm	0.0000	103.9946	-449.2792	754.9754	-713.5435	553.7764	1.0000
1800rpm	0.0000	1.2664	-226.0007	637.0774	-743.4773	585.3052	1.0000
Carbon Dioxide							
1400rpm	0.0000	917.8606	-2669.9849	3104.0459	-2248.7144	1519.1695	0.9999
1800rpm	0.0000	598.2500	-2087.4536	2880.2797	-2356.6961	1595.2129	1.0000
Carbon Monoxide							
ALL	0.0000	6.5903	-19.1832	22.9116	-15.3016	5.9798	1.0000
Hydrocarbons							
1400rpm	0.0000	19.5790	-53.2918	54.3159	-25.8159	5.8463	0.9997
1800rpm	0.0000	15.3569	-44.0253	47.6195	-24.1824	5.7629	0.9999
NOx 0.51	>=pedal						
1400rpm	278.0728	-325.1339	154.9024	-1.7266	4.1437	0.3643	1.0000
1800rpm	299.2315	-272.2874	77.2967	27.0217	5.5791	0.6136	1.0000
0.51	<pedal						
1400rpm	510.7227	-710.0101	-862.0452	1976.2520	-1105.4659	204.8508	0.9993
1800rpm	-716.6846	2643.8863	-3891.6135	2755.9354	-883.1561	108.3025	0.9998

Table D.10. Best-fit polynomial coefficients and correlation coefficients for case W-K.

W-K	pedal^5	pedal^4	pedal^3	pedal^2	pedal^1	pedal^0	R^2
f	0.0000	0.0000	0.0000	0.0000	0.0000	0.4300	
ϕ	0.0000	0.0000	0.0000	0.0000	0.5160	0.4100	
throttle	0.0000	0.0000	0.0000	0.0000	0.0000	1.0000	
Brake Power							
1400rpm	0.0000	-18.6915	41.8265	-34.7055	29.5064	10.3524	1.0000
1800rpm	0.0000	-21.7624	49.2520	-44.6994	41.0944	11.1143	1.0000
Electrolyser Power							
ALL	0.0000	0.0000	0.0000	0.0000	-4.5905	4.5905	
Fuel Consumption							
1400rpm	0.0000	310.0023	-819.0170	806.9219	-384.7946	337.0957	1.0000
1800rpm	0.0000	426.2298	-1184.4155	1235.9105	-609.8465	386.8211	1.0000
Carbon Dioxide							
1400rpm	0.0000	-102.1436	-267.6410	862.3032	-699.3242	822.7744	1.0000
1800rpm	0.0000	162.9865	-1085.6693	1808.9380	-1197.4648	937.5709	1.0000
Carbon Monoxide							
ALL	0.0000	7.0820	-20.4165	23.9115	-15.4284	5.8503	0.9999
Hydrocarbons							
1400rpm	0.0000	10.4062	-30.5571	35.2780	-19.2988	4.7720	1.0000
1800rpm	0.0000	14.5603	-42.1161	46.4211	-23.5047	5.1751	1.0000
NOx 0.51 >=pedal							
1400rpm	-477.4881	829.4857	-364.2038	58.2661	-1.5200	0.4353	0.9996
1800rpm	-526.7622	807.1560	-322.9648	51.3247	-0.8290	0.2663	0.9998
0.51 <pedal							
1400rpm	9061.2467	-33223.774	47619.054	-33462.191	11616.243	-1596.4793	0.9954
1800rpm	-4156.3803	16468.107	-25904.549	20024.705	-7508.493	1093.2536	0.9997

Table D.11. Best-fit polynomial coefficients and correlation coefficients for case X-K.

X-K	pedal^5	pedal^4	pedal^3	pedal^2	pedal^1	pedal^0	R^2
f	0.0000	0.0000	0.0000	0.0000	0.0000	0.4300	
ϕ	0.0000	0.0000	0.0000	0.0000	0.3460	0.5800	
throttle	0.0000	0.0000	0.0000	0.0000	0.0000	1.0000	
Brake Power							
1400rpm	0.0000	-3.7790	5.1846	-2.4907	11.7914	17.5820	1.0000
1800rpm	0.0000	-4.4005	6.2045	-4.5844	16.4730	21.3062	1.0000
Electrolyser Power							
*rpm/1000	0.0000	0.0000	0.0000	0.0000	-8.8578	8.8578	
Fuel Consumption							
1400rpm	0.0000	62.6709	-123.7581	89.6181	-50.5941	272.2715	1.0000
1800rpm	0.0000	86.0912	-187.6398	154.1328	-80.6071	282.7195	1.0000
Carbon Dioxide							
1400rpm	0.0000	-20.6501	-121.2750	238.8654	-156.1702	675.1989	1.0000
1800rpm	0.0000	32.9504	-262.5664	378.6041	-225.1268	702.5000	1.0000
Carbon Monoxide							
ALL	0.0000	0.5191	-1.8549	3.1357	-3.5519	2.7288	1.0000
Hydrocarbons							
1400rpm	0.0000	1.4630	-3.9789	4.8111	-2.9878	1.2794	1.0000
1800rpm	0.0000	2.0885	-5.4460	5.7281	-2.9971	1.1441	1.0000
NOx 1.00 >=pedal							
1400rpm	221.0565	-570.1999	403.0368	-55.4193	13.6833	1.1258	0.9969
1800rpm	247.1917	-561.7764	335.0130	-14.0245	9.4604	1.4635	0.9990
1.00 <pedal							
1400rpm	0.0000	0.0000	0.0000	0.0000	0.0000	0.0000	
1800rpm	0.0000	0.0000	0.0000	0.0000	0.0000	0.0000	

Table D.12. Best-fit polynomial coefficients and correlation coefficients for case Y-K.

Y-K	pedal^5	pedal^4	pedal^3	pedal^2	pedal^1	pedal^0	R^2
f	0.0000	0.0000	0.0000	0.0000	0.0000	0.4300	
ϕ	0.0000	0.0000	0.0000	0.0000	0.1860	0.7400	
throttle	0.0000	0.0000	0.0000	0.0000	0.0000	1.0000	
Brake Power							
1400rpm	0.0000	-0.3147	-0.2825	-0.0409	6.0845	22.8420	1.0000
1800rpm	0.0000	-0.3667	-0.3022	-0.4679	7.7799	28.3558	1.0000
Electrolyser Power							
*rpm/1000	0.0000	0.0000	0.0000	0.0000	-12.3282	12.3282	
Fuel Consumption							
1400rpm	0.0000	5.2342	-1.2181	-0.4792	-11.9958	258.6672	1.0000
1800rpm	0.0000	7.1894	-4.4108	1.2368	-13.1050	263.7861	1.0000
Carbon Dioxide							
1400rpm	0.0000	-1.7247	-24.7734	12.7518	-11.4084	641.1237	1.0000
1800rpm	0.0000	2.7526	-31.3232	16.3657	-16.3322	654.8984	1.0000
Carbon Monoxide							
ALL	0.0000	0.0212	-0.1116	0.3513	-0.8824	1.5972	1.0000
Hydrocarbons							
1400rpm	0.0000	0.0712	-0.1269	0.3185	-0.2781	0.6002	1.0000
1800rpm	0.0000	0.1071	-0.1533	0.2223	-0.2015	0.5403	1.0000
NOx 1.00 >=pedal							
1400rpm	188.7535	-372.3552	209.0185	-49.1527	24.4612	14.0978	0.9911
1800rpm	-9.8560	17.8622	-8.9452	-24.5044	26.2432	15.9252	0.9997
1.00 <pedal							
1400rpm	0.0000	0.0000	0.0000	0.0000	0.0000	0.0000	
1800rpm	0.0000	0.0000	0.0000	0.0000	0.0000	0.0000	

Table D.13. Best-fit polynomial coefficients and correlation coefficients for case Z-K.

Z-K	pedal^5	pedal^4	pedal^3	pedal^2	pedal^1	pedal^0	R^2
f	0.0000	0.0000	0.0000	0.0000	0.0000	0.4300	
ϕ	0.0000	0.0000	0.0000	0.0000	0.0230	0.9030	
throttle	0.0000	0.0000	0.0000	0.0000	0.0000	1.0000	
Brake Power							
1400rpm	0.0000	-0.0008	-0.0010	-0.0354	0.5586	27.7669	1.0000
1800rpm	0.0000	-0.0011	-0.0008	-0.0468	0.6529	34.3946	1.0000
Electrolyser Power							
X rpm/1000	0.0000	0.0000	0.0000	0.0000	-16.1392	16.1392	
Fuel Consumption							
1400rpm	0.0000	0.0011	0.0326	0.3124	-0.1918	250.0540	1.0000
1800rpm	0.0000	0.0010	0.0409	0.3469	-0.2154	254.5232	1.0000
Carbon Dioxide							
1400rpm	0.0000	-0.0002	-0.0588	-0.9220	-6.2791	623.2290	1.0000
1800rpm	0.0000	0.0007	-0.0411	-0.8149	-6.4802	633.6968	1.0000
Carbon Monoxide							
ALL	0.0000	-0.0007	0.0015	0.0011	-0.0574	1.0310	1.0000
Hydrocarbons							
1400rpm	0.0000	0.0007	-0.0015	0.0059	0.0218	0.5577	1.0000
1800rpm	0.0000	0.0009	-0.0017	0.0062	0.0148	0.4945	1.0000
NOx 1.00 >=pedal							
1400rpm	0.0000	0.0006	-0.0014	0.0974	-2.6571	16.7113	1.0000
1800rpm	0.0000	-0.8439	-0.1268	0.2434	-2.3047	19.5196	0.9995
1.00 <pedal							
1400rpm	0.0000	0.0000	0.0000	0.0000	0.0000	0.0000	
1800rpm	0.0000	0.0000	0.0000	0.0000	0.0000	0.0000	

Appendix E. Second by second model results

Second-by-second model results are shown for all cases in the SAE-J-227D schedule (Figures E.1 to E.13), the Highway schedule (Figures E.14 to E.26) and the Urban schedule (Figures E.27 to E.39).

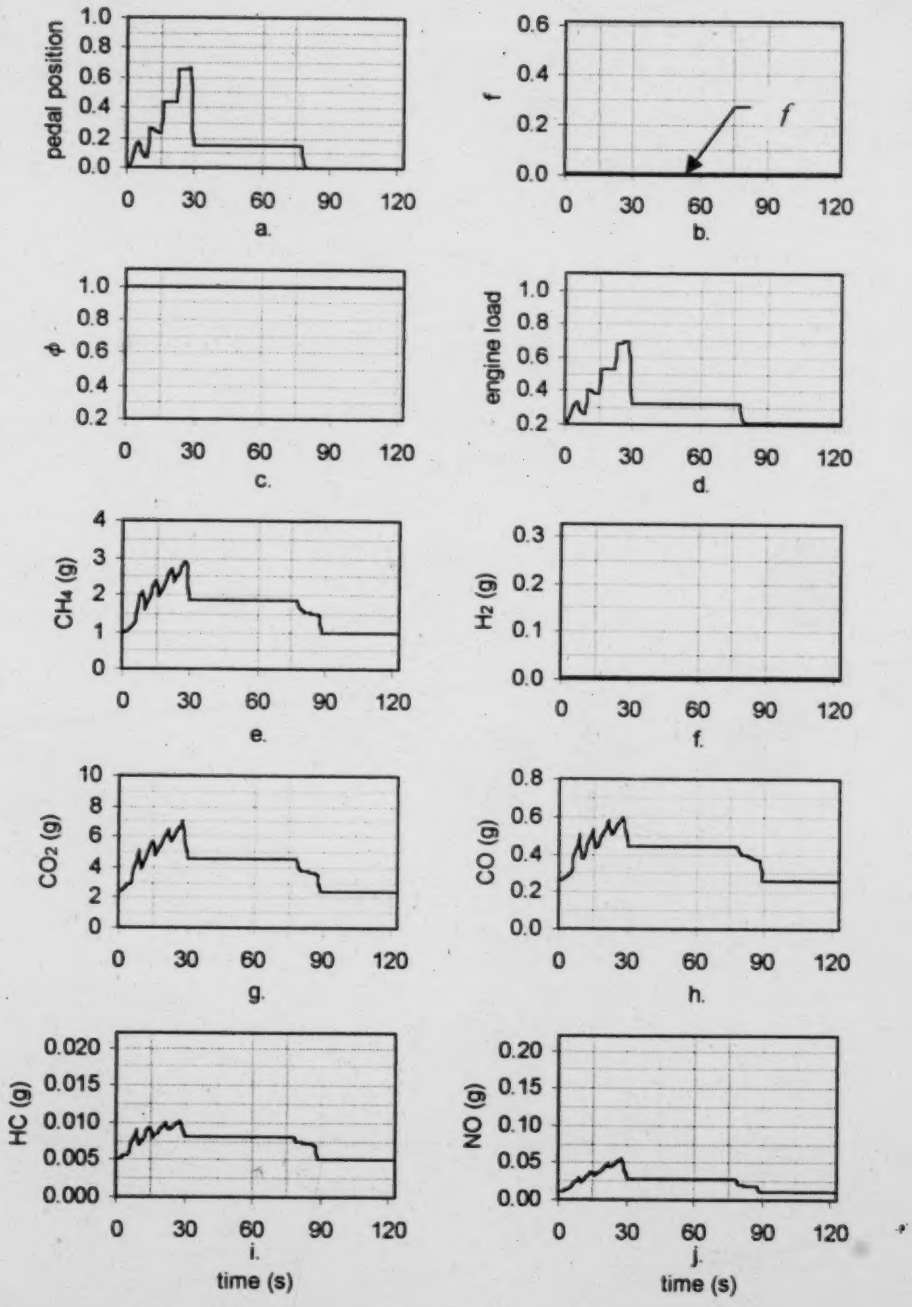

Figure E.1. Case A-G SAE J-227D schedule second-by-second results. (a.) Pedal position (b.) Fraction of hydrogen, (c.) Equivalence ratio (d.) Load (e.) Consumption of CH_4 and (f.) H_2. (g.) Production of CO_2 (h.) CO (i.) HC and (j) NO.

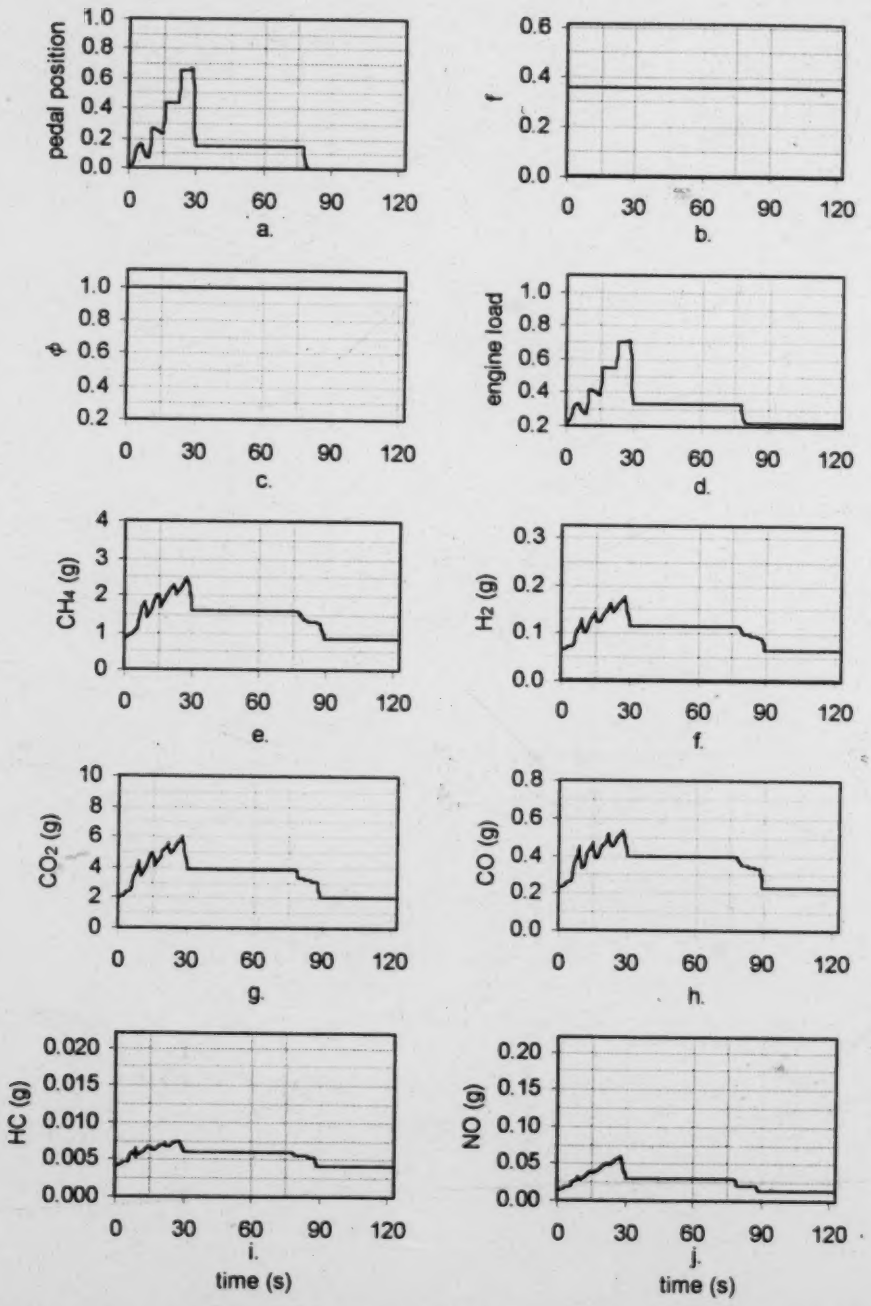

Figure E.2. Case B-H SAE J-227D schedule second-by-second results. (a.) Pedal position (b.) Fraction of hydrogen, (c.) Equivalence ratio (d.) Load (e.) Consumption of CH_4 and (f.) H_2. (g.) Production of CO_2 (h.) CO (i.) HC and (j) NO.

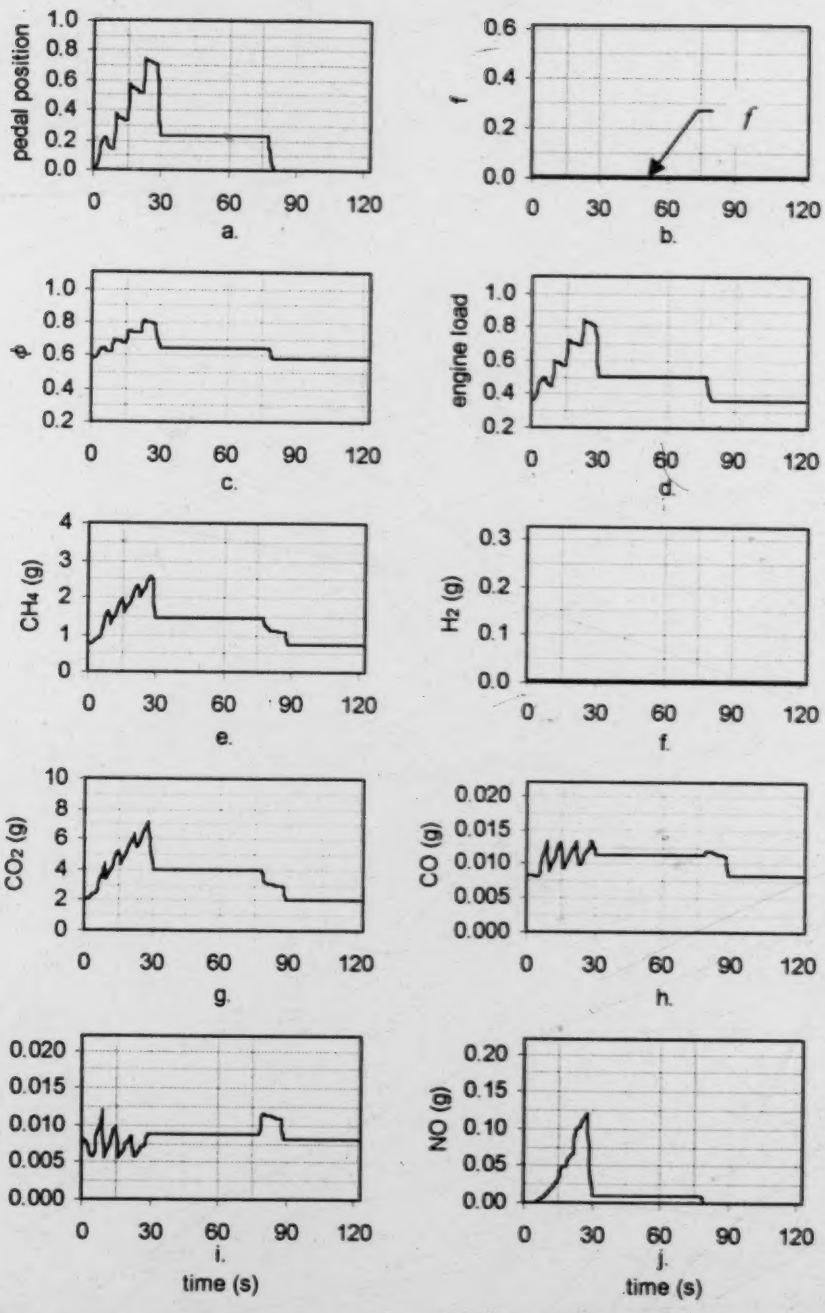

Figure E.3. Case C-I SAE J-227D schedule second-by-second results. (a.) Pedal position (b.) Fraction of hydrogen, (c.) Equivalence ratio (d.) Load (e.) Consumption of CH_4 and (f.) H_2. (g.) Production of CO_2 (h.) CO (i.) HC and (j) NO.

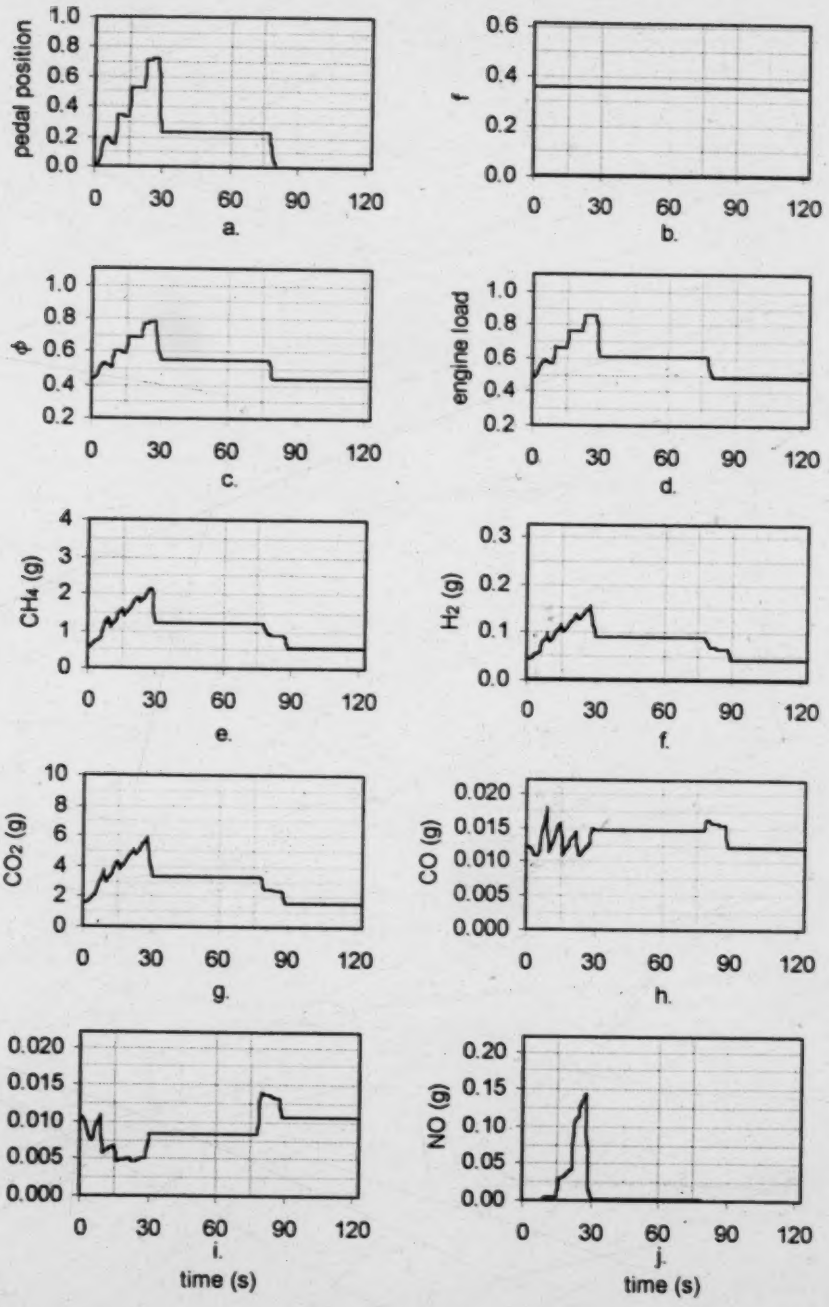

Figure E.4. Case D-J SAE J-227D schedule second-by-second results. (a.) Pedal position (b.) Fraction of hydrogen, (c.) Equivalence ratio (d.) Load (e.) Consumption of CH_4 and (f.) H_2. (g.) Production of CO_2 (h.) CO (i.) HC and (j) NO.

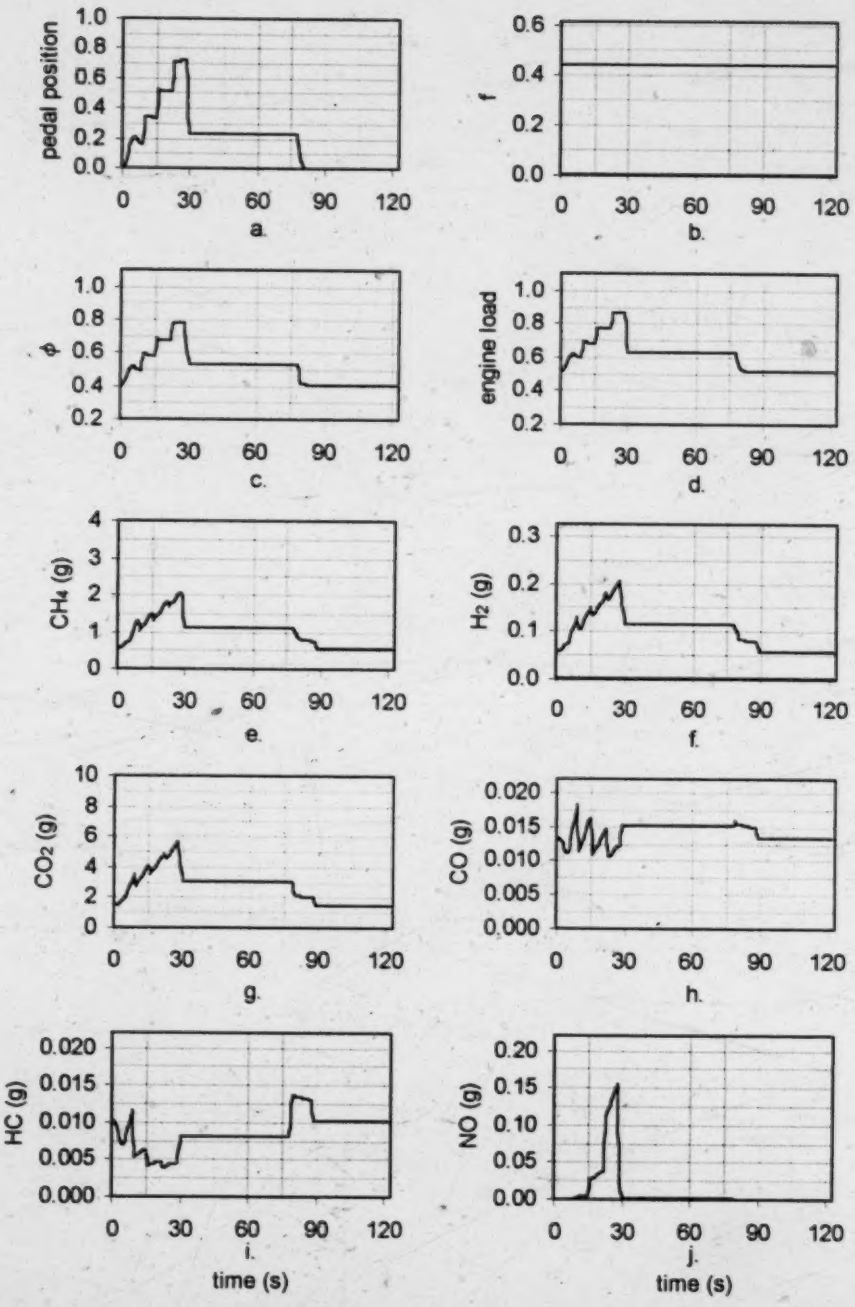

Figure E.5. Case E-K SAE J-227D schedule second-by-second results. (a.) Pedal position (b.) Fraction of hydrogen, (c.) Equivalence ratio (d.) Load (e.) Consumption of CH_4 and (f.) H_2. (g.) Production of CO_2 (h.) CO (i.) HC and (j) NO.

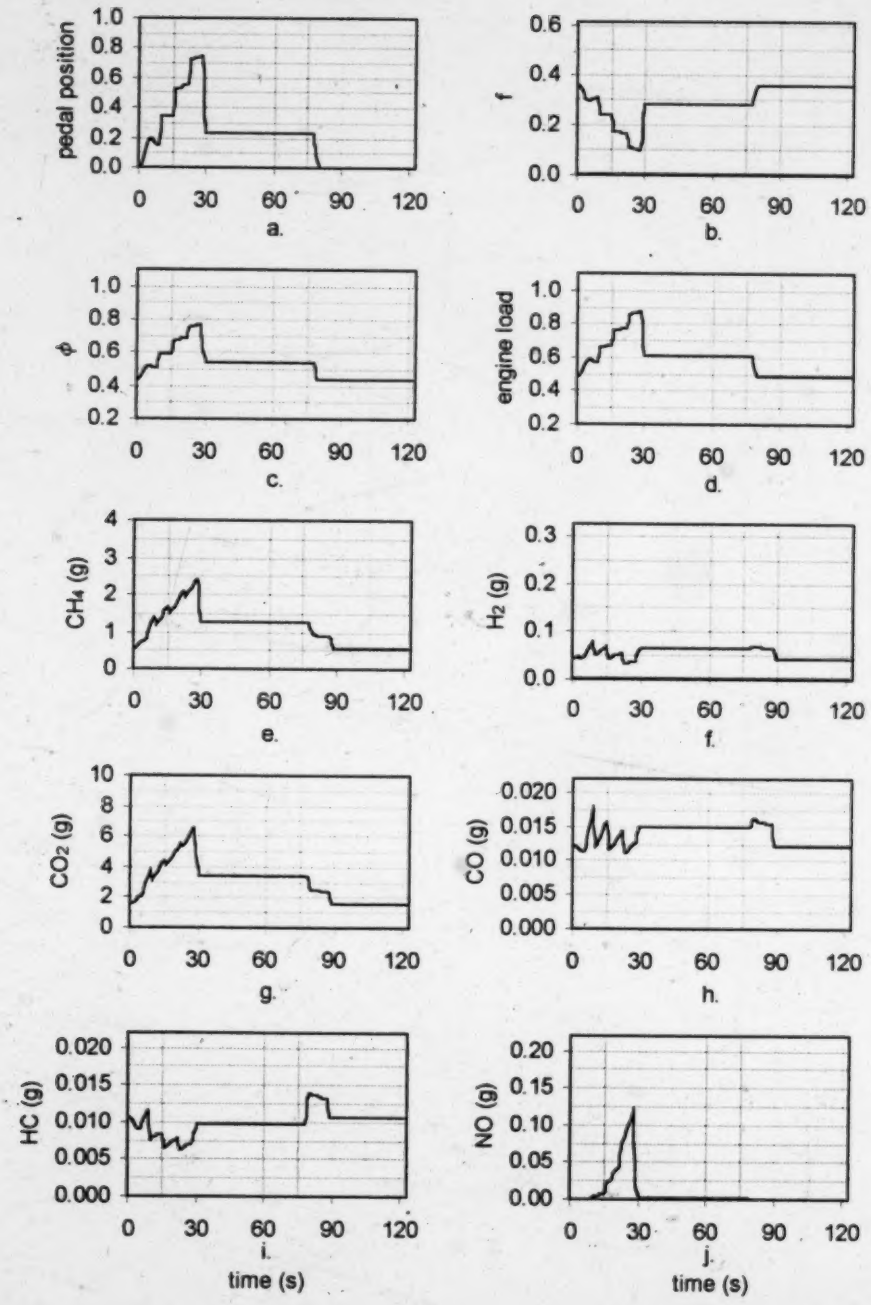

Figure E.6. Case D-I SAE J-227D schedule second-by-second results. (**a**.) Pedal position (**b**.) Fraction of hydrogen, (**c**.) Equivalence ratio (**d**.) Load (**e**.) Consumption of CH_4 and (**f**.) H_2. (**g**.) Production of CO_2 (**h**.) CO (**i**.) HC and (**j**) NO.

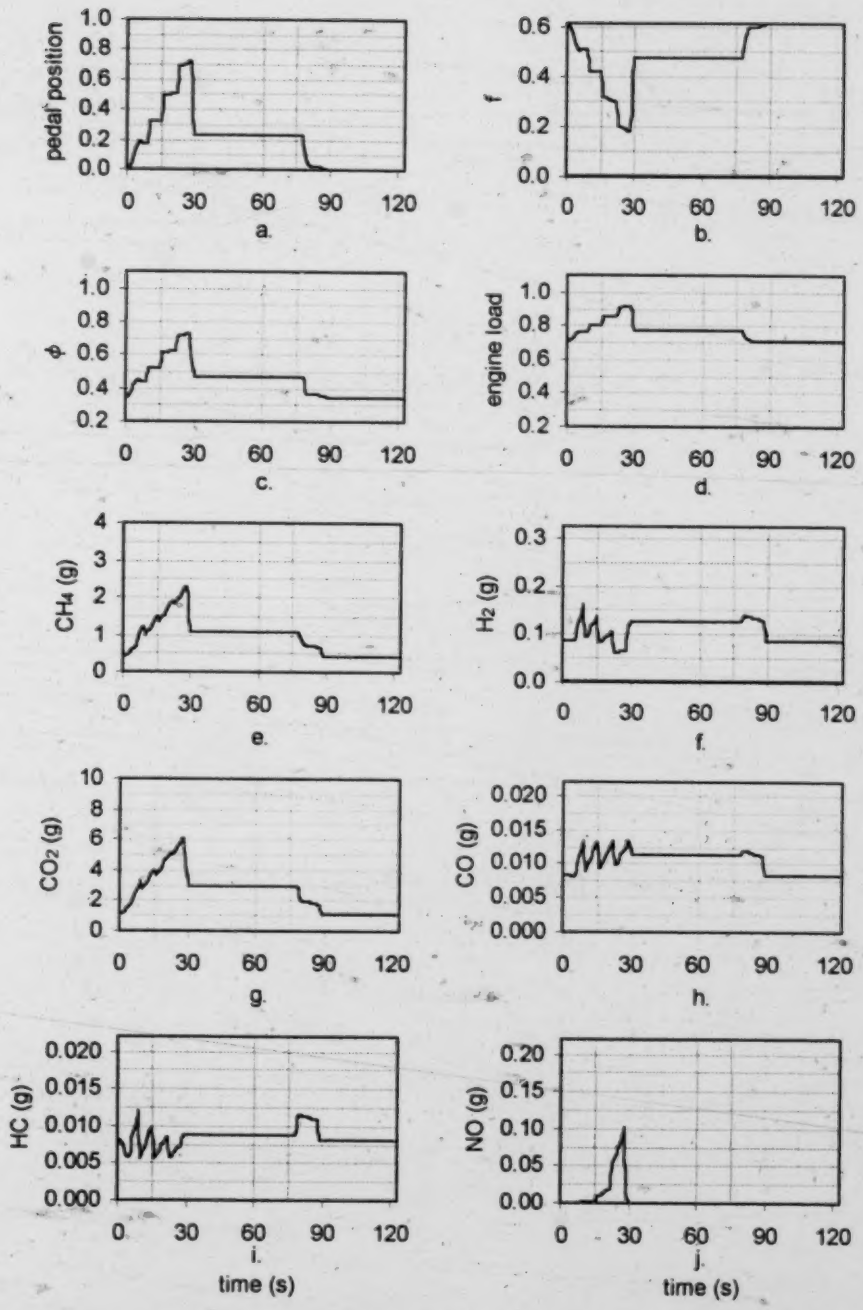

Figure E.7. Case F-I SAE J-227D schedule second-by-second results. (**a**.) Pedal position (**b**.) Fraction of hydrogen, (**c**.) Equivalence ratio (**d**.) Load (**e**.) Consumption of CH_4 and (**f**.) H_2. (**g**.) Production of CO_2 (**h**.) CO (**i**.) HC and (**j**) NO.

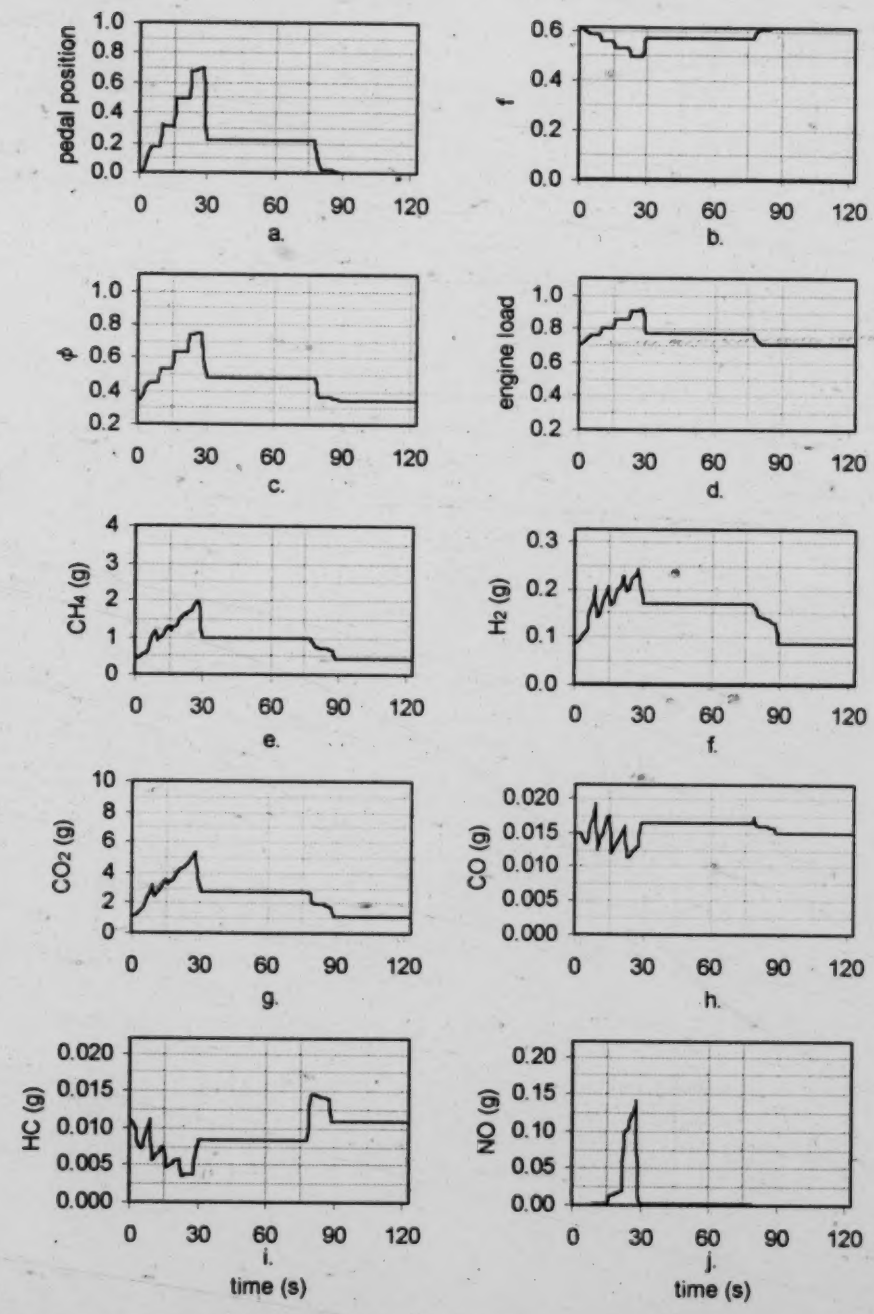

Figure E.8. Case F-K SAE J-227D schedule second-by-second results. (a.) Pedal position (b.) Fraction of hydrogen, (c.) Equivalence ratio (d.) Load (e.) Consumption of CH_4 and (f.) H_2. (g.) Production of CO_2 (h.) CO (i.) HC and (j) NO.

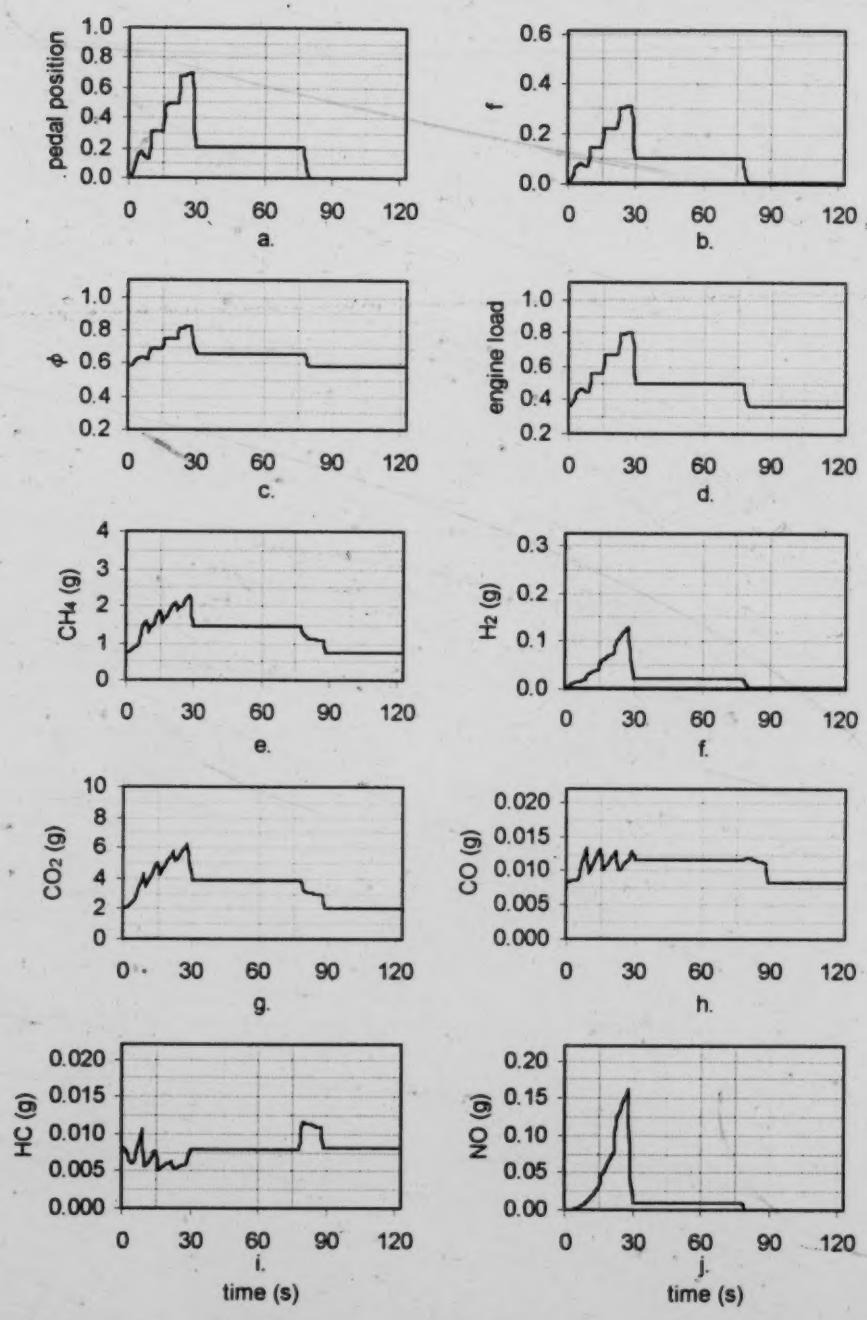

Figure E.9. Case C-K SAE J-227D schedule second-by-second results. (a.) Pedal position (b.) Fraction of hydrogen, (c.) Equivalence ratio (d.) Load (e.) Consumption of CH_4 and (f.) H_2. (g.) Production of CO_2 (h.) CO (i.) HC and (j) NO.

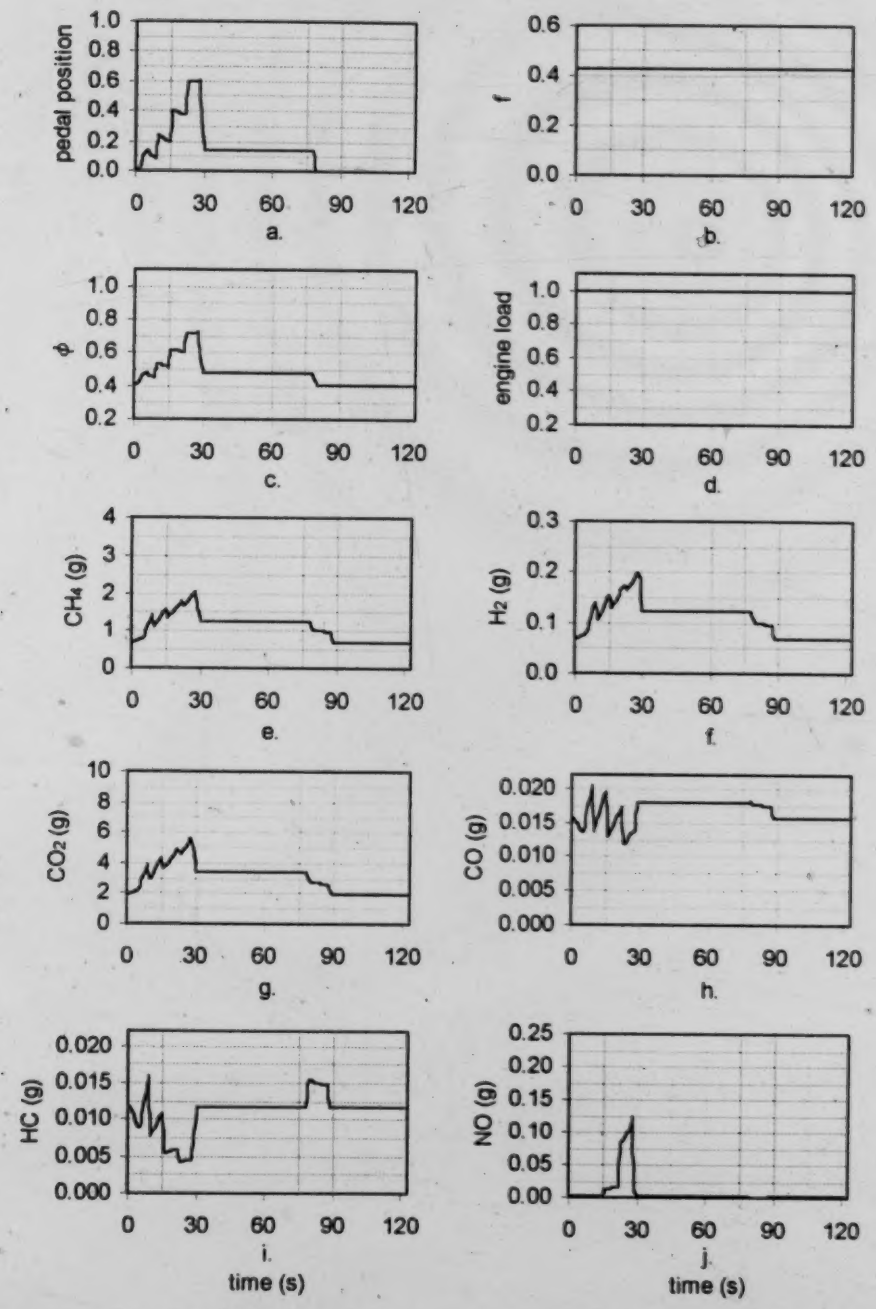

Figure E.10. Case W-K SAE J-227D schedule second-by-second results. (**a**.) Pedal position (**b**.) Fraction of hydrogen, (**c**.) Equivalence ratio (**d**.) Load (**e**.) Consumption of CH_4 and (**f**.) H_2. (**g**.) Production of CO_2 (**h**.) CO (**i**.) HC and (**j**) NO.

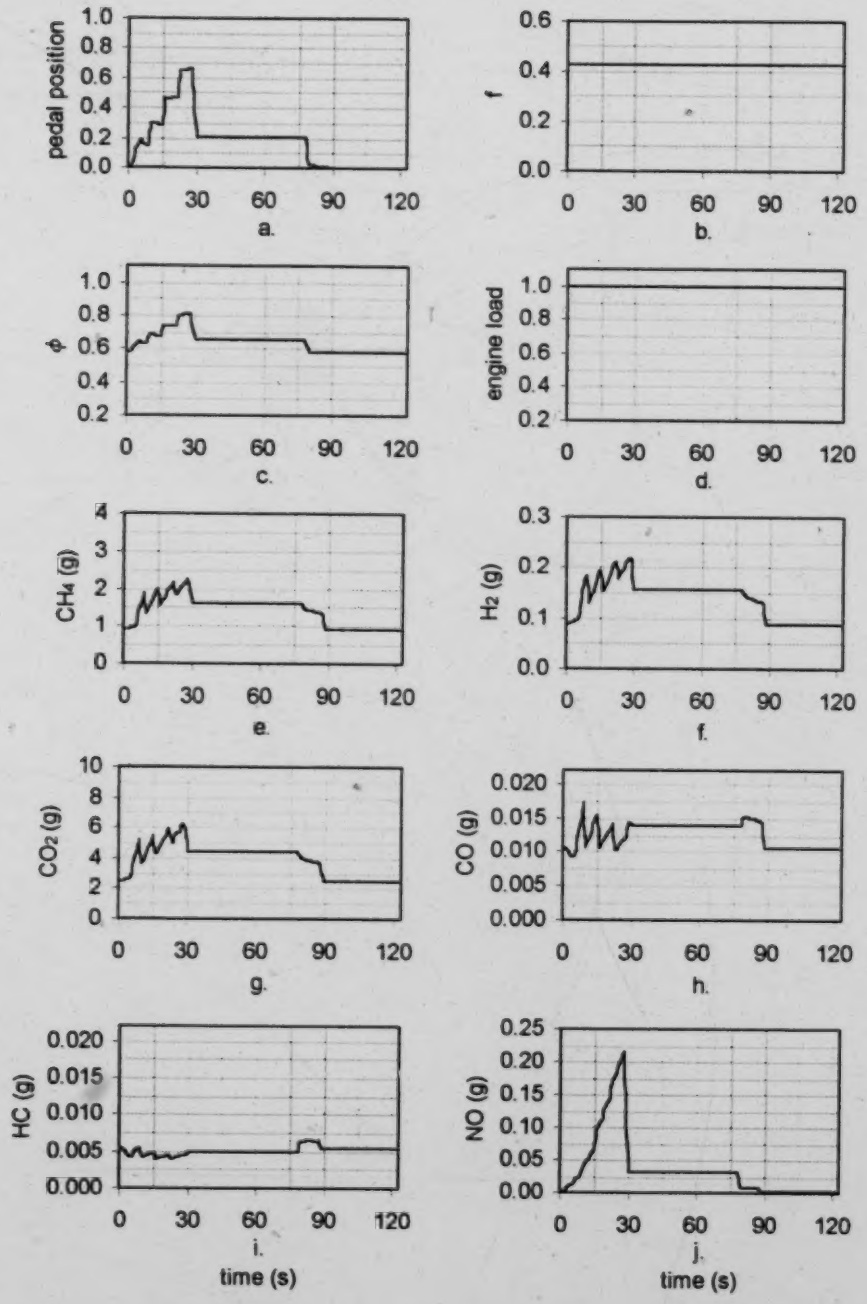

Figure E.11. Case X-K SAE J-227D schedule second-by-second results. (a.) Pedal position (b.) Fraction of hydrogen, (c.) Equivalence ratio (d.) Load (e.) Consumption of CH_4 and (f.) H_2. (g.) Production of CO_2 (h.) CO (i.) HC and (j) NO.

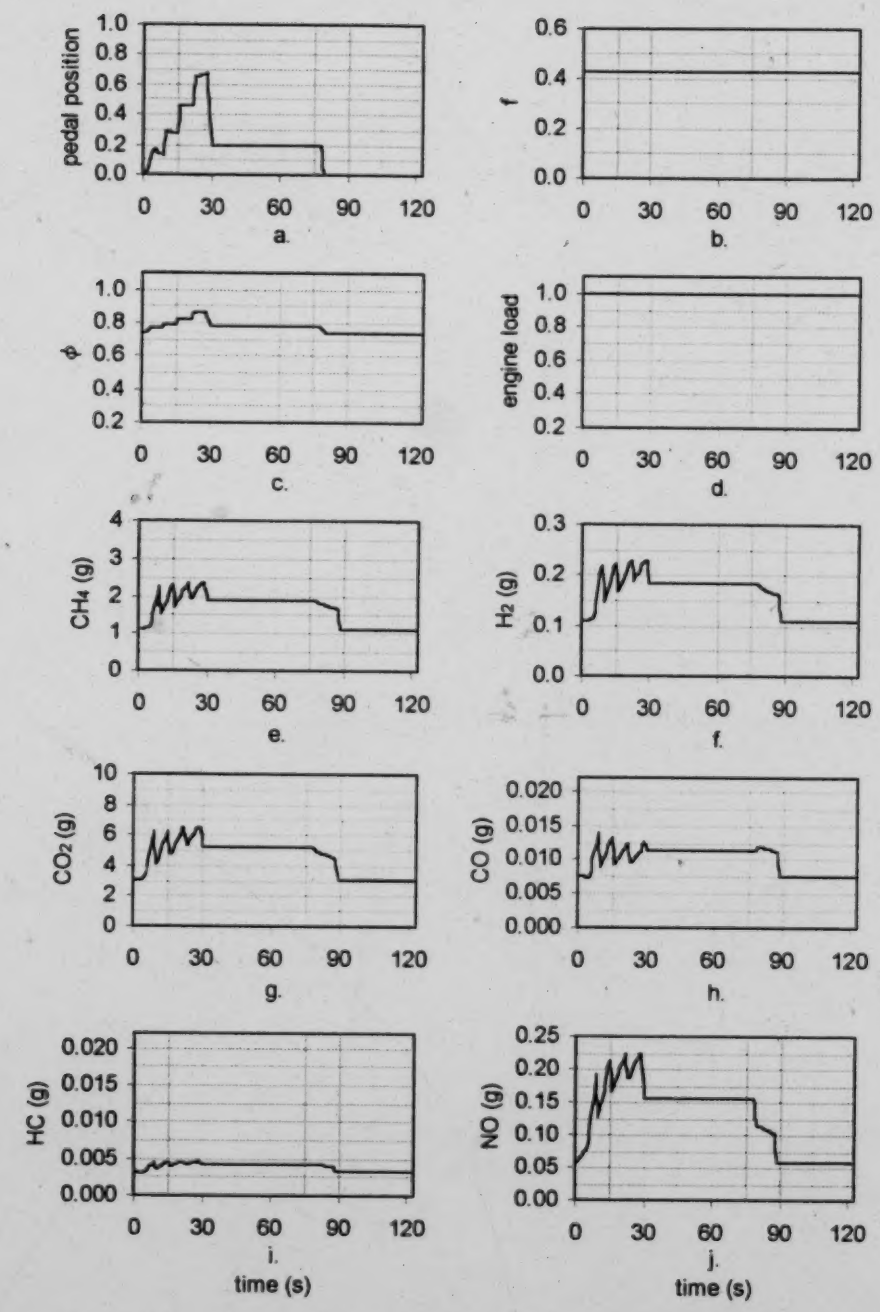

Figure E.12. Case Y-K SAE J-227D schedule second-by-second results. (a.) Pedal position (b.) Fraction of hydrogen, (c.) Equivalence ratio (d.) Load (e.) Consumption of CH_4 and (f.) H_2. (g.) Production of CO_2 (h.) CO (i.) HC and (j) NO.

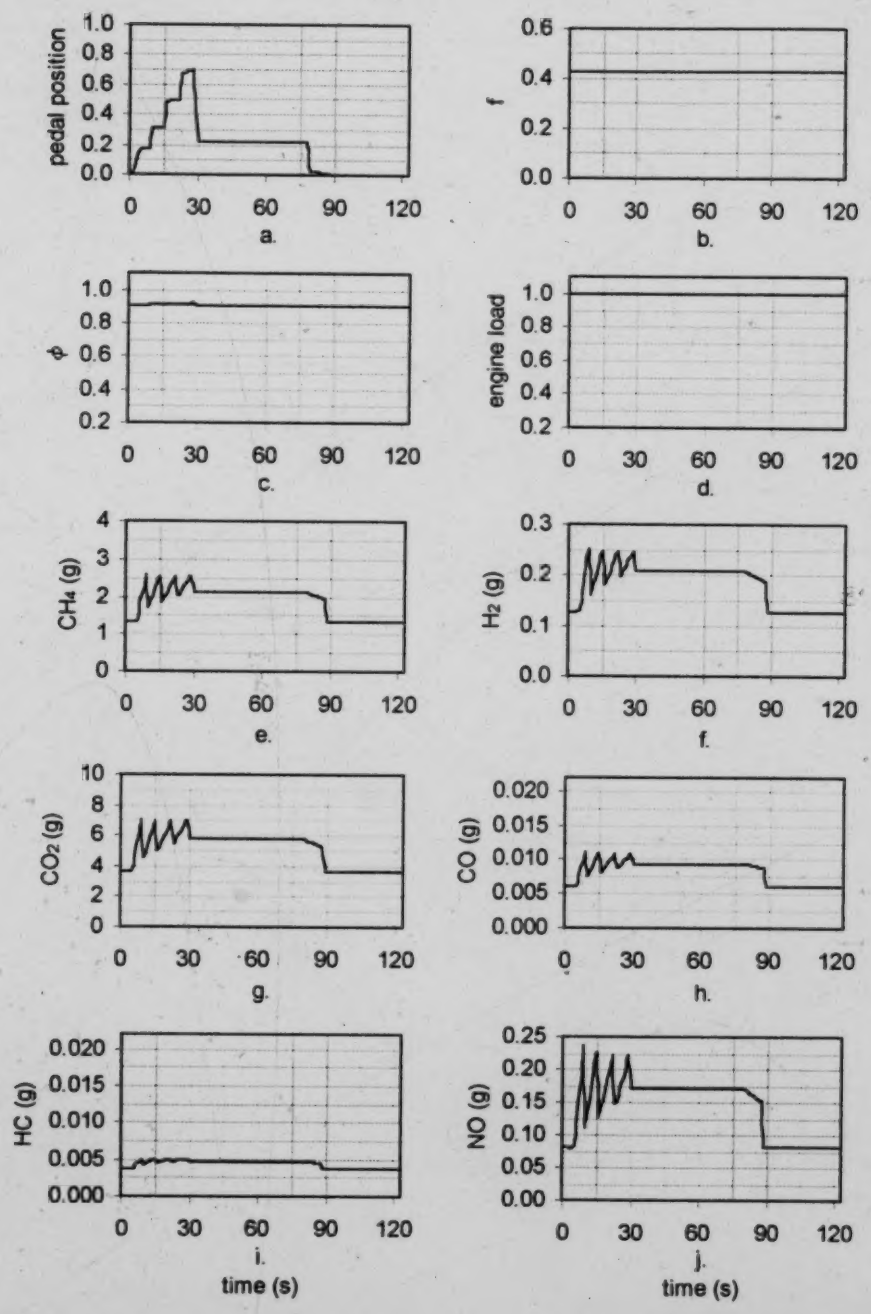

Figure E.13. Case Z-K SAE J-227D schedule second-by-second results. (a.) Pedal position (b.) Fraction of hydrogen, (c.) Equivalence ratio (d.) Load (e.) Consumption of CH_4 and (f.) H_2. (g.) Production of CO_2 (h.) CO (i.) HC and (j) NO.

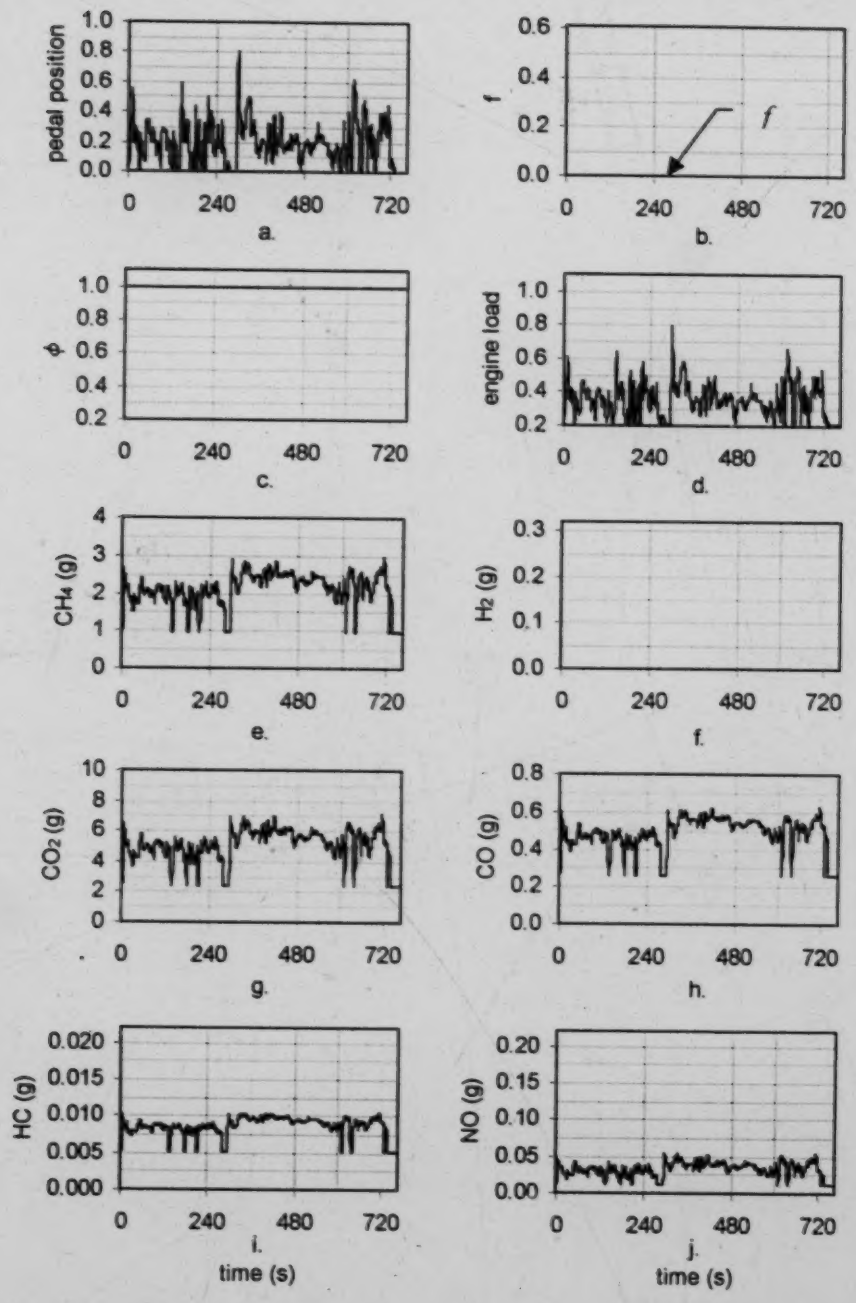

Figure E.14. Case A-G Highway schedule second-by-second results. (a.) Pedal position (b.) Fraction of hydrogen, (c.) Equivalence ratio (d.) Load (e.) Consumption of CH_4 and (f.) H_2. (g.) Production of CO_2 (h.) CO (i.) HC and (j) NO.

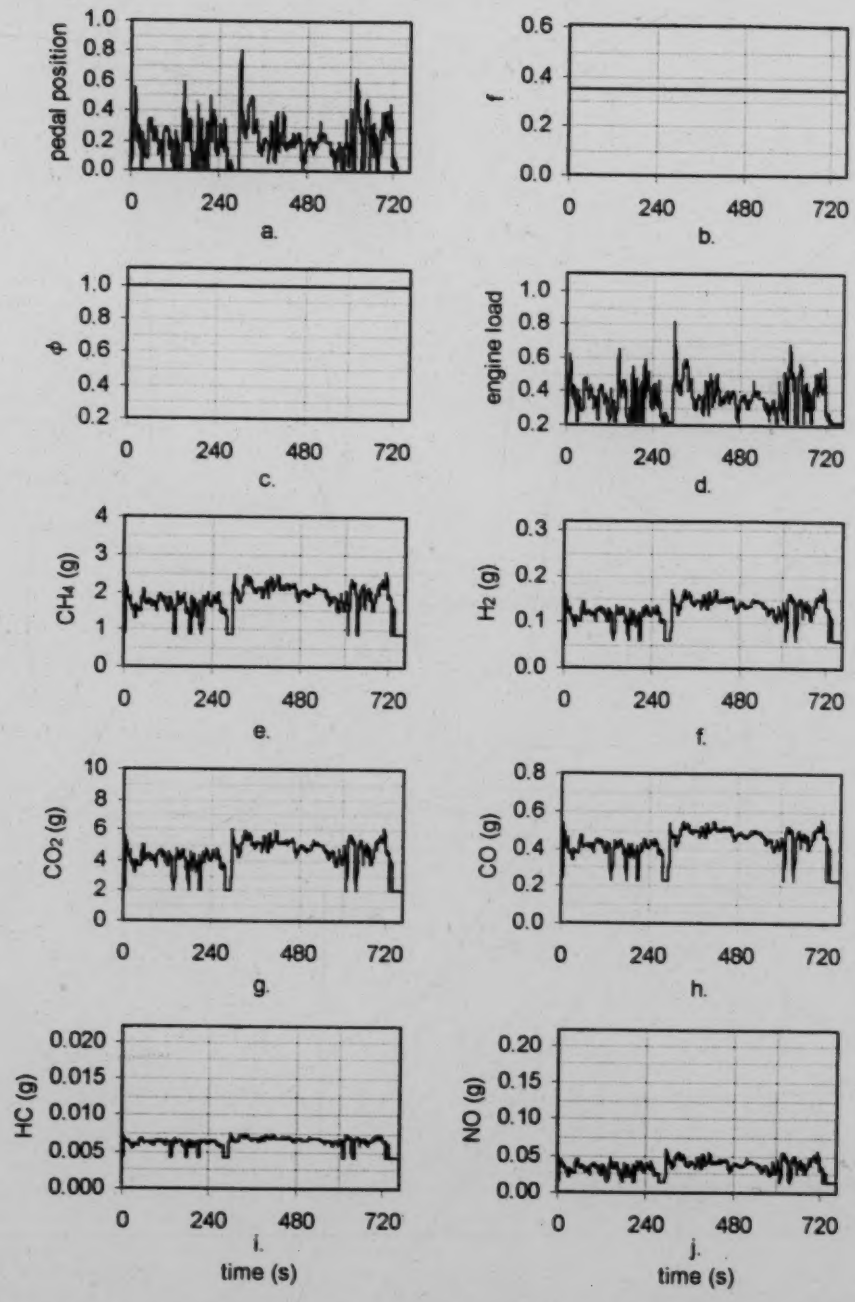

Figure E.15. Case B-H Highway schedule second-by-second results. (a.) Pedal position (b.) Fraction of hydrogen, (c.) Equivalence ratio (d.) Load (e.) Consumption of CH_4 and (f.) H_2. (g.) Production of CO_2 (h.) CO (i.) HC and (j) NO.

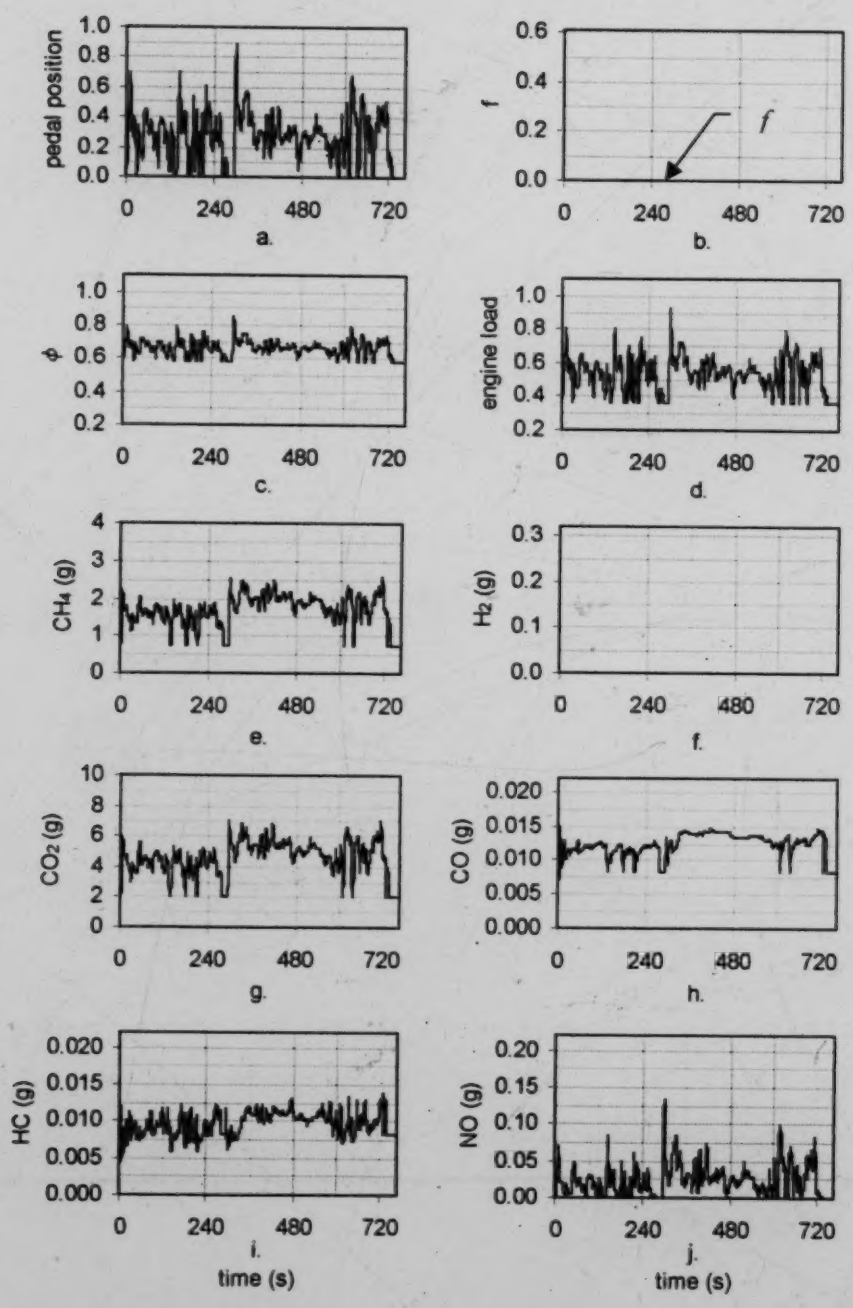

Figure E.16. Case C-I Highway schedule second-by-second results. (a.) Pedal position (b.) Fraction of hydrogen, (c.) Equivalence ratio (d.) Load (e.) Consumption of CH_4 and (f.) H_2. (g.) Production of CO_2 (h.) CO (i.) HC and (j) NO.

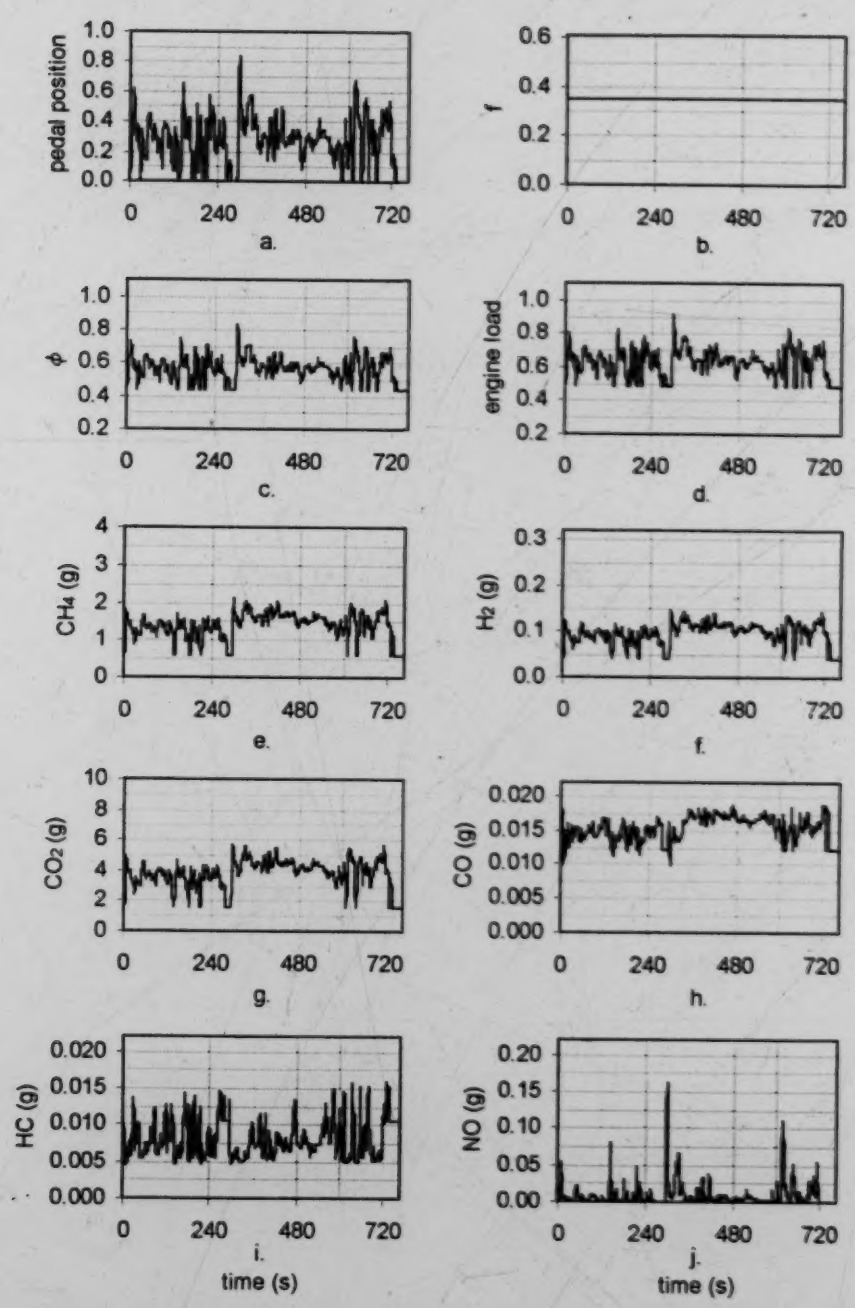

Figure E.17. Case D-J Highway schedule second-by-second results. (a.) Pedal position (b.) Fraction of hydrogen, (c.) Equivalence ratio (d.) Load (e.) Consumption of CH_4 and (f.) H_2. (g.) Production of CO_2 (h.) CO (i.) HC and (j) NO.

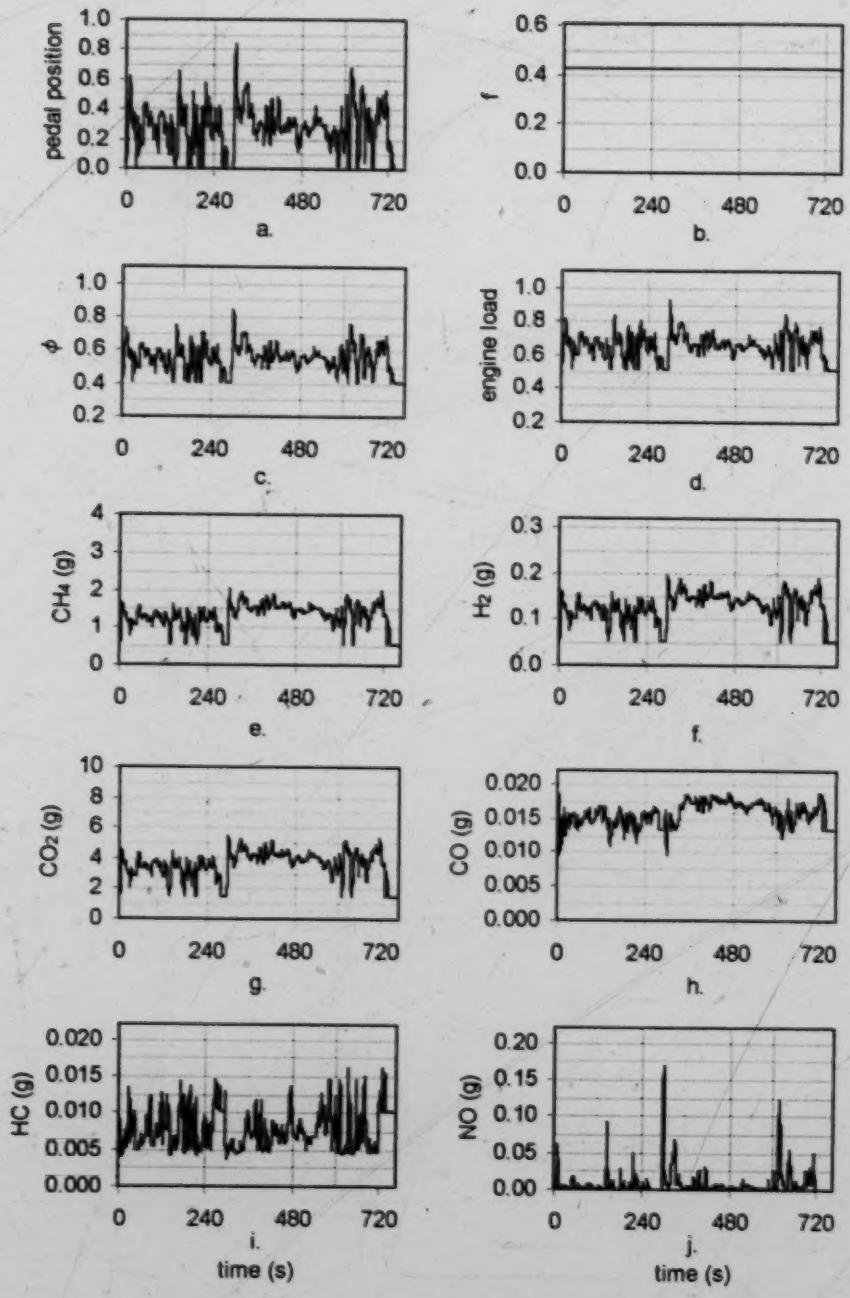

Figure E.18. Case E-K Highway schedule second-by-second results. (a.) Pedal position (b.) Fraction of hydrogen, (c.) Equivalence ratio (d.) Load (e.) Consumption of CH_4 and (f.) H_2. (g.) Production of CO_2 (h.) CO (i.) HC and (j) NO.

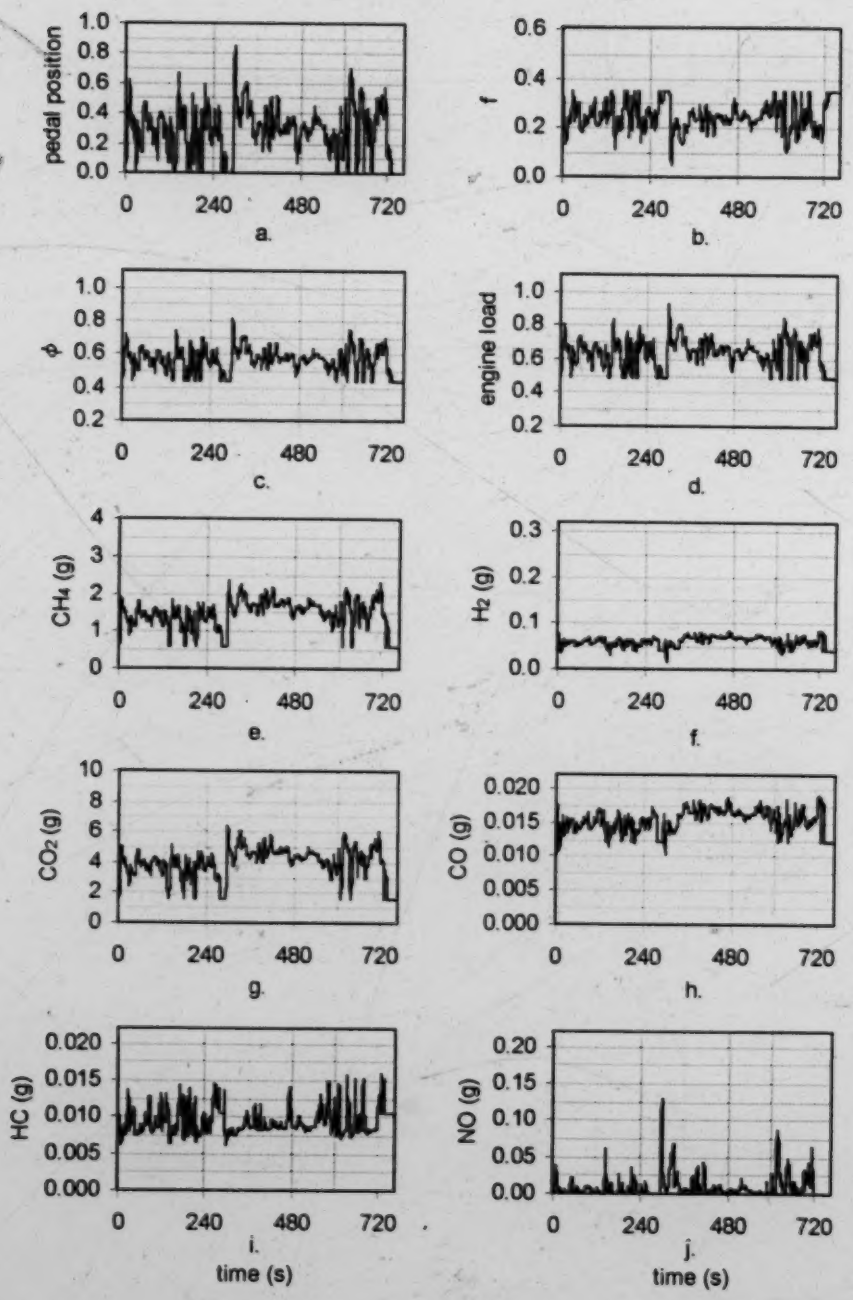

Figure E.19. Case D-I Highway schedule second-by-second results. (a.) Pedal position (b.) Fraction of hydrogen, (c.) Equivalence ratio (d.) Load (e.) Consumption of CH_4 and (f.) H_2. (g.) Production of CO_2 (h.) CO (i.) HC and (j) NO.

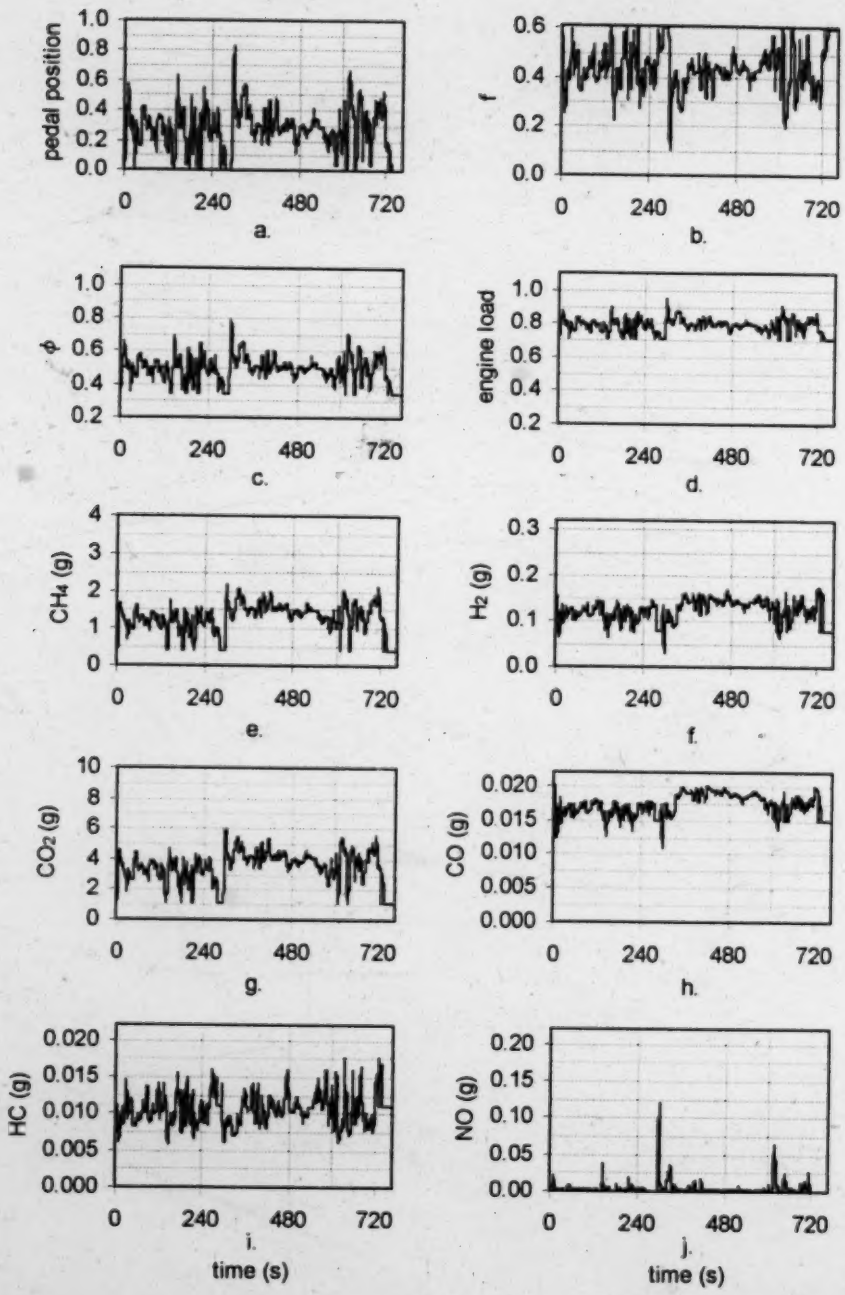

Figure E.20. Case F-I Highway schedule second-by-second results. (a.) Pedal position (b.) Fraction of hydrogen, (c.) Equivalence ratio (d.) Load (e.) Consumption of CH_4 and (f.) H_2. (g.) Production of CO_2 (h.) CO (i.) HC and (j) NO.

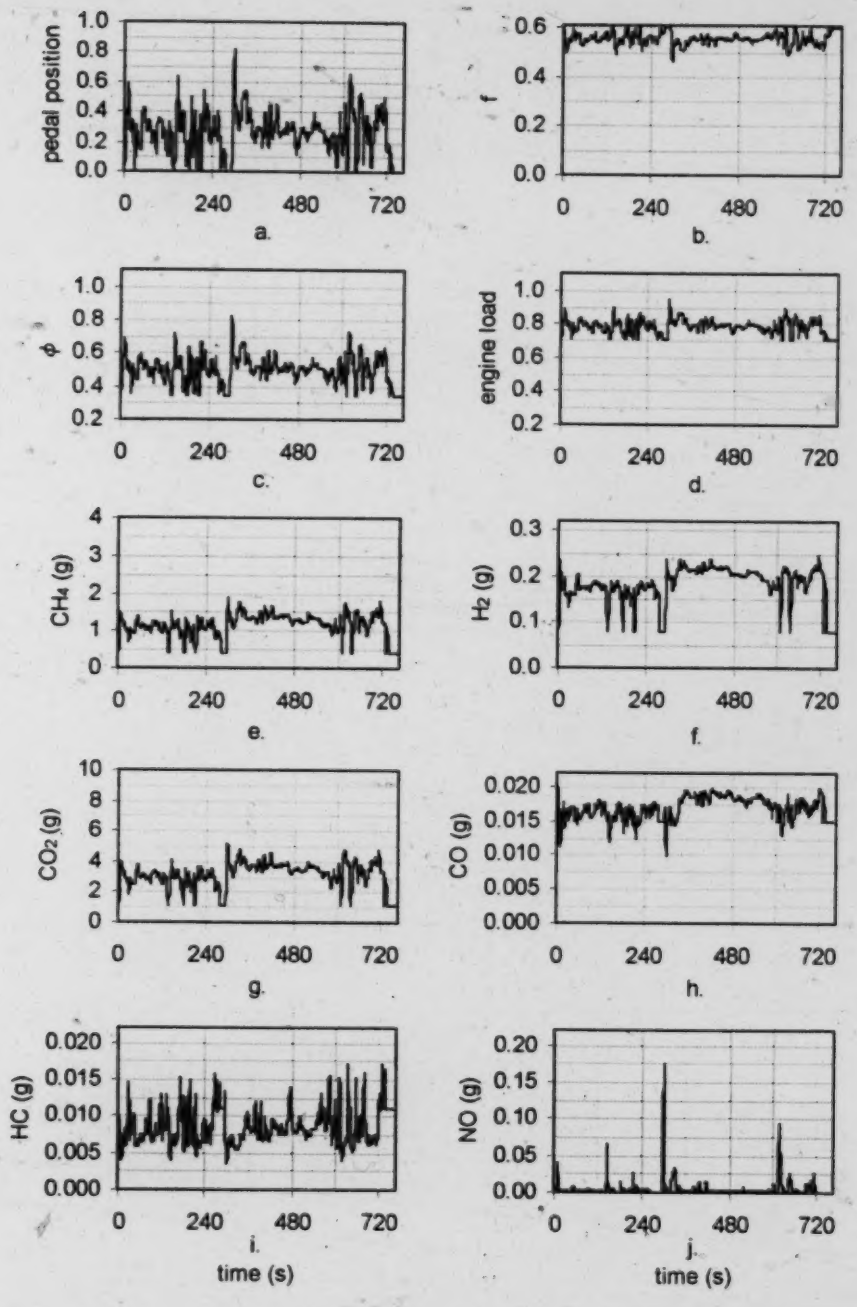

Figure E.21. Case F-K Highway schedule second-by-second results. (**a**.) Pedal position (**b**.) Fraction of hydrogen, (**c**.) Equivalence ratio (**d**.) Load (**e**.) Consumption of CH_4 and (**f**.) H_2. (**g**.) Production of CO_2 (**h**.) CO (**i**.) HC and (**j**) NO.

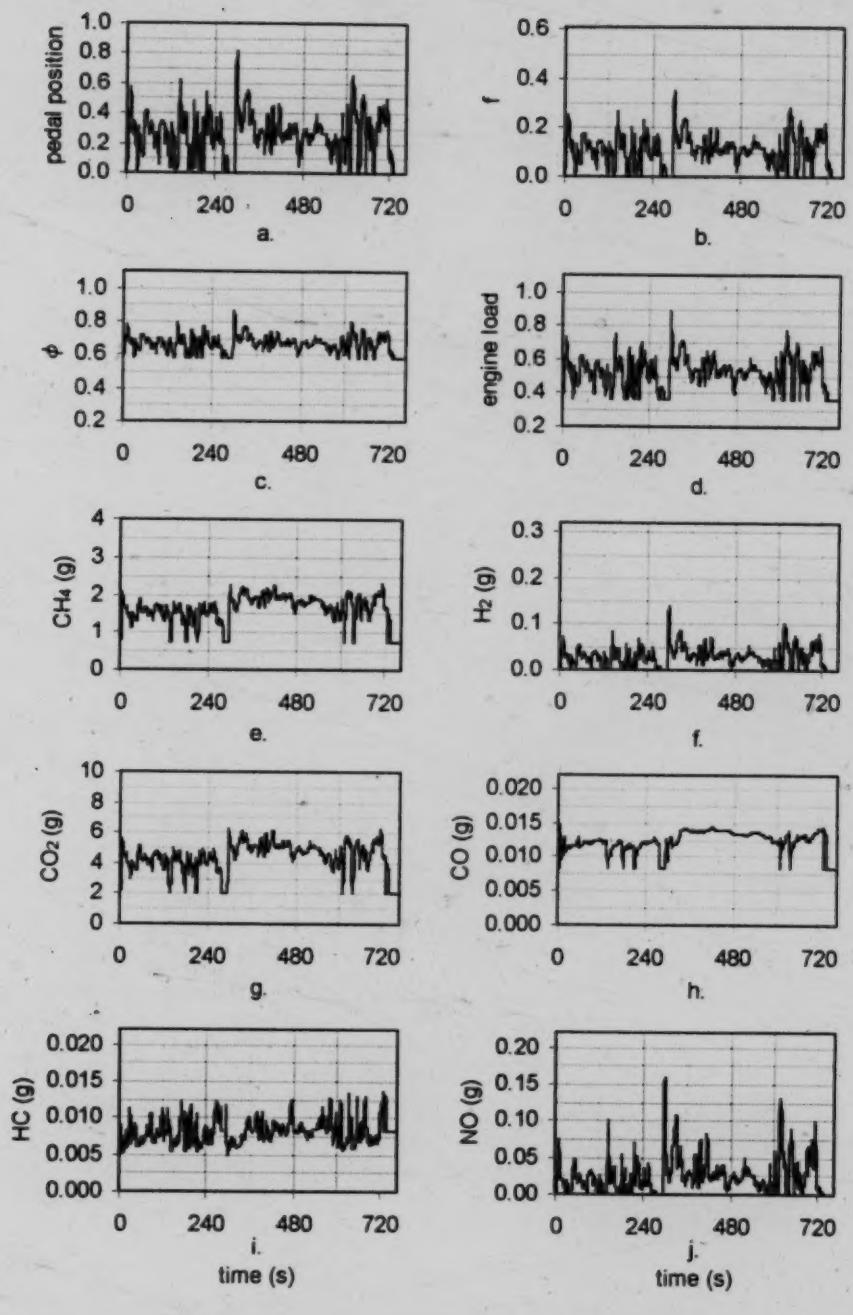

Figure E.22. Case C-K Highway schedule second-by-second results. (a.) Pedal position (b.) Fraction of hydrogen, (c.) Equivalence ratio (d.) Load (e.) Consumption of CH_4 and (f.) H_2. (g.) Production of CO_2 (h.) CO (i.) HC and (j) NO.

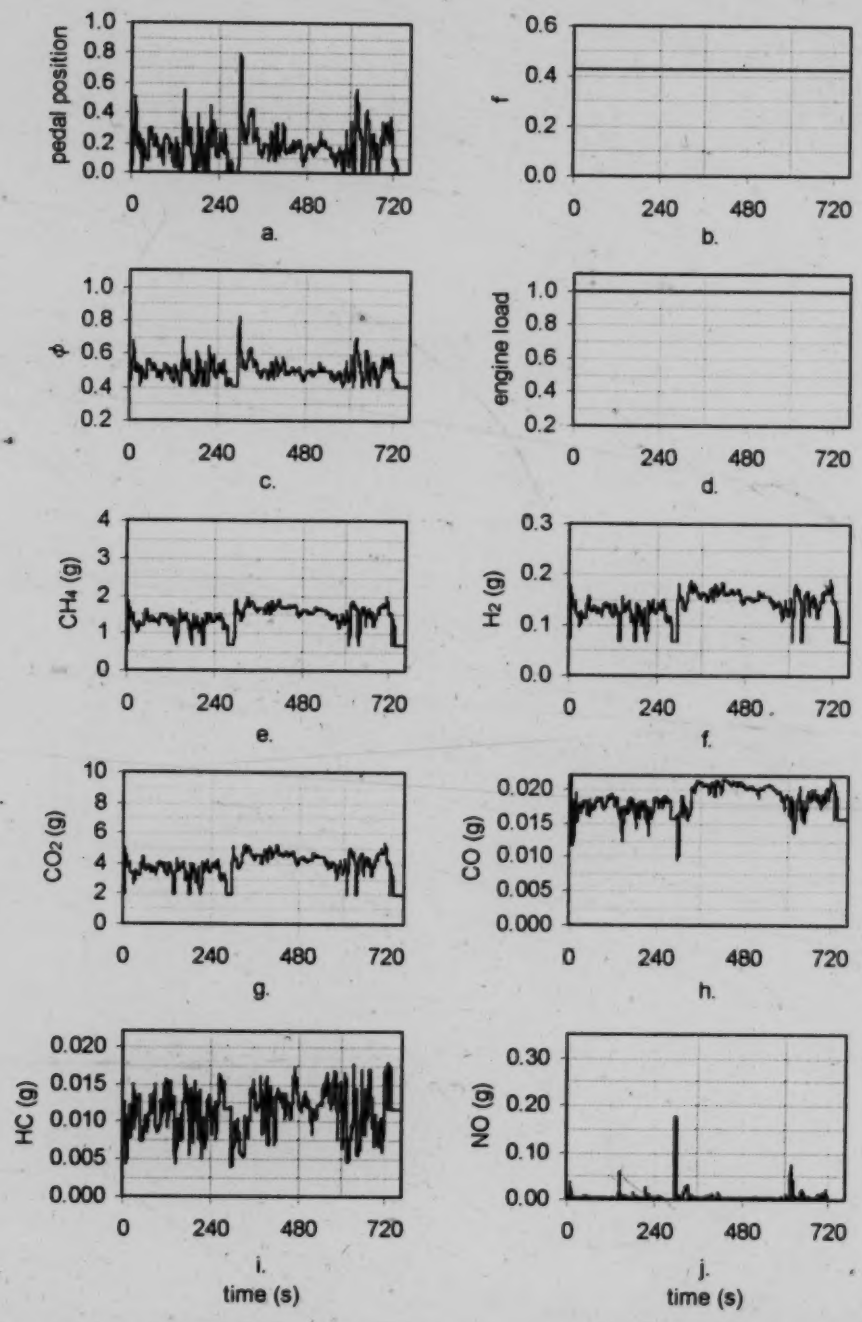

Figure E.23. Case W-K Highway schedule second-by-second results. (a.) Pedal position (b.) Fraction of hydrogen, (c.) Equivalence ratio (d.) Load (e.) Consumption of CH_4 and (f.) H_2. (g.) Production of CO_2 (h.) CO (i.) HC and (j) NO.

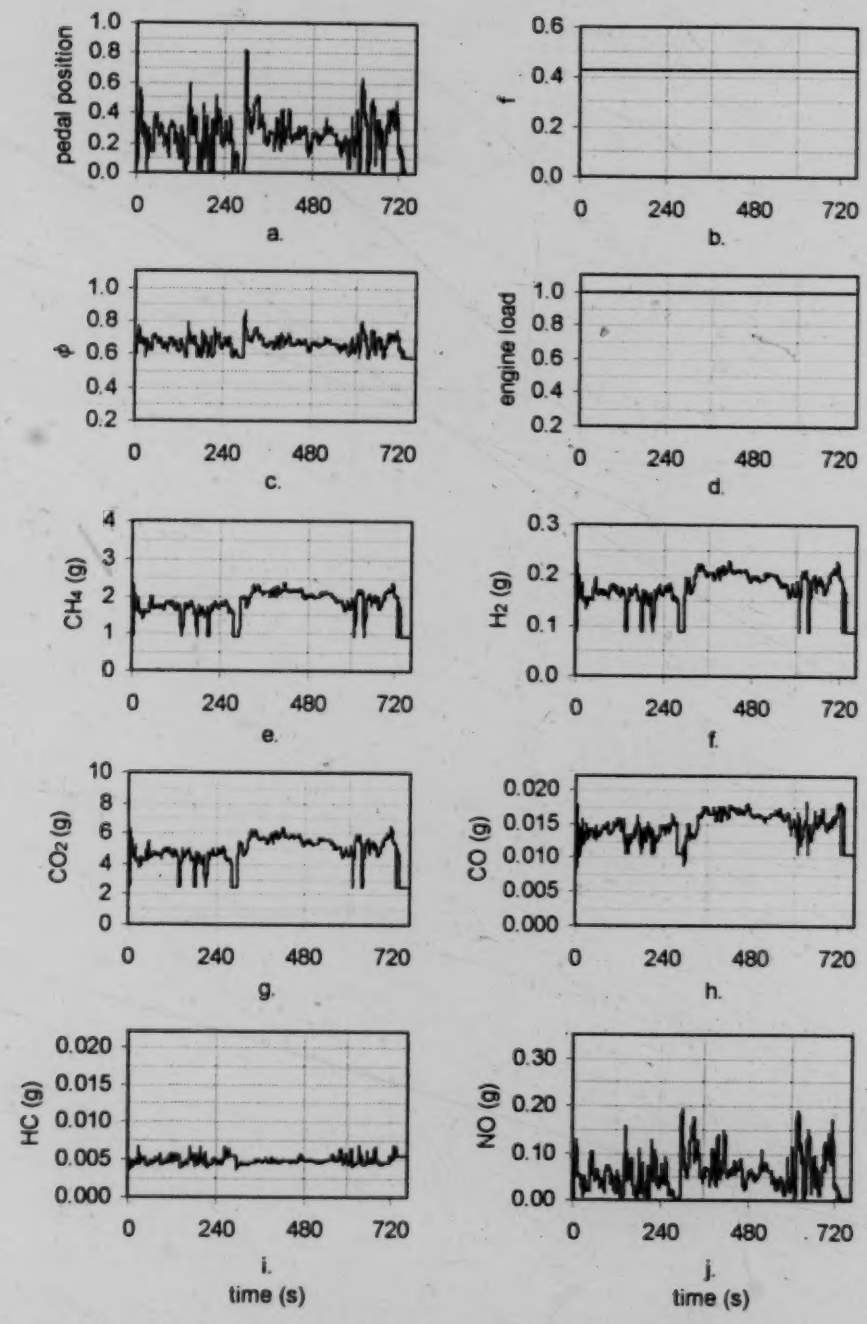

Figure E.24. Case X-K Highway schedule second-by-second results. (a.) Pedal position (b.) Fraction of hydrogen, (c.) Equivalence ratio (d.) Load (e.) Consumption of CH_4 and (f.) H_2. (g.) Production of CO_2 (h.) CO (i.) HC and (j) NO.

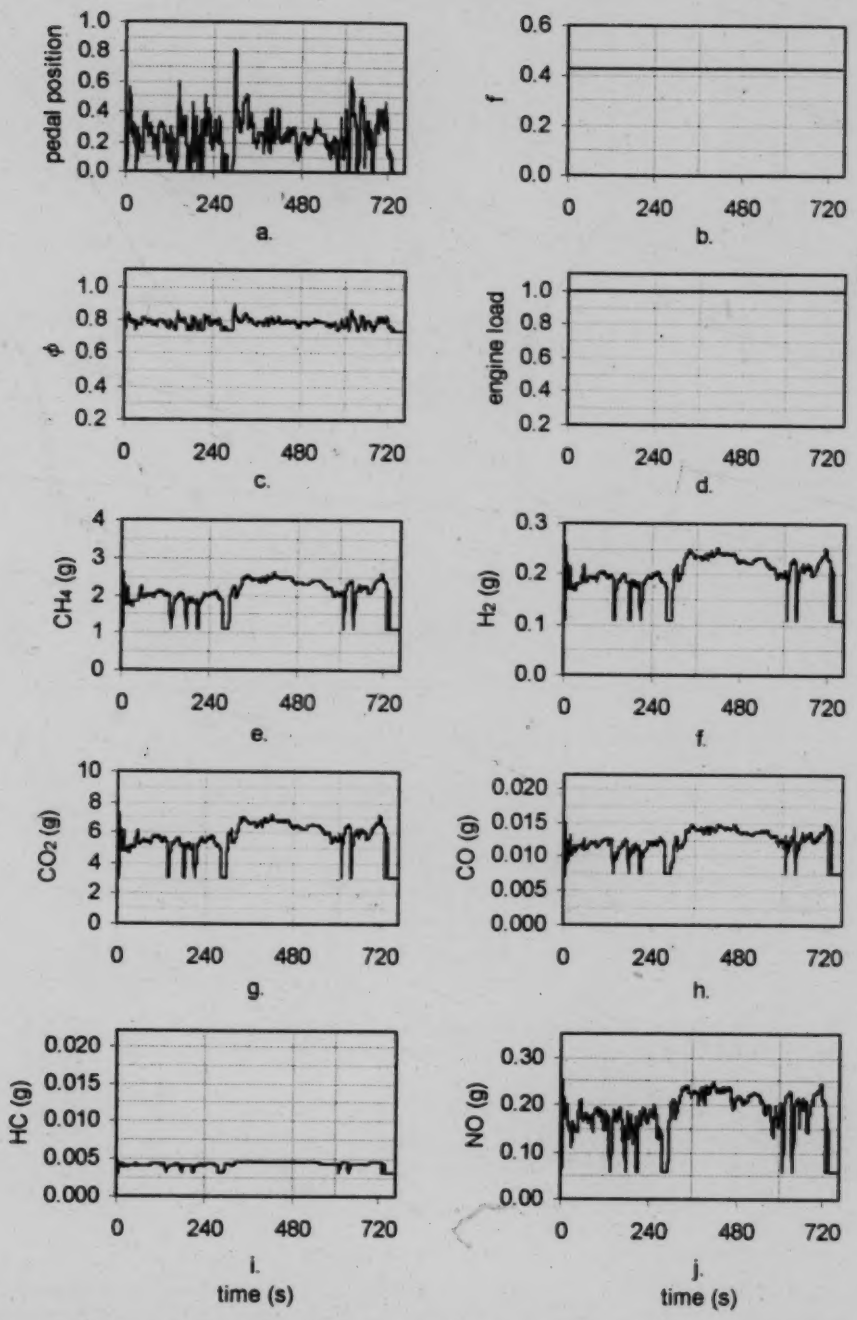

Figure E.25. Case Y-K Highway schedule second-by-second results. (a.) Pedal position (b.) Fraction of hydrogen, (c.) Equivalence ratio (d.) Load (e.) Consumption of CH_4 and (f.) H_2. (g.) Production of CO_2 (h.) CO (i.) HC and (j) NO.

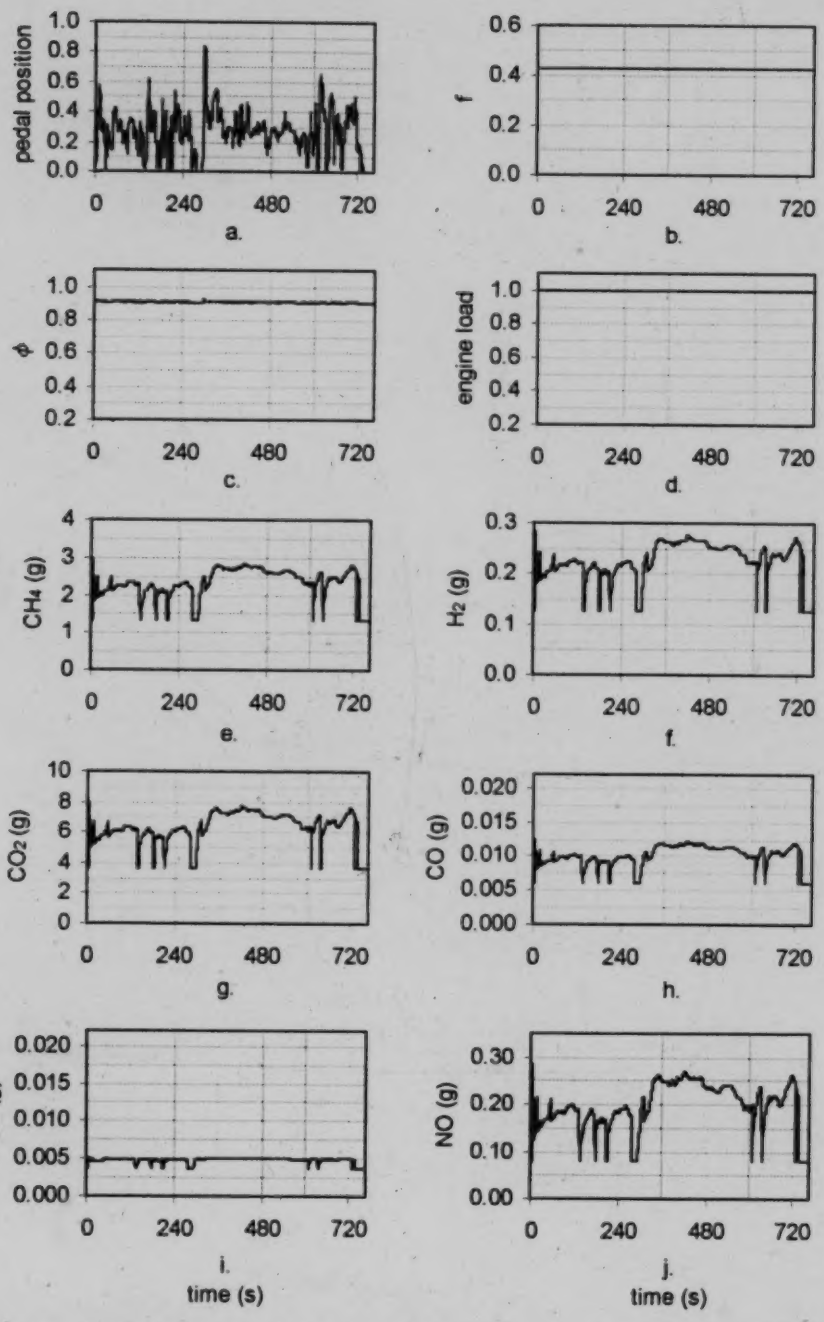

Figure E.26. Case Z-K Highway schedule second-by-second results. (a.) Pedal position (b.) Fraction of hydrogen, (c.) Equivalence ratio (d.) Load (e.) Consumption of CH_4 and (f.) H_2. (g.) Production of CO_2 (h.) CO (i.) HC and (j) NO.

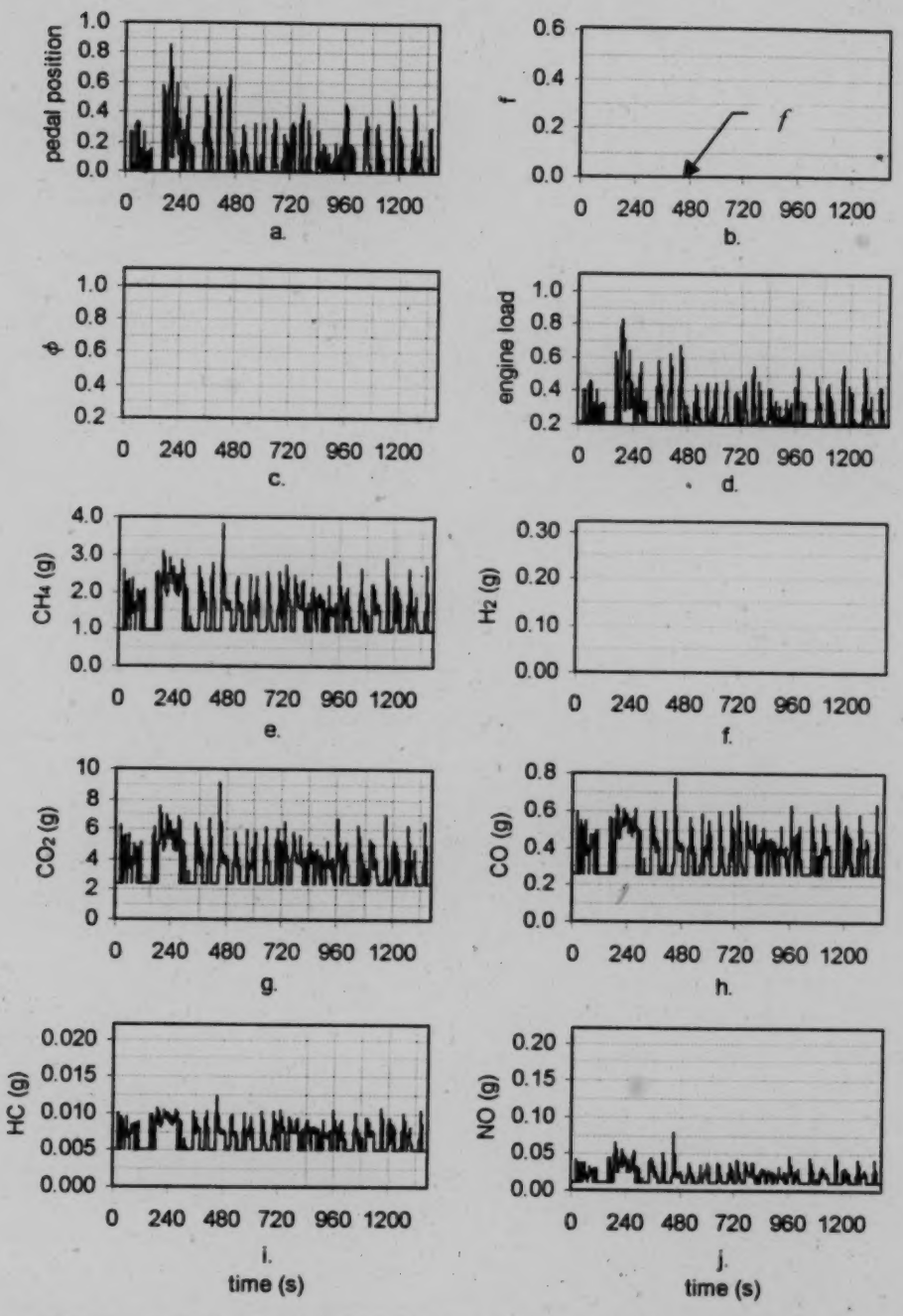

Figure E.27. Case A-G Urban schedule second-by-second results. (a.) Pedal position (b.) Fraction of hydrogen, (c.) Equivalence ratio (d.) Load (e.) Consumption of CH_4 and (f.) H_2. (g.) Production of CO_2 (h.) CO (i.) HC and (j) NO.

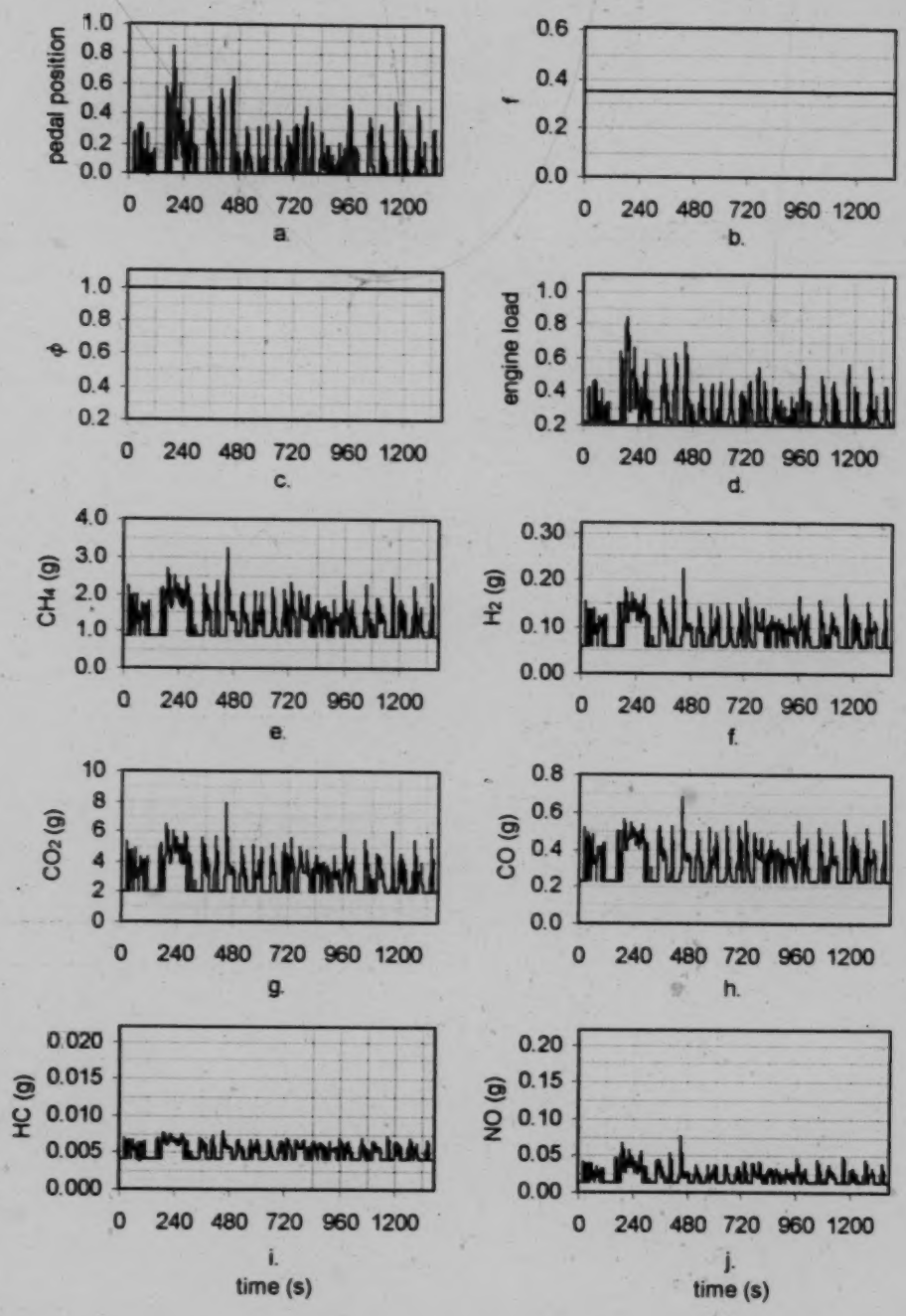

Figure E.28. Case B-H Urban schedule second-by-second results. (a.) Pedal position (b.) Fraction of hydrogen, (c.) Equivalence ratio (d.) Load (e.) Consumption of CH_4 and (f.) H_2. (g.) Production of CO_2 (h.) CO (i.) HC and (j) NO.

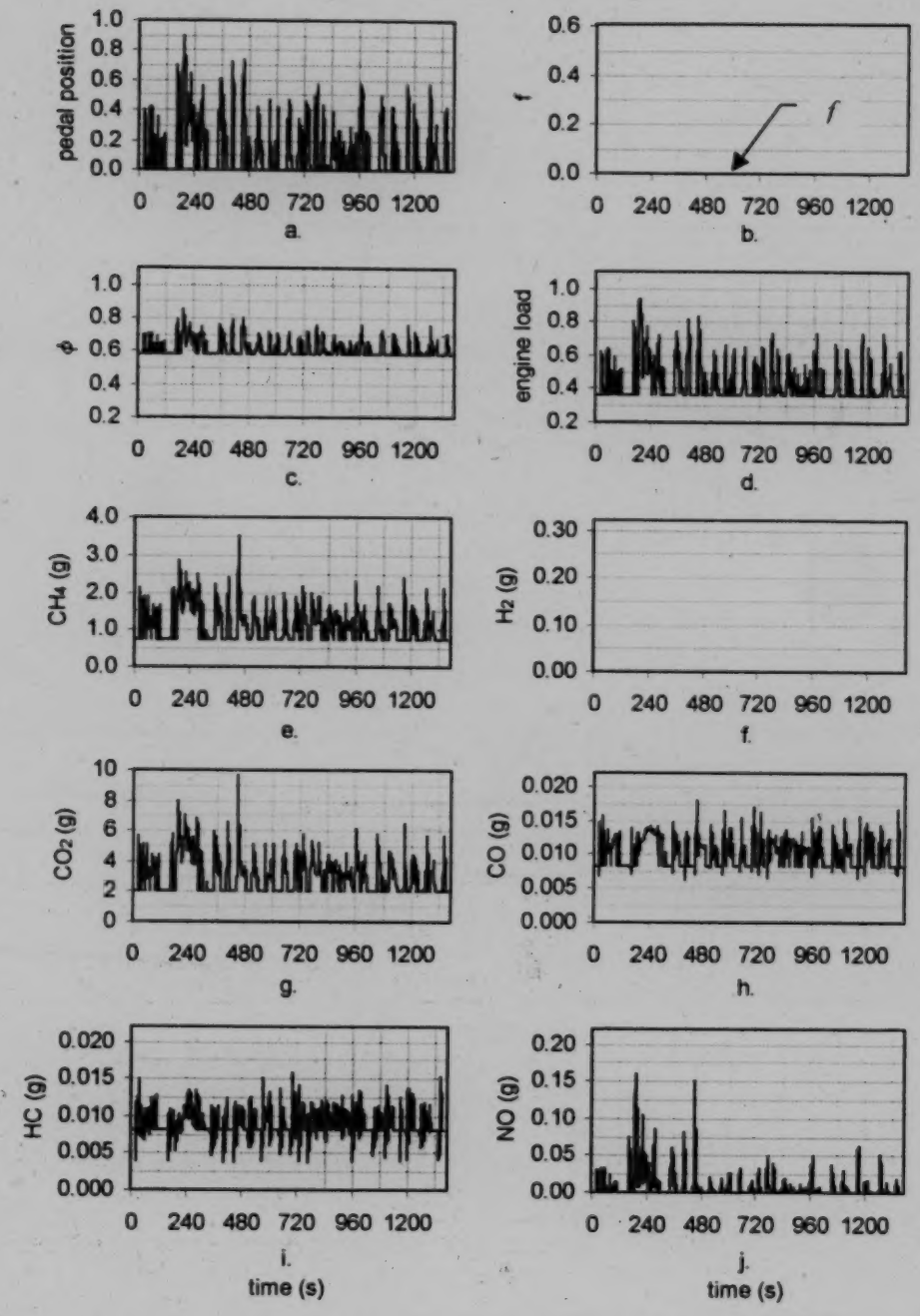

Figure E.29. Case C-I Urban schedule second-by-second results. (a.) Pedal position (b.) Fraction of hydrogen, (c.) Equivalence ratio (d.) Load (e.) Consumption of CH_4 and (f.) H_2. (g.) Production of CO_2 (h.) CO (i.) HC and (j) NO.

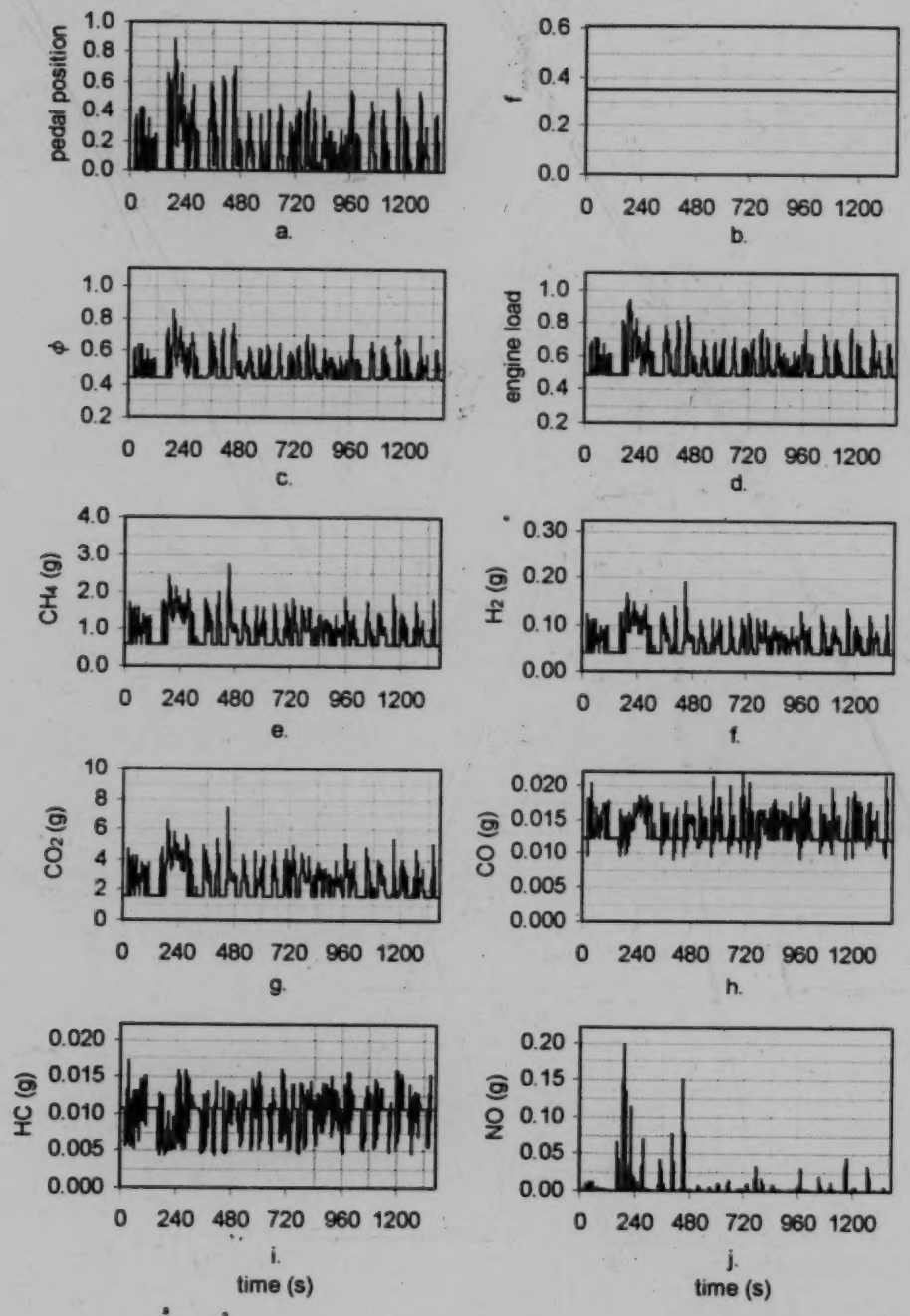

Figure E.30. Case D-J Urban schedule second-by-second results. (a.) Pedal position (b.) Fraction of hydrogen, (c.) Equivalence ratio (d.) Load (e.) Consumption of CH_4 and (f.) H_2. (g.) Production of CO_2 (h.) CO (i.) HC and (j) NO.

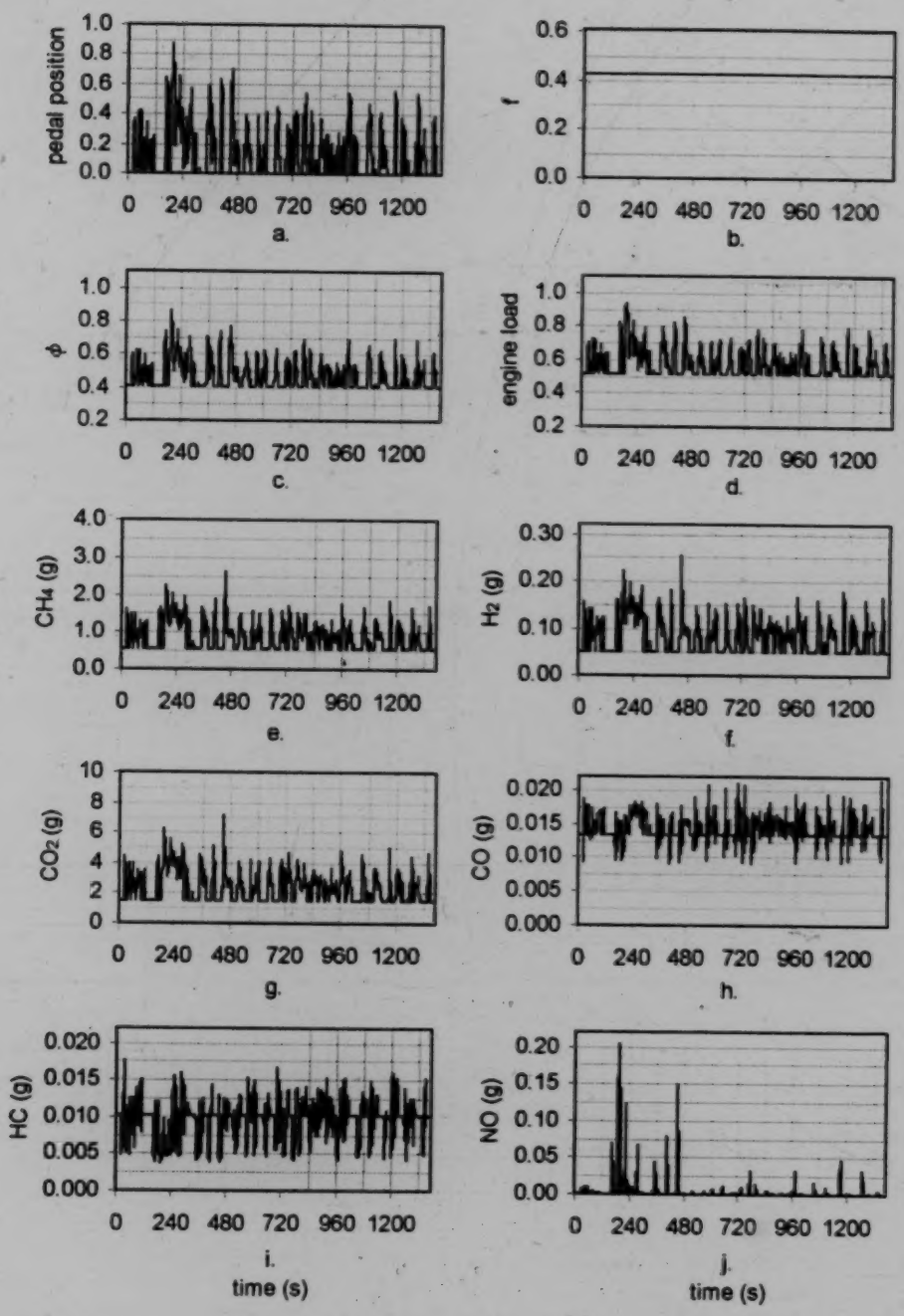

Figure E.31. Case E-K Urban schedule second-by-second results. (a.) Pedal position (b.) Fraction of hydrogen, (c.) Equivalence ratio (d.) Load (e.) Consumption of CH_4 and (f.) H_2. (g.) Production of CO_2 (h.) CO (i.) HC and (j) NO.

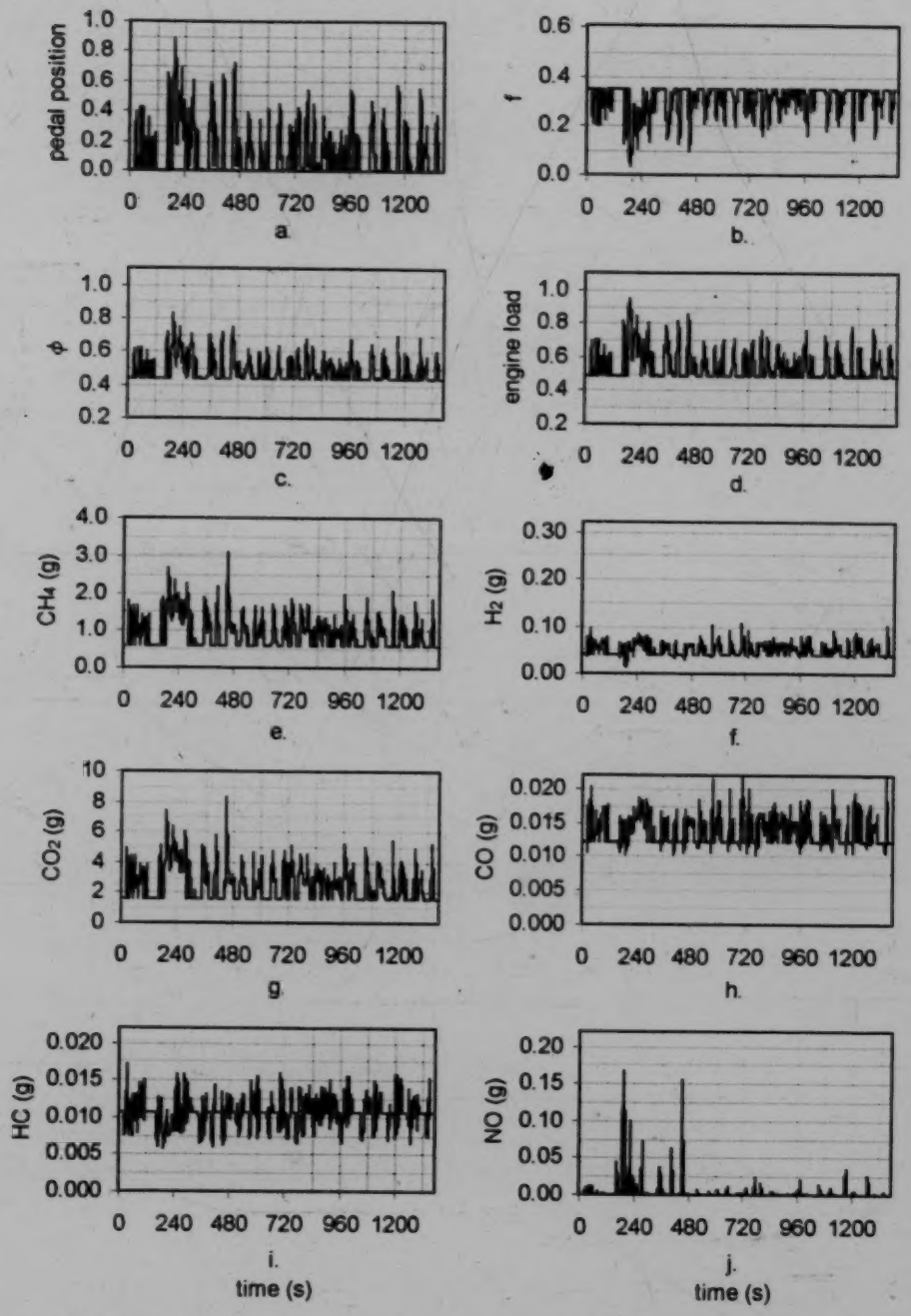

Figure E.32. Case D-I Urban schedule second-by-second results. (a.) Pedal position (b.) Fraction of hydrogen, (c.) Equivalence ratio (d.) Load (e.) Consumption of CH_4 and (f.) H_2. (g.) Production of CO_2 (h.) CO (i.) HC and (j) NO.

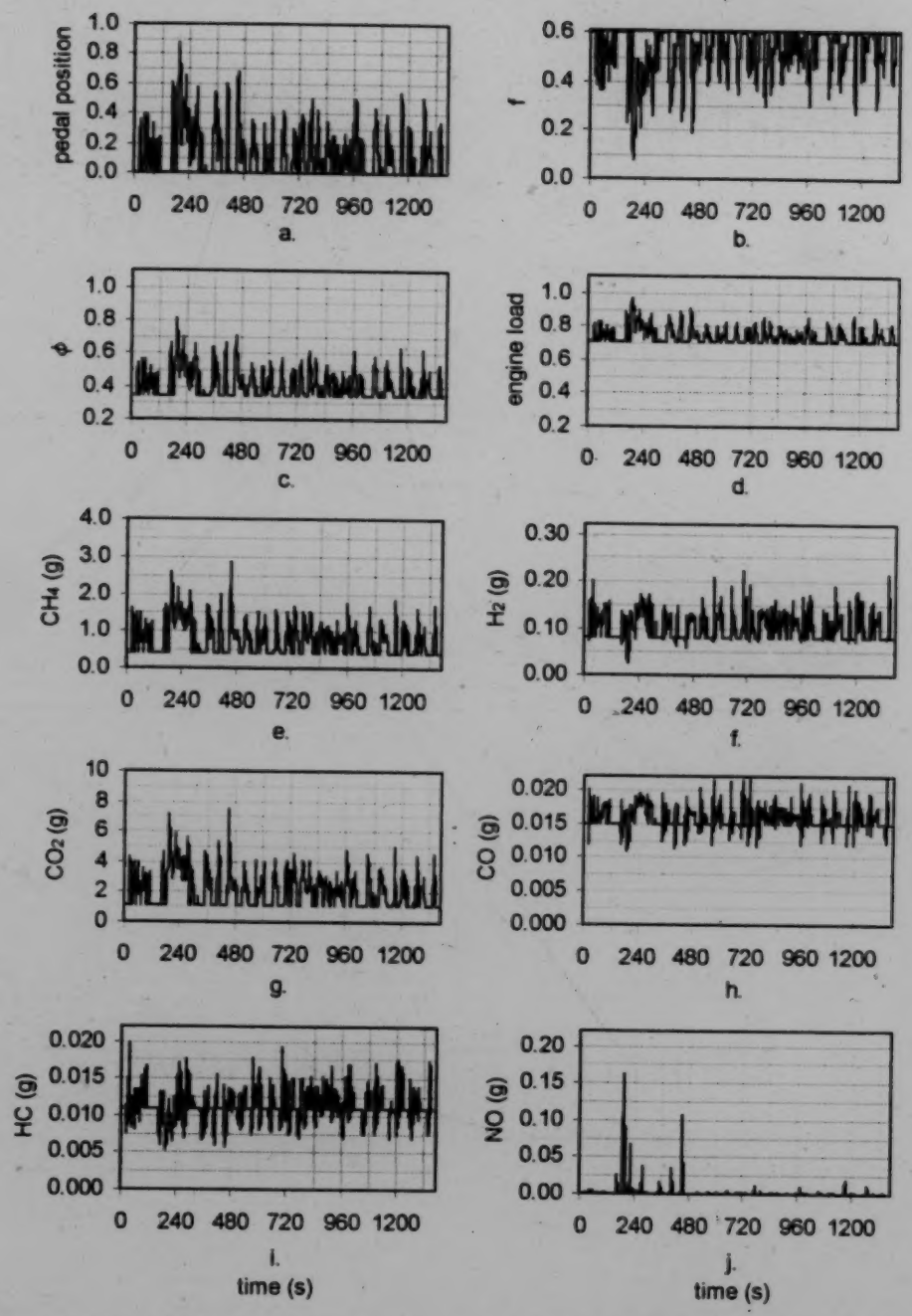

Figure E.33. Case F-I Urban schedule second-by-second results. (a.) Pedal position (b.) Fraction of hydrogen, (c.) Equivalence ratio (d.) Load (e.) Consumption of CH_4 and (f.) H_2. (g.) Production of CO_2 (h.) CO (i.) HC and (j) NO.

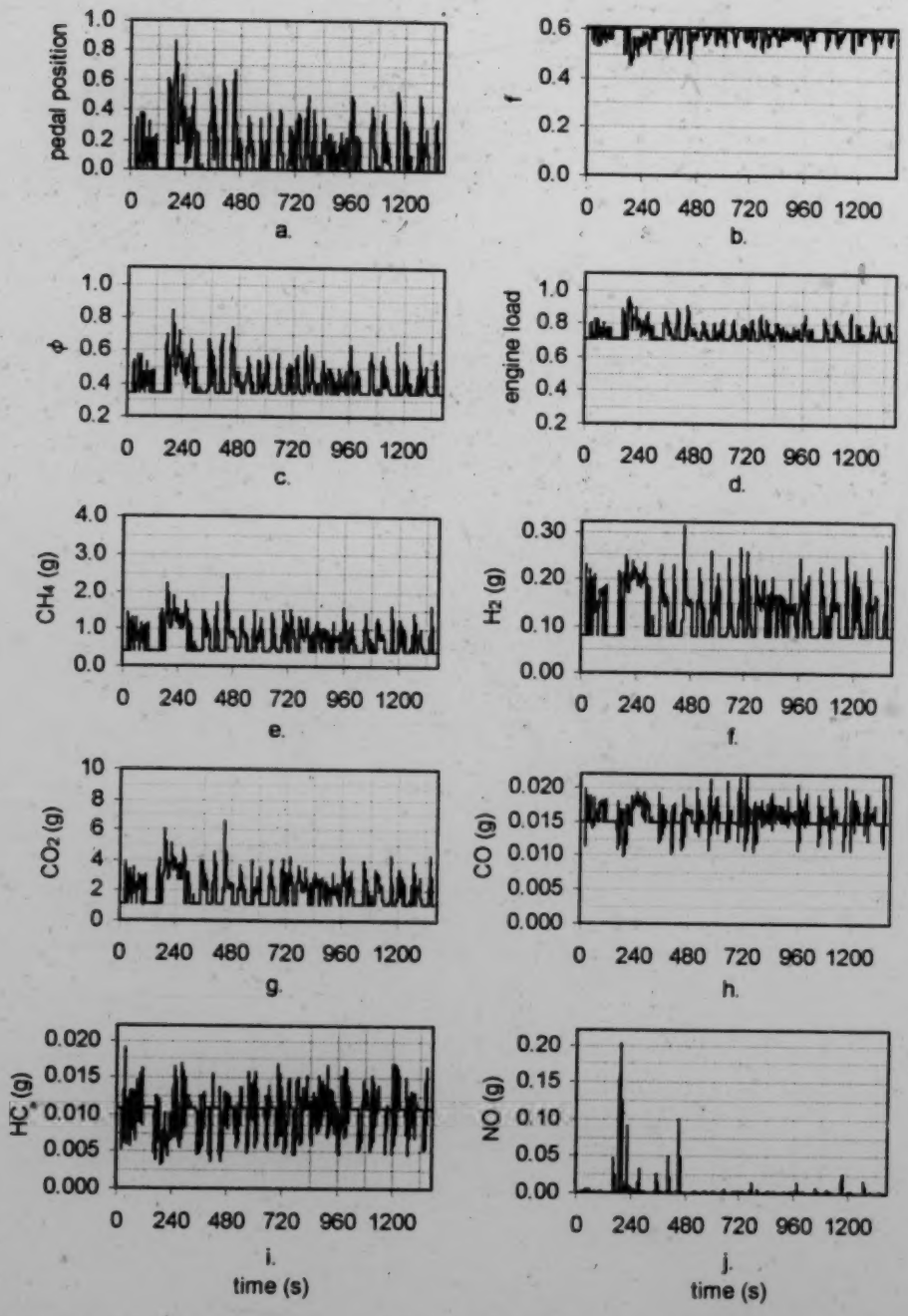

Figure E.34. Case F-K Urban schedule second-by-second results. (a.) Pedal position (b.) Fraction of hydrogen, (c.) Equivalence ratio (d.) Load (e.) Consumption of CH_4 and (f.) H_2. (g.) Production of CO_2 (h.) CO (i.) HC and (j) NO.

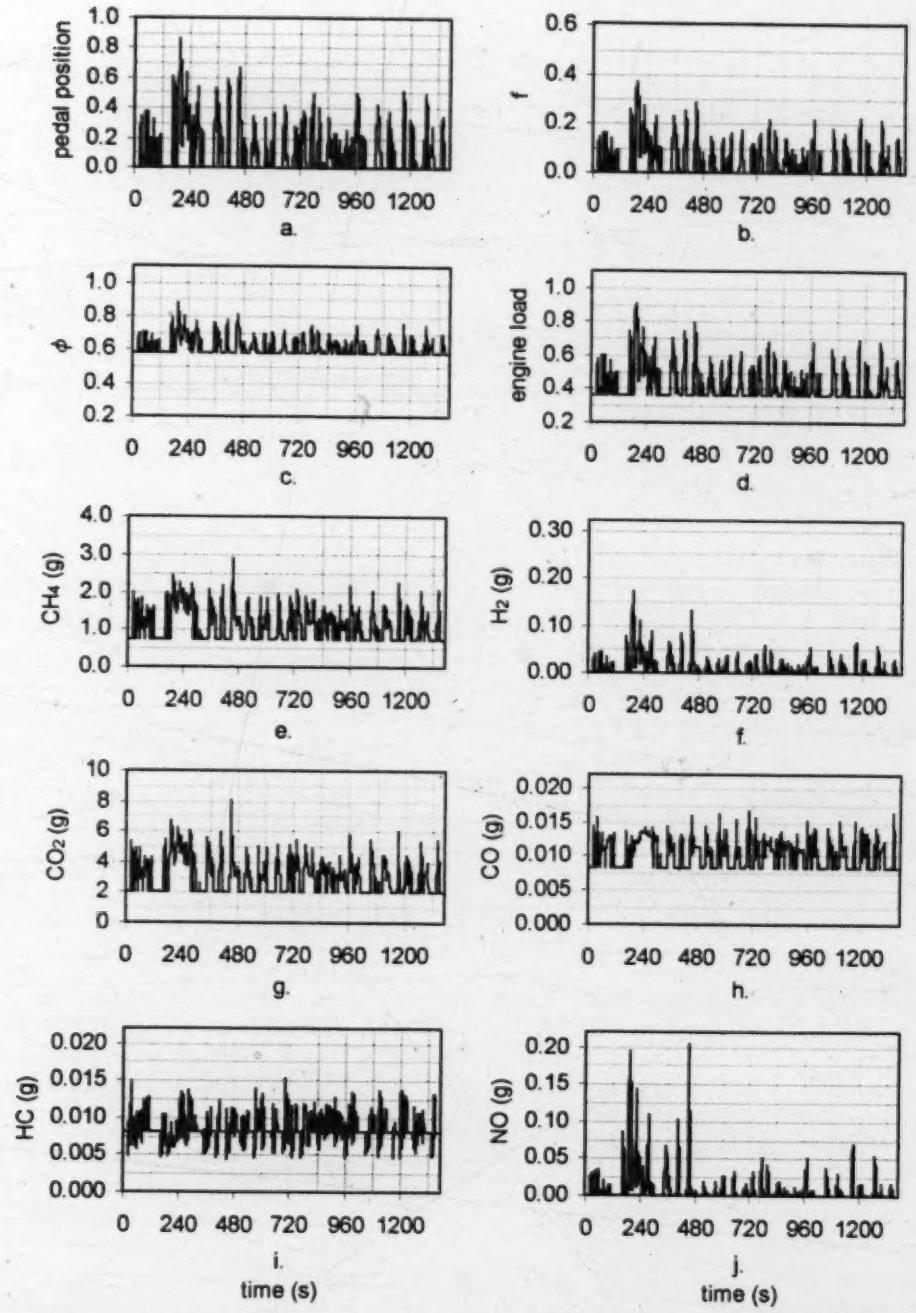

Figure E.35. Case C-K Urban schedule second-by-second results. (a.) Pedal position (b.) Fraction of hydrogen, (c.) Equivalence ratio (d.) Load (e.) Consumption of CH_4 and (f.) H_2. (g.) Production of CO_2 (h.) CO (i.) HC and (j) NO.

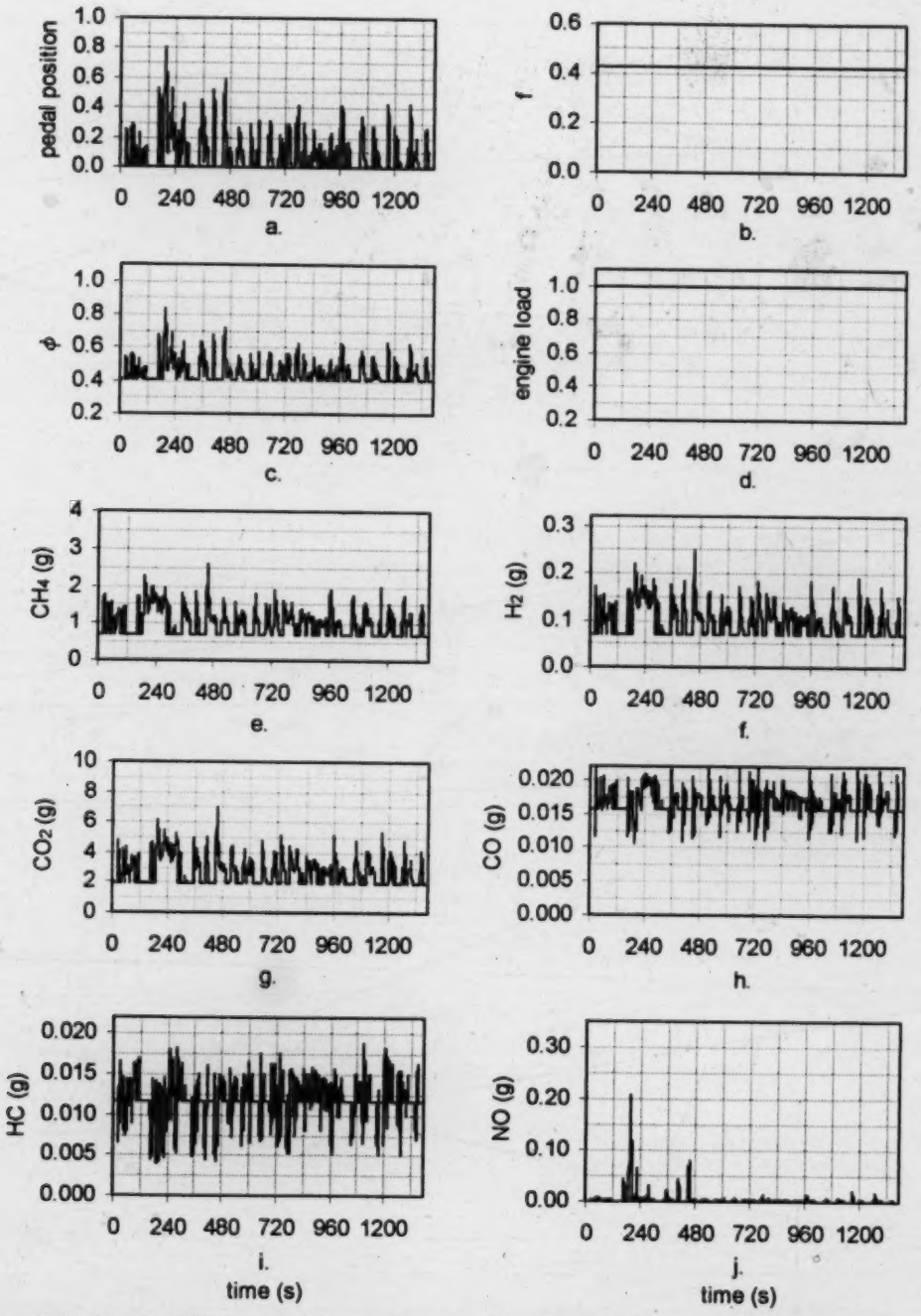

Figure E.36. Case W-K Urban schedule second-by-second results. (a.) Pedal position (b.) Fraction of hydrogen, (c.) Equivalence ratio (d.) Load (e.) Consumption of CH_4 and (f.) H_2. (g.) Production of CO_2 (h.) CO (i.) HC and (j) NO.

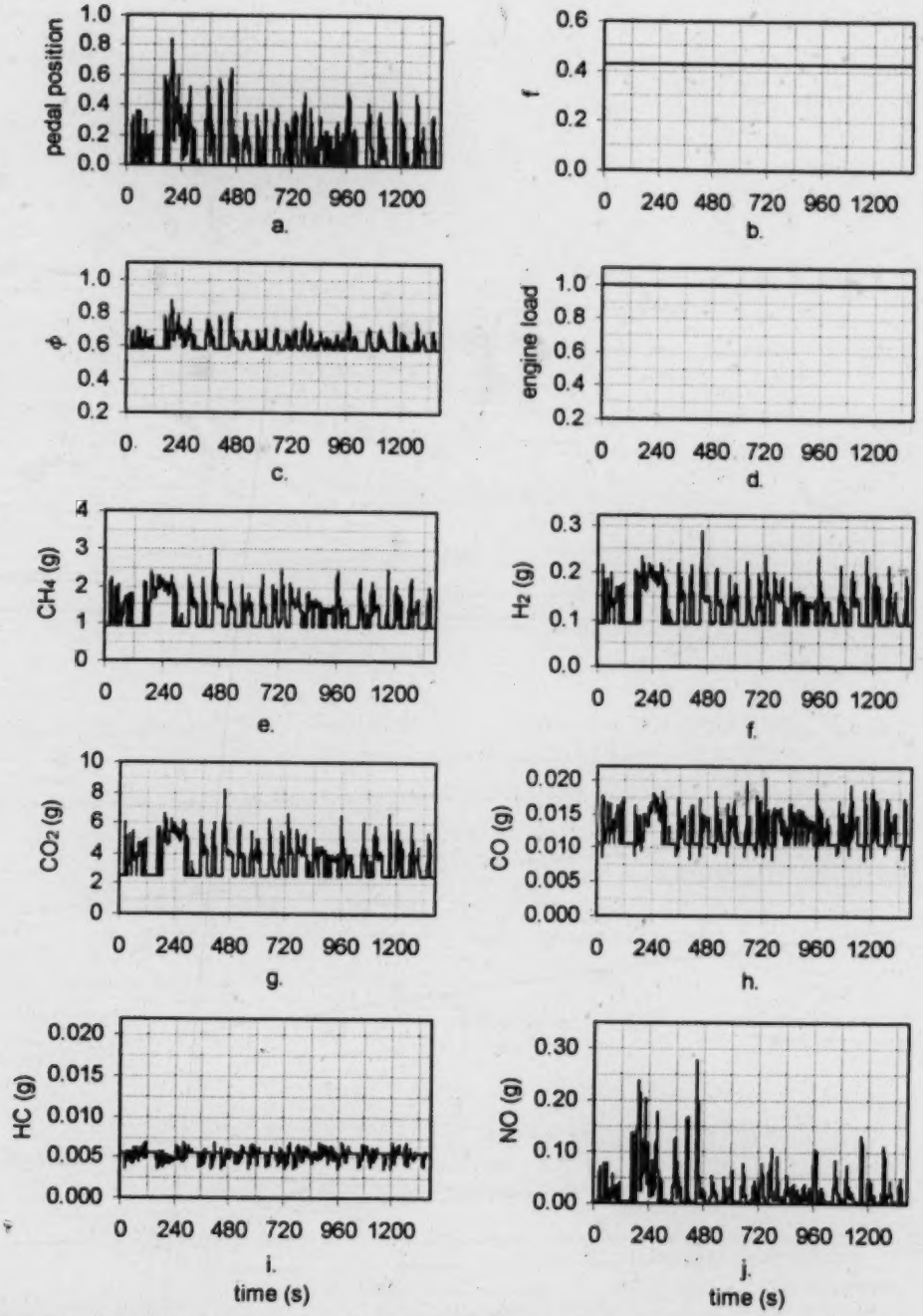

Figure E.37. Case X-K Urban schedule second-by-second results. (a.) Pedal position (b.) Fraction of hydrogen, (c.) Equivalence ratio (d.) Load (e.) Consumption of CH_4 and (f.) H_2. (g.) Production of CO_2 (h.) CO (i.) HC and (j) NO.

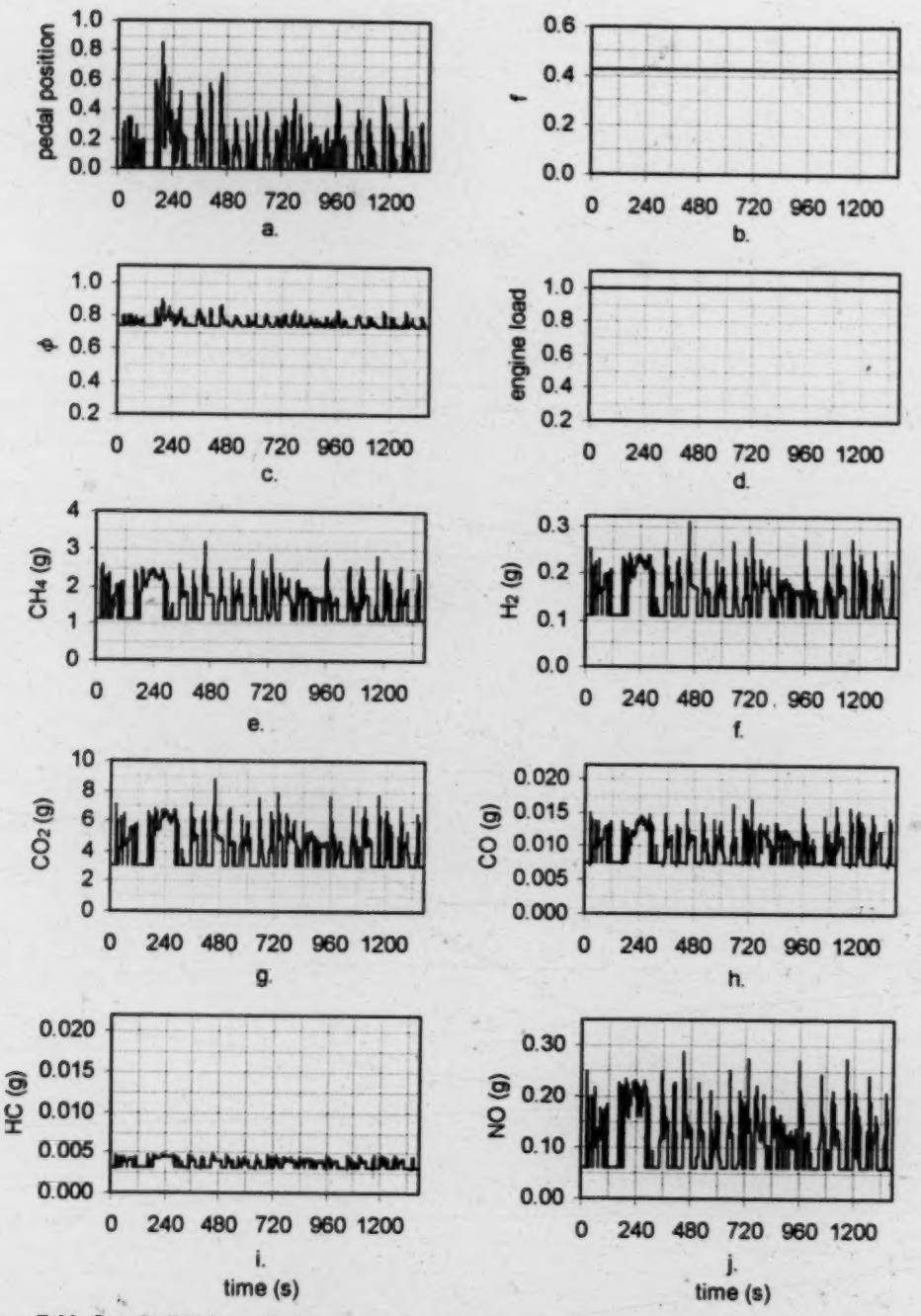

Figure E.38. Case Y-K Urban schedule second-by-second results. (a.) Pedal position (b.) Fraction of hydrogen, (c.) Equivalence ratio (d.) Load (e.) Consumption of CH_4 and (f.) H_2. (g.) Production of CO_2 (h.) CO (i.) HC and (j) NO.

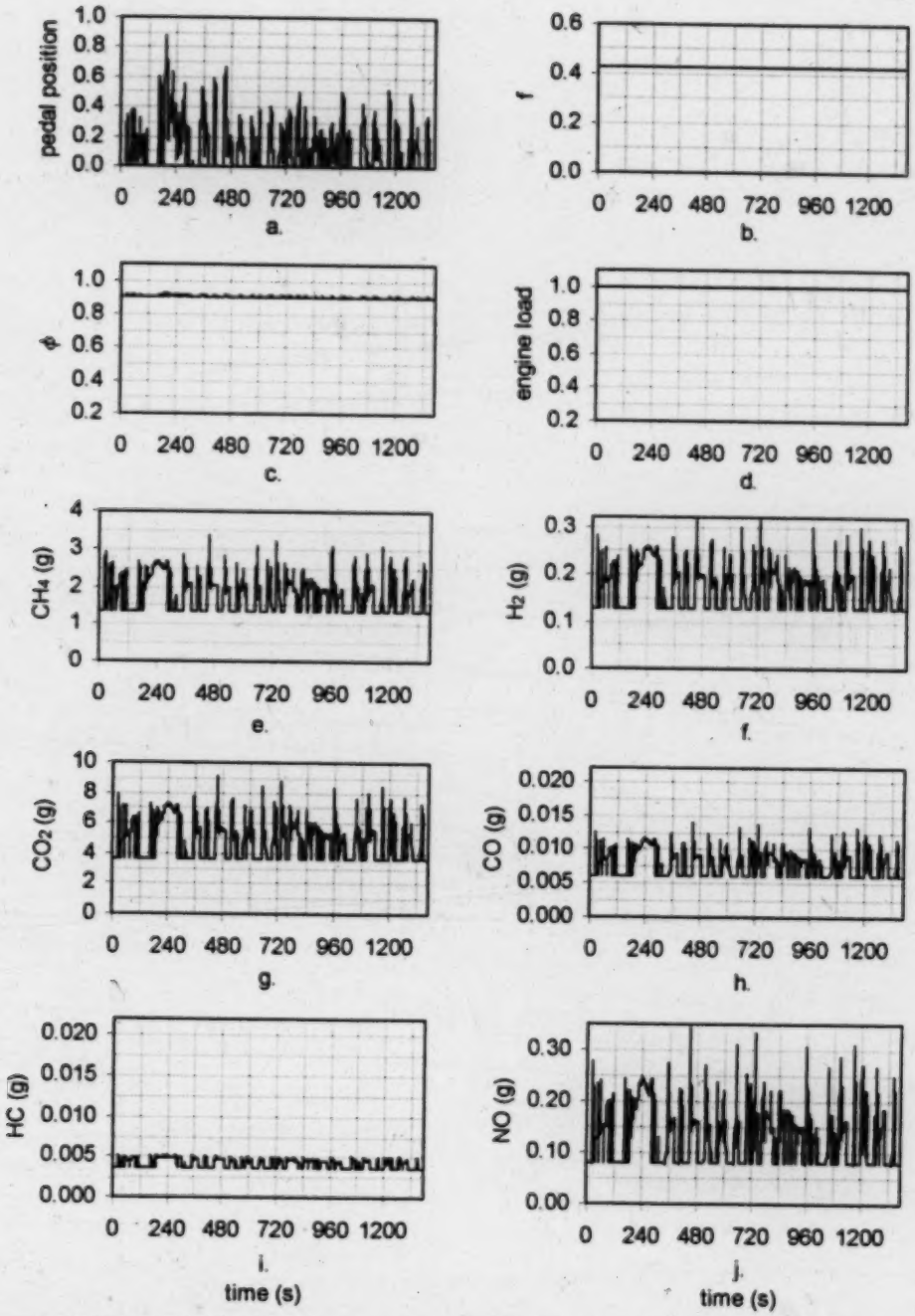

Figure E.39. Case Z-K Urban schedule second-by-second results. (a.) Pedal position (b.) Fraction of hydrogen, (c.) Equivalence ratio (d.) Load (e.) Consumption of CH_4 and (f.) H_2. (g.) Production of CO_2 (h.) CO (i.) HC and (j) NO.

Appendix F. Model sensitivity analysis

The addition of an electrolyser and its subsidiary components will add complexity and weight to the system. What is the impact of adding weight to the model? In order to evaluate this, case W-K at a mass of 1250kg was chosen for a baseline example, as this case contains an electrolyser. As seen in Figure F.1, increasing the mass 24% to 1550kg increases the positive tractive energy (p.t.e.) required to 113% to 120% of the 1250kg value. Negative tractive energy (n.t.e.) is increased to 120% to 125%. However the engine energy (e.e.) only increases to 104%, as the power required at idle is unchanged, and the vehicle requires less power while decelerating from high speeds. At the higher pedal positions required during acceleration, the full time hydrogen produced by the electrolyser decreases to approximately 96%. This is primarily a function of the operating system. Regenerative hydrogen produced increases to approximately 100% to 120%. The highway cycle showed the greatest increase in regenerative H_2 produced, as the increase in braking spikes are small enough to come under the 6.88kW maximum cutoff. The SAE-J-227D and Urban cycles are not as affected, as they contain large braking spikes above the 6.88kW cutoff. Although the engine power increases to 104%, the fuel consumption only increases to only 102%. This is because the higher pedal positions enable the engine to operate at lower *BSFC*. Production of CO_2 and CO are largely unaffected. However the average increase in pedal position is evident in that the average equivalence ratios used approach 0.8 to 0.9 where the production of HCs is low, but the production of NO increases.

It can be surmised that an engine could be redesigned for dedicated operation with hydrogen / methane mixtures. If such a redesign increased the thermal efficiency by 1% (absolute), then what would be the effect on fuel consumption? As seen in Figure F.2, increasing the thermal efficiency of the engine by 1% (absolute) decreases the fuel consumption to 95% for a 1250kg vehicle. Therefore, the impact of engine design and thermal efficiency on fuel consumption is significant.

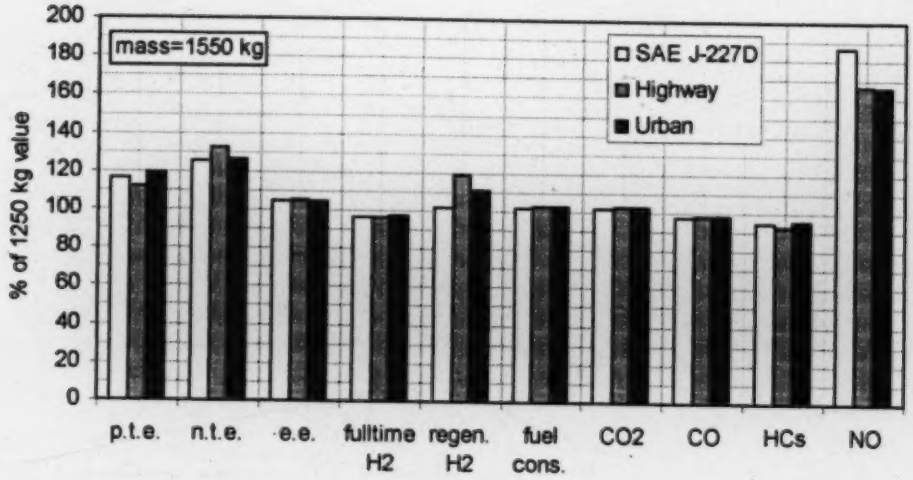

Figure F.1. Effect of increasing the mass of the vehicle model from 1250kg to 1550kg on energy, fuel consumption and pollutant production (using engine case W-K).

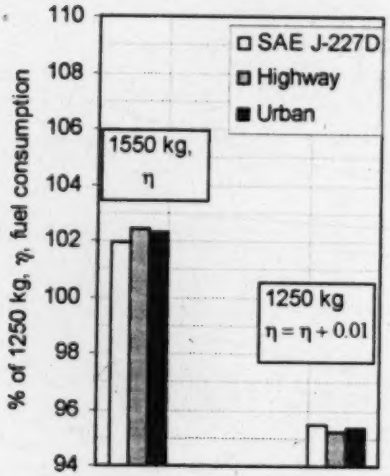

Figure F.2. The effect of increasing the thermal efficiency of the engine by 1% (absolute) compared to the effect of increasing mass on the fuel consumption (using engine case W-K).

Appendix G. Model computer code

The vehicle model was programmed in Visual Basic 5.0. The driving cycle data input was received in the form of a second-by-second text file. Equations for the engine model for each case were received in the form of a text file (see Appendix D). The code is presented here in edited form.

```
'Hydrogen/Methane mixtures
'Program by C.Bauer, 1998

Private Sub Command1_Click()
'Vehicle Model
    Cd = 0.38           'coefficient of drag
    Area = 1.85         'frontal area (m^2)
    mass = 1250         'base vehicle mass (kg)
    Cr = 0.013          'rolling resistance
    Gear1 = 3.46        'gear ratio 1
    Gear2 = 1.94        'gear ratio 2
    Gear3 = 1.29        'gear ratio 3
    Gear4 = 0.97        'gear ratio 4
    Gear5 = 0.81        'gear ratio 5
    FDR = 3.67          'final drive ratio
    tired = 26          'tire diameter (inches)
    rhoair = 1.17       'air density (kg/m^3)

    'Cycle variables
    't - time (s)
    'tmax - maximum cycle time (s)
    'v - velocity (km/kr)
    'd - distance(m)
    'a - acceleration (m/s^2)
    'aero - aerodynamic drag (N)
    'rolling - rolling resistance (N)
    'inertial - inertial resistance (N)
    'reqpower - required power (kW)
    'gear - gear, 0=neutral
```

```
'Engine Model
    shiftmax = 2000          'upper shift point (RPM)
    shiftmin = 1300          'lower shift point (RPM)
    idle = 1000              'idle speed (RPM)

    'Cycle variables
    'RPM – engine speed (RPM)
    'pedal - pedal position
    'f – hydrogen fraction
    'equiv – equivalence ratio
    'lode – engine load
    'power – engine power delivered to the ground (kW)
    'bsfc – brake specific fuel consumption (g/kWhr)
    'fc – fuel consumption (g)
    'h2 – H2 consumption (g)
    'ch4 – CH4 consumption (g)
    'bsco2 – brake specific production of CO2 (g/kWhr)
    'co2 – CO2 (g)
    'bsco– brake specific production of CO (g/kWhr)
    'co – CO (g)
    'bshc - brake specific production of HC (g/kWhr)
    'hc – HC (g)
    'bsno - brake specific production of NO (g/kWhr)
    'no – NO (g)
    'pengine – engine power (kW)
    'pgenerator – engine power sent to full-time generator (kW)
    'pfulltime – full time power sent to electrolyser (kW)
    'pregen – regenerative power sent to electrolyser (kW)
    'pelectro – total power received by electrolyser (kW)
    'h2fulltime – hydrogen produced by fulltime electrolysis (g)
    'h2regen - hydrogen produced by regeneration electrolysis (g)
    'h2pro – total hydrogen produced by electrolysis (g)

    'Input driving cycle
    If Option1.Value = True Then Open "c:\windows\desktop\model\urban.prn" For Input As #1
    If Option2.Value = True Then Open "c:\windows\desktop\model\hiway.prn" For Input As #1
    If Option3.Value = True Then Open "c:\windows\desktop\model\J-227D.prn" For Input As #1
```

```
Input #1, tmax
  ReDim v(0 To tmax + 2) As Single
  For i = 1 To tmax
    Input #1, t, v(i)
  Next I
 Close #1

'Input engine model case
 Input #2, A1, A2, A3, A4, A5, A6        'f
 Input #2, B1, B2, B3, B4, B5, B6        'equiv
 Input #2, C1, C2, C3, C4, C5, C6        'lode
 Input #2, D1, D2, D3, D4, D5, D6        'P1400
 Input #2, E1, E2, E3, E4, E5, E6        'P1800
 Input #2, F1, F2, F3, F4, F5, F6        'BSFC1400
 Input #2, G1, G2, G3, G4, G5, G6        'BSFC1800
 Input #2, I1, I2, I3, I4, I5, I6        'BSCO21400
 Input #2, J1, J2, J3, J4, J5, J6        'BSCO21800
 Input #2, K1, K2, K3, K4, K5, K6        'BSCO
 Input #2, L1, L2, L3, L4, L5, L6        'BSHC1400
 Input #2, M1, M2, M3, M4, M5, M6        'BSHC1800
 Input #2, N1                            'NO limit
 Input #2, O1, O2, O3, O4, O5, O6        'BSNO14001
 Input #2, P1, P2, P3, P4, P5, P6        'BSNO18002
 Input #2, Q1, Q2, Q3, Q4, Q5, Q6        'BSNO14002
 Input #2, R1, R2, R3, R4, R5, R6        'BSNO18002
 Input #2, S1, S2, S3, S4, S5, S6        'Electrolyser Power
 Input #2, T1, T2, T3                    'Electrolyser min. cutoff, max. cutoff, tag
 Close #2

'Second-by-second calculations
  'Set initial RPM and initial gear
  RPM(0) = idle
  gear(0) = 1

  For i = 1 To tmax
    'Vehicle model calculations
    If v(i) > 0 Then
```

```
    gear(i) = gear(i - 1)
    If RPM(i - 1) > shiftmax Then
      gear(i) = gear(i - 1) + 1
    End If

    If RPM(i - 1) < shiftmin Then
      gear(i) = gear(i - 1) - 1
    End If

    If gear(i) <= 0 Then
      gear(i) = 1
    End If
    If gear(i) >= 5 Then
      gear(i) = 5
    End If
    If gear(i) = 1 Then
      RPM(i) = (v(i) * Gear1 * FDR * 60) / (tired * 0.0254 * 3.14 * 3.6)
    End If
    If gear(i) = 2 Then
      RPM(i) = (v(i) * Gear2 * FDR * 60) / (tired * 0.0254 * 3.14 * 3.6)
    End If
    If gear(i) = 3 Then
      RPM(i) = (v(i) * Gear3 * FDR * 60) / (tired * 0.0254 * 3.14 * 3.6)
    End If
    If gear(i) = 4 Then
      RPM(i) = (v(i) * Gear4 * FDR * 60) / (tired * 0.0254 * 3.14 * 3.6)
    End If
    If gear(i) = 5 Then
      RPM(i) = (v(i) * Gear5 * FDR * 60) / (tired * 0.0254 * 3.14 * 3.6)
    End If

    'Slip clutch for low RPM when starting
    If RPM(i) < idle Then RPM(i) = idle

  Else
    gear(i) = 0
    RPM(i) = idle
```

```
End If

'Calculate vehicle model required power
d(i) = d(i - 1) + v(i) / 3.6
a(i) = (v(i + 1) - v(i - 1)) / (2 * 3.6)
aero = Cd * Area * rhoair * ((v(i) / 3.6) ^ 2) / 2
rolling = mass * 9.807 * Cr
inertial = mass * a(i)
reqpower(i) = v(i) * (aero + rolling + inertial) / 3600
'Add nominal power required (4.95 kW) due to engine idle setpoint
If reqpower(i) >= 0 Then reqpower(i) = reqpower(i) + 4.95

'Let engine idle while decelerating
If reqpower(i) <= 0 Then
  RPM1 = RPM(i)
  RPM(i) = idle
End If

'Engine model calculations
pedal(i) = 0

'Incremental increasing of pedal position until desired power is reached
For k = 1 To 100
    P1400 = D1 * pedal(i) ^ 5 + D2 * pedal(i) ^ 4 + D3 * pedal(i) ^ 3 + D4 * pedal(i) ^ 2 + D5 *
    pedal(i) + D6
    P1800 = E1 * pedal(i) ^ 5 + E2 * pedal(i) ^ 4 + E3 * pedal(i) ^ 3 + E4 * pedal(i) ^ 2 + E5 *
    pedal(i) + E6
    pengine(i) = (P1800 - P1400) / 400 * RPM(i) + 4.5 * P1400 - 3.5 * P1800

  If T3 = 1 Then
    pgenerator(i) = (S1 * pedal(i) ^ 5 + S2 * pedal(i) ^ 4 + S3 * pedal(i) ^ 3 + S4 * pedal(i) ^ 2 + S5 *
    pedal(i) + S6)
  End If
  If T3 = 2 Then
    pgenerator(i) = (S1 * pedal(i) ^ 5 + S2 * pedal(i) ^ 4 + S3 * pedal(i) ^ 3 + S4 * pedal(i) ^ 2 + S5 *
    pedal(i) + S6) * RPM(i) / 1000
  End If
```

```
    power(i) = pengine(i) - pgenerator(i)

    If power(i) - reqpower(i) < 0.001 Then pedal(i) = pedal(i) + 0.01
Next k

'Tracking hydrogen fraction, equivalence, & load
f(i) = A1 * pedal(i) ^ 5 + A2 * pedal(i) ^ 4 + A3 * pedal(i) ^ 3 + A4 * pedal(i) ^ 2 + A5 * pedal(i) +
A6
If f(i) = 0 Then f(i) = 0.0001
equiv(i) = B1 * pedal(i) ^ 5 + B2 * pedal(i) ^ 4 + B3 * pedal(i) ^ 3 + B4 * pedal(i) ^ 2 + B5 * pedal(i)
+ B6
lode(i) = C1 * pedal(i) ^ 5 + C2 * pedal(i) ^ 4 + C3 * pedal(i) ^ 3 + C4 * pedal(i) ^ 2 + C5 * pedal(i)
+ C6

'instantaneous consumption/production of fuel/pollutant (g)
bsfc1400 = F1 * pedal(i) ^ 5 + F2 * pedal(i) ^ 4 + F3 * pedal(i) ^ 3 + F4 * pedal(i) ^ 2 + F5 * pedal(i)
+ F6
bsfc1800 = G1 * pedal(i) ^ 5 + G2 * pedal(i) ^ 4 + G3 * pedal(i) ^ 3 + G4 * pedal(i) ^ 2 + G5 *
pedal(i) + G6
bsfc(i) = (bsfc1800 - bsfc1400) / 400 * RPM(i) + 4.5 * bsfc1400 - 3.5 * bsfc1800
fc(i) = (pengine(i) * bsfc(i)) / 3600
h2(i) = fc(i) / (1 + ((1 - f(i)) * 0.65119) / (f(i) * 0.083764))
h2c(i) = h2c(i - 1) + h2(i)
ch4(i) = fc(i) - h2(i)
ch4c(i) = ch4c(i - 1) + ch4(i)

bsco21400 = I1 * pedal(i) ^ 5 + I2 * pedal(i) ^ 4 + I3 * pedal(i) ^ 3 + I4 * pedal(i) ^ 2 + I5 * pedal(i)
+ I6
bsco21800 = J1 * pedal(i) ^ 5 + J2 * pedal(i) ^ 4 + J3 * pedal(i) ^ 3 + J4 * pedal(i) ^ 2 + J5 * pedal(i)
+ J6
bsco2(i) = (bsco21800 - bsco21400) / 400 * RPM(i) + 4.5 * bsco21400 - 3.5 * bsco21800
co2(i) = (pengine(i) * bsco2(i)) / 3600
co2c(i) = co2c(i - 1) + co2(i)

bsco(i) = K1 * pedal(i) ^ 5 + K2 * pedal(i) ^ 4 + K3 * pedal(i) ^ 3 + K4 * pedal(i) ^ 2 + K5 * pedal(i)
+ K6
```

```
co(i) = (pengine(i) * bsco(i)) / 3600
coc(i) = coc(i - 1) + co(i)

bshc1400 = L1 * pedal(i) ^ 5 + L2 * pedal(i) ^ 4 + L3 * pedal(i) ^ 3 + L4 * pedal(i) ^ 2 + L5 *
pedal(i) + L6
bshc1800 = M1 * pedal(i) ^ 5 + M2 * pedal(i) ^ 4 + M3 * pedal(i) ^ 3 + M4 * pedal(i) ^ 2 + M5 *
pedal(i) + M6
bshc(i) = (bshc1800 - bshc1400) / 400 * RPM(i) + 4.5 * bshc1400 - 3.5 * bshc1800
hc(i) = (pengine(i) * bshc(i)) / 3600
hcc(i) = hcc(i - 1) + hc(i)

If pedal(i) <= N1 Then
    bsno1400 = O1 * pedal(i) ^ 5 + O2 * pedal(i) ^ 4 + O3 * pedal(i) ^ 3 + O4 * pedal(i) ^ 2 + O5 *
    pedal(i) + O6
    bsno1800 = P1 * pedal(i) ^ 5 + P2 * pedal(i) ^ 4 + P3 * pedal(i) ^ 3 + P4 * pedal(i) ^ 2 + P5 *
    pedal(i) + P6
End If

If pedal(i) > N1 Then
    bsno1400 = Q1 * pedal(i) ^ 5 + Q2 * pedal(i) ^ 4 + Q3 * pedal(i) ^ 3 + Q4 * pedal(i) ^ 2 + Q5 *
    pedal(i) + Q6
    bsno1800 = R1 * pedal(i) ^ 5 + R2 * pedal(i) ^ 4 + R3 * pedal(i) ^ 3 + R4 * pedal(i) ^ 2 + R5 *
    pedal(i) + R6
End If

bsno(i) = (bsno1800 - bsno1400) / 400 * RPM(i) + 4.5 * bsno1400 - 3.5 * bsno1800
no(i) = (pengine(i) * bsno(i)) / 3600
noc(i) = noc(i - 1) + no(i)

'Electrolyser calculations
    'Cumulative engine energy
    penginec(i) = penginec(i - 1) + pengine(i)
    'Cumulative generator power
    pgeneratorc(i) = pgeneratorc(i - 1) + pgenerator(i)

    'Full-time electrolyser power
    h2pro(i) = 0
```

```
pfulltime(i) = 0.9 * pgenerator(i)

'Regenerative electrolyser power
If reqpower(i) <= -1 Then
    pregen(i) = Abs(reqpower(i))
Else
    pregen(i) = 0
End If

If reqpower(i) < -6.88 Then
    pregen(i) = 6.88
End If

factor = pfulltime(i) / (pregen(i) + pfulltime(i))
pelectro(i) = pfulltime(i) + pregen(i)
pelectroc(i) = pelectroc(i - 1) + pelectro(i)

'Conversion to H2
If pelectro(i) <= T2 Then
    h2pro(i) = 0.0045 * pelectro(i)
End If
If pelectro(i) > T2 Then
    h2pro(i) = 0.0045 * T2
End If

h2fulltime(i) = factor * h2pro(i)
h2regen(i) = (1 - factor) * h2pro(i)
h2fulltimec(i) = h2fulltimec(i - 1) + h2fulltime(i)
h2regenc(i) = h2regenc(i - 1) + h2regen(i)
h2proc(i) = h2proc(i - 1) + h2pro(i)

If reqpower(i) <= 0 Then
    RPM(i) = RPM1
End If

Next i
```